

ÉCOLE DE TECHNOLOGIE SUPÉRIEURE
UNIVERSITÉ DU QUÉBEC

MANUSCRIPT-BASED THESIS PRESENTED TO THE
ÉCOLE DE TECHNOLOGIE SUPÉRIEURE

IN PARTIAL FULFILLMENT OF THE REQUIREMENTS FOR
THE DEGREE OF DOCTOR OF PHILOSOPHY
Ph.D.

BY
Thomas HEID

INNOVATIVE NANOSTRUCTURED EPOXY COMPOSITES FOR ENHANCED HIGH
VOLTAGE INSULATION SYSTEMS

MONTREAL, AUGUST 18th, 2015



Thomas HEID, 2015



This Creative Commons licence allows readers to download this work and share it with others as long as the author is credited. The content of this work can't be modified in any way or used commercially.

BOARD OF EXAMINERS

THIS THESIS HAS BEEN EVALUATED

BY THE FOLLOWING BOARD OF EXAMINERS

Mr. Eric David, Thesis Supervisor
Department of Mechanical Engineering at École de Technologie Supérieure

Mr. Michel F. Fréchette, Thesis Co-supervisor
Department of Material Sciences at Hydro-Québec's Research Institute

Mr. Sylvain Cloutier, President of the Board of Examiners
Dean of Research at École de Technologie Supérieure

Mr. Martin Viens, Member of the jury
Department of Mechanical Engineering at École de Technologie Supérieure

Mr. Michael Muhr, External Evaluator
Institute of High Voltage Engineering and System Performance at Graz University of
Technology

THIS THESIS WAS PRESENTED AND DEFENDED

IN THE PRESENCE OF A BOARD OF EXAMINERS AND PUBLIC

ON AUGUST 12th, 2015

AT ÉCOLE DE TECHNOLOGIE SUPÉRIEURE

INNOVATIVE NANOSTRUCTURED EPOXY COMPOSITES FOR ENHANCED HIGH VOLTAGE INSULATION SYSTEMS

Thomas HEID

RÉSUMÉ

Afin de faire face à la demande croissante en électricité, les tensions et les puissances d'opération ont été amenées à augmenter au cours des dernières années. Ceci engendre inévitablement une augmentation des contraintes électrothermiques sur les systèmes d'isolation électrique existants. Cependant, les matériaux polymériques habituellement utilisés pour les systèmes d'isolation haute tension sont vulnérables à la dégradation due à la présence de décharges électriques et présentent généralement de faibles conductivités thermiques. Ces raisons, choisies parmi d'autres, expliquent pourquoi il y a un besoin de créer une nouvelle génération de matériaux isolants avec de meilleures performances diélectriques et thermiques.

Durant les dernières décennies, l'attention s'est portée sur une nouvelle classe de matériaux diélectriques: les nanocomposites polymériques ou nano diélectriques. Ces diélectriques, renforcés de particules de dimension nanométrique à la place des particules micrométriques habituellement utilisés, ont montré des performances considérablement améliorées, comme, par exemple, une amélioration de la rigidité diélectrique même à de très faibles teneurs en particules, ce qui suggère leur grand potentiel d'application dans les systèmes d'isolation HT. Néanmoins, ces matériaux ne peuvent atteindre leur potentiel maximum que lorsqu'une bonne dispersion et une bonne distribution des particules dans la matrice-polymère sont atteintes. Toutefois, des grappes de nanoparticules avec des dimensions micrométriques ou submicrométriques peuvent survenir, surtout à cause de l'incompatibilité entre les particules inorganiques et le polymère organique. Ces agglomérations peuvent limiter l'amélioration des propriétés diélectriques attendue dans le cas de nanoparticules bien dispersées. Afin d'améliorer l'interaction entre les particules inorganiques et la matrice organique, et par conséquent afin d'améliorer la dispersion de ces particules dans des polymères, la fonctionnalisation de nanocharges par l'intermédiaire de traitements de surface est souvent utilisée. Pourtant, on sait peu sur la stabilité à long terme de ces traitements de surface sous les contraintes électrothermiques d'opération, ce qui peut limiter leur utilisation à l'échelle industrielle, dans le domaine de la haute tension.

L'objectif de cette thèse a été le développement de matériaux innovants à base d'époxy nanostructurés, en vue d'améliorer les performances diélectriques et thermiques du polymère de base, ainsi que d'évaluer leur applicabilité pour les systèmes d'isolation à haute tension. Afin de réaliser une contribution originale au domaine des nano diélectriques, une nouvelle approche a été explorée par l'utilisation d'additifs fonctionnels nanométriques - des silsesquioxanes oligomères polyédriques (POSS) - au lieu d'appliquer une fonctionnalisation de surface pour des nanocharges habituellement utilisées. En outre, dans le cadre de ce travail, des composites nanostructurés à plusieurs phases ont été conçus, impliquant des

additifs fonctionnels (POSS) dans la matrice polymère ainsi que des particules micro ou submicrométriques avec une haute conductivité thermique - nitrure de bore (BN) - comme deuxième additif, afin d'augmenter la conductivité thermique des composites résultants.

Pour atteindre cet objectif, dans une première étape, des composites d'époxy avec du nitrure de bore ayant une structure cristalline hexagonale (h-BN) ou cubique (c-BN), ont été élaborés et analysés, avec des teneurs en charge bien en dessous du seuil de percolation. Notre objectif a été de trouver le type de renfort le plus prometteur, le pourcentage massique de celui-ci ainsi que la taille idéale, pour augmenter la conductivité thermique dans les composites à base d'époxy. Dans ce contexte, il a été montré que l'incorporation de faibles fractions massiques ($\leq 5\%$) de particules h-BN submicrométriques ou micrométriques dans la résine époxy conduit à des améliorations notables dans la résistance à la dégradation sous décharges couronne ainsi que dans la conductivité thermique résultantes des composites, par rapport au polymère de base. L'addition de 5 % (en poids) de c-BN submicrométriques, cependant, a généré l'amélioration la plus significative de la conductivité thermique par rapport aux matériaux composites époxy/h-BN. Toutefois, tous les composites époxy/BN ont vu une légère réduction de leur rigidité diélectrique, allant jusqu'à 18 % par rapport à la résine époxy de base, ce qui est un phénomène couramment observé quand des particules de ces tailles sont utilisées. Cependant, comme les valeurs retrouvés sont nettement plus élevés que les contraintes électriques courantes pour l'isolation à haute tension (des rigidités diélectriques au-dessus de 130 kV / mm pour le h-BN, et au-dessus de 170 kV / mm pour les composites c-BN), l'amélioration notable de la résistance à l'érosion ou de conductivité thermique dans le cas des composite restent des résultats qui pourraient avoir un impact notable dans le domaine de l'appareillage de haute tension.

Dans une deuxième étape, deux types différents de nanocharges fonctionnelles de type POSS ont été utilisées pour fabriquer des composites. POSS est un matériau hybride organique/inorganique, qui a un noyau en silice, entouré par des groupes fonctionnels. Ces groupes fonctionnels ont une nature réactive dans le cas des deux additifs POSS utilisés dans ce projet, et donc, peuvent créer des liaisons covalentes avec l'époxy. Le premier additif POSS a été un Triglycidylisobutyl-POSS (TG-POSS) avec 3 groupes fonctionnels, compatibles avec notre système époxy. Lors de notre étude, on a constaté que la création de liaisons covalentes entre la matrice époxy et POSS améliore de manière significative l'interaction nanocharge-matrice et, par conséquent, conduit à des améliorations significatives de la rigidité diélectrique et de la résistance aux décharges couronne pour les composites TG-POSS. De plus, des performances supérieures ont été retrouvées pour les composites avec des teneurs en particules allant de 1 à 2,5 % (en poids), cas pour lesquels aucune agglomération n'a été retrouvée, et par conséquent, lorsque la dispersion de POSS dans la résine époxy peut être considérée comme étant réalisée à un niveau moléculaire. La présence des agglomérations pour des teneurs plus élevées de TG-POSS et la dégradation concomitante des performances diélectriques pour ces composites (avec 5 ou 10 % en poids) a limité l'exploration des chargements plus élevés en POSS, initialement envisagée pour améliorer encore d'avantage la résistance aux décharges couronne. Par conséquent, un glycidyl-POSS (G-POSS) fortement fonctionnalisé a été choisi pour poursuivre l'étude. Cette fois-ci, il a été montré que les composites à faible teneur en G-POSS ont d'excellentes

propriétés en terme de rigidité diélectrique et des résistances notamment accrues aux décharges couronne. Plus encore, les mêmes composites ont présenté des conductivités thermiques améliorées ainsi que de faibles pertes diélectriques. Globalement, l'ajout de 2,5 % (en poids) de chaque type de POSS dans une matrice d'époxy a été retrouvé comme la valeur optimale en termes de rigidité diélectrique et pour les pertes diélectriques. Pour conclure cette partie de l'étude, des composites époxy avec des teneurs en particules de Glycidyl-POSS beaucoup plus élevés qu'avant (jusqu'à 20 % en poids) ont été investigués et ils ont montré une résistance encore plus élevée aux décharges couronne. Toutefois, pour ce qui est de la conductivité thermique pour les deux types POSS, les composites à faible teneur (2,5 % en poids POSS ou moins) ont vu la plus importante amélioration par rapport au polymère de base. Ce comportement a été investigué en détail plus loin dans ce travail de thèse.

Dans la troisième étape de notre étude, des composites multi-phases ont été produits en utilisant deux types de charges. Ces matériaux contiennent à la fois 1 % (en poids) de POSS et 5 % (en poids) de particules de c-BN, afin d'étudier l'interaction entre le POSS - un composant hybride organique/ inorganique et le c-BN, purement inorganique, dans la matrice organique d'époxy. Les échantillons obtenus ont été comparés en termes de leurs propriétés diélectriques et thermiques à chaque composite individuellement chargé (contenant seulement 1 % en poids POSS ou 5 % en poids de c-BN incorporés dans l'époxy). Cette partie de l'étude a révélé que, même si aucun traitement de surface chimique complexe n'a pas été appliquée pour les particules c-BN utilisées dans notre étude, une dispersion très homogène de ces particules c-BN inorganiques a été retrouvée dans les matériaux multi-phases. Ceci a été considéré comme l'effet de l'ajout de POSS dans la résine, qui semble agir comme un dispersant des charges submicrométriques de c-BN et, cet effet positif sur la dispersion des renforts doit être considéré comme un point d'intérêt majeur dans le domaine des nanodiélectriques ou nanocomposites en général, où la dispersion des charges inorganiques nanométriques dans les polymères est encore un problème courant. En conséquence, la possibilité de concevoir des composites d'époxy combinant le POSS réactive, en même temps que d'autres charges afin d'améliorer leur dispersion dans la matrice d'époxy, représente un résultat qui pourrait contribuer de manière significative à l'avancement de la mise en œuvre des nanocomposites à base d'époxy à l'échelle industrielle. En termes de conductivité thermique ou concernant la rigidité diélectrique, lorsque les deux POSS et les particules de c-BN ont été incorporés ensemble dans le même composite, aucune amélioration n'a pas été observée par rapport à ceux retrouvés auparavant pour les composites ayant 5 % (en poids) de c-BN. En conclusion, on peut affirmer que les composites comportant uniquement les nanoparticules G-POSS possèdent, dans l'ensemble, les meilleures performances diélectriques et ils sont appropriés pour une utilisation dans le domaine de l'isolation haute tension, après avoir montré des pertes diélectriques plus faibles, une plus grande rigidité diélectrique, ainsi qu'une augmentation de la conductivité thermique, par rapport à la résine d'époxy de base.

La dernière partie de ce travail de thèse présente une analyse par éléments finis basée sur le phénomène de transfert de chaleur observé pour les composites POSS. Par conséquent, des simulations 3D du transfert de chaleur par conduction dans les composites d'époxy

VIII

sélectionnés ont été développés dans COMSOL Multiphysics en vue d'analyser d'avantage le phénomène de transport de chaleur trouvé pour les matériaux mono ou pluri-composites, étant donné que nos résultats ont montré que les teneurs croissantes en POSS ont conduit à une diminution en termes de conductivité thermique, ce qui est en contradiction avec le comportement suggéré par les lois théoriques des mélanges. L'approche de calcul en utilisant des éléments finis a finalement conduit à la proposition d'un nouveau modèle, apte à expliquer le phénomène de transport de chaleur dans les composites POSS investigués. Basé sur ces résultats, il a été conclu que la nature réactive du POSS, avec ses groupes fonctionnalisés, doit avoir un impact sur la morphologie du réseau/POSS époxy, d'une manière qui améliore le transport des phonons à travers le composite. Cette conclusion a finalement abouti avec la proposition du modèle de restructuration d'interface (IFRM), pour expliquer les résultats particuliers de la conductivité thermique dans les composites en question.

Mots-clés: comptabilisant, composites époxy, conductivité thermique, nitrure de bore, polymères nanodiélectriques POSS, réponse diélectrique, résistance aux décharges corona, rigidité diélectrique, simulations par Éléments Finis,

INNOVATIVE NANOSTRUCTURED EPOXY COMPOSITES FOR ENHANCED HIGH VOLTAGE INSULATION SYSTEMS

Thomas HEID

ABSTRACT

In order to cope with the growing demand in electricity, operating voltages and power ratings have seen an increase in the past years. This means that electro-thermal stresses on the existing electrical insulation systems have increased concomitantly. However, polymeric materials used for high voltage insulation are prone to degradation due to electrical discharges and commonly boast rather low thermal conductivities, which is why there is an impelling need for a new generation of insulating materials with improved dielectric and thermal performances.

During the last decades, attention was drawn towards a novel class of dielectric materials: polymer nanocomposites or nanodielectrics. These dielectrics feature nanometric filler particles instead of micrometric particles, which can lead to significantly enhanced performances - such as improved dielectric breakdown strengths - already at very low contents, thus indicating their great potential for application in HV insulation systems. Nevertheless, such nanodielectrics only unfold their full potential when a good dispersion and distribution of those filler particles within the polymer matrix are achieved. Albeit, clusters of nanoparticles with submicrometric or micrometric dimensions are often found, which is due to the incompatibility of inorganic particles with the organic polymer. Such agglomerations will subsequently cancel the beneficial effect seen for well dispersed nanoparticles. In order to enhance the interaction between inorganic filler particles and organic matrix, and hence, improve the dispersion of such particles in polymers, the functionalization of nanofillers has become rather common. Still, little is known about the long-term stability of such functionalizers under electro-thermal stresses, which poses a drawback to their broad industrial use in high voltage engineering.

The objective of the presented thesis was to develop innovative, nanostructured epoxy composites that reveal enhanced dielectric and thermal performances, and to evaluate their applicability for high voltage insulation systems. In order to achieve an original contribution to the field of nanodielectrics, a novel approach was explored by using functional nanometric additives, so-called polyhedral oligomeric silsesquioxanes (POSS) instead of applying surface functionalization for the filler particles used. Even more, multifunctional nanostructured composites were to be designed, involving functional POSS additives along with thermally conductive filler, to further enhance the thermal conductivity of the resulting composites.

To achieve our objectives, in a first step, epoxy composites with hexagonal boron nitride (h-BN) and cubic boron nitride (c-BN) were developed and analyzed, with filler contents well below the percolation threshold, to find the most promising type of BN filler and its

respective size, to boost thermal conductivity in epoxy composites. In this context, it was shown that incorporation of low weight fractions (≤ 5 wt%), of submicrometric and micrometric h-BN particles in epoxy resin resulted in noticeable improvements in corona resistance and thermal conductivity of the resulting composites. Addition of 5 wt% c-BN in submicrometric particle sizes, however, was found to achieve the most significant improvement of the thermal conductivity compared to the h-BN composites. At the same time, all the BN composites have seen a slight reduction in their dielectric breakdown strength of up to 18 % compared to the base epoxy, which is a common phenomenon observed for the filler sizes used. With the respective breakdown strengths being above 130 kV/mm for the h-BN, and above 170 kV/mm for the c-BN composites, thus still significantly higher than common electric stresses in high voltage insulation systems, the improvements found in the composites' erosion resistance or thermal conductivity should be granted a higher emphasis.

In a second step, two different types of functional POSS fillers were used to fabricate composites. POSS is a hybrid inorganic/organic material, which has a silica-like core surrounded by functional groups. These functional groups were of reactive nature in the case of the two POSS additives used, and thus, could covalently bond with the epoxy. The first POSS additive was a Triglycidylisobutyl-POSS (TG-POSS) which had 3 functional groups that were compatible with our epoxy system. It was found that the formation of covalent bonds between POSS and the epoxy matrix significantly improved the filler/matrix interaction, and hence, led to significant improvements in dielectric breakdown (BD) strengths and corona resistances for the TG-POSS composites. This was further supported by the superior performances of the lower content composites with 1 and 2.5 wt% of TG-POSS, where no agglomerations were found, and hence, where the dispersion of POSS in the epoxy can be considered to be at a molecular level. The presence of agglomerations for higher TG-POSS contents (with 5 or 10 wt% POSS) and the concomitant deterioration of the dielectric performances for these composites prevented to exploit higher POSS loadings, to further enhance the resistance to corona discharges for instance. Therefore, a highly functionalized Glycidyl-POSS (G-POSS) was chosen to continue with the study. This time around, it was shown that composites with low G-POSS content have excelled in high BD strengths and notably increased resistances against corona discharges, as well as enhanced thermal conductivities and low dielectric losses. Overall, the addition of 2.5 wt% of both types of POSS in epoxy was found to be an optimal value in terms of dielectric strength and losses. Further increase of the Glycidyl-POSS loading would then contribute towards an even higher resistance to corona discharges, whereas in terms of thermal conductivity for both POSS types, the composites with low contents, of 2.5 wt% POSS and below, have seen the most significant enhancements.

In the third step of this study, multiphase composites were produced, which contained both, 1 wt% of POSS and 5 wt% of c-BN particles, in order to investigate the interaction between the hybrid inorganic/organic POSS and the inorganic c-BN. The obtained multiphase samples were compared in terms of their dielectric and thermal properties with the respective single-phase composites, where only 1 wt% POSS or 5 wt% c-BN were incorporated in epoxy. This part of the study revealed that although no complex chemical surface treatment was applied

for the c-BN particles used in our study, yet a homogeneous dispersion of the inorganic c-BN particles was seen in the multiphase composites. This effect of POSS, which was shown to act as a dispersant of the inorganic c-BN filler should be regarded as a major point of interest in nanodielectrics or nanocomposites in general, as the dispersion of nanometric inorganic filler particles within polymers is still a very current problematic. And thus, the approach of formulating epoxy composites combining reactive POSS and other filler particles to improve their dispersion within the epoxy matrix, could significantly contribute to the advancement of the implementation of epoxy-based nanocomposites on an industrial level. In terms of thermal conductivity or breakdown strengths no improvement compared to the 5 wt% c-BN composite was seen, when both POSS and c-BN were incorporated together in a multiphase sample. In conclusion, it can be stated that the G-POSS composites feature the overall best performance of a dielectric material for high voltage insulation, with lower dielectric losses, higher BD strength, as well as increased thermal conductivity, compared to the base epoxy.

The last part of this work presents a simulation-based analysis of the heat transfer phenomenon observed for the POSS composites. Therefore, 3D FEM simulations of the conductive heat transfer in selected epoxy composites were conducted in COMSOL Multiphysics, given that our results have shown that increasing POSS contents have led to a decrease in terms of thermal conductivity, which is in contradiction with the behavior suggested by theoretical mixing laws. The FEM computational approach finally led to the proposal of a novel model, which can explain the heat transport phenomenon in the presented POSS composites. The *Interfacial Restructuration Model* (IFRM) points out that the reactive nature of POSS, with its functionalized groups, must have an impact on the morphology of the epoxy/POSS network, in a way that enhances phonon transport through the bulk composite, thus explaining the particular results of thermal conductivities in the POSS composites in question.

Keywords: Boron nitride, compatibilizer, corona resistance, dielectric breakdown strength, dielectric response, epoxy composites, FEM modeling, polymer nanodielectrics, POSS, thermal conductivity

TABLE OF CONTENTS

	Page
INTRODUCTION	1
0.1 Research objectives and approach	2
0.2 Specific research objectives & structure of PhD thesis	2
0.3 Methodology	4
CHAPTER 1 DIELECTRICS VS. NANODIELECTRICS.....	5
1.1 Physical properties of dielectrics for high voltage applications	5
1.1.1 Thermal properties	6
1.1.2 Electrical properties	7
1.1.3 Mechanical properties.....	8
1.1.4 Chemical properties	8
1.2 From micro to nano – or is it sub-micro really?	8
1.2.1 When is “nano” really nano?	8
1.2.2 Introduction to nanocomposites.....	9
1.3 Theories and models for nanocomposites.....	10
1.3.1 Electric double layer	10
1.3.2 Intensity model.....	11
1.3.3 Multi-core model	12
1.3.4 Water shell model	13
1.4 Overview of the impact of nanoparticles on some electrical properties of NC	14
1.4.1 Impact on AC breakdown strength	15
1.4.2 Impact on the resistance to corona discharges.....	15
1.5 Materials Review	16
1.5.1 Epoxy resins.....	16
1.5.2 Boron nitride	20
1.5.3 Polyhedral oligomeric silsesquioxanes (POSS).....	21
CHAPTER 2 PHYSICAL PROPERTIES OF POLYMER DIELECTRICS.....	23
2.1 Electrostatics of dielectrics	23
2.2 Polarization mechanisms in dielectrics.....	24
2.2.1 Electronic or optical polarization.....	25
2.2.2 Atomic or ionic polarization	25
2.2.3 Dipolar or orientational polarization.....	26
2.3 Dielectric relaxation in polymers.....	26
2.3.1 Complex relative permittivity and the dielectric losses	27
2.3.2 Complex permittivity vs. polarization mechanisms in NC.....	29
2.3.3 Dielectric relaxation theory and models	30
2.3.4 Dielectric relaxation processes in polymers	33
2.4 Conduction mechanisms in polymers	36
2.4.1 Electronic conduction	36
2.4.2 Ionic conduction.....	37

2.4.3	Thermal conduction	38
CHAPTER 3 EPOXY/BN MICRO- AND SUBMICRO-COMPOSITES: DIELECTRIC AND THERMAL PROPERTIES OF ENHANCED MATERIALS FOR HIGH VOLTAGE INSULATION SYSTEMS		
3.1	Introduction.....	41
3.2	Materials and sample preparation	43
3.3	Experimental methods	44
3.3.1	Microstructure analysis.....	44
3.3.2	Differential scanning calorimetry	44
3.3.3	Dielectric spectroscopy	44
3.3.4	AC breakdown strength	45
3.3.5	Resistance to electrical discharge	45
3.3.6	Thermal conductivity	46
3.4	Experimental results and discussion	47
3.4.1	Microstructure analysis.....	47
3.4.2	Differential scanning calorimetry	47
3.4.3	Dielectric spectroscopy.....	50
3.4.4	AC breakdown strength	54
3.4.5	Resistance to electrical discharge	56
3.4.6	Thermal conductivity	58
3.5	Conclusions.....	60
3.6	Acknowledgment	62
CHAPTER 4 NANOSTRUCTURED EPOXY/POSS COMPOSITES: ENHANCED MATERIALS FOR HIGH VOLTAGE INSULATION APPLICATIONS		
4.1	Introduction.....	64
4.2	Materials and sample preparation	65
4.3	Experimental methods	67
4.3.1	Microstructure analysis.....	67
4.3.2	Differential scanning calorimetry	67
4.3.3	AC breakdown strength	67
4.3.4	Resistance to corona discharges.....	68
4.3.5	Thermal conductivity	69
4.3.6	Dielectric spectroscopy	69
4.4	Experimental results and discussion	70
4.4.1	Microstructure analysis.....	70
4.4.2	Differential scanning calorimetry	70
4.4.3	AC breakdown strength	73
4.4.4	Resistance to corona discharge	75
4.4.5	Thermal conductivity	76
4.4.6	Dielectric spectroscopy	78
4.4.7	Relaxation behavior	82
4.5	Concluding remarks	84

4.6	Acknowledgment	85
CHAPTER 5	ENHANCED ELECTRICAL AND THERMAL PERFORMANCES OF NANOSTRUCTURED EPOXY/POSS COMPOSITES	87
5.1	Introduction	88
5.2	Materials and sample preparation	89
5.3	Experimental methods	91
5.3.1	Microstructure analysis	91
5.3.2	Differential scanning calorimetry	91
5.3.3	AC breakdown strength	91
5.3.4	Resistance to corona discharges	92
5.3.5	Thermal conductivity	93
5.3.6	Dielectric spectroscopy	93
5.4	Results and discussion	93
5.4.1	Microstructure analysis	93
5.4.2	Differential scanning calorimetry	95
5.4.3	AC breakdown strength	96
5.4.4	Resistance to corona discharges	98
5.4.5	Thermal conductivity	99
5.4.6	Dielectric spectroscopy	103
5.4.7	Relaxation behavior	106
5.5	Concluding remarks	109
5.6	Acknowledgment	110
CHAPTER 6	FUNCTIONAL EPOXY COMPOSITES FOR HIGH VOLTAGE INSULATION INVOLVING C-BN AND REACTIVE POSS AS COMPATIBILIZER	111
6.1	Introduction	112
6.2	Materials and sample preparation	114
6.2.1	Materials	114
6.2.2	Compounding	115
6.3	Experimental methods	117
6.3.1	Microstructure analysis	117
6.3.2	Dielectric spectroscopy	117
6.3.3	Differential scanning calorimetry	118
6.3.4	AC breakdown strength	118
6.3.5	Thermal conductivity	118
6.4	Results and discussion	119
6.4.1	Microstructure analysis	119
6.4.2	Dielectric spectroscopy	121
6.4.3	Differential scanning calorimetry	122
6.4.4	AC breakdown strength	123
6.4.5	Thermal conductivity	125
6.5	Concluding remarks	127
6.6	Acknowledgment	128

CHAPTER 7	MATHEMATICAL VALIDATION AND ESTIMATION OF MATERIAL PROPERTIES	129
7.1	Theoretical models for the complex permittivity of composite materials	129
7.1.1	Two phase models.....	129
7.1.2	Three phase models.....	133
7.2	Theoretical models for the thermal conductivity of composite materials.....	134
7.3	Comparison of theoretical models with the experimental data.....	136
7.3.1	Estimation of the thermal conductivities of h-BN composites	136
7.3.2	Estimation of the thermal conductivities of c-BN composites	138
7.4	Conclusion on the applicability of mixing laws to estimate material properties	139
CHAPTER 8	3D FEM MODELING OF THE THERMAL CONDUCTIVITY OF COMPOSITE MATERIALS	141
8.1	Basics of heat transfer in solids	142
8.2	Modeling the thermal conductivity of epoxy/c-BN composites	143
8.3	Unraveling the thermal conductivity of the multiphase and functional POSS composites.....	148
8.4	Evaluation of POSS' contribution to the thermal conductivity in the multi-phase composites.....	149
8.4.1	Simulations based on the assumption that POSS is represented only by its silica core	150
8.4.2	Proposal of the Interfacial Restructuration Model (IFRM) for conductive heat transfer in functional POSS composites	153
8.4.3	Evaluation of the interfacial restructuration zone (IFRZ) of POSS by means of 3D FEM simulations	154
8.4.4	Validation of the proposed model of the interfacial restructuration zones	158
8.5	Concluding remarks on the interfacial restructuration zones in functional POSS composites.....	160
CONCLUSION.....		163
RECOMMENDATIONS.....		171
APPENDIX I	PERSONAL PUBLICATION LIST	173
LIST OF BIBLIOGRAPHICAL REFERENCES.....		177

LIST OF TABLES

		Page
Table 3.1	Specifications for BN filler particles as provided by supplier	43
Table 3.2	Glass transition temperatures of neat epoxy and the BN composites	49
Table 3.3	Weibull parameters obtained from Figure 3.9	55
Table 4.1	Glass transition temperatures of neat epoxy and TGIB-POSS composites	72
Table 4.2	Weibull parameters obtained from Figure 4.5	74
Table 4.3	Activation energies obtained by fitting the β -relaxation process	84
Table 5.1	Overview and nomenclature of prepared samples	90
Table 5.2	Glass transition temperatures T_g of test specimens	95
Table 5.3	Weibull parameters from the breakdown experiment	97
Table 5.4	Evaluation of the eroded sample volumes after exposure to corona discharges and the respective relative resistances against corona discharges of the composites compared to NE	99
Table 5.5	Evaluation of thermal conductivity measurements	100
Table 5.6	Activation energies obtained by fitting the β -relaxation process	108
Table 6.1	Overview and nomenclature of prepared samples	115
Table 6.2	Glass transition temperatures T_g of test specimens	122
Table 6.3	Weibull parameters from the breakdown experiment	124
Table 6.4	Evaluation of thermal conductivity measurements	126
Table 7.1	Parameters for the comparison between the theoretical mixing laws and the experimental data for the h-BN sample series	138
Table 7.2	Parameters for the comparison between the theoretical mixing laws and the experimental data for the c-BN sample series	139
Table 8.1	Resulting thermal conductivities obtained by COMSOL simulations (coherent results are highlighted in green, unmatched results in orange)	145

XVIII

Table 8.2	Comparison of simulation results with the experimental value for the thermal conductivity in the case of cBN 5wt% with clusters of c-BN particles (coherent results are highlighted in green, unmatched results in orange).....	146
Table 8.3	Overview of the sample natures and the respective measured thermal conductivities in case of cBN 5wt% and the two multiphase samples	148
Table 8.4	Simulation results of bulk thermal conductivity for the MP composite (right column) as a function of a variation in the matrix' thermal conductivity (left column). The values for λ_{matrix} which will lead to the measured values of $\lambda_{\text{MP composite}}$ are highlighted in green	151
Table 8.5	Simulation parameters and resulting thermal conductivities for the GP 1wt% composite, where POSS was embodied by 9 silica spheres (unmatched results highlighted in orange).....	152
Table 8.6	The calculated bulk thermal conductivities of GP 1wt% in W/m·K as a function of the interfacial restructuring zone's λ_{IFRZ} and its radius around the silica core. Possible combinations of λ_{IFRZ} and its radius giving the same bulk thermal conductivity as measured for GP 1wt% are highlighted in green	157
Table 8.7	Final results of the COMSOL simulations on the bulk thermal conductivity of the G-POSS composites showing matching parameter combinations for the IFRZs	158
Table 8.8	Final results of the COMSOL simulations presenting the matching combinations of IFRZ parameters to achieve a $\lambda_{\text{matrix}} = 0.166$ W/m·K by incorporation of 1wt% G-POSS in the multiphase composite	161

LIST OF FIGURES

	Page
Figure 1.1	Illustration of increasing dominance of interfacial areas with decreasing filler sizes Taken from Andritsch (2010, p. 3)9
Figure 1.2	A schematic of the electrical double layer surrounding a particle Taken from Andritsch (2010, p. 35) 11
Figure 1.3	Change of intensities I_α defining phases A and B over the distance across the interface Taken from Lewis (2005, p. 203) 12
Figure 1.4	Illustration of the multi-core model for polymeric NC Taken from Tanaka et al. (2005, p. 674)..... 13
Figure 1.5	Water shell model with quasi DC (QDC) conduction (a) no overlapping water shells (b) overlapping water shells Adapted from Zou et al. (2008, p. 114) 14
Figure 1.6	Relative impact on various nanofillers on the ACBD strength of polymer NCs compared to the base polymers Taken from David and Fréchet (2013, p. 31)..... 15
Figure 1.7	Simple molecule of diglycidyl ether of bisphenol A with two epoxide groups..... 17
Figure 1.8	Basic processing schematic for epoxy based composites 19
Figure 1.9	Different crystal structures of boron nitride Taken from Haubner et al. (2002, p. 6)..... 20
Figure 1.10	(a) shows a typical POSS molecule with the inorganic silica-like core and the organic side-groups “R” which are depending on the respective POSS-type; (b) and (c) show the proposed interaction with POSS and the epoxy matrix, rendering the amorphous epoxy resin (b) into a structured composite on a nanometric scale (c) 21
Figure 2.1	Polarization charges on a parallel plate condenser; a) with vacuum and b) with a dielectric medium between the plates 23
Figure 2.2	Polarization mechanisms in dielectrics 25

Figure 2.3	Dielectric between two electrodes forming a condenser (left) and the phase diagram of a complex current through the dielectric due to an applied AC voltage (right)	27
Figure 2.4	Frequency dependent polarization mechanisms Taken from Andritsch (2010, p. 147)	30
Figure 2.5	Schematic of dielectric relaxation processes observable in polymers (left) and their temperature dependence (right)	34
Figure 2.6	Relaxation map showing the dielectric losses (ϵ'') and the relaxation phenomena of neat epoxy as a function of frequency and temperature.....	36
Figure 2.7	Schematic of heat transfer by phonons in amorphous dielectrics. A phonon moves along a polymer chain until reaching its end, where phonon scattering occurs, resulting in reduced bulk thermal conductivity of the polymer	39
Figure 3.1	Schematic of surface erosion setup.....	46
Figure 3.2	Schematic of heat flow meter setup	47
Figure 3.3	SEM micrographs of epoxy/BN composites a) BN205 1wt%, b) BN205 2wt%, c) BN205 5wt%, d) BN600 1wt%, e) BN600 2wt%, f) BN600 5wt%.....	48
Figure 3.4	DSC graphs from the second thermal cycle for neat epoxy and the BN composites.....	49
Figure 3.5	3D plots of dielectric losses for all samples measured at either 3 or 500 V, showing the main relaxation phenomena. BN composites revealed lower dielectric losses at high temperatures and low frequencies with increasing filler loadings. Electrode polarization (EP) due to a delay in charge transport at electrode-composite interfaces could additionally be detected for all samples	51
Figure 3.6	Dielectric response of neat epoxy and BN composites measured at 3 V and 20 °C; a) real part and b) imaginary part of the complex permittivity.....	52
Figure 3.7	Neat epoxy temperature dependent real part (a), imaginary part (b) of complex permittivity and (c) loss tangent.....	53
Figure 3.8	BN205 5wt% temperature dependent real part (a), imaginary part (b) of complex permittivity and (c) loss tangent	53
Figure 3.9	Weibull plots of breakdown strengths with 95 % confidence intervals.....	55

Figure 3.10	Schematic evolution of the microstructure in epoxy resin with increasing filler and subsequently defect contents.....	57
Figure 3.11	Comparison of eroded sample volume after exposure to partial discharges for 30 hours at 4 kV _{RMS} and 300 Hz	57
Figure 3.12	Comparison of thermal conductivities; two measurements were taken on each sample type. The comparison of thermal conductivity was based on the average value for each	59
Figure 4.1	Proposed reaction of TGIB-POSS with curing agent and epoxy resin with the formation of covalent bonds, and hence, forming a nano-structured epoxy/POSS network.....	66
Figure 4.2	Schematic of point-to-plane setup for corona resistance experiment.....	68
Figure 4.3	SEM micrographs with increasing magnification from left to right, for a) neat epoxy, b) ePOSS 1wt%, c) ePOSS 2.5wt%, d) ePOSS 5wt% and e) ePOSS 10wt%.....	71
Figure 4.4	Overlaid DSC curves from the second thermal cycles	72
Figure 4.5	Weibull plot of breakdown data with 95 % confidence intervals.....	74
Figure 4.6	Evaluation of resistance to electrical discharges based on eroded sample volume after 30 hours of exposure to PD.....	76
Figure 4.7	Evaluation of thermal conductivities for the test specimens, with the first and second measurement series plotted as dashed columns and the respective average values in solid columns	77
Figure 4.8	Dielectric responses at 20 °C and 1 V of neat epoxy and the TGIB-POSS composites; a) real parts and b) imaginary parts of the complex permittivities	79
Figure 4.9	Temperature-dependent real part (left column) and imaginary part (right column) of complex permittivity for a) neat epoxy, b) ePOSS 1wt%, c) ePOSS 2.5wt%, d) ePOSS 5wt% and e) ePOSS 10wt%.....	81
Figure 4.10	Relaxation time plots of the β relaxation process	83
Figure 5.1	Structure of a Glycidyl-POSS molecule in its cage-form (with 8 epoxy groups) reacting with the curing agent and the epoxy resin (top) to form a nano-structured epoxy/POSS composite due to the formation of covalent bonds between the constituents (bottom)	90

Figure 5.2	Schematic of the erosion setup used (on the left) and a typical 3D erosion pattern retrieved on a NE sample (right) viewed from the top. The original sample surface is colored in red, and the zones with the deepest erosion traces are represented in blue92
Figure 5.3	SEM micrographs of the samples at a magnification of x200k (upper six images) and a TEM image showing a zoom on one crystalline structure found in the GP 20wt% composites (bottom right), which itself consists of several hexagonal substructures. The crystalline structures had sizes starting from just a few nanometers up to some hundreds of nanometers.....94
Figure 5.4	Weibull plot of the breakdown data with 95 % confidence intervals97
Figure 5.5	Evolution of the thermal conductivity for the POSS composites as estimated with mixing laws, compared to experimental values. While the calculations result in a continuously increasing thermal conductivity with increasing POSS content, the experimental values show a logarithmic decrease102
Figure 5.6	Dielectric response of NE and the POSS composites for a) 20°C, b) 60°C and c) 100°C.....104
Figure 5.7	Relaxation maps of the dielectric losses as a function of applied frequency and temperature; for a) NE, b) GP 2.5wt% and c) GP 20wt%106
Figure 5.8	Relaxation time plots of the β -relaxation process.....108
Figure 6.1	Proposed reaction of the two different POSS types with curing agent and epoxy resin, TG-POSS (left) with the three epoxy groups and the G-POSS (right) with the cage structure represented for the case of R=8 epoxy groups. The formation of covalent bonds between POSS and epoxy matrix results in nano-structured epoxy/POSS networks114
Figure 6.2	Micrographs of the composites captured at different magnifications: (a) G-POSS, (b) TG-POSS, (c) cBN, (d) MP/G-POSS and (e) MP/TG-POSS.....120
Figure 6.3	Dielectric response of test specimens at 20 °C and 1 V; (a) real part of complex permittivity, (b) imaginary part of complex permittivity and (c) the resulting loss tangent.....121
Figure 6.4	Weibull plot of the breakdown data with 95 % confidence intervals124

Figure 7.1	(a) Single spherical inclusion within a medium to develop Maxwell's equations for mixtures (b); the small inclusions in (b) are the same as the inclusion shown in (a) Adapted from Kremer (2003, p. 89)	130
Figure 7.2	Comparison of thermal conductivities between the experimental data obtained for the submicrometric BN205 sample series and the theoretical mixing laws	137
Figure 7.3	Comparison of thermal conductivities between the experimental data obtained for the micrometric BN600 sample series and the theoretical mixing laws	137
Figure 7.4	Comparison of thermal conductivities between the experimental data obtained for the submicrometric c-BN sample series and the theoretical mixing laws	138
Figure 8.1	Geometries for the cases of a) neat epoxy, b) cBN 1wt% and c) cBN 5wt%	143
Figure 8.2	The defined boundary conditions for the models, here in case of cBN 1wt%. The temperature difference over the sample volume will cause a heat flow from top to bottom of the model. The heat flux out of the unit cell with 2 μm side lengths was defined zero ($q_x = q_y = 0$)	144
Figure 8.3	Micrograph of the cBN 5wt% sample (with increasing magnification from left to right) showing that the c-BN particles were not well dispersed in the matrix, but formed clusters with c-BN agglomerations	146
Figure 8.4	New geometries for the cBN 5wt% sample with a) small distance between the particles, b) an agglomerated "X" structure and c) an agglomerated "⊥" structure	146
Figure 8.5	Scenario with 8 unit cells (cases b) and c) in equal numbers), representing a random structure of cBN 5wt%	148
Figure 8.6	Microstructures of a) cBN 5wt%, b) MP/G-POSS and c) MP/TG-POSS. In the two MP samples a clearly improved dispersion of the c-BN particles resulted	149
Figure 8.7	The geometry for the calculation of the thermal conductivity of GP 1wt%, with G-POSS represented by 9 well dispersed silica sphere	152

Figure 8.8	Schematic to explain the enhanced phonon transport in POSS composites compared to neat epoxy, caused by an interfacial restructuring of the polymeric network due to covalent bonding between epoxy and POSS154
Figure 8.9	Different geometries used for the simulations of the impact of the IFRZ on the thermal conductivity of GP 1wt%, showing the varying size of the IFRZ for a) no IFRZ at all (0 nm), b) with a 3 nm and c) with a 5 nm IFRZ155
Figure 8.10	Computed bulk thermal conductivity of the GP 1wt% composite as a function of radius and thermal conductivity of the IFRZs. The dashed red line shows the experimental value of the GP 1wt% composite, which is the desired bulk thermal conductivity for our model cases156
Figure 8.11	The final geometries for the cases of a) GP 5wt%, b) GP 10wt% and c) GP 20wt% with the IFRZ sizes that gave the matching results for the calculations compared with the experimental data159

LIST OF ABBREVIATIONS

AC	Alternating current
BD	Breakdown
BDS	Broadband dielectric spectroscopy
BN	Boron nitride
c-BN	Cubic boron nitride
DC	Direct current
DGEBA	Diglycidyl ether of bisphenol A
DSC	Differential scanning calorimetry
G-POSS	Glycidyl-POSS
h-BN	Hexagonal boron nitride
HV	High voltage
IFRM	Interfacial Restructuration Model
IFRZ	Interfacial restructuration zone
NC	Nanocomposite
PD	Partial discharge
POSS	Polyhedral Oligomeric SilSesquioxanes
SEM	Scanning electron microscopy
TEM	Transmission electron microscopy
T _g	Glass transition temperature
TGIB-POSS	Triglycidylisobutyl-POSS
TG-POSS	Triglycidylisobutyl-POSS

INTRODUCTION

Insulating systems are a key part of any high voltage (HV) apparatus used in power generation, energy transformation and energy transportation. Bushings, rotating machines, spacers and cable terminations are only some examples of applications that require well designed and reliable insulating systems. In an ongoing effort to make power systems more reliable, sustainable, as well as meeting the growing demand in electricity, changes in the existing insulating materials are inevitable. However, most of the organic materials used for high voltage insulation like, e.g. epoxy resins, are prone to degradation due to electrical discharges and usually feature rather low thermal conductivities. Further, considering the increasing electro-thermal stresses on electrical insulation systems due to growing operating voltages and power ratings, there is an impelling need for a new generation of insulating materials with improved dielectric and thermal performances.

In the past, the above mentioned deficient properties of HV insulating materials have been counteracted by the addition of micrometric inorganic filler materials, e.g. silica, which can render the resulting microcomposites more resilient to electro-thermal stresses and improve parameters such as thermal conductivity and erosion resistance.

During the last decade though, much has been reported about a novel class of dielectric materials: the so-called polymer nanocomposites or nanodielectrics, featuring nanometric filler particles (Fabiani et al., 2010; Fréchette et al., 2001; Iyer et al., 2011; Krivda et al., 2012; Tanaka et Imai, 2013). However, such nanodielectrics only unfold their full potential when good dispersion and distribution of those filler particles within the matrix are achieved. Albeit, due to the incompatibility of inorganic particles with the organic polymer, dispersion and distribution are regularly compromised, resulting in agglomerations of nano particles, often leading to aggregates with submicrometric or micrometric dimensions.

In order to enhance the interaction between inorganic filler particles and the organic matrix, and hence, improve the dispersion of such particles in polymers, the functionalization of

nanofillers has become rather common. Surface treatments with coupling agents such as silane (Dongling et al., 2005b; Huang et al., 2012; Preda et al., 2013), or more complex processes, like grafting organic brushes on particle surfaces (Virtanen et al., 2014), have been explored with varying success in the past. Still, little is known about the long-term stability of such functionalizers under electro-thermal stresses, which might pose a drawback to a broad industrial use in high voltage engineering. For example, when the surface functionalization was conducted just by surface coating of the filler particles, thermal degradation of the used agents, and hence, the loss of the compatibilizing effect has been shown by (Wen et Ding, 2004) and by (Vahid, Mostafa et Pascal, 2012). In the latter case, the degradation of the surface coating occurred during polymer processing.

0.1 Research objectives and approach

In this context, my PhD was started in May 2012 as a part of a bigger research project, called “*recherche et développement cooperative*” (RDC), in collaboration between *École de Technologie Supérieure (ETS)* and *Hydro Québec’s Research Institute (IREQ)*, aiming to tailor the dielectric and thermal properties of polymer composites by nanostructuring. In this framework, the objective of my thesis was to develop innovative, nanostructured epoxy composites that reveal enhanced dielectric and thermal performances, and to evaluate their applicability for high voltage insulation systems. Due to the above mentioned reasons of thermal degradation of common surface treatments, a novel approach was explored by using functional fillers, instead of applying surface functionalization for the used filler particles.

0.2 Specific research objectives & structure of PhD thesis

This PhD project was divided into three main steps:

In the first step, hexagonal boron nitride (h-BN) and cubic boron nitride (c-BN) with submicrometric and micrometric particle sizes are used to fabricate epoxy/BN composites with improved thermal conductivities. The results of this part led to the publication of Article I (Chapter 3) and two conference papers (Heid et al., 2013a; Heid et al., 2013b).

In the second step, nanostructured epoxy/POSS (Polyhedral Oligomeric Silsesquioxanes) composites are fabricated, using various reactive liquid POSS additives, which are compatible with our used epoxy system. Accordingly, the filler can form covalent bonds with the epoxy matrix, which is supposed to change the morphology of the epoxy by increasing the order locally, and consequently, structure the epoxy network on a nanometric scale. The findings of this part were published in Article II (Chapter 4) and Article III (Chapter 5) as well as in multiple conference papers (Heid, Fréchet et David, 2013; Heid, Fréchet et David, 2014b; 2014c).

For all of the retrieved epoxy/POSS and epoxy/BN composites, the dielectric and thermal properties are evaluated for various filler types and concentrations, in order to find the most promising constituents and their optimal concentrations for designing multiphase composites in the third step.

In the third and final step, novel nanostructured multiphase epoxy composites featuring both POSS and BN are designed and characterized. These materials were expected to have both enhanced dielectric and thermal properties due to the impact of both fillers. Considering that the incorporated POSS is forming covalent bonds with the epoxy matrix, the additional BN filler will now be integrated in an organized and structured epoxy/POSS network instead of an amorphous epoxy. This change in morphology and the polymer chain structure is assumed to affect the interaction of BN with the network. Based on this, we aimed on achieving a synergetic effect, where the hybrid POSS with its inorganic core and the organic side-groups could act like a functionalizing agent, and thus, improve the integration of BN in the epoxy/POSS matrix. The conclusions found for this part were published in Article IV (Chapter 6) and in one conference paper (Heid, Fréchet et David, 2015a).

Subsequently, the aim of this PhD project is to design and analyze innovative nanostructured multiphase epoxy composites, which should take advantage of the specific features of both POSS and BN as filler materials, thus exhibiting improvements such as reduced degradation due to electrical discharges and enhanced thermal conductivities.

0.3 Methodology

In order to evaluate the potential of our created composites for industrial use in HV insulation systems, all single filler and multiphase composites are characterized by means of broadband dielectric spectroscopy (BDS), AC breakdown testing, surface erosion due to partial discharges and thermal conductivity measurements.

Thermal analysis like Differential Scanning Calorimetry (DSC) will give deeper insights on the materials morphology and reticulation states of our composites, while chemical analysis like Fourier Transform Infrared Spectroscopy (FTIR) will help understand changes of dielectric properties due to chemical processes and changes of the composites' chemistry due to the subjected treatments.

In addition, morphological investigations will help to understand the achieved results of incorporating the various fillers in epoxy, by revealing the intrinsic structures of the composites. Therefore Scanning Electron Microscopy (SEM), Transmission Electron Microscopy (TEM) and Atomic Force microscopy (AFM) are used. In some special cases, more specifically for the POSS composites, X-Ray Diffraction spectroscopy (XRD) is used to assess the level of molecular dispersion of the POSS additives in the respective composites.

Finally, analytical and numerical modelization based on the *finite element method* (FEM) will be conducted, to further understand the underlying heat transfer mechanisms observed for our composites.

CHAPTER 1

DIELECTRICS VS. NANODIELECTRICS

Insulation is a key part of any electrical insulation system and therefore of any high voltage equipment. Per definition, an electrical insulation system is an “*Insulating structure containing one or more electrical insulating materials (EIM) together with associated conducting parts employed in an electrotechnical device.*” according to the IEC 62332-1 standard. Due to the technical development towards higher electrical field strengths and frequently concomitant increased thermal loads, improved materials are needed to meet the demands. Consequently this embodies a continuous point of interest in research in order to achieve better performances and longer lifetimes. There are three basic groups of electrical insulating materials, also called dielectrics:

- solid dielectrics;
- fluid dielectrics;
- and gaseous dielectrics.

Common solid dielectrics, along numerous types of polymers (e.g. epoxy resin, PE), are ceramics and glass. Well known representatives of fluid dielectrics would be mineral oils and more recent their biodegradable pendants, whereas air is probably the most common gaseous dielectric in high voltage power transmission and distribution grids besides various other gases like SF₆.

1.1 Physical properties of dielectrics for high voltage applications

During operation, an electrical insulation system can be exposed to several kinds of stress factors, which can be of thermal, electrical, ambient and mechanical nature, often referred to as the “T.E.A.M.” stresses, each leading to corresponding ageing mechanisms. Accordingly,

the functionality of insulation systems can generally be characterized by four main categories of material's properties:

- thermal properties;
- electrical properties;
- mechanical properties;
- chemical properties.

1.1.1 Thermal properties

A known limiting factor for high voltage insulation systems is their thermal conductivity. If the heat generated, mainly due to Joule heating in conducting parts, cannot be dissipated properly, it causes an increase of the temperature in the insulation system. With such an increase in temperature, the thermal degradation, and hence the ageing process, is accelerated, leading to shorter lifetimes of polymeric insulation materials according to the Arrhenius model given by

$$L = L_0 e^{\left(\frac{E}{RT}\right)} \quad (1.1)$$

where L is the lifetime in hours, L_0 a material specific constant, E the activation energy in eV, R the universal gas constant and T the temperature in Kelvin. Additional information on the topic of thermal ageing in electrical insulation can be found in literature, e.g. (Mazzanti, Montanari et Motori, 1994).

A crucial temperature for polymeric materials, and especially for epoxy resins, is given by their glass transition temperature T_g . When the temperature of an epoxy-based insulation system exceeds its T_g , the insulating material experiences a permanent weakening of both, mechanical and electrical strengths. Accordingly, the optimal operating temperatures of apparatus with epoxy-based insulation systems lie well below their T_g .

Furthermore, the thermal stability of the insulation systems' properties is an important parameter as well. In this aspect epoxy resins are known to have comparably stable electrical properties below their glass transition temperatures (Arora et Mosch, 2011).

1.1.2 Electrical properties

Obviously, the electrical or dielectric properties are amongst the most important parameters for electrical insulating materials. The specific resistivity is a basic parameter of an electrical insulator, since it defines the ability of a material to prevent electric currents from passing through it and lies in the range of $10^{16} \Omega\text{m}$ for epoxies in high voltage applications. Its inverse value, the specific conductivity, thus ranges around 10^{-16}S/m . For some particular applications like field grading systems, higher values of the specific conductivity or non-linear conductivity behaviors might be required.

Additionally, the dielectric breakdown strength (in kV/mm) is another important aspect of insulating materials. It describes the maximum electric field strength a material can withstand without having an intrinsic breakdown (BD) and therefore losing its ability to prevent an electric current from flowing. The BD strength of dielectrics strongly depends on the thickness of the material and generally decreases with increasing thickness. In literature, this dependency is described by an empiric inverse power law (Chen et al., 2012):

$$E_{BD}(d) = kd^{-n} \quad (1.2)$$

with E_{BD} , the electric field strength applied at breakdown, as a function of the thickness d and the empiric materials constants k and n .

Another parameter which is very important in describing dielectric material is the complex permittivity ε^* which will be treated in more detail in chapter 2.3. Besides those already mentioned parameters, the resistance to erosion due to partial discharge and the resistance of materials to electrical treeing represent two additional crucial features of dielectrics.

1.1.3 Mechanical properties

Depending on the application, mechanical properties like the mechanical strength of dielectric material can be of importance as well. In case of epoxy, winding insulations of electric machines would be a prominent example of an application where high mechanical stresses act on the insulation system during operation and especially during transient states.

Based on the application for which the dielectric material is used, it is always of importance to find an adequate balance between rigidity and flexibility of the insulation system, according to possible stresses during operational states.

1.1.4 Chemical properties

Further important properties for dielectrics are their resistance to environmental (ambient) aspects, like UV radiation or air pollution for outdoor insulators, as well as hydrophobicity. In some applications the chemical resistance to degradation due to reactants caused by partial discharge (PD), for instance in gas insulated lines (GIL) filled with SF₆ gas, embodies one more point of interest for insulating materials (Küchler, 2009).

1.2 From micro to nano – or is it sub-micro really?

1.2.1 When is “nano” really nano?

Nanodielectrics are commonly defined as electrical insulation materials, with incorporated fillers of particle sizes in the range of some tens of nanometers, forming structures of less than 100 nm in one dimension. Composites showing dimensions above 100 nm up to 500 nm are specified as mesocomposites and those with internal structures exceeding 500 nm are considered microcomposites.

1.2.2 Introduction to nanocomposites

It is commonly agreed today that the key point for the improved or altered properties of nanocomposites (NC) lies within the particle-host interfaces (Fr chet te, 2009; Lewis, 2005; Nelson et Hu, 2005; Raetzke et Kindersberger, 2006; Roy et al., 2005), which become more and more prominent with decreasing filler sizes (see Figure 1.1). Those interfacial layers, or interaction zones are estimated to be of approximately 10 nm thickness around the particle surfaces, and possibly more if certain prerequisites are met (Lewis, 2004). Models like the ‘‘Multi-Core Model’’ of Tanaka et al. (Tanaka et al., 2005), the ‘‘Polymer Chain Alignment Model’’ of Andritsch et al. (Andritsch et al., 2011) or the ‘‘Overlap Model’’ of Preda et al. (Preda et al., 2014) try to predict the properties of NC or explain their structural composition, respectively.

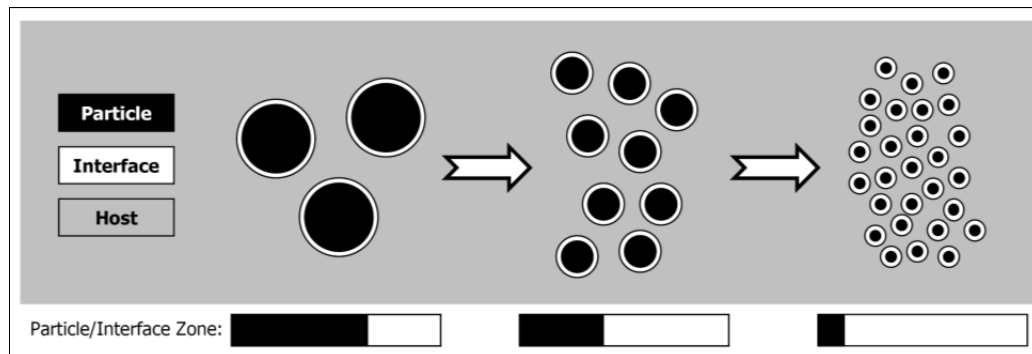


Figure 1.1 Illustration of increasing dominance of interfacial areas with decreasing filler sizes

Taken from Andritsch (2010, p. 3)

Often, such nanocomposites expose very distinct properties which cannot easily be explained and might derive from the characteristics of their meso- and microscopic pendants, respectively. The origins of those compartments are thought to be due to several factors (Nelson, 2010; Roy et al., 2005):

- the large surface area of nanoparticles;
- the surface of particles affecting the polymer morphology;

- a reduction in the internal field caused by the decrease in size of particles;
- change in space charge distribution;
- scattering mechanisms.

In addition many other aspects like filler size, aspect ratio, dispersion and distribution of introduced particles in the polymer matrix, may strongly affect the resulting composites' electric, dielectric, thermal as well as mechanical parameters.

The polymeric matrix in NC can be of diverse origin: rubbers, Polyethylene and epoxy resins, to name just a few important polymeric materials in electrical insulation engineering. This thesis focuses on epoxy based composites and their characteristics, although many of the following properties and models are generally applicable to polymeric NCs.

1.3 Theories and models for nanocomposites

Several models for describing the special dielectric characteristics of NC exist, all of them stressing the importance of the particle-matrix interface. But as there are still many unknowns to be understood, probably none of these following models can claim to fully explain all processes in NC.

1.3.1 Electric double layer

The electric double layer introduced by Lewis (Lewis, 2004) describes a coulombic interaction between a filler particle and the surrounding polymer matrix. It consists of two layers (see Figure 1.2) formed at the particle-host interface, the inner Stern layer where ions are bound to the particle surface and the outer layer, also called diffuse Gouy-Chapman layer, which represents a diffuse region where the charge decreases exponentially with the distance from the particle.

Any ions beyond the so called slipping plane are not affected by the charges surrounding the particle. The electric double layer forms a long distance dipole, with a slow time response,

which affects electrical conduction and dielectric properties in the low frequency domain. Regarding the triboelectric series, epoxy resins tend to get negatively charged (Andritsch, 2010; Nelson, 2010).

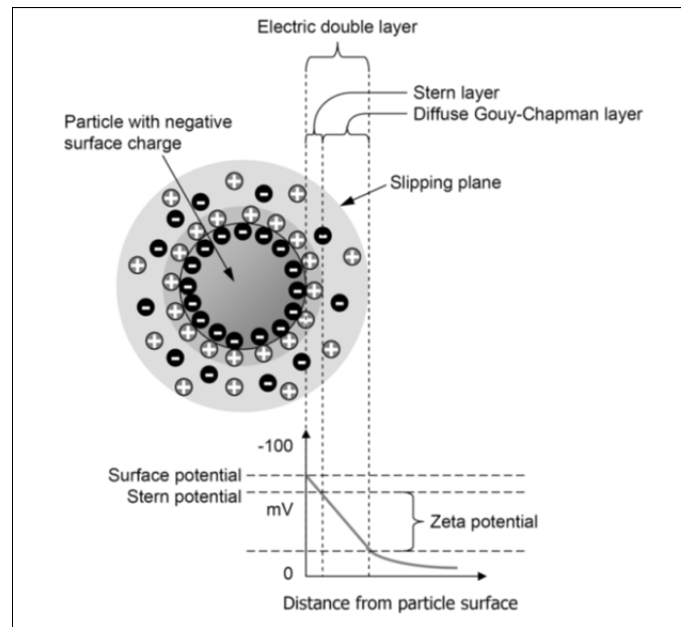


Figure 1.2 A schematic of the electrical double layer surrounding a particle
Taken from Andritsch (2010, p. 35)

1.3.2 Intensity model

Proposed by Lewis in 2005 (Lewis, 2005), the intensity model is built on the idea that a material property α embodied by its intensity I_α can only change gradually with the distance over an interfacial area between two different phases (see Figure 1.3), meaning there are no abrupt borders for those properties. The intensity I_α does not necessarily have to stay between the values for phases A and B, but can reach intensities exceeding or even deceeding both of those values, depending on the nature of the phases.

Atoms along with molecules located in this interfacial area interact with their surrounding media via short and long ranged forces. This model provides only a general view on the impact of nanoscale fillers on macroscopic composites.

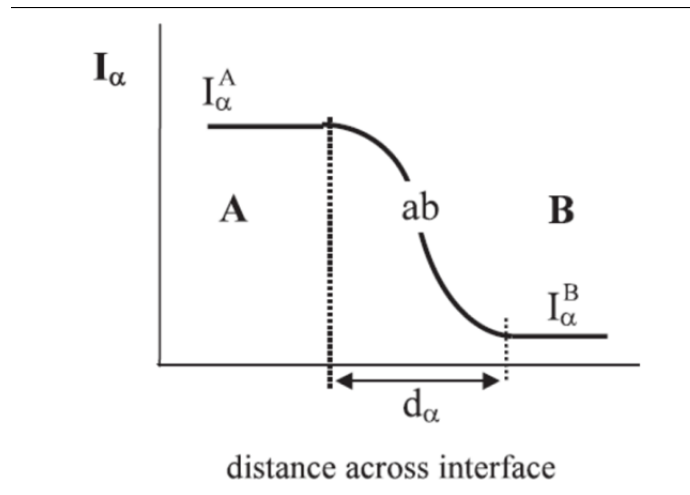


Figure 1.3 Change of intensities I_α defining phases A and B over the distance across the interface
Taken from Lewis (2005, p. 203)

1.3.3 Multi-core model

The multi-core model developed by Tanaka et. al (Tanaka et al., 2005) is a theoretical approach to explain the possible interactions of filler particle and matrix. It is based on a three layer geometry (see Figure 1.4), which are overlapped by a fourth, the electric double layer (as described in paragraph 1.3.1):

Bonded layer:

This is a transition layer physically bonded to the particle surface, approximately of 1 nm thickness. It is formed by ionic, covalent, hydrogen and Van-der-Waals bindings (with strength decreasing from first to last).

Bound layer:

Interfacial region between a layer of polymer chains strongly bound to the first layer, as well as the surface of the inorganic particle. A perpendicular alignment of surrounding polymer chains to the filler surface results in a rather structured morphology, and therefore affects the mobility of polymer chains in the proximity of filler particles. The thickness of this layer is assumed to measure between 2 and 9 nm.

Loose layer:

Measuring several tens of nm, this layer is supposed to be loosely coupled with the second layer, consisting of polymer chains with affected morphology due to the presence of the inorganic filler, leading to changes in chain formations and mobility, as well as free volume or crystallinity.

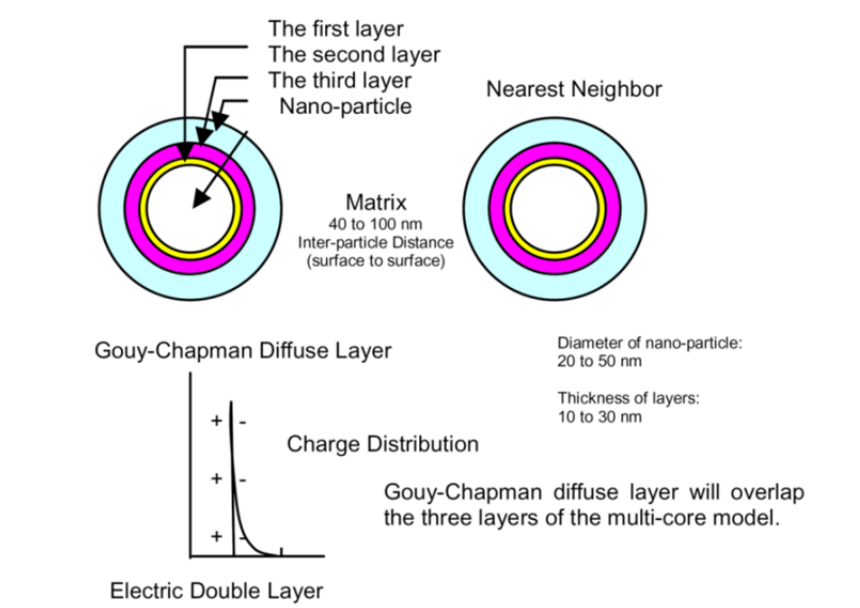


Figure 1.4 Illustration of the multi-core model for polymeric NC
Taken from Tanaka et al. (2005, p. 674)

1.3.4 Water shell model

The water shell model (Figure 1.5) as proposed by Zou et al. (Zou, Fothergill et Rowe, 2008) considers water absorption in the interfacial areas between filler particles and polymer. It suggests that water is primarily existing in the second layer shown in the multi-core model (see chapter 1.3.3) providing conductive paths (see Figure 1.5b) compared to a polymer with “dry” filler particles (see Figure 1.5a). In the case of dry nanoparticles, and hence, without water shells, no conductive pathways will be formed through the bulk composite. Once enough water is adsorbed by hydrophilic nanoparticles (like silica) though, overlapping water shells will provide conductive pathways for charges, and thus, quasi DC behavior will result at low frequencies.

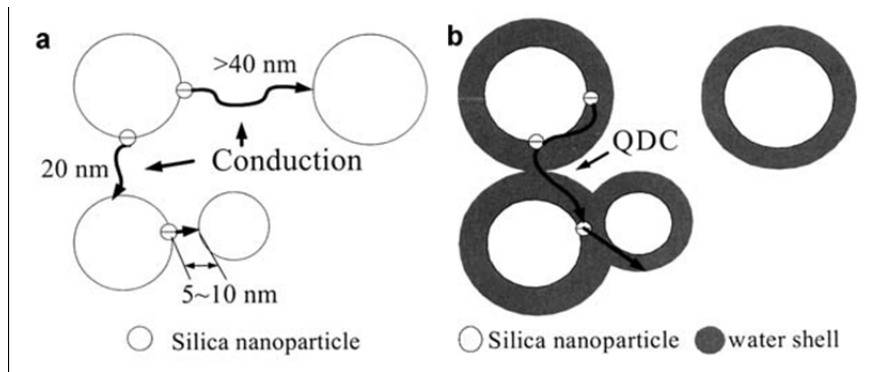


Figure 1.5 Water shell model with quasi DC (QDC) conduction
 (a) no overlapping water shells (b) overlapping water shells
 Adapted from Zou et al. (2008, p. 114)

1.4 Overview of the impact of nanoparticles on some electrical properties of NC

Using nanometric filler particles instead of micrometric particles was found to lead to significantly enhanced performances of the resulting composites, such as improved dielectric breakdown strengths for instance, already at very low contents. Considering that the incorporation of micrometric filler particles in polymer matrices usually causes a diminishment in dielectric strength, it is evident that nanodielectrics have a great potential for application in HV insulation systems.

When inorganic nanoparticles are incorporated in a polymer matrix, the electric field distortion in the bulk composite around these particles, which arises due to the mismatch in permittivity between the polymer and the inorganic filler, will be less pronounced, because of the smaller sizes of nanoparticles compared to their micrometric counterparts. Thus, leading to more homogeneous electric field stresses over the bulk composite compared to the case when micrometric particles are involved. This, however, only holds for well dispersed nanoparticles, as in the case of agglomerated clusters of nanoparticles this beneficial size effect will get lost. In the following paragraph a comprehensive review on specific improvements of dielectric properties is presented, which were achieved by incorporation of nanometric fillers in polymers like epoxy resin or polyethylene.

1.4.1 Impact on AC breakdown strength

In Figure 1.6, an illustration by David and Fr chet te (David et Fr chet te, 2013) is presented, which gives an overview of the relative improvements in AC breakdown (ACBD) strengths of NCs reported in literature. It summarizes the effects on ACBD strength of metallic oxides, such as silica and titanium dioxide, or POSS along with layered silicates, when such fillers were incorporated in a polymer matrix. It can be seen, that low contents of metallic oxides and layered silicates, below 5 wt%, have resulted in increased ACBD strengths of the respective NC by up to 20 % compared to the base polymers. Higher nanofiller loadings would usually show no additional improvement. This might be attributable to the formation of agglomerates of micrometric dimensions for such high loadings of nanoparticles, subsequently counteracting the beneficial effect found for low contents of nanoparticles.

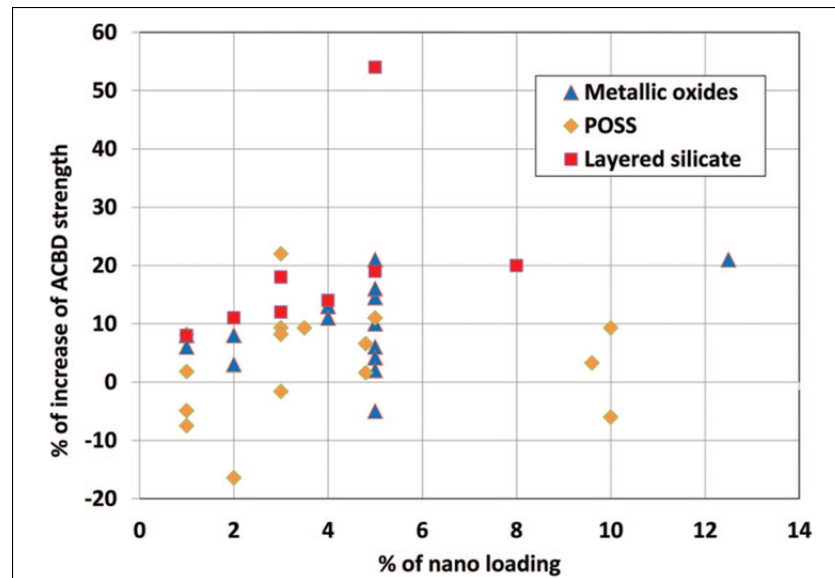


Figure 1.6 Relative impact on various nanofillers on the ACBD strength of polymer NCs compared to the base polymers
Taken from David and Fr chet te (2013, p. 31)

1.4.2 Impact on the resistance to corona discharges

The resistance to corona discharges or partial discharges in general is one of the key factors for a HV insulation material. Volumetric replacement of the organic polymer by inorganic

materials, such as micrometric silica for instance, was commonly applied in the past to render the composite more resilient to electrical discharges, as the inorganic particles act like a shield towards the electrical discharges, and thus, protect the organic matrix from degradation due to the highly energetic discharges. However, due to the micrometric size of these particles, often a decrease in BD strength would concur. Therefore, nanofillers have come to interest to improve polymer composites' resistance to electrical discharges, without causing a diminishment in dielectric breakdown strength at the same time, as it was discussed before.

It was shown by (Iyer, Gorur et Krivda, 2012) that the corona resistance for samples containing 5 wt% of nano-silica would result in erosion depths half as profound as measured for neat epoxy. In the same time, the composites with 5 wt% nano-silica performed slightly better than composites involving 65 wt% of micrometric silica particles. It was further pointed out, that a combination of 62.5 wt% micrometric and 2.5 wt% nanometric silica resulted in the best resistance to corona discharges, with erosion depths of less than $\frac{1}{4}$ compared to neat epoxy. A similar study by (Fr chet te et al., 2012) comparing nanocomposites with either 2.5 wt% of nano- or micrometric silica has shown a similar trend, where the silica NC had a better resistance to corona discharges than their micrometric pendants. A work by (Tanaka, Matsuo et Uchida, 2008) showed that nanometric SiC with contents up to 5 wt% have reduced the erosion depth of the respective epoxy composites by more than factor 7 in the case 5 wt% SiC were incorporated in the epoxy. Also in terms of POSS some notable improvements in erosion resistance were reported by (Huang et al., 2014), who achieved a by factor 2 enhanced resistance to corona by addition of 5 wt% POSS in epoxy.

1.5 Materials Review

1.5.1 Epoxy resins

Amongst the polymeric dielectrics, epoxy resins are a frequently used insulating material in various types of high voltage applications, due to their excellent mechanical, electrical and

chemical properties, as well as their advantageous processing opportunities. Epoxy resins allow a variety of different production processes such as casting, injection molding or laminating methods, which enables their use as insulating materials for numerous applications, such as spacers, cable terminations, bushings and machine insulation.

Epoxies, which belong to the group of thermosetting polymers, are commonly produced from two constituents: the epoxy resin which, for the use in electrical insulation materials, is often a diglycidyl ether of bisphenol A (DGEBA) (see Figure 1.7) combined with a curing agent, although in some cases the addition of catalysts can be necessary. During the cross-linking process, the curing agent opens the epoxide “rings” and initiates the connection between several epoxy monomers to form polymer chains.

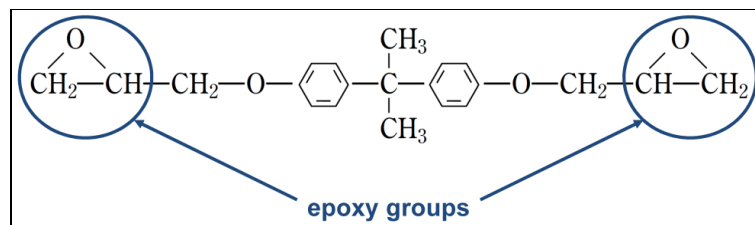


Figure 1.7 Simple molecule of diglycidyl ether of bisphenol A with two epoxide groups

The chosen epoxy system for this research project consists of two components, the DER332 epoxy resin (bisphenol A type) which is mixed in a ratio of 1000:344 parts with the second component, a Jeffamine D230 curing agent (commonly called “hardener”). This epoxy system is known for its good electrical insulation properties and further allows relatively long processing times at room temperature (Fr chet te et al., 2012; Reading et al., 2011a).

1.5.1.1 Chemical considerations and its effects on physical properties of epoxy resins

The stoichiometric ratio *phr* (parts by weight of curing agent per 100 parts of epoxy resin mixture) for the neat epoxy samples, with its constituents the DER332 epoxy resin, with its two oxirane groups, and the Jeffamine D230 curing agent, with its di-amine structure, were based on the average epoxy equivalent weight for the epoxy (EEW) and the amine hydrogen

equivalent weight (AHEW) of the Jeffamine D230, both provided by the manufacturers (DOW Chemicals and Huntsman Corp., respectively). The calculation follows to

$$phr = \frac{AHEW}{EEW} \cdot 100 \quad (1.3)$$

$$phr = \frac{60}{174} \cdot 100 = 34.48 \quad (1.4)$$

The optimal ratio of resin and curing agent is crucial to produce an epoxy composite with good dielectric properties and the optimal cross-linking degree. It was found that excess epoxy can increase the amount of free molecules or epoxide chains and therefore the free volume (Calventus, Montserrat et Hutchinson, 2001), which is leading to increased permittivity and lower breakdown (BD) strengths along with lower values in glass transition temperature (T_g) (Nguyen et al., 2011). Additionally, it has been reported that a surplus in epoxy had worse effects on T_g than a surplus in hardener (Calventus, Montserrat et Hutchinson, 2001; Park et Lee, 1998). Whereas in terms of dielectric breakdown performance, an excess of hardener has shown to cause heterogeneous areas with comparably lower densities, leading to more significant decrease in BD strength, compared to a surplus of epoxy (Nguyen et al., 2011).

Considering that the BD strength is a very crucial parameter of high voltage insulation systems, the calculated stoichiometric ratio in equation (1.4) was hence rounded down to a $phr = 34.4$ (equal to a ratio of 1000:344) to avoid excess of the anhydride hardener. The incorporation of filler particles can, however, further influence the molecular mobility of the epoxy resin molecules during the curing reaction. Thus the optimal stoichiometric ratio of epoxy and curing agent, with respect to achieving the best possible dielectric properties of the resulting composites, may vary as a function of filler size and loading, as was recently shown in (Nguyen et al., 2015).

1.5.1.2 Basic epoxy composite fabrication process

The epoxy based sample fabrication consists of several steps which are illustrated in Figure 1.8. After introducing the filler particles in the epoxy resin, the mixture is sonicated to attain a uniform distribution of particles in the matrix. In the second step, the curing agent as well as the particle-containing epoxy are degased, while they are still separated in different beakers. Afterwards the hardener is mixed with epoxy resin for an appropriate time to reach a good distribution of the curing agent. Following another degasing procedure the liquid composite is finally cast into a mould and cured.

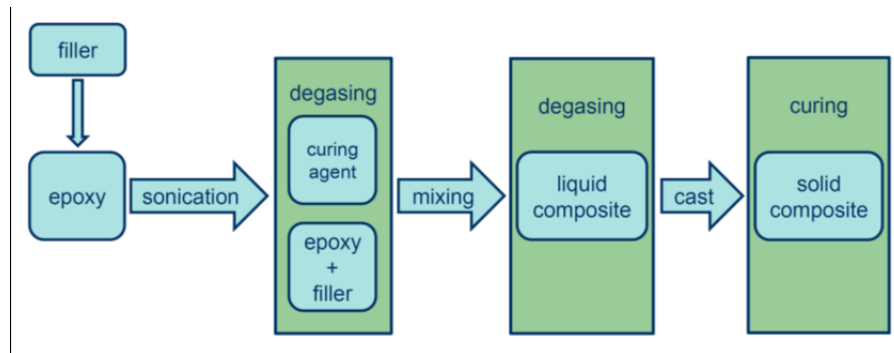


Figure 1.8 Basic processing schematic for epoxy based composites

Degasing and sonication of the composites are the vital points in this procedure. Sonication has been found to be a very effective method to achieve good dispersion of the filler particles in the epoxy (Reading et al., 2011b). Further it has been postulated, that sonication could improve epoxy based composites' mechanical properties due to enhanced cross-linking processes (Chisholm et al., 2005). Degasing the composites before mixing and curing respectively, is crucial to remove introduced air inclusions along with prospective humidity to achieve homogeneous and void free samples after curing. Consequently, the fabrication process has been improved during this thesis to an extent, that vacuum could also be applied during the mixing processes (see Chapters 3 to 6).

1.5.2 Boron nitride

Boron nitride (BN) is a very promising material for dielectric composites due to its high thermal conductivity, excellent mechanical features as well for its electrical insulating properties (Haubner et al., 2002; Pakdel et al., 2012). In addition, its chemical inertness (Pakdel et al., 2012) could be of benefit for surface degradation processes of electrical insulation systems. The different crystal structures of boron nitride are represented in Figure 1.9.

Recent studies have shown an improved thermal conductivity of composites after incorporating BN in an epoxy matrix with increasing filler amount (Kochetov et al., 2009a; Kochetov et al., 2010) and decreasing filler sizes (Reading, Vaughan et Lewin, 2011). It has also been discovered that, besides filler size, the aspect ratio of the filler plays an important role in thermal conductivity, where BN-platelets showed superior properties over spherical particles (Kochetov et al., 2010; Zengbin et al., 2011b). Further on, dielectric BD strength could be improved by lowering the filler sizes (Andritsch et al., 2010; Reading, Vaughan et Lewin, 2011), along with the resistance to surface erosion due to PD (Zengbin et al., 2011a).

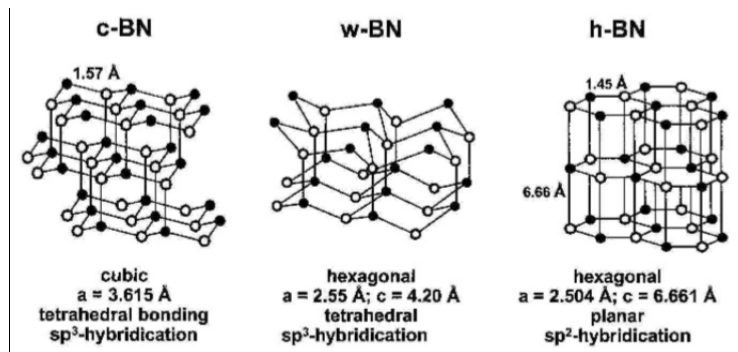


Figure 1.9 Different crystal structures of boron nitride
Taken from Haubner et al. (2002, p. 6)

1.5.3 Polyhedral oligomeric silsesquioxanes (POSS)

POSS is a hybrid material, consisting of an inorganic silica-like core surrounded by organic side-groups (Figure 1.10a). These organic groups can be of either reactive or non-reactive nature and therefore offer compatibility with a multitude of polymers, depending on the respective organic side group configuration. POSS, being a hybrid inorganic-organic material, further combines the beneficial material properties of ceramics, like inertness and electrical insulating properties, with the processability of polymers. It has been denoted as a “Nano-building-block” in the past, because of its crystalline structure (Bocek et al., 2011; Chen, 2012), which enables POSS to organize a polymeric matrix through its reactive groups on a nanometric scale (compare Figure 1.10b and Figure 1.10c). These features have shown to result in improved thermo-mechanical properties, like increased T_g values, due to reduced molecular chain mobility (Bocek et al., 2011; Kuo et Chang, 2011; Strachota et al., 2007).

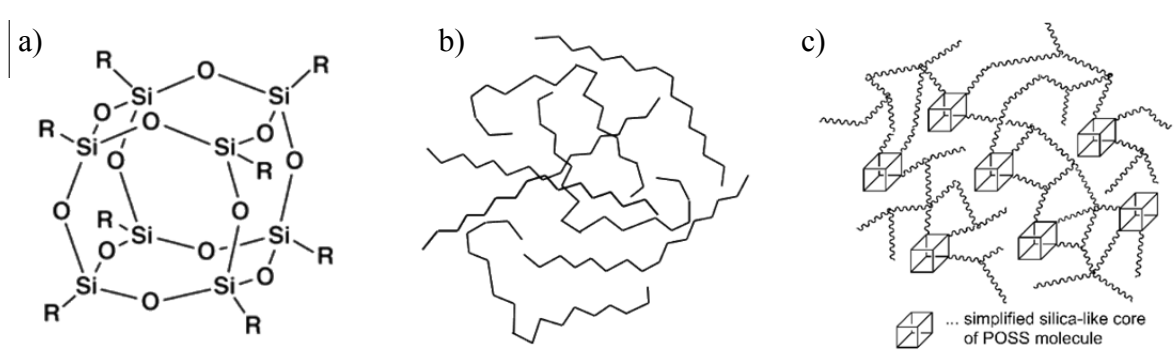


Figure 1.10 (a) shows a typical POSS molecule with the inorganic silica-like core and the organic side-groups “R” which are depending on the respective POSS-type; (b) and (c) show the proposed interaction with POSS and the epoxy matrix, rendering the amorphous epoxy resin (b) into a structured composite on a nanometric scale (c)

POSS molecules, commonly with sizes below 2 nm, are assumed to be able to dissolve within a polymer without forming agglomerations known from conventional nano-particles (Kuo et Chang, 2011). Epoxy/POSS composites have not been much explored yet in terms of their dielectric properties, but due to the nature and chemistry of POSS along with some preliminary studies on other polymer based materials, epoxy/POSS composites could be promising dielectrics for high voltage applications.

Besides the advantages on thermo-mechanical aspects, recently some dielectric properties of epoxy/POSS composites have been analyzed. It has been shown that low contents of solid crystalline POSS, in the range of 1 - 10 wt%, could improve the resistivity of the composite along with achieving comparably low dielectric losses, especially at elevated temperatures (Bocek et al., 2011) , which could be interesting for high voltage applications. In this study it was also reported that for high filler grades of POSS an increased thermal conductivity could be found.

Further, different types of liquid POSS have shown to affect an epoxy matrix in dielectric terms (Takala et al., 2008). Introducing Octaglycidyl dimethylsilyl POSS by 1 wt% in a bisphenol A based epoxy resulted in composites with low permittivity, improved BD strength and low dielectric losses. Using another type, to be specific a glycidyl POSS, in 3 – 4 wt% could as well increase the BD strength of the composite materials, along with low dielectric losses and high resistivity values. The authors stated that the POSS molecules possibly serve as some sort of nanocapacitors in the polymer, scavenging charges and therefore decreasing the electrical volume conductivity. In addition, POSS has shown to improve other dielectric properties like the resistance to surface discharge for different base polymers, such as XLPE (Takala et al., 2008).

CHAPTER 2

PHYSICAL PROPERTIES OF POLYMER DIELECTRICS

2.1 Electrostatics of dielectrics

When a voltage U is applied between two plates of a condenser, with plate surfaces A , in vacuum (see Figure 2.1a), an electric field E equal to the ratio of applied voltage and the distance d between the two condenser plates occurs. The accumulated charges on the condenser's plates $\pm Q$ will then be

$$Q_0 = \varepsilon_0 EA \quad (2.1)$$

where ε_0 is the vacuum permittivity. If a real dielectric is placed between the condenser plates instead of a vacuum, the dipoles within the dielectric will re-orientate parallel to the electric field lines, with the charges now facing the opposite polarity, leading to the polarization of the dielectric medium (Figure 2.1b).

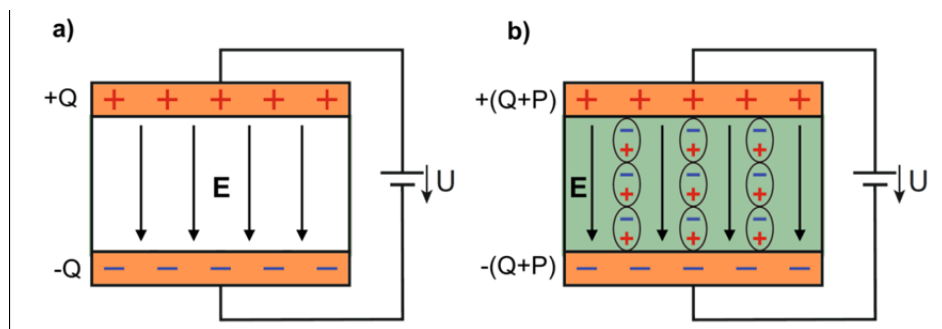


Figure 2.1 Polarization charges on a parallel plate condenser; a) with vacuum and b) with a dielectric medium between the plates

Accordingly, due to the additional charges Q_P caused by the polarization, the sum of charges will increase depending on the relative dielectric permittivity ε_r , also called the dielectric constant of the medium, resulting in (Osswald et Menges, 2012):

$$Q = \varepsilon_r Q_0 = Q_0 + Q_P . \quad (2.2)$$

In the case of small electric field strengths E , the dielectric displacement D caused by the charges can be written as

$$D_0 = \varepsilon_0 E \quad (2.3)$$

in the case of vacuum, and as

$$D = \varepsilon_0 \varepsilon_r E \quad (2.4)$$

for a dielectric medium. Hence, the polarization P , which describes the dielectric displacement arising from charges in a dielectric medium as a result of an applied external electric field, can be defined as

$$P = D - D_0 = (\varepsilon_r - 1)\varepsilon_0 E = \chi \varepsilon_0 E \quad (2.5)$$

with the dielectric susceptibility χ of the medium in an electric field, where

$$\chi = \varepsilon_r - 1 . \quad (2.6)$$

2.2 Polarization mechanisms in dielectrics

There are several polarization mechanisms that can occur in matter (Blythe et Bloor, 2005; Jonscher, 1983; Raju, 2003):

- electronic or optical polarization;
- atomic or ionic polarization;
- orientational polarization;
- and interfacial polarization.

The first three mechanisms should be considered as molecular or microscopic polarizations (schematically represented in Figure 2.2) due to displacement of bound charges, and the latter as a macroscopic mechanism that can occur on boundaries of the dielectric as well as at imperfections inside the dielectric (Raju, 2003). In epoxy based dielectrics this can often be observed in their dielectric response at elevated temperatures (close to or above the glass transition temperatures) and at low frequencies, and is thus also known as *low frequency dispersion* (Jonscher, 1983), which will be discussed in more depth in the chapters dealing with dielectric spectroscopy results.

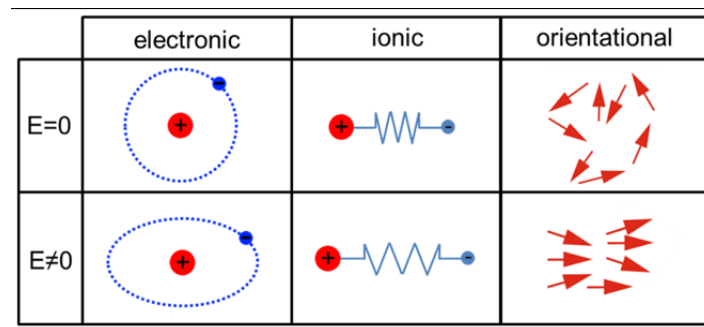


Figure 2.2 Polarization mechanisms in dielectrics

2.2.1 Electronic or optical polarization

When matter is exposed to an external applied electric field, a displacement of the electrons surrounding the positively charged nucleus of the affected atoms occurs. The displacement is relatively small, as the forces due to the electric field are much lower than intra-atomic forces. Electronic polarization appears at very high frequencies, also in the spectrum of visible light, and causes the refraction of light (Blythe et Bloor, 2005). Hence, it's often referred to as optical polarization.

2.2.2 Atomic or ionic polarization

Exposed to an applied electric field, atomic nuclei in a molecule can be displaced relative to each other. Permanent dipoles or polar bonds of molecules, which are often found in polymeric dielectrics, are affected by this displacement. Atomic polarization occurs for all

molecules, but is more distinct in molecules with weaker bonds (Raju, 2003). The displacement due to atomic polarization is superimposed with the one caused by electronic polarization, but as heavier nuclei are affected, it does not occur for frequencies above infrared (Blythe et Bloor, 2005).

2.2.3 Dipolar or orientational polarization

All the above mentioned polarization mechanisms occur at rather high frequencies of the electric field, as we will see in more detail in paragraph 2.3.2 (also see Figure 2.4), and are thus not of major interest for dielectrics in high voltage engineering. If dielectric materials now have molecules with permanent dipoles, which is the case for polar materials like epoxy resins, these dipoles will align under the influence of an electric field, and hence cause a polarization in the respective direction, which is called orientational polarization (Blythe et Bloor, 2005). This effect occurs at medium frequencies and represents the physical basis for the analysis of the frequency dependent dielectric response of insulating materials by the means of dielectric spectroscopy. In epoxy based dielectrics, changes in chain mobility due to reticulation states or after incorporation of filler particles for instance, will lead to differences in orientational polarization.

2.3 Dielectric relaxation in polymers

Profound reviews of dielectric relaxation theory and the complex permittivity can be found in (Blythe et Bloor, 2005; Jonscher, 1983; 1996; Kremer, 2003; Raju, 2003). In the framework of this thesis, a concise summary will be presented on these topics. The process of dielectric relaxation is of deep interest in insulation engineering and can be studied by dielectric spectroscopy, in order to understand and reduce losses, which will occur in dielectrics during operation due to polarization mechanisms. Additionally, the dielectric constant and the loss tangent can be derived, which are important parameters in electrical insulation engineering.

2.3.1 Complex relative permittivity and the dielectric losses

When a dielectric is placed between two parallel electrodes, forming a condenser with complex impedance Z^* (Figure 2.3 on the left) on which an alternating voltage U is applied, Ohm's law follows to

$$Z^* = \frac{1}{j\omega C^*} = \frac{U}{I^*}. \quad (2.7)$$

In an ideal condenser, the resulting current I^* through the medium would be shifted in an angle of 90° to the applied voltage. However, in a real dielectric, the current will lead the voltage by an angle φ

$$\varphi = 90^\circ - \delta \quad (2.8)$$

where δ is the *loss angle* attributed to the dielectric medium (see Figure 2.3 on the right). When we rewrite equation (2.7) as

$$I^* = j\omega C^* U \quad (2.9)$$

and further consider that the complex relative permittivity is given by

$$\varepsilon_r^* = \varepsilon_r' - j\varepsilon_r'' \quad (2.10)$$

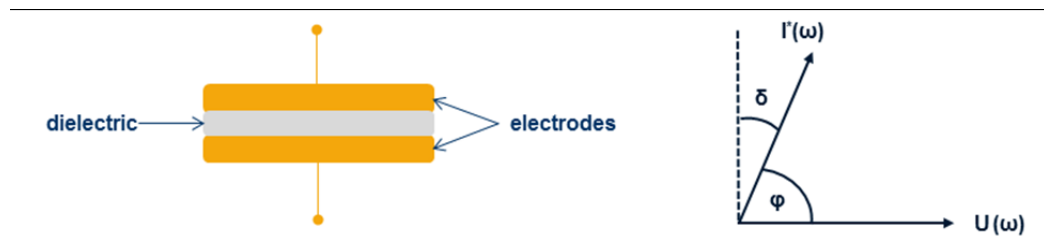


Figure 2.3 Dielectric between two electrodes forming a condenser (left) and the phase diagram of a complex current through the dielectric due to an applied AC voltage (right)

where ε_r' and ε_r'' are the real and the imaginary part of the complex relative permittivity, respectively, and that the complex capacity C^* can be expressed as

$$C^* = \varepsilon_r^* C_0 \quad (2.11)$$

equation (2.9) then follows to

$$I^* = j\omega\varepsilon_r^* C_0 U = \omega C_0 (j\varepsilon_r' + \varepsilon_r'') U. \quad (2.12)$$

Accordingly, the complex current through the dielectric can be divided into a real part, caused by a resistive component, which is responsible for the dielectric losses of the medium

$$I_{real} = \omega C_0 \varepsilon_r'' U \quad (2.13)$$

and an imaginary part, which is purely capacitive

$$I_{imag} = j\omega C_0 \varepsilon_r' U. \quad (2.14)$$

It should be noted at this point that the imaginary part of the complex permittivity ε_r'' obtained by measurements is composed by two parts: The contribution from the relaxation phenomena derived by the Fourier transform of the polarization and the contribution of the conductivity σ of the dielectric. It can thus be expressed by

$$\varepsilon_r'' = \varepsilon_{relaxation}'' + \frac{\sigma}{\varepsilon_0 \omega}. \quad (2.15)$$

These relations show why the real part ε_r' of the complex permittivity is often associated with the energy storage capacity of a dielectric, whereas the imaginary part ε_r'' is commonly referred to as the dielectric losses of a medium. The ratio between imaginary and real part of the complex relative permittivity (or simply complex permittivity)

$$\tan\delta = \frac{\varepsilon_r''}{\varepsilon_r'} \quad (2.16)$$

is the so called *loss tangent* or *dissipation factor*, another important parameter often used in high voltage engineering. The smaller the loss angle δ , and thus the lower the loss tangent, the better the insulating properties of the dielectric. Designing dielectrics with low loss tangents is hence one important motivation for applications in energy generation, transmission and distribution, to render the complete process more efficient.

2.3.2 Complex permittivity vs. polarization mechanisms in NC

The introduction of filler materials in epoxy resin will result in changes of the dielectric properties of the bulk material. Whereas for micrometric filler some mixture rules exist to predict e.g. the relative permittivity of composites, they seem not to be applicable on nanometric filler materials, as the interface gets more and more dominant. Therefore NC often showed deriving values from predicted ones, repeatedly lower permittivities.

Speaking of permittivity, we usually mean the complex relative permittivity ε_r^* (see equation (2.10)) given by its real part ε' , a measure for the energy storage capacity of a dielectric, and the imaginary part ε'' , which is representing the losses due to the polarization mechanisms. The permittivity is depending on frequency and temperature and further provides information about material changes due to filler introduction or e.g. ageing processes. An overview of the above mentioned frequency-dependent polarization mechanisms is presented in Figure 2.4.

The polarization spectrum is the result of superimposed polarization mechanisms at different frequencies, as shown in chapter 2.2. Starting at very high (optical) frequencies where even electrons can't follow the changing electric field and therefore no polarization occurs, both ε' and ε'' begin increasing towards lower frequencies. For rapid changes in ε' very distinct loss peaks for ε'' can be found.

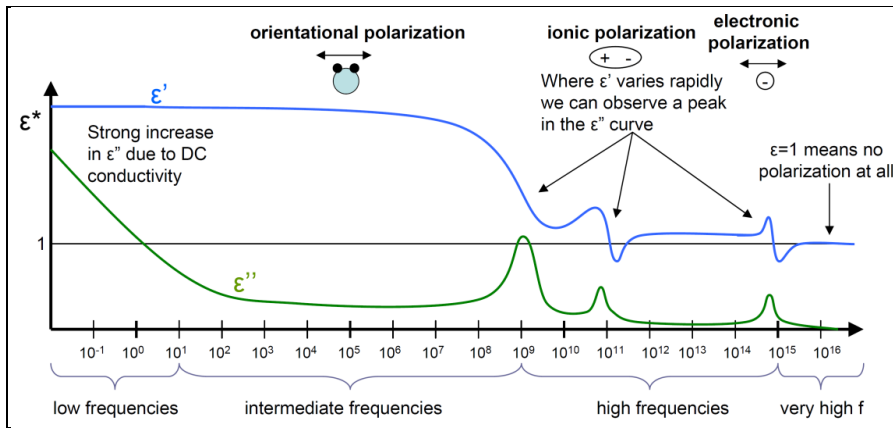


Figure 2.4 Frequency dependent polarization mechanisms
Taken from Andritsch (2010, p. 147)

Decreasing to high frequencies (in UV and IR range) electronic and ionic polarization occur (see chapters 2.2.1 and 2.2.2). Anyway, those frequencies are still too high for power applications making them not the primary interesting mechanisms for dielectric spectroscopy of insulating materials. For intermediate frequencies, the orientation polarization becomes governing, which enables us to see changes in chain mobilities due to reticulation processes or introduction of filler particles for instance (Dakin, 2006). Finally for low frequencies, two more mechanisms influence the dielectric response of an insulating material, the interfacial polarization between two phases in a composite, also called *Maxwell-Wagner-Sillars polarization*, and the *DC conductivity* σ_{DC} eventually causing increasing losses with lower frequencies, as we will see in chapter 2.3.4 (see Figure 2.5).

2.3.3 Dielectric relaxation theory and models

After a dielectric material is poled under a static electric field for a long time and the poling field is suddenly removed, the following decrease of polarization of the material will not occur without a certain, finite time delay. The oriented dipoles due the electric field will require time to rearrange from their aligned state into random, electrically stable positions. In the same way, dipoles will not react to an applied polarizing field instantaneously, but align with a certain time delay till the polarization reaches a maximum (Raju, 2003). This is called *dielectric relaxation* or *dielectric retardation*. The time needed for the orientation of dipoles

is dependent on molecular mobilities, and hence, on factors such as size of dipoles and the rigidity of the polymer matrix, which will be elaborated more in later chapters.

Dielectric relaxation processes are often analyzed as a function of applied voltage over a wide range of frequencies, as well as varying temperatures. The measurement principles are based on the physical relations presented before in chapter 2.3.1. In order to interpret the dielectric response of a medium, several theoretical models have been proposed to describe the complex permittivity. The most basic one was established by *Debye* (Kremer, 2003), which is limited to rather narrow and symmetric relaxation peaks though:

$$\varepsilon^* = \frac{D^*(\omega)}{\varepsilon_0 E^*(\omega)} = \varepsilon_\infty + \frac{\varepsilon_s - \varepsilon_\infty}{1 + j\omega\tau_D}. \quad (2.17)$$

In equation (2.17), ε_∞ is the high frequency value of the real part of the relative permittivity, ε_s the low frequency value or static permittivity, ω the angular frequency ($\omega=2\pi f$) and τ_D the Debye relaxation time. The Debye relaxation time is dependent on the frequency where the maximum loss, and hence, a relaxation peak occurs. Thus $\tau_D = 1/\omega_{peak}$ (Kremer, 2003). The real and complex parts of the relative permittivity can further be expressed by

$$\varepsilon'(\omega) = \varepsilon_\infty + \frac{\varepsilon_s - \varepsilon_\infty}{1 + \omega^2\tau^2} \quad (2.18)$$

$$\varepsilon''(\omega) = \frac{\varepsilon_s - \varepsilon_\infty}{1 + \omega^2\tau^2} \omega\tau. \quad (2.19)$$

The difference between the static and high frequency permittivity is further called the dielectric strength $\Delta\varepsilon$ (Blythe et Bloor, 2005):

$$\Delta\varepsilon = (\varepsilon_s - \varepsilon_\infty) = \int_{-\infty}^{+\infty} \varepsilon''(\omega) d(\ln\omega). \quad (2.20)$$

In polymeric dielectrics the relaxation behavior commonly derives from the ideal, or Debye behavior, leading to broader and/or asymmetric peaks in the permittivity spectra. *Cole and Cole* proposed a modified Debye model accounting for broader peaks for non-ideal or non-Debye relaxations (Kremer, 2003)

$$\varepsilon^* = \varepsilon_\infty + \frac{\Delta\varepsilon}{1 + (j\omega\tau_{CC})^\alpha} \quad (2.21)$$

with a shape factor $0 < \alpha \leq 1$. If $\alpha = 1$ a symmetrical peak follows and the formula simplifies to the Debye equation (2.17). The relaxation time τ_{CC} relates to the frequency of the loss peak $\tau_{CC} = 1/\omega_{peak}$. The Cole-Cole formula (2.21) was later extended by *Cole and Davidson* to account for asymmetric peaks, leading to

$$\varepsilon^* = \varepsilon_\infty + \frac{\Delta\varepsilon}{(1 + j\omega\tau_{CD})^\beta} \quad (2.22)$$

with the shape factor $0 < \beta \leq 1$. For $\beta = 1$ the Debye relation is retrieved again. Due to the asymmetric nature of the relaxation process the relaxation time τ_{CD} does not coincide with the position of maximum loss in the frequency spectrum, but the following relation holds (Kremer, 2003)

$$\omega_{peak} = \frac{1}{\tau_{CD}} \tan\left(\frac{\pi}{2\beta + 2}\right). \quad (2.23)$$

Havriliak and Negami later proposed a combination of the Cole-Cole and Cole-Davidson models, which can describe both asymmetric and broader peaks (Kremer, 2003) and is known to be valid for polymers as well as inorganic materials:

$$\varepsilon^*(\omega) = \varepsilon_\infty + \frac{\Delta\varepsilon}{(1 + (j\omega\tau_{HN})^{\alpha_{HN}})^{\beta_{HN}}}. \quad (2.24)$$

In equation (2.24), again ε_∞ is the high frequency permittivity, $\Delta\varepsilon$ the dielectric relaxation strength, ω the angular frequency ($\omega=2\pi f$), τ_{HN} the relaxation time, α_{HN} and β_{HN} (with $0 < \alpha_{HN} \leq 1$ and $0 < \alpha_{HN}\beta_{HN} \leq 0$) the Havriliak-Negami parameters which designate the symmetric and asymmetric broadening of the relaxation time distribution function, respectively (Kremer, 2003). When α_{HN} and β_{HN} are equal to 1, equation (2.24) is simplified, and the relaxation law proposed by Debye (equation (2.17)) is obtained. The Havriliak-Negami function can be split in real and imaginary part, which read (Kremer, 2003)

$$\varepsilon'(\omega) = \varepsilon_\infty + \Delta\varepsilon \left[1 + 2(\omega\tau_{HN})^\alpha \cos\left(\frac{\alpha\pi}{2}\right) + (\omega\tau_{HN})^{2\alpha} \right]^{-\beta/2} \cos[\beta\Psi(\omega)] \quad (2.25)$$

$$\varepsilon''(\omega) = \Delta\varepsilon \left[1 + 2(\omega\tau_{HN})^\alpha \cos\left(\frac{\alpha\pi}{2}\right) + (\omega\tau_{HN})^{2\alpha} \right]^{-\beta/2} \sin[\beta\Psi(\omega)] \quad (2.26)$$

with

$$\Psi(\omega) = \arctan \left[\frac{\sin\left(\frac{\alpha\pi}{2}\right)}{(\omega\tau_{HN})^{-\alpha_{HN}} + \cos\left(\frac{\alpha\pi}{2}\right)} \right]. \quad (2.27)$$

The Havriliak-Negami equation is frequently used to treat data, or to “fit” dielectric responses of polymer composites, to further understand the effect of incorporating filler particles in a polymeric matrix on the respective polarization mechanisms or molecular mobilities of the polymeric chains, i.e. (Couderc et al., 2013; Preda et al., 2013), and will thus be discussed in more detail in Chapters 4 and 5.

2.3.4 Dielectric relaxation processes in polymers

In solid polymers, we can differentiate between several discrete relaxation processes that occur depending on the frequency of the polarizing field and the applied temperature. An overview of the most prominent relaxation phenomena and their respective contribution to the dielectric losses (ε''), observable by dielectric spectroscopy, is presented in Figure 2.5. At very low temperatures - in epoxies this can be as low as -100 °C to -50 °C - the *γ-relaxation*

can be observed. It is a secondary relaxation mechanism due to movement of small polar groups, which are rather mobile and can thus be excited at low temperatures and also higher frequencies. In epoxy resins, this relaxation is characteristic for unreacted epoxy groups (oxirane groups).

When we go to slightly higher temperatures, another secondary relaxation phenomenon - the β -relaxation - can be observed in epoxies. It is associated with secondary relaxation processes due to local crankshaft movements of the hydroxyl ether groups in the case of epoxy resin, and it can appear for a wide range of frequencies and temperatures, e.g. $-80\text{ }^{\circ}\text{C}$ to $+50\text{ }^{\circ}\text{C}$, as in the case of the epoxy system used during this thesis (see Figure 2.6).

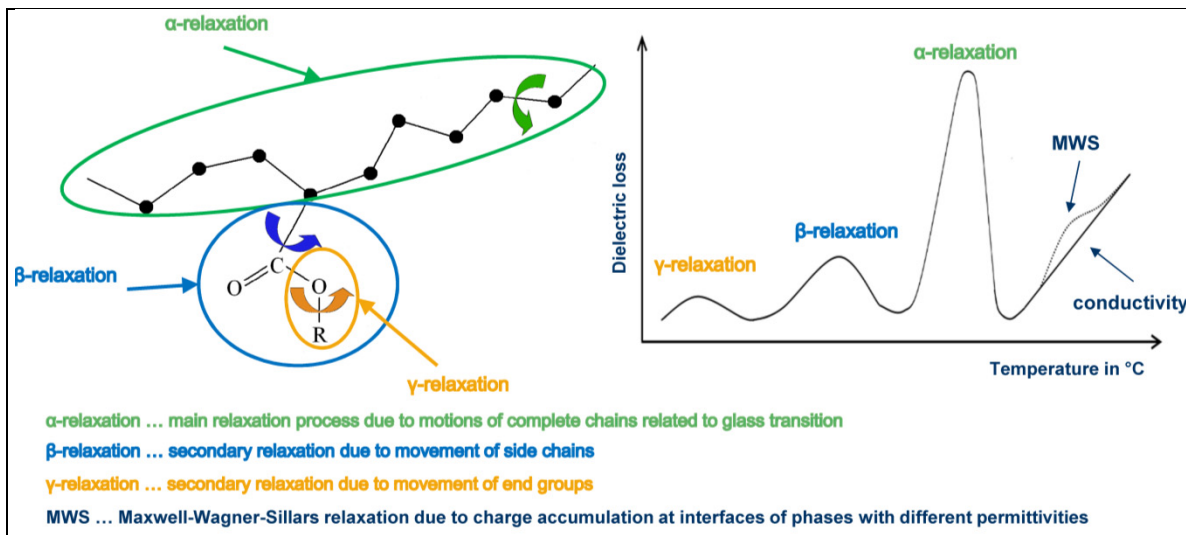


Figure 2.5 Schematic of dielectric relaxation processes observable in polymers (left) and their temperature dependence (right)

In amorphous polymers, the α -relaxation is correlated to relaxation processes of the main polymer backbone due to micro-Brownian chain movement as a result of the glass transition phenomenon (Blythe et Bloor, 2005), and thus occurs at higher temperatures around T_g of the polymer. At such elevated temperatures, the volume of the polymer composite increases, which will then lead to an increased mobility of the long polymer backbone, as a result of a reduction in density of the polymer.

When the T_g is approached and most significantly for higher temperatures and low frequencies, an additional phenomenon can be observed, revealing itself by an increase in dielectric losses. This increase in ε'' is due to contribution from charge fluctuations, as given by (Jonscher, 1996)

$$\varepsilon^*(\omega) = B(j\omega)^{n-1} \quad (2.28)$$

where B represents the intensity of the conductivity phenomenon and n the frequency dependence ($0 < n < 1$), with the real and imaginary parts of the complex permittivity reading

$$\varepsilon'(\omega) = B \sin \left[\frac{n\pi}{2} \right] \omega^{n-1} \quad (2.29)$$

$$\varepsilon''(\omega) = B \cos \left[\frac{n\pi}{2} \right] \omega^{n-1} . \quad (2.30)$$

This increase in dielectric losses due to charge fluctuations is often also called *quasi DC conduction* or *low frequency dispersion* and is defined by its distinct slope close to -1 on the log-log scale. In the case of real DC conductivity, $n = 0$ for equations (2.28) to (2.30).

On a more practical aspect, during dielectric spectroscopy measurements at elevated temperatures, deviations from this slope are rather commonly seen for polymeric materials. This is caused by additional charges, possibly of ionic nature, which are getting trapped at the interface of sample and electrodes. This parasitic phenomenon is called *electrode polarization* (EP) and occurs at high temperatures and is most distinct at low frequencies (see Figure 2.6).

In polymer composites another relaxation phenomenon, the so-called *Maxwell-Wagner-Sillars relaxation* (MWS) might arise in the high temperature domain (Figure 2.5). This relaxation process is caused by charge accumulations at interfaces of entities with different complex permittivities (Kremer, 2003), and thus, it can occur at prominent interfaces

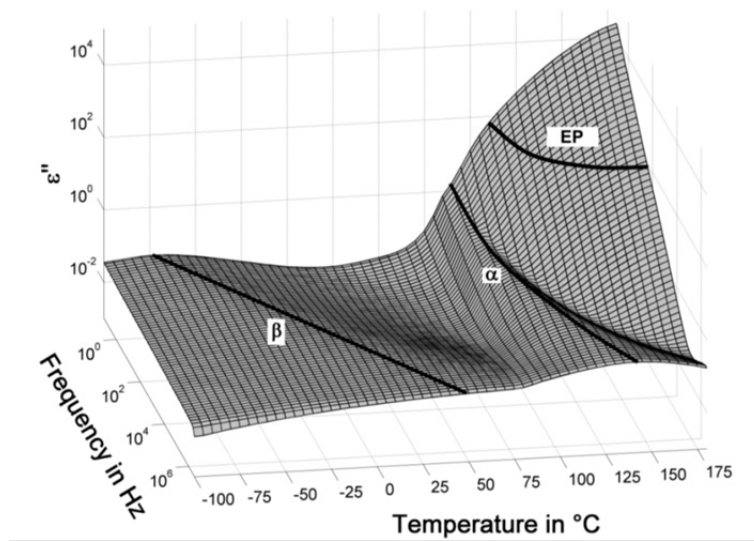


Figure 2.6 Relaxation map showing the dielectric losses (ϵ'') and the relaxation phenomena of neat epoxy as a function of frequency and temperature

between the polymeric matrix and incorporated filler particles. It has been reported in literature that this peak is closely related to the dispersion of nanometric filler particles in the case of NC, and will therefore disappear as a result of successful dispersion of nanoparticles in a polymer (Fr chet te et al., 2014).

2.4 Conduction mechanisms in polymers

Although electrical insulation is mainly used for its low conductivity values, this can embody a limiting factor for their usage at the same time, which makes it essential to understand the underlying effects and their extent. Comprehensive reviews on this topic can be found in literature (Blythe et Bloor, 2005; Dakin, 2006; Raju, 2003).

2.4.1 Electronic conduction

The electronic conduction in solids is basically determined by the atomic, crystal or amorphous structures. Very good electronic conductors are embodied by metals, as they have

free electrons on their outer shell, which can easily move and contribute to electric conduction.

The band theory describes this kind of conductivity: Usually an energy gap “separates” the valence band from the conduction band, so that electrons have to get shifted from the former to the latter band in order to contribute to electronic conduction. Therefore a certain amount of excitation energy (either of thermal nature or due to ionizing radiation) is necessary which is low for conductors (e.g. metals), as for metals both bands overlap, and relatively high for insulating materials. The electronic conductivity is proportional to the energy of the band gap E_{gap} as shown in equation (2.31), where $kT = 0.02518$ eV at 298 K (Dakin, 2006):

$$\sigma_e \propto \exp\left(\frac{E_{gap}}{k \cdot T}\right). \quad (2.31)$$

In epoxies, such electronic conductivity can be found at elevated temperatures, usually above the T_g of the epoxy system, and at low frequencies. This phenomenon is often referred to as *quasi DC conductivity*.

2.4.2 Ionic conduction

Ionic conduction mechanisms in amorphous dielectrics, e.g. epoxy resin composites, are similar to those present in solutions of electrolytes, whereby they may differ from each other in degree of intensity. The ionic conduction is based on impurities in the epoxy resin and depends on the mobilities μ_+ and μ_- , the concentrations n_+ and n_- as well as the number of unit charges z_+ and z_- on the positive and negative ions, respectively (Dakin, 2006). It can be described by

$$\sigma = (\Sigma \mu_+ n_+ z_+ + \Sigma \mu_- n_- z_-) \cdot e \quad \left[\frac{S}{m} \right] \quad (2.32)$$

with e being the electron charge in Coulomb. The velocity v of ions with a radius r moving in a resin with viscosity η due to an applied electric field E is given by

$$v = \frac{F}{6\pi\eta r} = \frac{zeE}{6\pi\eta r} \quad (2.33)$$

and the mobility μ of the ions is defined by the ratio of velocity to the force F :

$$\mu = \frac{v}{zeE} = \frac{1}{6\pi\eta r}. \quad (2.34)$$

Ionic conduction is further depending on temperature and it is increasing with rising temperatures due to the decreasing viscosity (inverse proportional) and the higher dissociation to ions. The underlying conduction mechanism in resins can be described as electron hopping between lattice sites, instead of diffusion flow in liquids (Dakin, 2006).

2.4.3 Thermal conduction

Thermal conduction or the transport of thermal energy in solid materials happens via electrons, phonons (atom vibrations) or photons. Whereas in dielectric materials phonon conductivity is predominant, in semi-conductive material both electrons and phonons can contribute to thermal conduction. In perfect crystals, phonons can propagate unhindered (via lattice vibrations) between different atoms throughout the material, but as real crystals have imperfections and deviations in atomic vibrations, phonon scattering can occur (Cui et al., 2011; Huang et al., 2012; Takezawa, Akatsuka et Farren, 2003).

In amorphous materials like epoxy resins, phonon scattering is the dominating process, which occurs at either particle-particle, particle-matrix (equally at defects or pores), as well as interfaces of the amorphous structure in epoxy resin itself (Takezawa, Akatsuka et Farren, 2003), as schematically depicted in Figure 2.7. Phonon scattering thus causes a diminishment of thermal conductivity within a material.

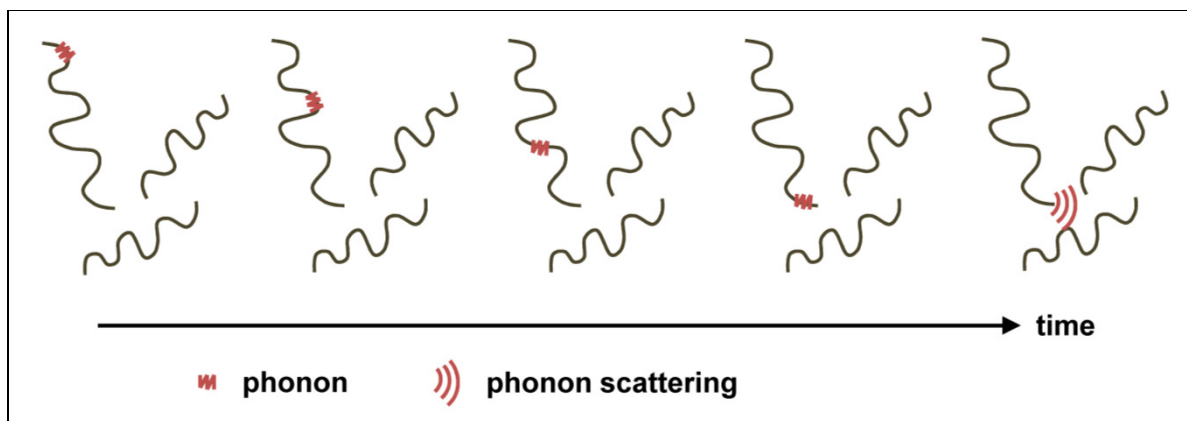


Figure 2.7 Schematic of heat transfer by phonons in amorphous dielectrics. A phonon moves along a polymer chain until reaching its end, where phonon scattering occurs, resulting in reduced bulk thermal conductivity of the polymer

CHAPTER 3

EPOXY/BN MICRO- AND SUBMICRO-COMPOSITES: DIELECTRIC AND THERMAL PROPERTIES OF ENHANCED MATERIALS FOR HIGH VOLTAGE INSULATION SYSTEMS

Thomas Heid^{1,2}, Michel Fréchette², Eric David¹

¹ Department of Mechanical Engineering, École de Technologie Supérieure,
1100 Notre-Dame West, Montreal, Quebec, (H3C 1K3) Canada

² Hydro-Québec's Research Institute,
1800 Boulevard Lionel-Boulet, Varennes, Quebec, (J3X 1S1) Canada

This article has been published in:

IEEE Transactions on Dielectrics and Electrical Insulation

04/2015, vol. 22, issue 02, pp. 1176-1185

<http://dx.doi.org/10.1109/TDEI.2015.7076820>

Abstract

In order to study the effect of incorporating hexagonal boron nitride (h-BN) particles in epoxy resin, composites with different filler sizes and several BN loadings have been fabricated. Two different filler sizes, one micrometric with an average grain size of 9 μm and a submicrometric one with 0.5 μm , have been used to form composites. The amount of either type of BN in the matrix has been varied from 1 to 5 wt%. It has been found that incorporation of h-BN particles in the epoxy resin resulted in significant improvements of parameters such as resistance to electrical discharge, as well as diminished dielectric losses for the composites at higher temperatures. Furthermore, BN composites with 5 wt% filler loadings have shown a noteworthy enhancement of thermal conductivities, which was more distinct for the submicrometric BN composite.

Keywords: AC breakdown strength, boron nitride, dielectric spectroscopy, electrical discharge, polymer composites, surface erosion, thermal conductivity

3.1 Introduction

Epoxy resins are commonly used dielectric materials for power applications such as spacers, cable terminations and machine insulation. Naturally such dielectrics are exposed to high electric, thermal and mechanical stresses during operation. Due to the technical development towards higher electrical field strengths and frequently concomitant increased thermal loads, improved materials are needed to meet those demands. Boron nitride (BN) is a very promising material for dielectric composites due to its high thermal conductivity, excellent mechanical features as well as for its electrical insulating properties (Haubner et al., 2002; Pakdel et al., 2012).

Recent studies have shown an improved thermal conductivity of composites after incorporating BN in an epoxy matrix (Kochetov et al., 2009a; Kochetov et al., 2010; Zengbin et al., 2011a; 2011b), with a trend of superior performances by reducing filler sizes in non-percolating networks (Kochetov et al., 2010; Reading, Vaughan et Lewin, 2011). Partially very high BN particle loadings of 20 wt% (Kochetov et al., 2010) and up to 90 wt% (Tanaka et al., 2011; Zengbin et al., 2011a; 2011b) in epoxy resins have been studied. It has also been shown in the literature that dielectric breakdown strength could be slightly improved with nanometric filler sizes (Andritsch et al., 2010) whereas incorporation of submicrometric and micrometric particles in epoxy resin resulted in similar breakdown strengths compared to the neat epoxy at BN loadings of 10 wt% (Andritsch et al., 2010; Reading, Vaughan et Lewin, 2011).

In this work, we aimed to affect the morphology of epoxy resin composites by adding either submicrometric or micrometric BN particles in comparatively low weight percentages (≤ 5 wt%) and verify the effects on dielectric and thermal performances of the resulting composites.

3.2 Materials and sample preparation

DER332 epoxy resin (DOW Chemicals) and Jeffamine D230 (Huntsman Corp.) curing agent were mixed in a ratio of 1000:344 parts. As filler materials, hexagonal boron nitride (h-BN) particles (Henze Boron Nitride Products AG) with two different average particle sizes, BN205 with average dimensions of 500 nm, or BN600, which were of 9 μm average size, were used to fabricate the composites (see Table 3.1 for details).

The filler particles were dispersed in the epoxy using manual stirring, followed by extensive mixing with a high energetic ultrasonic probe, to generate a homogeneous dispersion of the particles within the matrix. The resulting mixture and the curing agent were degassed separately, before subsequently adding the hardener to that mixture and dispersing it using a magnetic stir. After the final mixing procedure, the liquid composite was degassed again, cast into a stainless steel mold and cured for six hours at 100 $^{\circ}\text{C}$, followed by a gradient cool down to ambient temperature. A release agent (QZ13) was applied on the mold before casting the epoxy, to facilitate removing the samples after the curing process. The samples were post-cured subsequently under vacuum for 48 hours at 140 $^{\circ}\text{C}$.

Composites with loadings of 1, 2 and 5 % per weight for either filler type were produced. The nomenclature for the resulting composites, consisting of epoxy and BN particles, will be referred to as e.g. BN205 1wt% for epoxy with 1 wt% of BN205 throughout this work.

Table 3.1 Specifications for BN filler particles as provided by supplier

Filler type	Particle size in μm	Specific surface area in m^2/g	Bulk density in g/cm^3
BN205	0.5	16-26	0.2
BN600	9	35-40	0.5

3.3 Experimental methods

3.3.1 Microstructure analysis

Samples were prepared by cutting with a diamond knife in a microtome (Leica RM2265) while being cooled to -80 °C inside a nitrogen chamber. Subsequently they were sputtered with a 2 nm Platinum layer to prevent charging, before the samples were observed with a Hitachi S-3600N Scanning Electron Microscope (SEM).

3.3.2 Differential scanning calorimetry

Glass transition temperatures were measured by Differential Scanning Calorimetry (DSC) with a heat flow calorimeter (Q20, TA Instruments) on samples not exposed to the thermal post-treatment. Each sample was subjected to two thermal cycles with a heating rate of 10 °C/min from 20 to 250 °C, followed by a gradual cool down to 20 °C at 10 °C/min. The glass transition temperatures T_g were obtained from the second cycle to ensure no thermal history of the samples.

3.3.3 Dielectric spectroscopy

The frequency and temperature dependent dielectric response of the samples was obtained by Broadband Dielectric Spectroscopy (BDS, Novocontrol) for temperatures ranging from -100 °C to +180 °C (± 0.1 °C), in isothermal steps of 5 °C, for either low or high excitation voltages. Low excitation voltages of 3 V with a frequency range of 0.1 Hz to 1 MHz were applied on one series of samples, whereas for high excitation voltages of 500 V the dielectric response was analyzed for frequencies from 0.1 Hz to 10 kHz for the second sample series.

BDS measurements were performed on samples with 20 mm diameter on a parallel plate electrode setup, on samples with average thickness of $275 \mu\text{m} \pm 5\%$. The complex

permittivity ε^* as given in (3.1) was retrieved, with the real permittivity ε' representing the storage part and ε'' as imaginary or dielectric loss part.

$$\varepsilon^* = \varepsilon'(f, T) - j\varepsilon''(f, T) \quad (3.1)$$

3.3.4 AC breakdown strength

The dielectric breakdown strength was measured based on ASTM D149. Samples were immersed in transformer oil (Luminol TR-i) and placed between two symmetrical ball tip electrodes with a diameter of 4 mm. The short term test was used, where a 60 Hz voltage with a ramp rate of 2 kV/s was applied between the electrodes until the breakdown occurred. On each sample type 16 breakdowns were conducted, after which the ball tips have been replaced by new ones to avoid pitting.

3.3.5 Resistance to electrical discharge

To evaluate the resistance to electrical discharges, each sample was exposed to partial discharges (PD) using a point-to-plane geometry which was operated in open air. A sinusoidal voltage of 4 kV_{RMS} at an enhanced frequency of 300 Hz, to accelerate the ageing effect, was applied to the high voltage rod electrode, bearing a titanium ball tip with 4 mm in diameter. The samples were placed centrally on a ground electrode framed by an acrylic base plate, with the tip of the rod electrode facing the sample surface, separated by an air gap of 200 μm (see Figure 3.1). Samples were exposed to the electrical discharges for 30 hours, equaling 150 hours of 60 Hz and 180 hours of 50 Hz equivalent time respectively.

The resistance to erosion due to electrical discharge was further evaluated by the use of a mechanical profilometer, based on the eroded volume that has been calculated from the attained data. The values of eroded sample volume can thus be seen as an inverse reference value of the resistance to partial discharge. Before passing the samples in the profilometer they were carefully cleaned in an ultrasonic bath, to remove the debris caused by the PD.

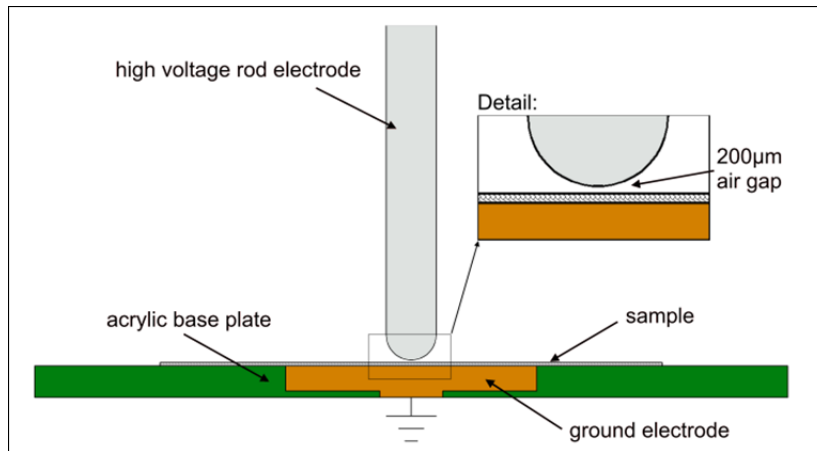


Figure 3.1 Schematic of surface erosion setup

3.3.6 Thermal conductivity

The thermal conductivity was obtained with a DTC-25 guarded heat flow meter (TA Instruments) in accordance with ASTM E1530 standard. Samples with 50.8 mm (2 inches) diameter were subsequently placed between an upper heating plate and a lower cooling plate of the device (see Figure 3.2). A pressure of 15 psi applied on the upper plate assured an intimate contact between the sample, the heating and the cooling plate. The upper plate was heated, whereas the lower one was cooled, creating a ΔT over the sample with thickness t and surface A , leading to a medium sample temperature of 25 °C.

The samples have been allowed for thermal stabilization, which occurred within one hour, in the measuring chamber. A heat flux transducer in the lower plate measures the heat flow Q through the sample, with which the thermal conductivity λ can be expressed by equation (3.2):

$$\lambda = \frac{Q/A}{\Delta T/t} \quad (3.2)$$

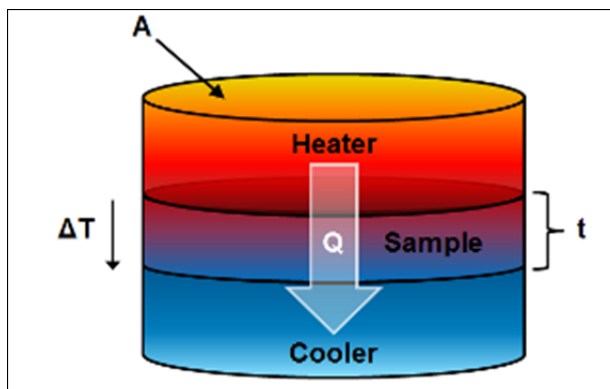


Figure 3.2 Schematic of heat flow meter setup

3.4 Experimental results and discussion

3.4.1 Microstructure analysis

In Figure 3.3 the SEM micrographs of the epoxy/BN composites are displayed. The left column (Figure 3.3a to Figure 3.3c) represents the BN205 composites with increasing filler amount, whereas the right column (Figure 3.3d to Figure 3.3f) represents the BN600 types. The dispersion of BN particles in the epoxy matrix has been qualitatively assessed by eye based on the SEM observations. The particles were found to be evenly dispersed throughout the composite volumes. For the submicrometric BN composite some agglomerations could be seen though, especially with increasing amount of filler. Those agglomerations had dimensions of only a few microns in size, being below the 9 μm average size of the micrometric filler particles.

3.4.2 Differential scanning calorimetry

In Figure 3.4 the DSC graphs from the second thermal cycle for all samples are presented. The derived glass transition temperatures T_g are displayed in Table 3.2. It was found that the addition of boron nitride into the epoxy matrix would slightly increase the glass transition temperature. The composites with 5 wt% of either submicrometric or micrometric BN type have exposed the highest T_g values of approximately 96 $^{\circ}\text{C}$ and 95 $^{\circ}\text{C}$ respectively. The glass

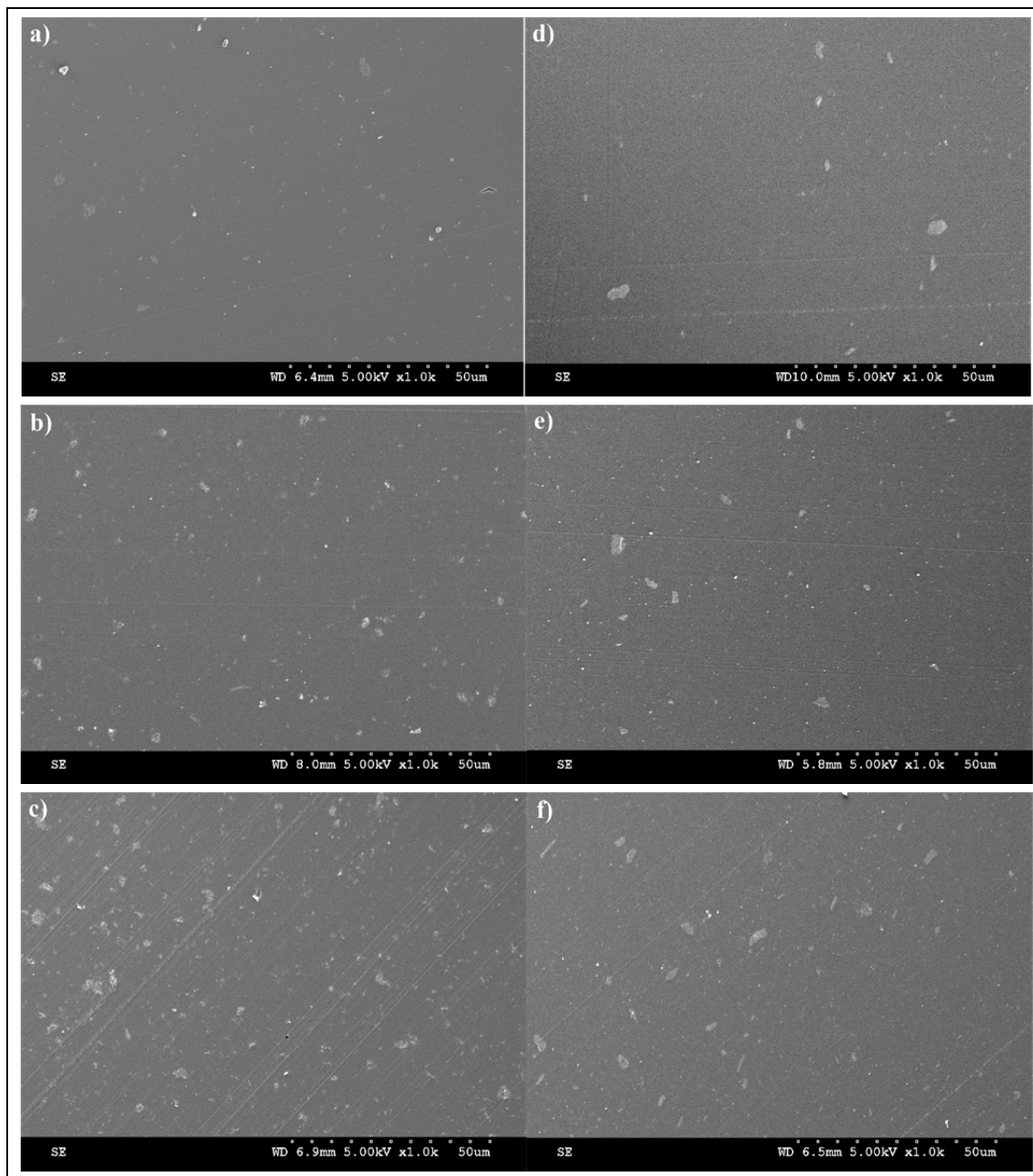


Figure 3.3 SEM micrographs of epoxy/BN composites a) BN205 1wt%, b) BN205 2wt%, c) BN205 5wt%, d) BN600 1wt%, e) BN600 2wt%, f) BN600 5wt%

transition phenomenon is linked to the movement of the main chains within the epoxy network, therefore it can be derived that the incorporation of BN particles in the epoxy matrix slightly reduces the mobility of the epoxy chains, subsequently leading to the minor increase in T_g .

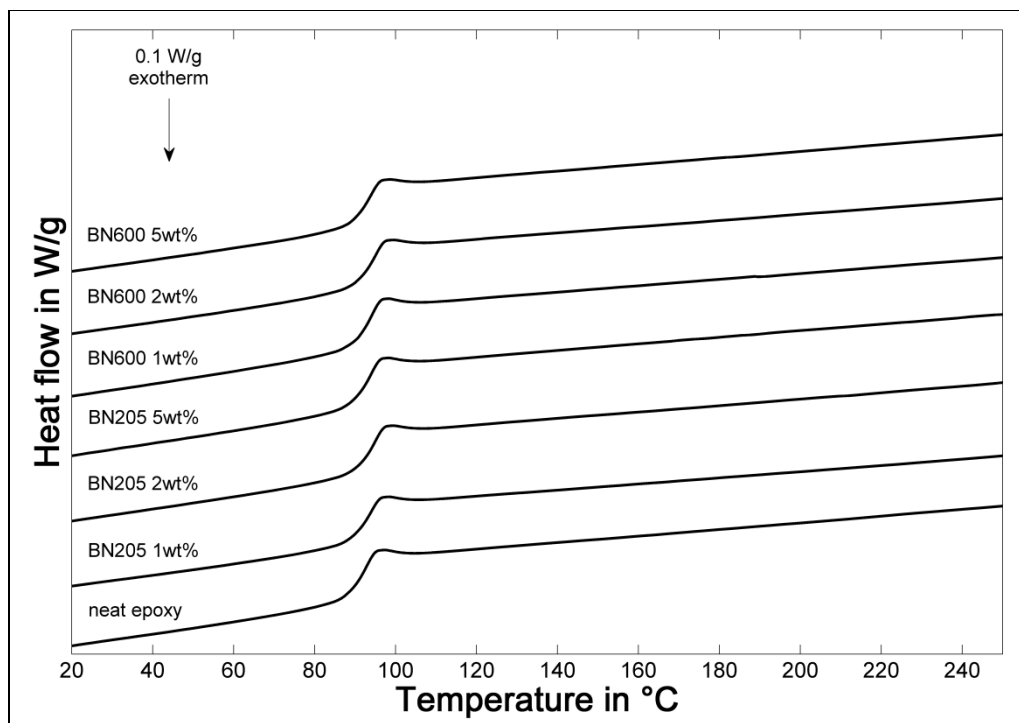


Figure 3.4 DSC graphs from the second thermal cycle for neat epoxy and the BN composites

Table 3.2 Glass transition temperatures of neat epoxy and the BN composites

Sample type	T_g in °C
Neat epoxy	93
BN205 1wt%	94
BN205 2wt%	94
BN205 5wt%	96
BN600 1wt%	94
BN600 2wt%	94
BN600 5wt%	95

3.4.3 Dielectric spectroscopy

Dielectric responses of the test specimens have been taken at excitation voltages of 3 and 500 V (see chapter 3.3.3), leading to low field strengths of close to 11 V/mm, or high field strengths of approximately 1.8 kV/mm. Measurements at low and high excitation voltages were found to be quite similar for the respective sample types.

The dielectric spectroscopy experiments, both at low and high excitation voltages have revealed α - and β -relaxation peaks for all test specimens (see Figure 3.5). In amorphous polymers those relaxation peaks can be related to relaxation processes of the main chains of the cross-linked epoxy chains due to the glass transition process in the case of α -relaxation, or secondary relaxation processes due to movement of local groups attached to the main chain, as in the case of the β -relaxation.

An additional phenomenon has been observed at high temperatures and low frequencies for neat epoxy and all BN composites likewise, the so-called electrode polarization (EP). This is a parasitic phenomenon well known for epoxy resin and its composites (Ishai P.B et al., 2013; Preda et al., 2013; Tian et Ohki, 2014), which can be related to a delay in charge transfer at interfaces between sample and electrodes, giving rise to additional interfacial polarization on a macroscopic level.

This peak due to EP at high temperatures and low frequencies is overshadowed by low-frequency dispersion due to charge fluctuation, possibly superimposed by electronic conductivity, which is a rather common behavior for solid insulating materials at elevated temperatures. Lower losses due to conductivity for the BN composites, as compared to neat epoxy, lead to more prominent peaks due to electrode polarization (EP) for the composites (Figure 3.5).

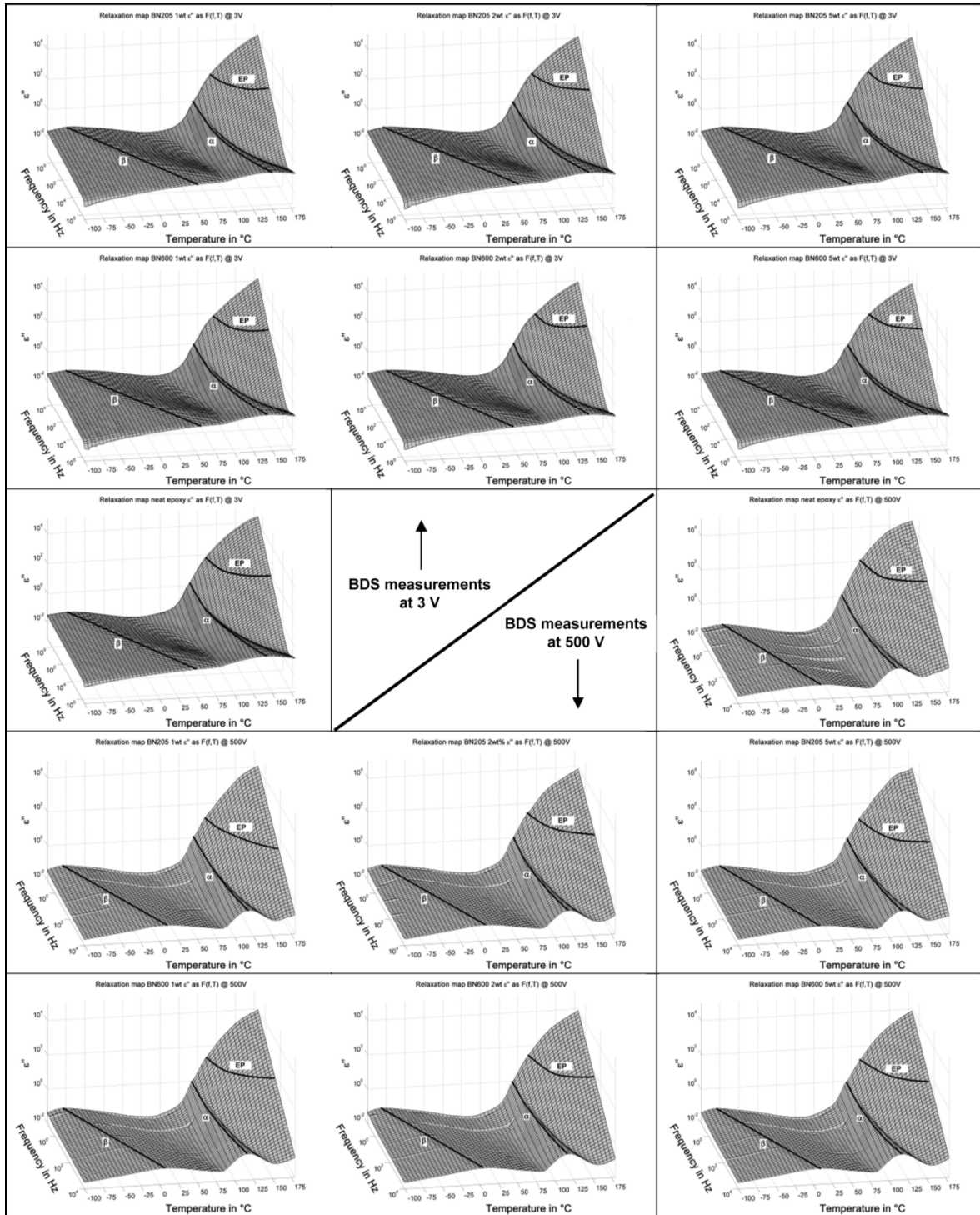


Figure 3.5 3D plots of dielectric losses for all samples measured at either 3 or 500 V, showing the main relaxation phenomena. BN composites revealed lower dielectric losses at high temperatures and low frequencies with increasing filler loadings. Electrode polarization (EP) due to a delay in charge transport at electrode-composite interfaces could additionally be detected for all samples

The dielectric responses measured at 20 °C have shown a rather similar ϵ' for all samples (see Figure 3.6a), whereas for ϵ'' a slight increase in dielectric losses could be detected (see Figure 3.6b). This is possibly due to the appearance of a low-magnitude interfacial loss peak in the mid-frequency range, leading to a local conduction phenomenon. The additional loss peak is overshadowed by the low frequency wing of the β -relaxation peak, causing a slight shift of the β -peaks for the BN composites towards lower frequencies, as compared to neat epoxy, for which the β -peak was located in the vicinity of 10^5 Hz. Dielectric responses for all BN composites were found to be quite similar, like it has been discussed in (Heid et al., 2013a), as a consequence of which the further discussion will be based on neat epoxy and the BN205 5wt% composite (see Figure 3.7 and Figure 3.8).

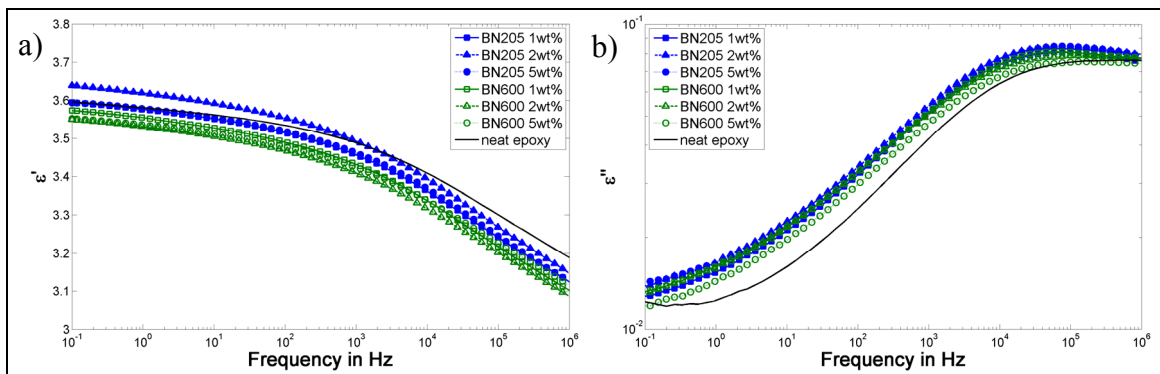


Figure 3.6 Dielectric response of neat epoxy and BN composites measured at 3 V and 20 °C; a) real part and b) imaginary part of the complex permittivity

Analogous to the observations made at 20 °C, introduction of BN particles in the epoxy matrix did not lead to significant changes of ϵ' for the composites as compared to neat epoxy, for temperatures of 60 °C and below (see Figure 3.7a and Figure 3.8a). However, considering the temperatures above 60 °C, a reduced ϵ' for the BN composites was found over the complete frequency range, getting more and more significant towards lower frequencies. Additionally the step in ϵ' at 100 °C representing the α -relaxation step, which was located around 100 Hz for neat epoxy, was found to be shifted about one order of magnitude towards lower frequencies for BN composites.

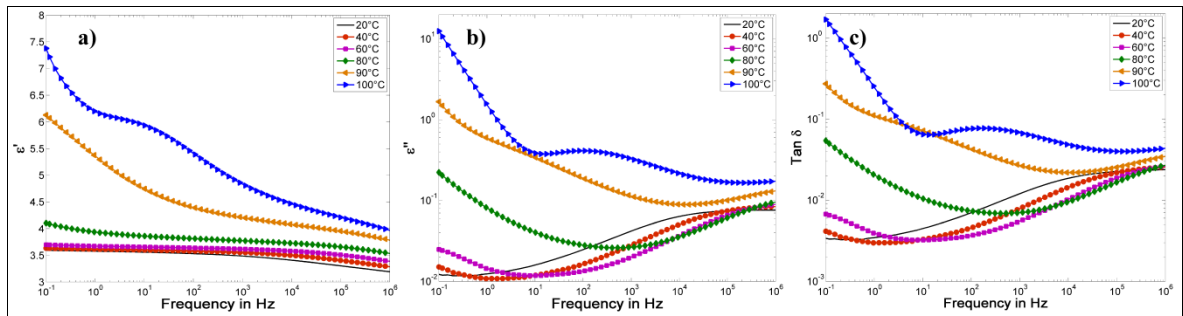


Figure 3.7 Neat epoxy temperature dependent real part (a), imaginary part (b) of complex permittivity and (c) loss tangent

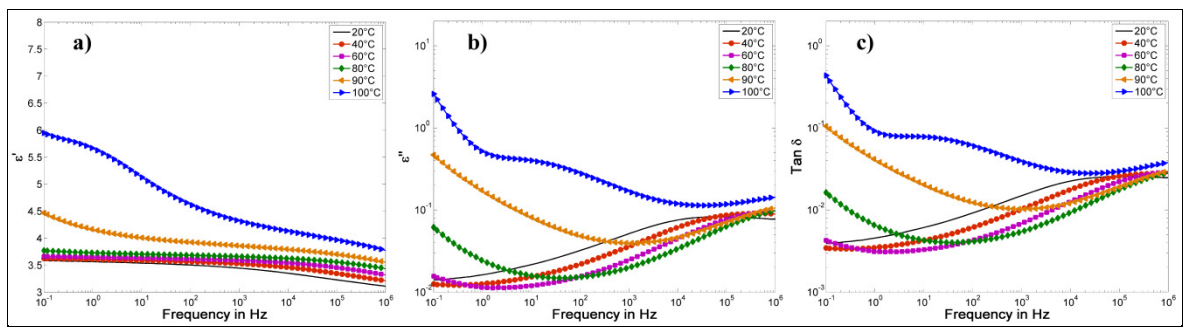


Figure 3.8 BN205 5wt% temperature dependent real part (a), imaginary part (b) of complex permittivity and (c) loss tangent

Evaluating ϵ'' of neat epoxy (Figure 3.7b) and BN205 5wt% (Figure 3.8b), the BN composites were found to have marginally increased dielectric losses, for temperatures between 20 °C and 60 °C, over the complete frequency range. This increase of dielectric losses supposedly originates in the abovementioned appearance of a low-magnitude interfacial loss peak in the mid-frequency range due to introduction of BN particles in the epoxy matrix (as it has been presented above for the results at 20 °C in Figure 3.6b). Nevertheless, exceeding 60 °C, the incorporation of BN filler in the organic matrix was found to significantly decrease dielectric losses of BN composites (Figure 3.8b) compared to neat epoxy (Figure 3.7b), especially for power frequencies and below. The α -relaxation peak found around 100 Hz for neat epoxy at 100 °C, was shifted about one order of magnitude towards lower frequencies for BN205 5wt%. In contrast to the BN composites, neat epoxy showed a precursor of the α -relaxation peak at 90 °C in the vicinity of 10 Hz. This phenomenon, along with the findings of higher dielectric losses due to conductivity at

elevated temperatures and low frequencies for the neat epoxy, as well as the shift of the α -peak towards lower frequencies for the BN composites, can partially be explained by higher chain mobility in the neat epoxy as compared to the BN composites. It is further known that free ionic species, remaining from the synthesis process, contribute to the increased dielectric losses in epoxy resins at high temperatures (Friedrich et al., 2001; Katayama et al., 2013; Tian et Ohki, 2014; Ulański et al., 1997). Introducing BN particles in the epoxy matrix subsequently results in less mobile ionic charge carriers in the composite, leading to lower losses due to conductivity with increasing BN filler amount.

Lastly the quotient of ϵ'' and ϵ' , the loss tangent or $\tan \delta$, which is of interest in high voltage insulation engineering since it is often related to engineering requirements, is shown in the third column of Figure 3.7 and Figure 3.8. Analogous to the aforementioned results, significantly lower values for the loss tangent of BN composites (Figure 3.8c) have been found at temperatures above 60 °C, compared to neat epoxy (Figure 3.7c). To give an example, for power frequencies at 80 °C, neat epoxy had a loss tangent of almost two times the one for BN205 5wt%, whereas at 60 °C and below the loss tangent of neat epoxy was between 10 to 20 % lower than for the BN composites.

3.4.4 AC breakdown strength

The retrieved AC breakdown (BD) data were treated by two parameter Weibull distribution according to the IEEE 930 standard to assess the breakdown strength of the tested specimens. The relevant parameters are the scale parameter α , representing the dielectric breakdown strength in kV/mm at the cumulative failure probability (62.3 %), as well as the shape parameter β , which is an inverse measurement for the scatter of BD data, thus higher values mean less scattering. The Weibull plots for the experimental data are displayed in Figure 3.9 and the corresponding Weibull parameters are summarized in Table 3.3.

It has been found that the introduction of either submicrometric (BN205) or micrometric (BN600) boron nitride particles in the epoxy matrix resulted in decreased breakdown

strengths of the composites compared to neat epoxy, even more so with increasing amount of filler. Thus, for both filler types, the 1 wt% composites had the least deterioration of dielectric BD strength, at values of approximately 140 kV/mm. For the submicrometric composite BN205 2wt%, addition of BN did not result in a significant reduction of BD strength though, as compared to the micrometric BN600 2wt%.

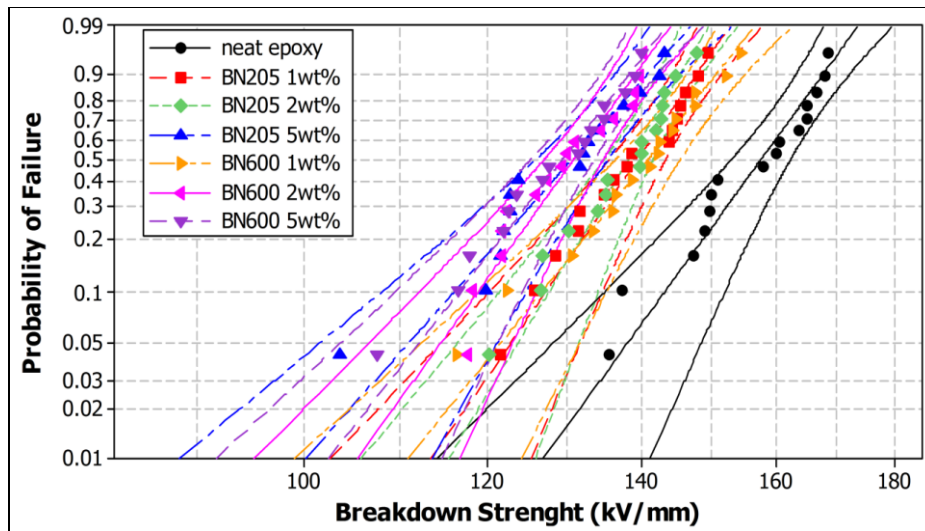


Figure 3.9 Weibull plots of breakdown strengths with 95 % confidence intervals

Table 3.3 Weibull parameters obtained from Figure 3.9

Sample type	α	β	Avg. sample thickness in mm
Neat epoxy	160.4	19.62	0.233
BN205 1wt%	141.8	20.63	0.217
BN205 2wt%	140.2	23.69	0.223
BN205 5wt%	133.5	16.03	0.209
BN600 1wt%	143.7	17.80	0.208
BN600 2wt%	133.2	19.71	0.223
BN600 5wt%	131.9	18.26	0.216

It has repeatedly been reported in the literature, that incorporation of micrometric filler particles in epoxy resins resulted in diminishment of BD strength compared to the neat epoxy resins (Li et al., 2009; 2011; Lovell, 1976; Wang et al., 2012; Zengbin et al., 2011a). This effect can be associated with locally enhanced electric field strengths in proximity of those filler particles, due to the mismatch of permittivity as well as orientation and shape of those particles, giving rise to electrical discharges.

Additionally, despite all the care taken during sample preparation, defects (voids) are likely to be introduced in the epoxy matrix by micrometric particles during the compounding process (Lovell, 1976; Preetha et Thomas, 2011; Wang et al., 2012). Those defects, present at the filler surface, will cause additional field enhancement. The combination of abovementioned effects will subsequently lead to earlier BD of the composites at lower BD strengths as the neat polymer.

Bearing in mind these observations, along with the rather close values for BN205 1wt% and BN205 2wt%, it seems that submicrometric composites suffer less from diminished BD strengths as micrometric composites, at least as long as a good dispersion of the particles can be achieved. For BN205 5wt% agglomerates with sizes close to the one of BN600 particles were found during SEM observation (see Figure 3.3), explaining the similar results for the two types of composites containing 5 wt% of either filler type.

In Figure 3.10 the evolution of the composites' microstructures depending on filler content and consequentially introduced defects is depicted, to better illustrate the effects of incorporating filler particles in a polymeric matrix along with their dispersion within it.

3.4.5 Resistance to electrical discharge

The results of the surface erosion experiment based on the eroded sample volumes are presented in Figure 3.11. It has been discovered that incorporation of low contents of BN

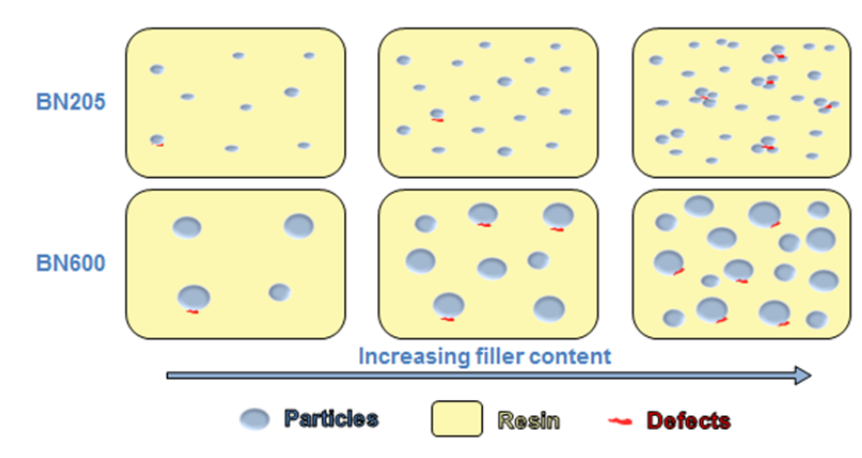


Figure 3.10 Schematic evolution of the microstructure in epoxy resin with increasing filler and subsequently defect contents

particles in the epoxy resin has significantly improved the composites' resistances to electrical discharges by up to 50 % less eroded volume, as in the case of BN600 1wt%. The resistance to electrical discharges however diminished marginally with increase in filler content, a trend similar to the BD strength.

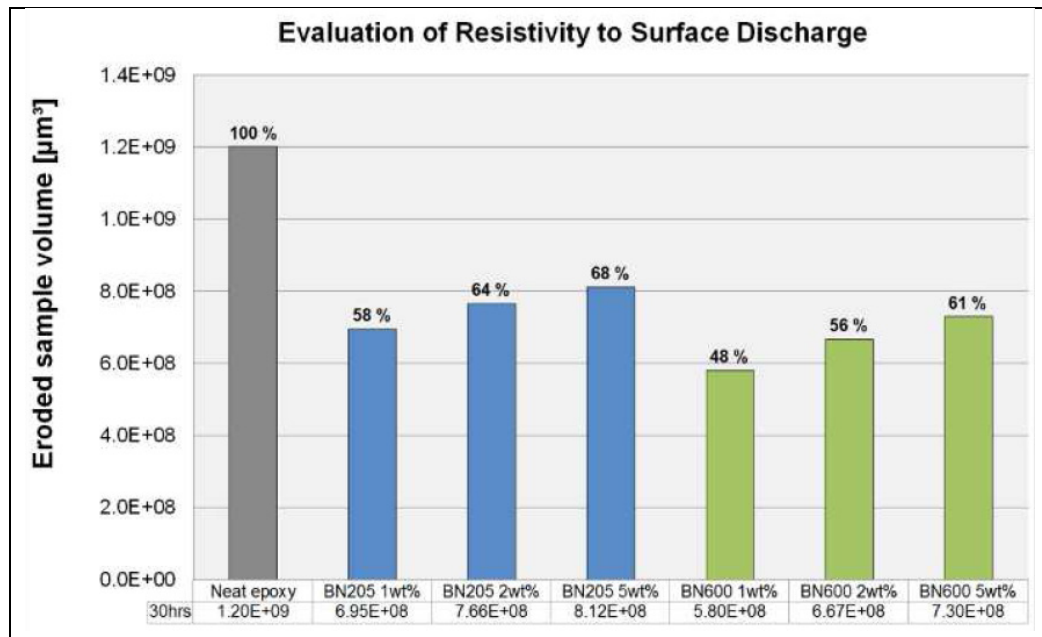


Figure 3.11 Comparison of eroded sample volume after exposure to partial discharges for 30 hours at 4 kV_{RMS} and 300 Hz

Considering that polymeric composites with inorganic fillers are mainly eroded in the organic phase, hence in the polymeric region, one would expect to have less eroded volume on composites with higher contents of inorganic filler particles, as it has been reported in (Li et al., 2011) for instance. The sole change of morphology due to incorporation of inorganic filler, along with the “shielding” effect of such inorganic particles cannot explain that deviating behavior for low and high filler contents. It is more likely that, at low filler contents, the introduction of defects in the matrix along with the micrometric particles, as well as electric field enhancement due to the mismatch of permittivity, give rise to the slight deterioration of resistance to electrical discharge with increased BN contents.

Additionally, it has been found in our study that the micrometric BN600 composites had an overall better performance than their submicrometric BN205 counterparts. This is assumed to be due to the considerably larger specific surface area of the BN600 particles, which is approximately two times higher than for BN205 (see Table 3.1). Thus a larger protective or “shielding” area is provided by the same amount of BN600 in comparison to the BN205 particles when incorporated in the polymeric matrix.

3.4.6 Thermal conductivity

Thermal conductivities of all composite types have been measured twice and the further discussion of thermal conductivities is based on the average value taken from the two measurement series. Based on the results presented in Figure 3.12 it has been found that incorporation of very low BN particle contents of 1 wt% and 2 wt% did not lead to a significant increase of thermal conductivity compared to the neat epoxy resin. Only marginally improved thermal conductivities by up to 5 % have been found for those composites, contrary to the composites featuring 5 wt% of BN particles. For the submicrometric BN205 5wt% composite a noteworthy increase of 17 % in thermal conductivity has been attained, in contrast to 11 % increased thermal conductivity for the micrometric BN600 5wt% specimen.

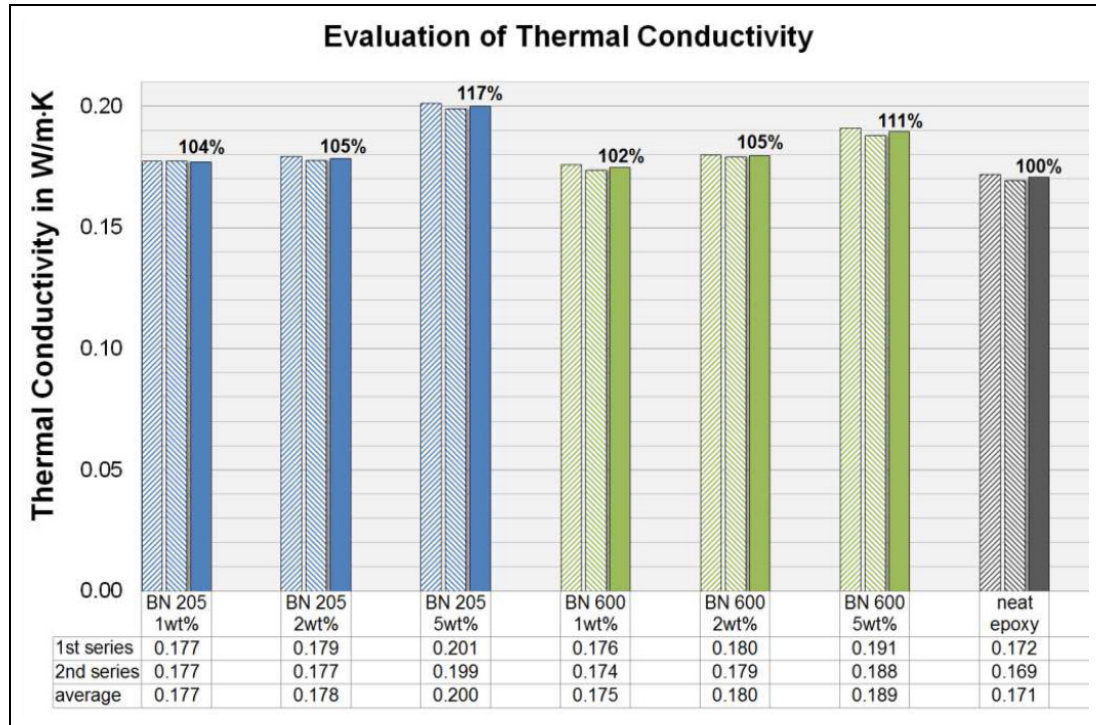


Figure 3.12 Comparison of thermal conductivities; two measurements were taken on each sample type. The comparison of thermal conductivity was based on the average value for each

It is commonly known that thermal conduction in solid materials is based on phonons (lattice vibrations) (Cui et al., 2011; Huang et al., 2012; Takezawa, Akatsuka et Farren, 2003). In amorphous materials, i.e. epoxy resins, phonon scattering is the dominating process, which occurs at either particle-particle, particle-matrix (equally at defects or pores), as well as interfaces of the amorphous structure in epoxy resin itself (Takezawa, Akatsuka et Farren, 2003). Phonon scattering causes diminishment of thermal conductivity within a material.

Introduction of high thermally conductive filler particles, i.e. BN, into the amorphous epoxy resin will consequently result in local zones with good thermal conductivity, on a microscopic level. Thus, an improvement of the resulting composite's thermal conductivity with increasing content of BN particles can be expected, as the BN takes up more and more volume. However, increasing the filler content in a composite multiplies the number of interfaces, in particular those between filler and the matrix, as well as particle to particle interfaces in case of agglomerations. Both phenomena can limit the amelioration of thermal

conductivity. Subsequently phonon scattering becomes more and more important with rising BN particle content.

Comparing the thermal conductivities of BN205 5wt% and BN600 5wt%, viz. 0.2 and 0.189 W/m·K, it is evident, that the submicrometric BN composite exhibits better thermal conductivity compared to the micrometric one. Two main factors will cause this behavior: firstly, the volume factor and secondly, the specific surface area. While BN205 has a density of 0.2 g/cm³ in contrary to 0.5 g/cm³ for BN600 (see Table 3.1), the submicrometric BN205 occupies 2.5 times more volume than the micrometric BN600, when introduced in equal wt% into the epoxy matrix. In the same time, the surface area of BN600 particles is approximately two times larger than the BN205 particles' (as depicted in Table 3.1), which will result in more prominent phonon scattering at the particle-matrix interfaces within the BN600 composites, thus rendering their thermal conductivity lower in comparison to BN205 composites.

3.5 Conclusions

In this study, epoxy composites with rather low contents of submicrometric and micrometric boron nitride particles have been fabricated and analyzed in regards to their respective effects on morphology, as well as the dielectric and thermal performance.

It has been shown that incorporation of BN resulted in marginally increased glass transition temperatures for the 5 wt% composites.

Significantly lower dielectric losses resulted for BN composites at temperatures above 60 °C, getting more and more pronounced with higher BN loadings.

The AC breakdown strength of BN composites was found to be diminished with increasing content of BN particles, although the deterioration of breakdown strength for submicrometric BN205 composites was found to be less distinct as compared to their micrometric BN

counterparts, as micrometric BN particles are more likely to introduce defects in the epoxy matrix during the fabrication process.

Resistance to erosion due to electrical discharge has been remarkably increased by up to 50 % less eroded volume for the BN composites. Composites with only 1 wt% BN content were found to have the best erosion resistance due to less introduced defects in the epoxy matrix with less filler particles. The micrometric BN600 composites performed better than the submicrometric BN205 ones, which was attributed to the larger specific surface area of BN600 (see Table 3.1), offering better protection against the electrical discharges.

The thermal conductivity of composites after addition of less than 5 wt% BN didn't show any significant increase. The submicrometric BN205 5wt% composite revealed a noteworthy increase of 17 % in thermal conductivity compared to neat epoxy, the micrometric BN600 5wt% composite however an increase of 11 %. The superior performance of the submicrometric BN composite over the micrometric one could be attributed to the larger volume fraction in the composites for submicrometric BN particles, as well as augmented phonon scattering at particle-matrix interfaces for the micrometric BN particles with a larger specific surface area.

To conclude, it has been shown in this study that incorporation of very low weight fractions of BN particles in an epoxy resin could result in noticeable improvements of dielectric and thermal performance of the resulting composites. Although the composites with a loading of 5 wt% BN revealed deterioration in AC breakdown strength, it should be mentioned that the respective breakdown strengths of more than 130 kV/mm are still significantly higher than common electric stresses in high voltage insulation systems (e.g. 2 to 3 kV/mm in stator bars for rotating machines). Therefore the improvements in erosion resistance and thermal conductivity should be granted a higher emphasis.

3.6 Acknowledgment

The authors want to thank Prof. Alun Vaughan of the University of Southampton as well as Prof. Paul Lewin of the Tony Davies High Voltage Laboratory along with their teams, for the kind opportunity to produce our first set of epoxy samples there, as well as the much appreciated formation on how to do so. Hydro-Québec and the Natural Sciences and Engineering Research Council of Canada (NSERC) are gratefully recognized for their financial support.

CHAPTER 4

NANOSTRUCTURED EPOXY/POSS COMPOSITES: ENHANCED MATERIALS FOR HIGH VOLTAGE INSULATION APPLICATIONS

Thomas Heid^{1,2}, Michel Fréchette², Eric David¹

¹ Department of Mechanical Engineering, École de Technologie Supérieure,
1100 Notre-Dame West, Montreal, Quebec, (H3C 1K3) Canada

² Hydro-Québec's Research Institute,
1800 Boulevard Lionel-Boulet, Varennes, Quebec, (J3X 1S1) Canada

This article has been published in:

IEEE Transactions on Dielectrics and Electrical Insulation

06/2015, vol. 22, issue 03, pp. 1594-1604

<http://dx.doi.org/10.1109/TDEI.2015.7116355>

Abstract

In this study, the dielectric and thermal properties of nanostructured epoxy/POSS (Polyhedral Oligomeric Silsesquioxanes) composites were investigated, using a reactive Triglycidylisobutyl-POSS (TGIB-POSS) additive from 1 up to 10 wt%. TGIB-POSS has been successfully dispersed at a molecular level for low content composites, which show a remarkably improved resistance to corona discharges, with up to 60 % less eroded sample volume, along with significantly increased dielectric breakdown strengths and thermal conductivities. Epoxy/POSS composites containing 5 wt% and more of the Triglycidylisobutyl-POSS additive exhibit agglomerations, which have been observed by SEM. Furthermore, dielectric spectroscopy revealed additional interfacial loss peaks for such composites containing 5 wt% TGIB-POSS and more, in addition to the α - and β -peaks known for epoxy.

Keywords: AC breakdown strength, dielectric spectroscopy, epoxy, electrical discharge, interface, polymer composites, POSS, surface erosion, thermal conductivity

4.1 Introduction

Epoxy resins are an important dielectric material in the high voltage insulation industry, and they are widely used in insulation systems for bushings, rotating machines and cable terminations, to name a few. However, as an organic material, it is prone to degradation due to electrical discharges and usually features rather low thermal conductivities, which can constitute a limiting factor for power ratings. These deficient properties have been counteracted in the past by the addition of micrometric inorganic filler materials, such as silica, which can render the resulting composite more resilient to electro-thermal stresses and improve parameters such as the thermal conductivity.

In the last decade though, much has been reported about a novel class of dielectric materials, namely polymer nanocomposites or nanodielectrics, which feature nanometric filler particles (Fr chet te et al., 2001; Nelson, 2010). However, such nanodielectrics can only unfold their full potential, when good dispersion and distribution of those filler particles within the matrix are achieved. Albeit, due to the incompatibility of inorganic particles with the organic polymer, dispersion and distribution are regularly compromised, resulting in agglomerations of nano particles, often leading to agglomerates with submicrometric or micrometric dimensions. In order to enhance the interaction between inorganic filler particles and the organic matrix, and hence, improve the dispersion of such particles in polymers, their functionalization has become rather common. Surface treatments with coupling agents, such as silane (Dongling et al., 2005b; Huang et al., 2012; Preda et al., 2013), or more complex processes, including grafting organic brushes on particle surfaces (Virtanen et al., 2014), have been explored with varying degrees of success.

As an alternative to nanometric silica, Polyhedral Oligomeric Silsesquioxanes (POSS) could be of interest for electrical insulation applications, as it is a hybrid material, consisting of an inorganic silica-like core surrounded by organic side-groups. These organic groups can be either reactive or non-reactive and therefore offer compatibility with a multitude of polymers, depending on the specific organic side-group configuration. POSS, being a hybrid inorganic-

organic material, further combines the beneficial material properties of ceramics, such as inertness and electrical insulating properties, with the processability of polymers. It was previously denoted as a “Nano-building-block”, because of its crystalline structure (Bocek et al., 2011; Chen, 2012), enabling POSS to organize a polymeric matrix through its reactive groups on a nanometric scale. POSS molecules, commonly with sizes below 2 nm, are assumed to be able to dissolve within a polymer without forming agglomerations known from conventional nano-particles (Kuo et Chang, 2011).

The successful incorporation of POSS into epoxy has been shown to significantly improve the composite’s dielectric performance, in terms of corona resistance (Heid, Fréchette et David, 2014c; Horwath et al., 2005; Huang et al., 2014) and dielectric breakdown strengths (Heid, Fréchette et David, 2014b; Horwath et al., 2006; Takala et al., 2008). Furthermore, higher thermal stabilities of POSS composites have been reported in (Chen, 2012; Yang et al., 2012), as well as improved thermo-mechanical properties of such nanostructured materials (Bocek et al., 2011).

The aim of this study was to investigate the dielectric and thermal properties of epoxy/POSS composites, by incorporating a reactive Triglycidylisobutyl-POSS, which we intended to disperse at a molecular level within the matrix.

4.2 Materials and sample preparation

DER332 epoxy resin (DOW Chemicals) and Jeffamine D230 curing agent (Huntsman Corp.) were used as the base epoxy system in a ratio of 1000:344 parts (epoxy to curing agent). Liquid Triglycidylisobutyl-POSS (Hybrid Plastics) was used as an additive to fabricate composites. Triglycidylisobutyl-POSS (TGIB-POSS) has three mono-directionally oriented epoxy groups which are attached to the cage-like silica core (see Figure 4.1). These epoxy groups are compatible with those of the epoxy system used and can therefore form covalent bonds with the matrix, as schematically shown in Figure 4.1. Due to the fact that each TGIB-POSS molecule features three additional epoxy groups that will consume curing agent during

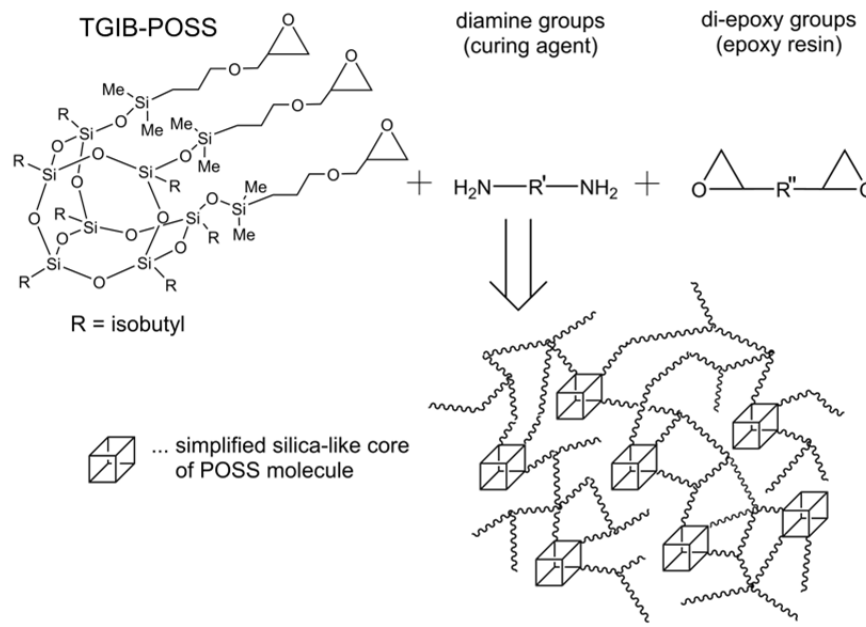


Figure 4.1 Proposed reaction of TGIB-POSS with curing agent and epoxy resin with the formation of covalent bonds, and hence, forming a nano-structured epoxy/POSS network

the reticulation process, a distinct stoichiometric ratio for each epoxy/POSS composite was established, in order to match the amount of reactive epoxy groups with the amine groups of the curing agent within the composite.

During the compounding process, the liquid TGIB-POSS, whose viscosity is similar to that of the epoxy system, was dispersed in the epoxy resin using a magnetic stir on a hot plate at 40 °C. Subsequently the curing agent was added to the mixture. The complete mixing procedures were conducted under vacuum, in order to ensure proper degassing of the liquid composites before they were cast in stainless steel molds. All test specimens were cured for six hours at 100 °C under vacuum, followed by a gradient cool down to ambient temperature. A release agent (QZ13) was applied on the mold before the epoxy was cast to facilitate the removal of the samples after the curing process. Subsequently, the samples were post-cured for 12 hours at 130 °C, also under vacuum. More details about the fabrication process and the stoichiometry can be found in (Heid, Fréchet et David, 2013).

Along with neat epoxy resin specimens, epoxy/POSS composites with TGIB-POSS contents of 1, 2.5, 5 and 10 wt% were fabricated. The POSS composites are further referred to as e.g. ePOSS 1wt%, for the epoxy/POSS composite containing 1 wt% of TGIB-POSS, and so on.

4.3 Experimental methods

4.3.1 Microstructure analysis

The test specimens were mounted in epoxy resin and subsequently polished with grain sizes down to 50 nm to assure a smooth sample surface for Scanning Electron Microscope (SEM) observations. A TM3030 tabletop SEM (Hitachi High Technologies America) was used for low magnification pictures (x5k), whereas a SU-70 high resolution SEM (Hitachi High Technologies America) was used for micrographs with magnifications of x20k and x50k, to further investigate some features found on the composites with higher POSS contents.

4.3.2 Differential scanning calorimetry

Glass transition temperatures were measured by Differential Scanning Calorimetry (DSC) with a heat flow calorimeter (Q20, TA Instruments) on samples which had not previously been exposed to the thermal post-treatment. Each sample was subjected to two thermal cycles with a heating rate of 10 °C/min from 20 °C to 250 °C, followed by a gradual cool down to 20 °C at 10 °C/min. The glass transition temperatures T_g were obtained from the second heating cycle to ensure no thermal history of the samples.

4.3.3 AC breakdown strength

The dielectric breakdown strength was measured based on the ASTM D149 standard. Samples were immersed in transformer oil (Luminol TR-i) and placed between two symmetrical ball tip electrodes with diameters of 4 mm. The short-term test was used, where a 60 Hz voltage with a ramp rate of 2 kV/s was applied between the electrodes until

breakdown occurred. On each sample type, 15 breakdowns were performed, after which the ball tips were exchanged and replaced with new ones to avoid pitting. The breakdown test specimens had an average thickness of $130\ \mu\text{m} \pm 5\%$.

4.3.4 Resistance to corona discharges

To evaluate the resistance to corona discharges, each sample was subjected to partial discharges (PD) using a point-to-plane geometry operated in open air. A sinusoidal voltage of $4\ \text{kV}_{\text{RMS}}$ at a frequency of 300 Hz was applied between the high voltage rod electrode, bearing a 4 mm diameter tungsten carbide ball tip, and the ground electrode. The samples were placed centrally on the ground electrode framed by an acrylic base plate, with the tip of the rod electrode facing the sample surface. The high voltage electrode rod and the sample surface were separated by a $200\ \mu\text{m}$ air gap (see Figure 4.2). All test specimens were exposed to electrical discharges for a duration of 30 hours, which is equal to exposures for 150 hours at 60 Hz and 180 hours at 50 Hz equivalent time, respectively.

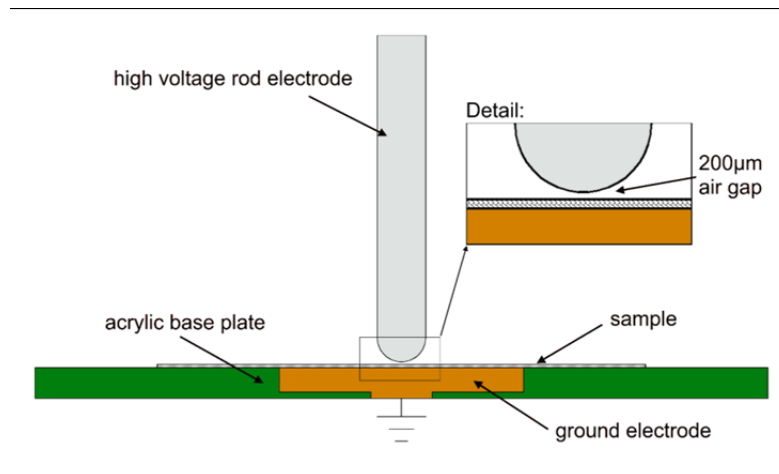


Figure 4.2 Schematic of point-to-plane setup for corona resistance experiment

The resistance to erosion due to corona discharges was subsequently evaluated by the use of a mechanical profilometer, based on the eroded volume calculated from the obtained data. The values of the eroded sample volumes can thus be seen as inverse reference values of the

resistance to partial discharge. Before the samples were analyzed with the profilometer, they were carefully cleaned in an ultrasonic bath in order to remove the debris caused by the PD.

4.3.5 Thermal conductivity

The thermal conductivity was obtained with a DTC-25 guarded heat flow meter (TA Instruments) in accordance with the ASTM E1530 standard. Test specimens with 50.8 mm (2 inches) diameter were subsequently placed between the upper heating plate and the lower cooling plate of the device. A pressure of 20 psi applied on the upper plate ensured intimate contact between the sample, the heating and the cooling plates. A heat flux transducer in the lower plate measured the heat flow Q through the sample. The thermal conductivity λ is defined by (4.1), with the sample surface A , its thickness t and the temperature drop over the sample volume ΔT . The measurements were conducted for a medium sample temperature of 25 °C. In order to assure the thermal stability of all test specimens during the measurements, each sample was left inside the test chamber for two hours before the thermal conductivity values were obtained.

$$\lambda = \frac{Q/A}{\Delta T/t} \quad (4.1)$$

4.3.6 Dielectric spectroscopy

The frequency- and temperature-dependent dielectric responses of the samples were obtained by Broadband Dielectric Spectroscopy (BDS, Novocontrol) for a temperature range from 20 °C to 100 °C (± 0.1 °C), in several distinct isothermal steps. The test specimens were subjected to an excitation voltage of 1 V with a frequency ranging from 0.1 Hz to 1 MHz. The BDS measurements were performed on 40 mm diameter samples on a parallel plate electrode setup. The complex permittivity ε^* as given in (4.2) was retrieved, with the real permittivity ε' representing the storage part, and ε'' the imaginary or dielectric loss part.

$$\varepsilon^* = \varepsilon'(f, T) - j\varepsilon''(f, T) \quad (4.2)$$

4.4 Experimental results and discussion

4.4.1 Microstructure analysis

In Figure 4.3, the SEM micrographs of neat epoxy and the POSS-composites are presented. The left column shows the microstructure obtained with low magnification (x5k) on the TM3030 SEM. The next two columns represent SEM micrographs obtained with the high resolution Hitachi SU-70 microscope using x20k and x50k magnification, respectively. For the ePOSS 1wt% and ePOSS 2.5wt% composites (Figure 4.3b and Figure 4.3c), the micrographs obtained up to a magnification of x50k did not show any particular trace of the presence of POSS additive, and hence, the revealed microstructures resemble those obtained for the neat epoxy (Figure 4.3a). The POSS additive thus appears to be dispersed into the epoxy matrix at a molecular level or to very small agglomerates of less than 10 nm if any, which allows us to consider these specific materials as actual nanocomposites. However, for the composites with higher filler contents, viz. ePOSS 5wt% (Figure 4.3d) and ePOSS 10wt% (Figure 4.3e), agglomerations of submicrometric dimensions ($< 1 \mu\text{m}$) were found. Further, both the size and the occurrence of these agglomerated structures increased with the POSS content.

4.4.2 Differential scanning calorimetry

The resulting graphs obtained from the DSC experiments are presented in Figure 4.4. The derived glass transition temperatures T_g are summarized in Table 4.1. It was found that incorporating POSS into the epoxy matrix led to a slight diminishment of T_g for all composites, compared to the neat polymer. The highest difference was found for the ePOSS 10wt% composite, which exhibited a glass transition temperature of almost 6 °C lower than that of neat epoxy.

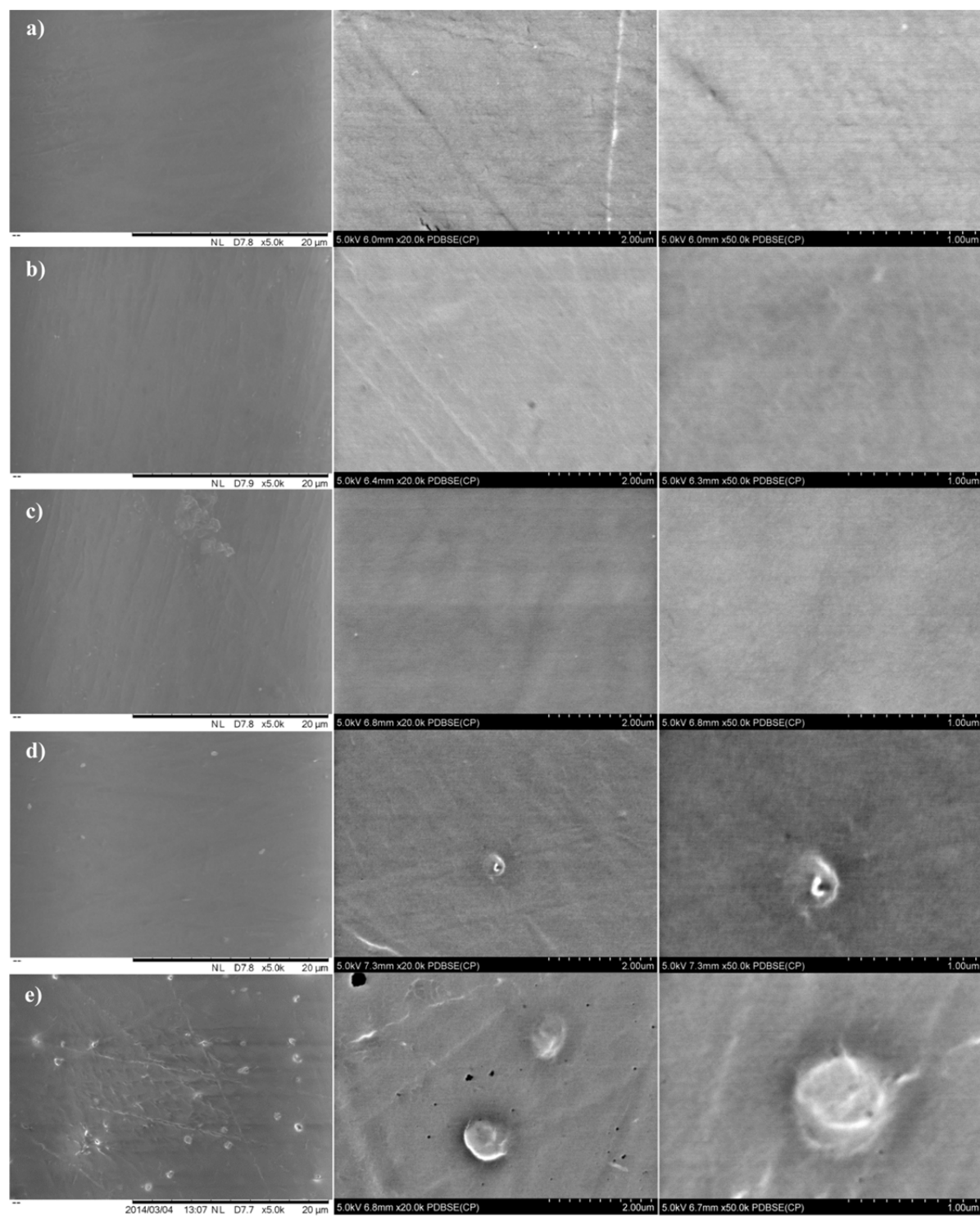


Figure 4.3 SEM micrographs with increasing magnification from left to right, for a) neat epoxy, b) ePOSS 1wt%, c) ePOSS 2.5wt%, d) ePOSS 5wt% and e) ePOSS 10wt%

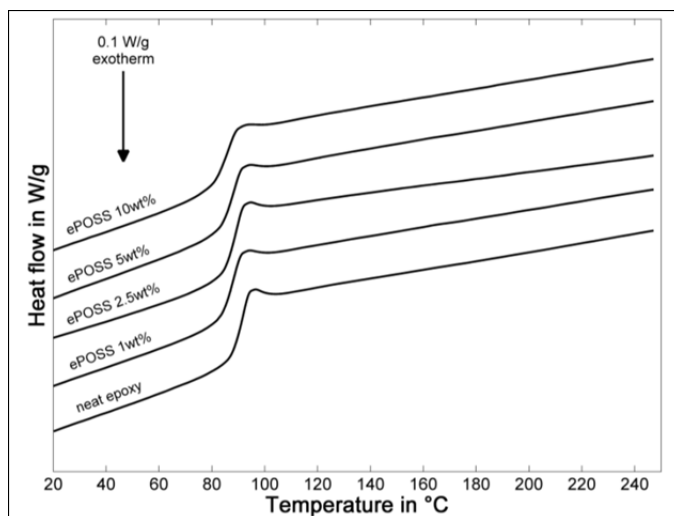


Figure 4.4 Overlaid DSC curves from the second thermal cycles

It is common understanding that T_g is closely related to the mobility of the molecular chains of the epoxy network. The mobility of the chains will further depend on factors such as the degree of cross-linking, chain lengths, flexibility of side-groups and chains, as well as free volume, as has been elaborated in detail in this extensive review (Nakka, 2010).

Considering the slight decrease in T_g for the POSS composites compared to the neat polymer, it is assumed that the cross-linking of the epoxy matrix is hindered in the presence of Triglycidylisobutyl-POSS. Additionally, the mono-directional alignment of epoxy groups on

Table 4.1 Glass transition temperatures of neat epoxy and TGIB-POSS composites

Sample type	T_g in °C
Neat epoxy	92.0
ePOSS 1wt%	88.6
ePOSS 2.5wt%	89.6
ePOSS 5wt%	88.6
ePOSS 10wt%	86.5

these particular POSS molecules might lead to shorter polymer chains, given that the chain “growth” during the cross-linking process is limited to one side of the TGIB-POSS molecule. Also, auto cross-linking between TGIB-POSS molecules themselves could further contribute to the reduction of chain lengths and cross-linking degree of the resulting epoxy/POSS network. Lastly, it should be mentioned that for the composites containing 5 wt% and 10 wt%, it is possible that the involved POSS molecules in the agglomerates shown by the SEM micrographs (see Figure 4.3d and Figure 4.3e), will not, or not completely react with hardener molecules. This would lead to free volume due to excess hardener in those composites with high POSS content, which would support the lowest values of T_g for the ePOSS 10wt% composite.

4.4.3 AC breakdown strength

The obtained AC breakdown (BD) data were treated by the two-parameter Weibull distribution in accordance with the IEEE 930 standard in order to evaluate the breakdown strengths of the test specimens. In Figure 4.5, the Weibull plots are depicted, and the corresponding Weibull parameters α and β are summarized in Table 4.2. The scale parameter α represents the breakdown strengths in kV/mm at which 62.3 % of the samples experienced electric BD, while the shape parameter β is an inverse measure for the scatter of the BD data, meaning the higher it is, the lower the variation of the data to the Weibull distribution.

Compared to neat epoxy, which had a BD strength of 214.9 kV/mm, all POSS composites, with the exception of ePOSS 10wt%, exhibited significant increase in BD strength. The highest BD value was found for ePOSS 2.5wt% (241.7 kV/mm), followed by ePOSS 5wt% (234.6 kV/mm) and ePOSS 1wt% (225.6 kV/mm), whereas the 10 wt% composite (214.7 kV/mm) would perform just as neat epoxy. Thus, it seems there is an optimal TGIB-POSS content around 2.5 wt%, where this POSS additive is still homogeneously dispersed within the epoxy at a molecular level, without showing agglomerations. With a further increase of filler content, the presence of TGIB-POSS agglomerations, as observed by SEM (see Figure 4.3), will consecutively counteract the beneficial effect of POSS. Those

agglomerations will cause local electric field enhancements, which subsequently lead to higher electric stress in the vicinity of agglomerates, and further results in a decrease of the BD strength for the composites, until the amount and size of agglomerations have completely nullified the POSS contribution as in the case of the 10 wt% composite.

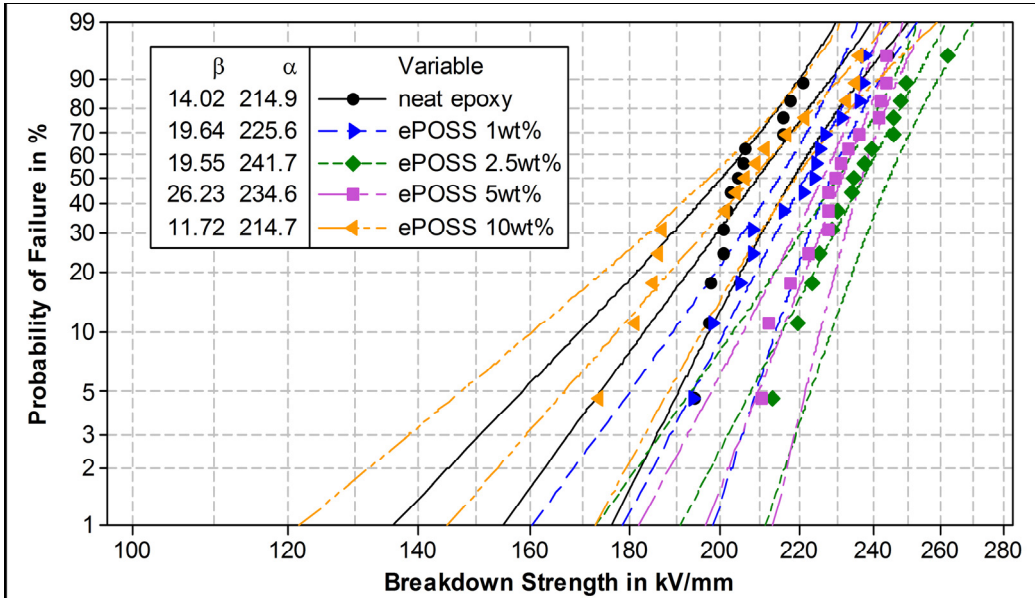


Figure 4.5 Weibull plot of breakdown data with 95 % confidence intervals

Table 4.2 Weibull parameters obtained from Figure 4.5

Sample type	α in kV/mm	β
Neat epoxy	214.9	14.02
ePOSS 1wt%	225.6	19.64
ePOSS 2.5wt%	241.7	19.55
ePOSS 5wt%	234.6	26.23
ePOSS 10wt%	214.7	11.72

Previous studies have shown increased BD strengths for epoxy composites with up to 2.5 wt% nano-silica, while incorporation of larger contents resulted in decreased BD values in comparison with the neat epoxy (Iyer et al., 2011; Preetha et Thomas, 2011). This could

most likely be attributed to conductive interfacial layers forming around silica nano-particles due to the hydrophilic nature of silica, creating conductive paths (Zou, Fothergill et Rowe, 2008), and thus, corrupting the BD strength of such composites.

The hydrophilicity of silica results from the formation of silanol groups at the silica particle surface (Laskowski et Kitchener, 1969). By using reactive TGIB-POSS molecules in our study, where organic groups surround the silica core, the resulting composites are not subject to the phenomenon of conductive paths around the filler. Thus, significant improvements of the dielectric strength of the resulting TGIB-POSS composites, as compared to neat epoxy, could be also achieved for comparably higher filler contents. Even more so, when agglomerations of POSS molecules can be avoided at higher filler loadings, as presented in one of our recent studies (Heid, Fréchette et David, 2014b).

4.4.4 Resistance to corona discharge

The results of the surface erosion experiment based on the respective eroded sample volumes after exposure to PD for 30 hours are presented in Figure 4.6. A decrease of eroded sample volume can be associated with an increase in resistance to electrical discharges. The experiment showed remarkable improvements in resistance to electrical discharge of all POSS composites, as compared to the neat polymer. With a 60 % and 59 % reduction in ablated material, for ePOSS 1wt% and ePOSS 2.5wt% respectively, the low content POSS composites revealed the best resistance to electrical discharges among all test specimens. With further increases of the POSS content, a continuous diminishment of resistance to PD was however noted for the resulting POSS composites with 5 and 10 wt% additive. This worsening of performance should be attributed to the occurrence of cumulative agglomerations with increasing POSS contents, as observed by SEM for ePOSS 5wt% and ePOSS 10wt% composites, and shown in Figure 4.3d and Figure 4.3e. Such agglomerations cause local electric field enhancements, which subsequently lead to locally increased electric and thermal stresses of the composite, resulting in intensified erosion of the surrounding organic matrix.

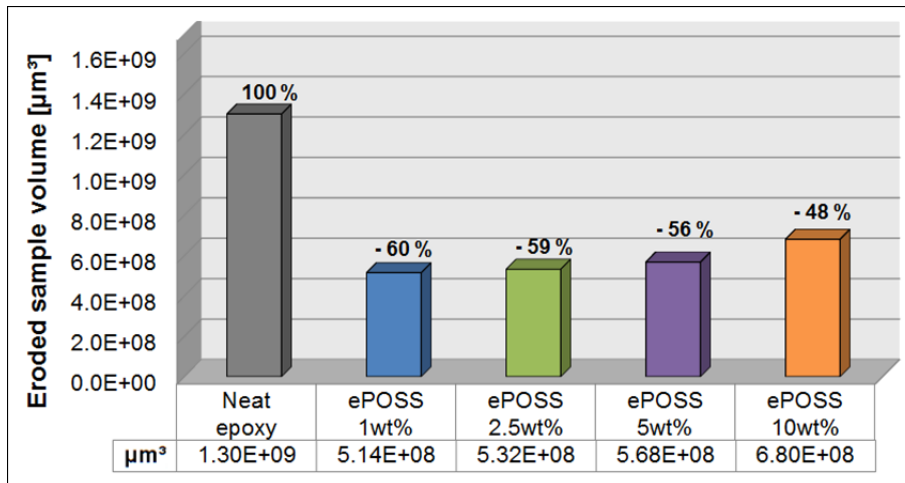


Figure 4.6 Evaluation of resistance to electrical discharges based on eroded sample volume after 30 hours of exposure to PD

Similar results for improved corona resistance of epoxy composites featuring inorganic nanofillers such as silica have been reported in the past (Brockschmidt et al., 2011; Kozako et al., 2005; Tanaka, Matsuo et Uchida, 2008). However, in some cases, very high nano-silica contents of 26 wt% and above (Brockschmidt et al., 2011) were needed to attain improvements comparable to those observed in this study, by incorporating 1 wt% of TGIB-POSS in epoxy. Thus, it is assumed that by dispersing POSS at a molecular level in epoxy, and because of the formation of covalent bonds between the POSS molecules with their inorganic cores and the epoxy matrix, the resulting change of morphology, and hence, the nanostructuring of the respective composite, gives rise to the significant resistance to corona discharges for the ePOSS 1wt% and ePOSS 2.5wt%. Coherent results with a different reactive POSS additive have been recently published in (Huang et al., 2014).

4.4.5 Thermal conductivity

The thermal conductivities were measured twice on each sample type, while considering that the reproducibility of the method used may vary by approximately 5 %. Further, the respective average values of thermal conductivities from those two measurement series were taken for the following discussion. The experimental results are displayed in Figure 4.7.

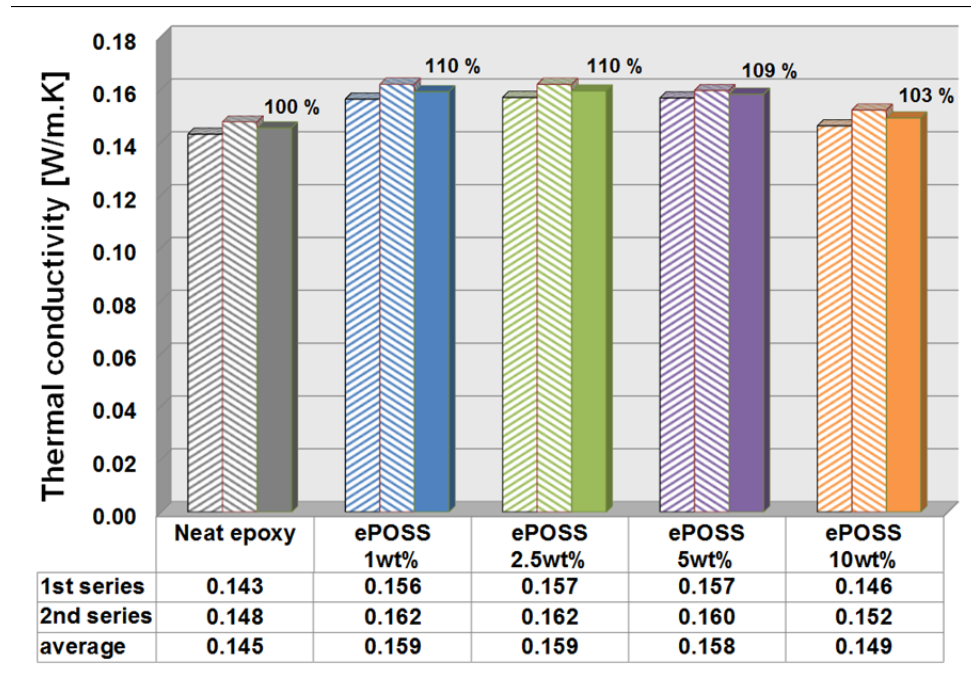


Figure 4.7 Evaluation of thermal conductivities for the test specimens, with the first and second measurement series plotted as dashed columns and the respective average values in solid columns

It was found that addition of TGIB-POSS in the epoxy matrix resulted in an increase in thermal conductivities of approximately 10 % for the respective composites with up to 5 wt% POSS content. The highest thermal conductivities were exhibited by both ePOSS 1wt% (0.159 W/m·K) and ePOSS 2.5wt% (0.159 W/m·K), followed by ePOSS 5wt% (0.158 W/m·K). However, ePOSS 10wt% (0.149 W/m·K) did not reveal a significant change in thermal conductivity, as compared to the neat polymer (0.145 W/m·K).

It is well established that thermal conduction in solid dielectrics is based on phonons (lattice vibrations) (Cui et al., 2011; Takezawa, Akatsuka et Farren, 2003). Phonon scattering, which appears at either particle-particle or particle-matrix interfaces, or at the interfaces of the amorphous structure in epoxy resins itself (Takezawa, Akatsuka et Farren, 2003), lead to attenuation of the thermal conductivity within a material. As a consequence, the addition of low contents (i.e. 1 wt%) of high thermally conductive filler was deemed insufficient for significant enhancements of the thermal conductivities of the resulting composites, as indicated in several studies (Heid, Fr chet te et David, 2014a; 2015b; Kochetov et al., 2009b).

However, it was established in (Takezawa, Akatsuka et Farren, 2003) that creating ordered, crystalline-like structures on a nanometric level within epoxy resins, which are characterized by their amorphous structure, would cause a diminishment of phonon scattering, and hence, significantly improve the thermal conductivity of the polymer. Accordingly, by adding POSS in the epoxy resin, which forms covalent bonds with the epoxy matrix, we succeeded in nanostructuring the resulting composites, which further resulted in reduced phonon scattering within the composite. In conclusion, the thermal conductivity of the POSS composites could be improved as compared to neat epoxy.

Nevertheless, there seems to be a threshold limit in the case of TGIB-POSS, due to agglomerations seen for the 5 wt% and especially the 10 wt% POSS composites. These agglomerations cause an augmentation of phonon scattering at matrix-particle interfaces, and hence, consecutively nullify the effect of nanostructuring. Consequently, this results in more or less equivalent thermal conductivities of ePOSS 1wt%, ePOSS 2.5wt% and ePOSS 5wt%. Moreover, in the case of ePOSS 10wt%, the numerous agglomerations might cause pronounced phonon scattering, which suppresses the beneficial effect seen for the composites with lower TGIB-POSS contents.

4.4.6 Dielectric spectroscopy

The dielectric responses obtained at 20 °C for all the investigated materials are presented in Figure 4.8. Both the real part of the complex permittivity (Figure 4.8a) and its imaginary component (Figure 4.8b) show that all composites exhibit dielectric responses similar to that of neat epoxy for power frequencies and above. For lower frequencies though, additional interfacial loss peaks were found for ePOSS 5wt% and ePOSS 10wt% (Figure 4.8b), being more pronounced for the 10 wt% composite. The corresponding steps in real permittivity could also be seen for lower frequencies in Figure 4.8a. However, ePOSS 1wt% and ePOSS 2.5wt% did not reveal such interfacial loss peaks, and hence, their dielectric responses are similar to that of neat epoxy.

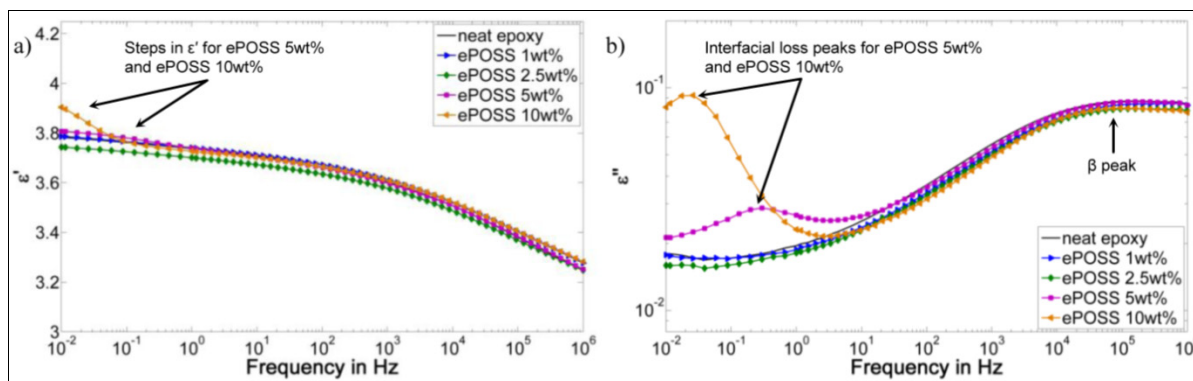


Figure 4.8 Dielectric responses at 20 °C and 1 V of neat epoxy and the TGIB-POSS composites; a) real parts and b) imaginary parts of the complex permittivities

The appearing interfacial loss peaks found for the composites containing 5 or 10 wt% POSS can be linked to the aforementioned agglomerations observed using SEM microscopy, as presented in Figure 4.3d and Figure 4.3e. These agglomerations give rise to interfacial polarization for the composites with high filler content. This is further supported by the lack of an additional loss peak for the 1 and 2.5 wt% composites, as well as by the microstructure analysis where no agglomerations were found for these two composites (Figure 4.3b and Figure 4.3c). It therefore seems, analogous to the results already presented in the previous subsections, that for low TGIB-POSS contents a good dissolution in epoxy is possible, allowing a dispersion of POSS at a molecular level. Consequently, no additional interfacial polarization occurs (Fr chet te et al., 2014).

Figure 4.9a to Figure 4.9e show the temperature- and frequency-dependent dielectric response of all test specimens. The α - and β -relaxation peaks could be located for neat epoxy and the epoxy/POSS composites, for both the real and imaginary parts of the complex permittivity. In amorphous polymers, the α -relaxation is correlated to relaxation processes of the main polymer backbone due to chain movement as a result of the glass transition phenomenon. The β -peak however, is associated with secondary relaxation processes due to local crankshaft movements of hydroxyl ether groups in the case of epoxy resin (Lee et al., 2003).

For all investigated materials, the β -peak was located for temperatures below 80 °C, in the vicinity of 100 kHz. The α -peak was found at 100 °C, with a loss maximum around 100 Hz for neat epoxy, ePOSS 1wt%, ePOSS 2.5 wt% and ePOSS 5 wt% (see Figure 4.9a' to Figure 4.9d'). With the incorporation of 10 wt% POSS, the α -peak was shifted slightly towards higher frequencies though, as shown in Figure 4.9e'. This result is in good correlation with the glass transition values presented in paragraph 4.4.2. Given that the 10 wt% composite has the lowest T_g , the α -relaxation process is initiated at lower temperatures, as compared to neat epoxy, and hence, the peak is shifted to slightly higher frequencies at 100 °C.

Analogous to the observations made at 20 °C (see Figure 4.8), at temperatures of 80 °C and below, the BDS analysis revealed similar ϵ' for neat epoxy, ePOSS 1wt% and ePOSS 2.5wt%, while ePOSS 5wt% and ePOSS 10wt% exhibited steps in ϵ' in the low frequency domain (see Figure 4.9a to Figure 4.9e). Those steps were much more distinct for the 10 wt% composite. According to these steps in ϵ' , additional interfacial loss peaks in ϵ'' could be seen for ePOSS 5wt% and ePOSS 10wt%, with higher magnitudes for the 10 wt% composite (Figure 4.9d' and Figure 4.9e').

This interfacial loss peak was more difficult to detect at a temperature of 80 °C in the case of ePOSS 5wt% and it was completely overshadowed by low-frequency dispersion due to charge fluctuations for a temperature of 100 °C for both, ePOSS 5wt% and ePOSS 10wt%.

The increasing dielectric losses at 100 °C for lower frequencies with a slope $\neq -1$ on the log-log scale, accompanied with the increasing real part of the permittivity for frequencies below 1 Hz, translates a more complex behavior than simple DC conductivity of being responsible for the increasing dielectric losses (Iyer et al., 2011). The low frequency dispersion at 100 °C can be explained by interfacial polarization on a macroscopic level at the electrode/sample interface, the so called electrode polarization (Kremer, 2003), possibly superimposed by electronic conductivity. This is a rather common behavior for solid insulating materials at elevated temperatures (Preda et al., 2013).

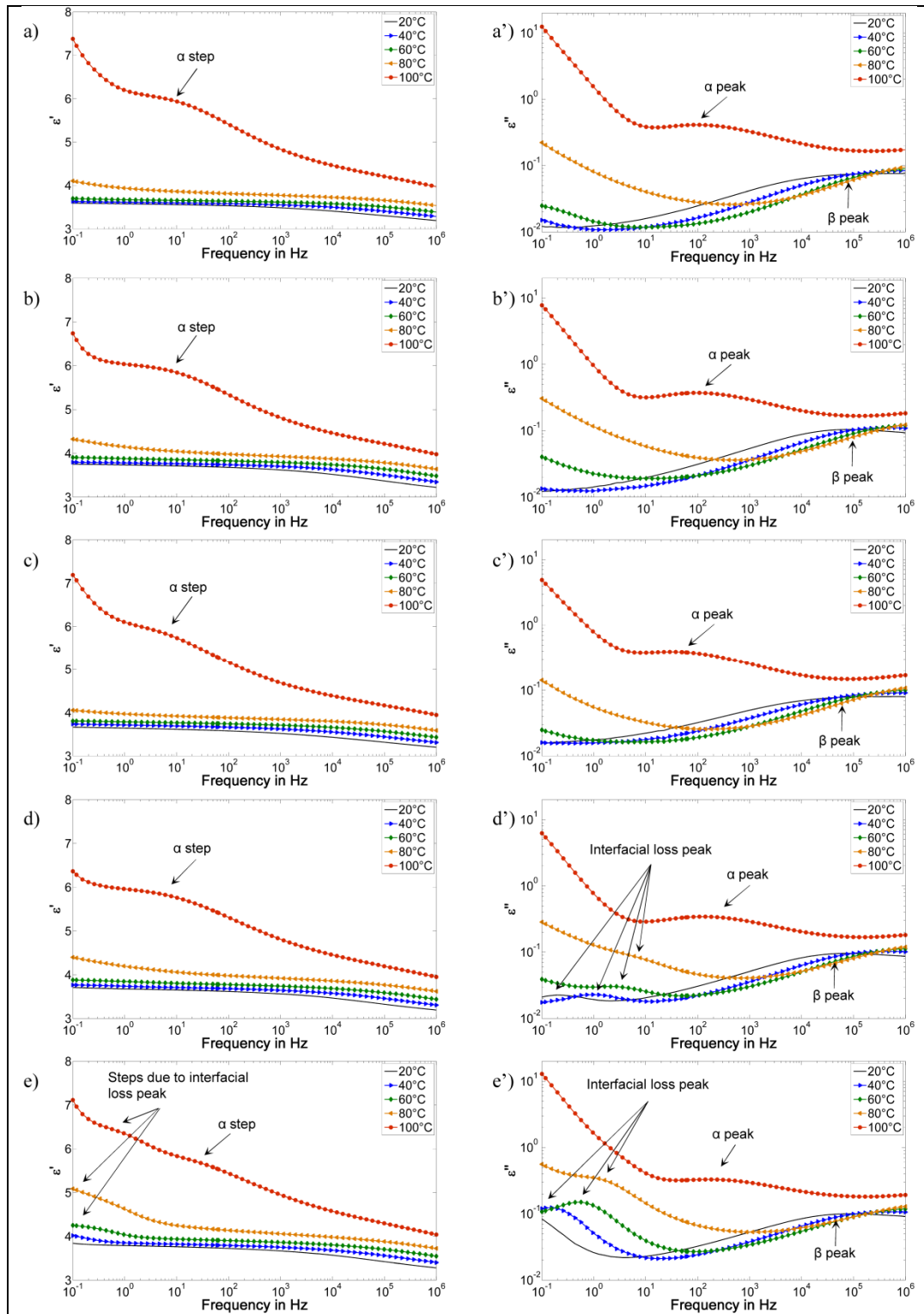


Figure 4.9 Temperature-dependent real part (left column) and imaginary part (right column) of complex permittivity for a) neat epoxy, b) ePOSS 1wt%, c) ePOSS 2.5wt%, d) ePOSS 5wt% and e) ePOSS 10wt%

4.4.7 Relaxation behavior

For further understanding of the relaxation behavior of polymer composites, their dielectric responses are frequently fitted by an empirical equation (4.3) proposed by Havriliak and Negami (Kremer, 2003), as it is known to be valid for polymers as well as inorganic materials:

$$\varepsilon^*(\omega) = \varepsilon_{\infty} + \frac{\Delta\varepsilon}{(1 + (i\omega\tau)^{\alpha_{HN}})^{\beta_{HN}}} \quad (4.3)$$

The frequency-dependent complex permittivity $\varepsilon^*(\omega)$ can be approximated by (4.3), where ε_{∞} is the high frequency permittivity, $\Delta\varepsilon$ the dielectric relaxation strength, ω the angular frequency ($\omega=2\pi \cdot f$), τ the relaxation time, α_{HN} and β_{HN} (with $0 < \alpha_{HN} < 1$ and $\beta_{HN} > 0$) the Havriliak-Negami parameters which designate, respectively, the symmetric and asymmetric broadening of the relaxation time distribution function. When the shape parameters (α_{HN} and β_{HN}) are equal to 1, equation (4.3) is simplified, and the relaxation law proposed by Debye (Raju, 2003) is obtained.

In this study, the relaxation behavior of our test specimens was further analyzed by fitting the β -relaxation peaks of the imaginary part of the complex permittivity in order to obtain the corresponding relaxation times. After the corresponding relaxation times were obtained for all the investigated temperatures, the molecular mobility of polymer chains participating in the β -relaxation process was investigated, as described by the Arrhenius law:

$$\tau_{\beta} = \tau_{0,\beta} \exp\left(\frac{E_a}{k_B T}\right) \quad (4.4)$$

According to the Arrhenius law, the relaxation time τ_{β} , which is inversely proportional to the molecular mobility, can be described with the pre-exponential factor $\tau_{0,\beta}$, the activation energy E_a of the β -relaxation process and the Boltzmann's constant k_B . The global error, obtained after both the fitting of the β -relaxation and the derivation of the parameters of the Arrhenius law, was below 10 %.

The relaxation plots and activation energies for the samples are depicted in Figure 4.10 and Table 4.3, respectively. It can be seen that neat epoxy and all POSS composites, with the exception of the 2.5 wt% composite, show very similar β -relaxation behaviors and activation energies. However, ePOSS 2.5wt% differs significantly, resulting in over 65 % increased activation energy. This means, that by addition of 2.5 wt% POSS to the epoxy matrix, the molecular movements during the β -relaxation process are notably hindered. It appears that due to the good dispersion of POSS, along with the formation of covalent bonds between the filler and the epoxy, a more rigid epoxy/POSS network is obtained. Such an increase in the rigidity of the epoxy/POSS network is the result of incorporating the rigid silica-like cage structure of POSS into the matrix.

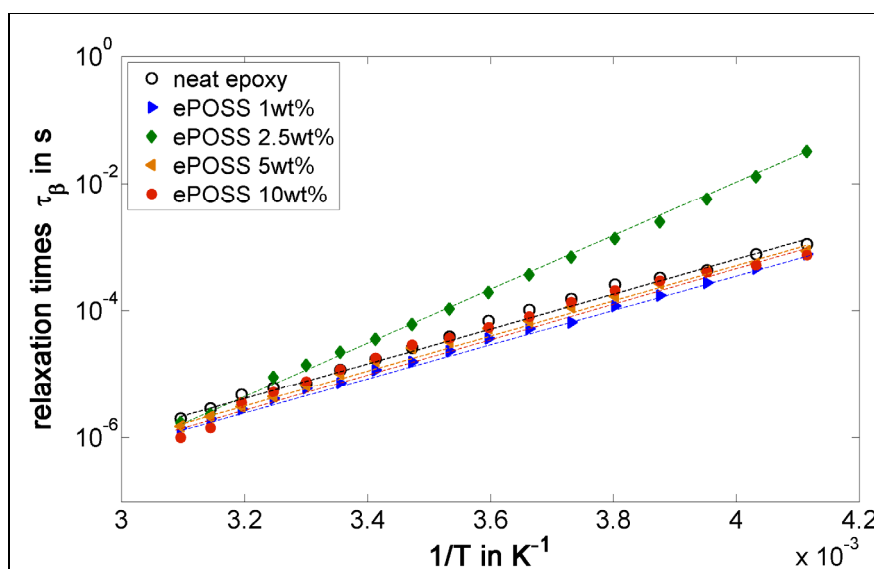


Figure 4.10 Relaxation time plots of the β -relaxation process

However, if only 1 wt% POSS is added to the epoxy, this effect might not be that significant, and similarly, for the higher filler content composites with 5 wt% and 10 wt% POSS, where due to the formation of agglomerations not enough POSS could be integrated into the epoxy network, and hence, no distinct change in the rigidity of the molecular web resulted. These findings are supported by the aforementioned improvements in BD strength, erosion resistance and thermal conductivity, where the ePOSS 2.5wt% composite out-performed neat epoxy and the other POSS composites, significantly in some cases.

Table 4.3 Activation energies obtained by fitting the β -relaxation process

Sample type	E_a in eV
Neat epoxy	0.526
ePOSS 1wt%	0.526
ePOSS 2.5wt%	0.875
ePOSS 5wt%	0.523
ePOSS 10wt%	0.504

4.5 Concluding remarks

The aim of this study was to investigate the dielectric and thermal properties of epoxy/POSS composites, along with the effect of nanostructurization of composites, by incorporating a reactive TGIB-POSS and dispersing it at a molecular level.

It has been shown that the addition of low amounts of TGIB-POSS (≤ 5 wt%) leads to significantly improved dielectric breakdown strengths, corona resistances, as well as thermal conductivities of the resulting epoxy/POSS composites. It is assumed that the formation of covalent bonds between the filler and the epoxy matrix significantly improves the filler/matrix interaction, leading to intimate *interfaces* instead of undefined *interphases*, and hence, contributes to a distinct improvement in performance for the resulting composites. This is supported by the superior performances of the lower content composites ePOSS 1wt% and ePOSS 2.5wt%, where no agglomerations were found, and hence, the dispersion of POSS at a molecular level in the epoxy has been successfully achieved.

In conclusion, although we used a reactive additive, agglomerations could not be avoided for higher filler contents. This prohibited the incorporation of a larger POSS content in the epoxy network, which should be beneficial for further improvements in dielectric performance, such as the resistance to corona discharges. The limited dissolubility of the used TGIB-POSS

in epoxy can be attributed to its low degree of reactivity (only 3 epoxy side groups around the silica-like core). In fact, when a different POSS additive with a higher degree of reactivity, and hence, a higher amount of epoxy side-groups, was used to fabricate epoxy composites, we successfully incorporated even larger contents of POSS into the epoxy matrix, without finding agglomerations. Consequently, the corona resistance of these composites could be enhanced even more significantly (Heid, Fréchette et David, 2014b).

4.6 Acknowledgment

Hydro-Québec and the Natural Sciences and Engineering Research Council of Canada (NSERC) are gratefully recognized for their financial support.

CHAPTER 5

ENHANCED ELECTRICAL AND THERMAL PERFORMANCES OF NANOSTRUCTURED EPOXY/POSS COMPOSITES

Thomas Heid^{1,2}, Michel Fréchet², Eric David¹

¹ Department of Mechanical Engineering, École de Technologie Supérieure,
1100 Notre-Dame West, Montreal, Quebec, (H3C 1K3) Canada

² Hydro-Québec's Research Institute,
1800 Boulevard Lionel-Boulet, Varennes, Quebec, (J3X 1S1) Canada

This article has been submitted for publication to:

IEEE Transactions on Dielectrics and Electrical Insulation

Abstract

Epoxy resins modified with Glycidyl-POSS (Polyhedral Oligomeric Silsesquioxanes) in contents of up to 20 wt% were fabricated and studied in terms of dielectric spectroscopy, differential scanning calorimetry, AC breakdown tests, thermal conductivity measurements and corona resistance. Microstructure analysis have revealed a molecular dispersion of Glycidyl-POSS up to contents of 10 wt%, whereas in the 20 wt% Glycidyl-POSS composites crystalline zones due to POSS could be observed by both scanning electron microscopy (SEM) and transmission electron microscopy (TEM). All Glycidyl-POSS composites have seen a significant improvement in AC breakdown strength, as well as an enhanced resistance to corona discharges, which in the latter case was getting more pronounced with higher Glycidyl-POSS loadings. On the contrary, low Glycidyl-POSS contents proofed most effective in improving the thermal conductivity, which should be attributed to the effect of POSS on the nanostructure of the polymeric network.

Keywords: Corona resistance, dielectric spectroscopy, dielectric breakdown strength, epoxy composites, polymer nanodielectric, POSS, silica, thermal conductivity

5.1 Introduction

Polymer-based electrical insulating materials, also called polymer dielectrics, are widely found in insulation systems in power generation, transformation and distribution systems. Due to the organic nature of these materials used for high voltage insulation, such as epoxy resins, they are subject to electrical degradation as a result of corona discharges, for instance (Dissado et Fothergill, 1992; Iyer, Gorur et Krivda, 2014; Li et al., 2011; Tanaka, Matsuo et Uchida, 2008). Additionally, polymers commonly feature low thermal conductivities (Heid, Fréchette et David, 2015b; Kochetov et al., 2009b; Takezawa, Akatsuka et Farren, 2003; Tanaka et al., 2011; Tsekmes et al., 2014), which is a major limiting factor for dielectrics that undergo high electro-thermal stresses during operation.

Accordingly, there is an increasing interest in nano-composite research in the scientific community in terms of dielectric materials, for more than one decade (Heid, Fréchette et David, 2015c; Nelson et Hu, 2005; Nelson et Fothergill, 2004; Nelson, 2010; Tanaka et Imai, 2013; Tuncer et al., 2007a). This novel class of dielectric materials is commonly called polymer nanodielectrics. The presence of inorganic nanometer-sized particles in the organic polymer matrix can render the resulting composites more resilient to electro-thermal stresses and improve parameters such as thermal conductivity or dielectric breakdown strength (Andritsch et al., 2010; Nelson, 2010; Tuncer et al., 2010; Tuncer et al., 2007b).

Promising filler materials, especially in the case of epoxy resins, are Polyhedral Oligomeric Silsesquioxanes (POSS). Unlike other commonly used inorganic nanofillers such as silica (Brockschmidt et al., 2011; Fabiani et al., 2010; Nguyen et al., 2015), POSS is a hybrid material that features an inorganic silica-like core and organic side-groups. When these organic side-groups are of reactive nature and compatible with the epoxy system used, as is the case for the POSS additives further used in this study, the POSS molecules can covalently bond with the epoxy matrix. This thus leads to an intimate interaction between the POSS molecules (approx. 2 nm in size) and the polymer, resulting in a re-structuration of the polymer network on a nanometric scale. As a result, epoxy/POSS composites have revealed

notable improvements in both, dielectric and thermal performances, as published in recent studies (Heid, Fréchette et David, 2014b; 2014c; 2015c; Huang et al., 2014).

In this study, the potential of nanostructured epoxy/POSS composites for high voltage insulation is evaluated using a highly reactive Glycidyl-POSS as an additive that can covalently bond with the epoxy system used. Due to its high reactivity, meaning a high amount of reactive epoxy groups attached to the inorganic silica core, this specific POSS type is thought to be dispersible within the epoxy matrix at a molecular level.

5.2 Materials and sample preparation

DER332 epoxy resin (DOW Chemical Company) and Jeffamine D230 curing agent (Huntsman Corp.) were used as the base polymer in a ratio of 344 parts curing agent to 1000 parts of resin. The base epoxy was further modified with a liquid Glycidyl-POSS (from Hybrid Plastics Inc.), in contents ranging from 1 to 20 wt%, to fabricate composites. This specific type of POSS features 8 to 12 epoxy groups attached to the silica core (see Figure 5.1 on top left), and thus can form covalent bonds during the curing reaction with the epoxy system used. The formation of covalent bonds between the POSS additive and the base epoxy will lead to a structuration of the epoxy network on a nanometric level, as it is proposed in Figure 5.1 (bottom).

In case of neat epoxy specimens (NE), the DER332 resin and the D230 curing agent were mixed on a hot plate at 40 °C, employing a magnetic stir. The mixing process was conducted in a special vessel that could be evacuated, so that air inclusions and residual humidity in the liquid composite could be removed. When epoxy/POSS composites were to be fabricated, the liquid Glycidyl-POSS (G-POSS) additive was first dispersed in the epoxy resin with the magnetic stir on a hot plate at 40 °C. After dispersing the POSS additive in the epoxy resin, the curing agent was added to the mixture, and likewise dispersed with the magnetic stir on the hotplate at 40 °C. All these mixing processes were conducted in the above-mentioned evacuated vessel. Considering that each POSS molecule introduces reactive epoxy groups in

the mixture, which will then consume curing agent during the reticulation process, a distinct stoichiometric ratio between epoxy resin, curing agent and POSS was established for each composite, depending of the respective amount of G-POSS added. A summary of the produced samples and the sample codes used during the discussion of this work is provided in Table 5.1.

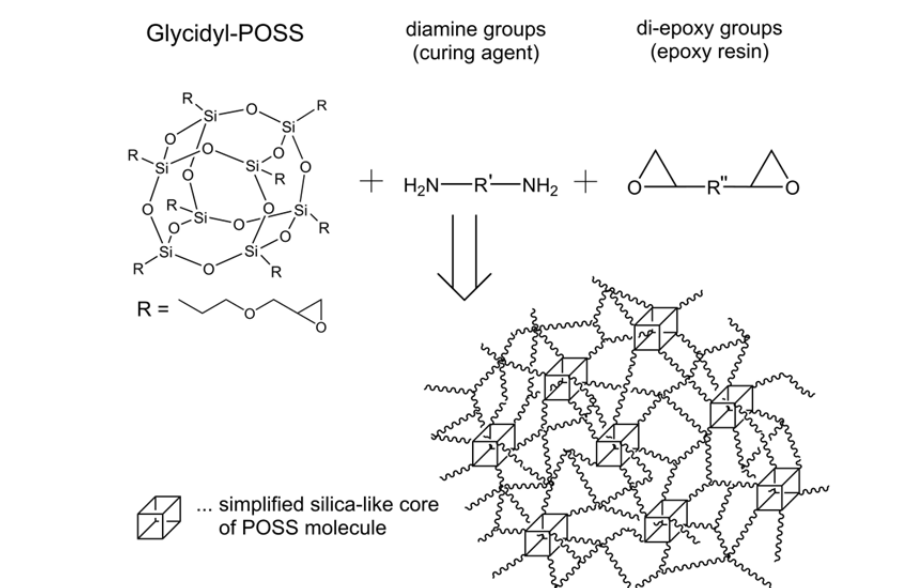


Figure 5.1 Structure of a Glycidyl-POSS molecule in its cage-form (with 8 epoxy groups) reacting with the curing agent and the epoxy resin (top) to form a nano-structured epoxy/POSS composite due to the formation of covalent bonds between the constituents (bottom)

Table 5.1 Overview and nomenclature of prepared samples

Sample code	Sample nature
NE	Neat epoxy
GP 1wt%	Epoxy + G-POSS 1wt%
GP 2.5wt%	Epoxy + G-POSS 2.5wt%
GP 5wt%	Epoxy + G-POSS 5wt%
GP 10wt%	Epoxy + G-POSS 10wt%
GP 20wt%	Epoxy + G-POSS 20wt%

5.3 Experimental methods

5.3.1 Microstructure analysis

The microstructure of the test specimens was evaluated with scanning electron microscopy (SEM) and transmission electron microscopy (TEM). For SEM observations, the samples were mounted in an electrically conductive epoxy and subsequently polished with abrasive materials of gradually decreasing particle sizes down to 50 nm, to obtain a smooth surface for high magnification observations with the SEM. The specimens were additionally sputter-coated with a 2 nm Platinum layer. Both, the conductive epoxy as a mount and the coated Platinum layer, helped to avoid charging phenomena due to the electron beam during SEM observations, and allowed us to obtain highly resolved images even at high magnifications of up to x200k. The employed SEM was a SU-70 high resolution SEM (Hitachi High Technologies America). For TEM observations, thin sections of approximately 50 to 80 nm were first cut from the specimen using a cryogenic ultra-microtome at -100 °C, and then deposited on copper grids. The used TEM was a JEM-2100F (Jeol USA, Inc.).

5.3.2 Differential scanning calorimetry

Glass transition temperatures T_g were measured by Differential Scanning Calorimetry (DSC) with a heat flow calorimeter (Q20, TA Instruments). Each specimen was subjected to two thermal cycles with a heating rate of 10 °C/min from 20 °C to 250 °C and a gradual cool down to 20 °C also at 10 °C/min between the two heating cycles. The T_g were obtained from the second heating cycle to avoid any thermal history of the test specimens.

5.3.3 AC breakdown strength

The AC breakdown strength was retrieved based on the ASTM D149 standard. Samples were immersed in transformer oil and positioned between two ball tip electrodes with a 4 mm diameter. The short-term test was used, where a 60 Hz voltage with a ramp rate of 2 kV/s was applied between the electrodes until breakdown occurred. Ten breakdowns were carried

out for each sample type, after which the ball tip electrodes were replaced by new ones, in order to avoid pitting. The test specimens used for this experiment had a thickness of 135 μm .

5.3.4 Resistance to corona discharges

In order to evaluate the resistance of our materials to electrical discharges, each specimen was first subjected to corona discharges during a period of 30 hours at ambient temperature. Therefore the test specimens, with a diameter of 40 mm, were placed in a self-built setup (see Figure 5.2), aligned concentrically between the upper high voltage (HV) rod electrode and the ground electrode at the bottom. The tungsten carbide ball tip of the HV electrode had a diameter of 4 mm and was adjusted at 200 μm distance to the sample surface. A sinusoidal voltage with 4 kV_{RMS} at a frequency of 300 Hz was applied between the HV and ground electrodes. After 30 hours of exposure to the corona discharges, the samples were removed from the setup and carefully cleaned in an ultrasonic bath to remove surface debris left after the erosion process. As an inverse reference for the materials' resistances to corona discharges, the respective eroded sample volumes (in μm^3) were then assessed using a mechanical profilometer. Accordingly, the less sample material was ablated during the exposure to corona, the higher is the sample's resistance to erosion.

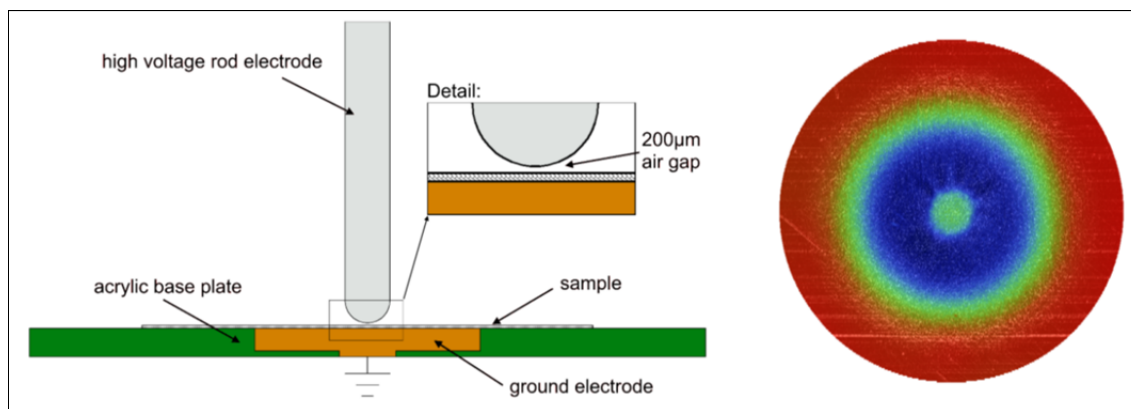


Figure 5.2 Schematic of the erosion setup used (on the left) and a typical 3D erosion pattern retrieved on a NE sample (right) viewed from the top. The original sample surface is colored in red, and the zones with the deepest erosion traces are represented in blue

5.3.5 Thermal conductivity

The thermal conductivities of the test specimens were measured with a DTC-25 guarded heat flow meter (TA Instruments) in accordance with the ASTM E1530 standard. Circular samples with 50.8 mm (2 inches) in diameter were placed between the upper heating plate and the lower cooling plate of the instrument. Applying a pressure of 20 psi on the upper plate ensured intimate contact between the sample, the heating and the cooling plates. The thermal conductivity values were assessed for a mean sample temperature of 25 °C. The specimens remained inside the test chamber of the DTC-25 setup for two hours, before obtaining the thermal conductivity values, to allow a thermal stabilization of the samples.

5.3.6 Dielectric spectroscopy

The dielectric response was evaluated on samples 40 mm in diameter and with an average thickness of 300 µm by the use of Broadband Dielectric Spectroscopy (BDS, Novocontrol Technologies GmbH), as a function of applied voltage, frequency and temperature. An excitation voltage of 1 V was applied and the complex dielectric permittivity was measured for temperatures from -100 °C to +180 °C, and for a frequency range of 0.1 Hz to 1 MHz. The complex permittivity ε^* as given in (5.1) was obtained with the real permittivity ε' representing the storage part and ε'' the imaginary or dielectric loss part.

$$\varepsilon^*(f, T) = \varepsilon'(f, T) - i\varepsilon''(f, T) \quad (5.1)$$

5.4 Results and discussion

5.4.1 Microstructure analysis

The microstructure of the test specimens was assessed by SEM with magnifications from x10k up to x200k. Only the SEM micrographs taken with the highest magnifications (x200k) are presented in Figure 5.3, for the sake of brevity.

It was found, that all composites containing from 1 wt% up to 10 wt% of Glycidyl-POSS revealed a homogeneous microstructure, similar to the one found for NE. Therefore, it can be concluded that in these composites a molecular dispersion of the POSS additive could be achieved. However, numerous zones of a darker contrast and with varying sizes were observed for the GP 20wt% composite. With TEM it could be seen, that these darker regions were in fact crystalline structures (see Figure 5.3, on the bottom right), which consisted of several hexagonal substructures itself. The observed crystalline regions had sizes starting from just a few nanometers up to some hundreds of nanometers. Thus, it appears that for high concentrations, the Glycidyl-POSS molecules react with each other to form crystalline regions within the otherwise amorphous epoxy.

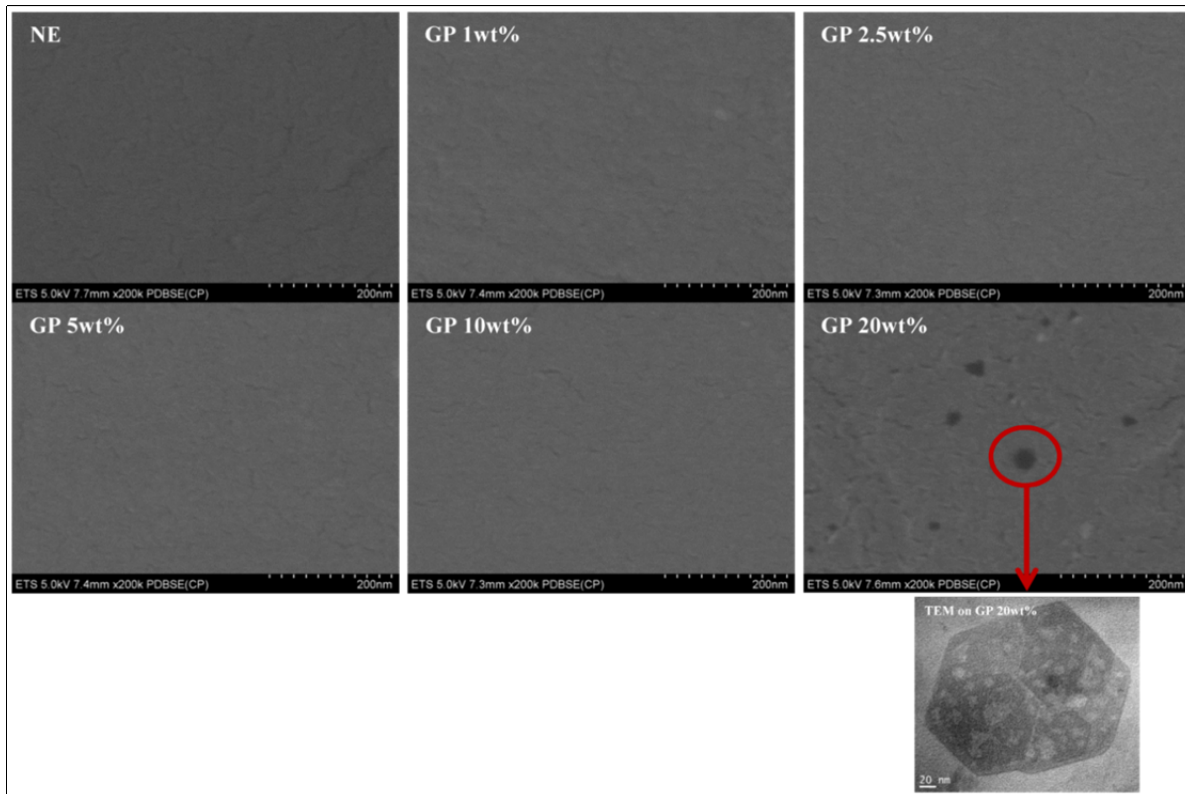


Figure 5.3 SEM micrographs of the samples at a magnification of x200k (upper six images) and a TEM image showing a zoom on one crystalline structure found in the GP 20wt% composites (bottom right), which itself consists of several hexagonal substructures. The crystalline structures had sizes starting from just a few nanometers up to some hundreds of nanometers

5.4.2 Differential scanning calorimetry

The glass transition temperatures retrieved from the DSC experiment are presented in Table 5.2. It was found, that the composites containing 1 wt% to 10 wt% G-POSS showed very similar values of T_g compared to the one of NE, which was 92°C. GP 1wt% and GP 10wt% have seen a marginally decreased T_g by 1.5 °C compared with NE though. More importantly, the incorporation of 20 wt% G-POSS has led to a significant decrease in T_g by 7 °C.

It is common understanding that T_g is closely related to the mobility of the molecular chains of the epoxy network. The mobility of the chains will further depend on factors such as the degree of cross-linking, chain lengths, flexibility of side-groups and chains, as well as free volume, as has been elaborated in detail in this extensive review (Nakka, 2010). Thus, it appears that the GP 20wt% composite has seen a lower degree of crosslinking, most likely due to inter-reaction of POSS molecules with each other, to form the crystalline zones observed by SEM and TEM (see Figure 5.3). This decrease in cross-linking degree, will result in a higher chain mobility of the polymeric backbone during the glass transition process, and hence lead to a lower T_g of the composite.

Table 5.2 Glass transition temperatures T_g of test specimens

Sample code	T_g (°C)
NE	92.0
GP 1wt%	90.5
GP 2.5wt%	91.5
GP 5wt%	92.0
GP 10wt%	90.5
GP 20wt%	85.0

5.4.3 AC breakdown strength

The AC breakdown (BD) data obtained were processed with the two-parameter Weibull distribution according to the IEEE 930 standard, to evaluate the AC breakdown strengths of the test specimens. The cumulative failure probability $P(E_{BD})$ in % reads:

$$P(E_{BD}) = 1 - \exp \left[- \left(\frac{E_{BD}}{\alpha} \right)^\beta \right] \quad (5.2)$$

where E_{BD} is the experimental value of the dielectric breakdown strength in kV/mm, α is the scale parameter representing the breakdown strengths in kV/mm at which 62.3 % of the samples experienced electric BD, and the shape parameter β , which is an inverse measure for the scatter of the BD data, meaning the higher it is, the lower the variation of the data to the Weibull distribution. In accordance with the IEEE 930 standard, the cumulative failure probability for the experimental data of E_{BD} can be approximated by:

$$P(i, n) = \frac{i - 0.44}{n + 0.25} \quad (5.3)$$

where i denotes the result of the i^{th} rank, when all values of $E_{BD,i}$ are sorted in ascending order, and n represents the number of data points. In this work, $n=10$.

The Weibull plots of the BD experiment are presented in Figure 5.4 and the respective Weibull parameters are listed in Table 5.3. It was found that all the POSS composites have seen a significant improvement in AC BD strength compared to the neat epoxy sample, which itself had a BD strength of 208 kV/mm. The GP 2.5wt% composite has seen the highest increase in BD strength by 17 % to 244 kV/mm, whereas the other POSS composites have revealed very similar BD strengths, with the exception of GP 20wt%. This composite's BD strength only has seen an improvement by approximately 13 % compared to NE.

It is assumed, that by incorporation of POSS in the epoxy matrix, a reorganization or re-structuration of the epoxy matrix follows during the reticulation process. Due to the reactivity of the Glycidyl-POSS used, additional cross-linking sites are introduced in the epoxy/POSS composites, which might increase the cross-linking density in the composite materials, compared to the amorphous epoxy resin itself, thus leading to lower free volume, and accordingly, to increased BD strengths for the POSS composites compared to the neat polymer.

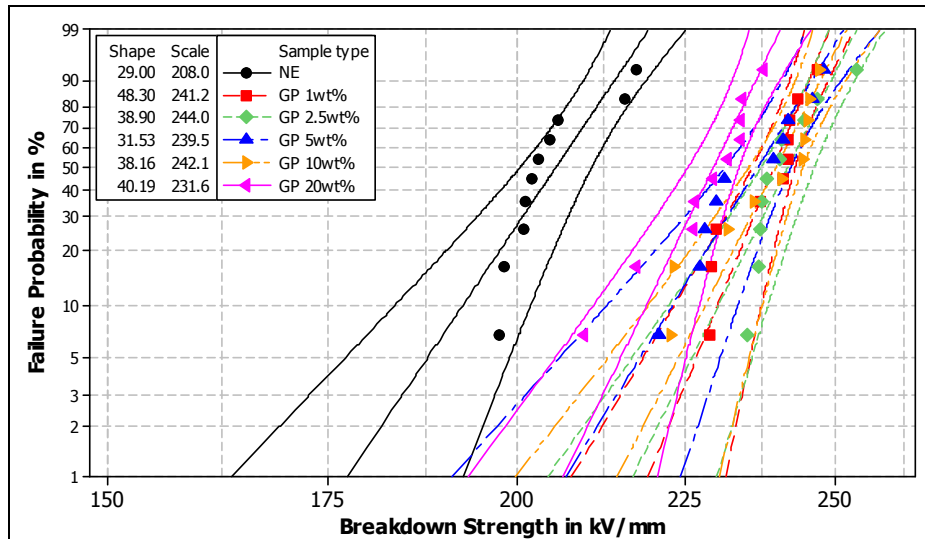


Figure 5.4 Weibull plots with 95 % confidence intervals

Table 5.3 Weibull parameters from the breakdown experiment

Sample	α (kV/mm)	β	Relative BD strengths
NE	208.0	29.0	100 %
GP 1wt%	241.2	48.3	116 %
GP 2.5wt%	244.0	38.9	117 %
GP 5wt%	239.5	31.5	115 %
GP 10wt%	242.1	38.2	116 %
GP 20wt%	231.6	40.2	113 %

Similar results of increased BD strengths for POSS modified epoxy composites were reported in (Heid, Fréchet et David, 2015c; Horwath et al., 2006; Takala et al., 2008). Horwath et al. (Horwath et al., 2006) reasoned, that the nanometric POSS additives might allow localized charge movement under the influence of an electric field, which would prevent internal charge accumulations in the bulk composite, further resulting in a more homogeneous electric field stress over the bulk. Thus, higher breakdown strengths will follow for the POSS composites, compared to the neat epoxy. These assumptions are paralleled by an earlier study of Nelson and Fothergill (Nelson et Fothergill, 2004) conducted in epoxy resin modified with titanium dioxide nano-particles.

In the case of the GP 20wt%, where we have observed a slightly retrogressive trend of BD strength, it can be concluded that, firstly, the appearing crystalline zones (as observed by SEM and TEM in Figure 5.3) might cause local electric field enhancements due to their shape and an eventual mismatch in permittivity, leading to locally increased electric field stresses, which will then result in decreasing BD strengths. Secondly, those crystalline inclusions could furthermore cause local charge accumulations due the resulting inhomogeneity at the interfaces between the matrix and the crystalline zones, and hence, additional electric field distortions will result in their vicinity.

5.4.4 Resistance to corona discharges

In Table 5.4, the evaluation of the erosion experiment is shown based on the eroded sample volumes. With the addition of POSS, significant improvements of the resulting composites' resistances to corona discharges were found; an improvement by a factor two after addition of 1 wt% Glycidyl-POSS, which got more distinct with higher amounts of the POSS added. GP 20wt% has seen an enhanced resistance to corona by more than seven times, compared to the neat epoxy.

Similar results for improved corona resistances of epoxy composites featuring inorganic nanofillers such as silica have been reported in the past (Brockschmidt et al., 2011; Kozako

et al., 2005; Tanaka, Matsuo et Uchida, 2008), and more recently in the more specific case of POSS additives as well (Heid, Fréchet et David, 2015c; Huang et al., 2014). Considering that the core of the Glycidyl-POSS consists of silica, which represents approximately 45 % of the overall Glycidyl-POSS' weight, we can conclude that the replacement of inorganic volume of epoxy by silica, contributes to the increased resistance to electrical discharges. When the organic epoxy chains of the composite break under the impact of the energy introduced from the electrical discharges, the organic material gets ablated. What remains on the surface of the composite will then be very small silica particles, considering that the overall size of a Glycidyl-POSS molecule is ranging somewhere around 2 nm. With increasing amount of POSS incorporated in the composites, the number of remaining silica particles on the surface will increase accordingly. These inorganic silica particles function as a shield against the corona discharges and thus protect the composite from further erosion, leading to the increased corona resistance of the composites with increasing POSS contents.

Table 5.4 Evaluation of the eroded sample volumes after exposure to corona discharges and the respective relative resistances against corona discharges of the composites compared to NE

Sample	Eroded volumes (μm^3)	Relative resistances to corona discharges
NE	1.30E+9	100 %
GP 1wt%	0.63E+9	206 %
GP 2.5wt%	0.62E+9	210 %
GP 5wt%	0.45E+9	289 %
GP 10wt%	0.33E+9	394 %
GP 20wt%	0.18E+9	722 %

5.4.5 Thermal conductivity

In terms of the thermal conductivity, we have found some intriguing results during this study, which are listed in Table 5.5. Based on the NE sample where we measured a value of

0.143 W/m·K, all G-POSS composites have seen an improvement in thermal conductivity, with exception of GP 20wt% which, with 0.145 W/m·K, showed a similar value to NE. In the case of the GP 1wt% the highest enhancement of thermal conductivity was found, being by 20 % higher than for the NE specimen. Further addition of G-POSS in the composites would then result in continuously decreasing values of the respective composites' thermal conductivity, until in the case of the GP 20wt% nearly the same values compared to the neat polymer were measured again.

Table 5.5 Evaluation of thermal conductivity measurements

Sample	Thermal conductivity (W/(m·K))	Relative values
NE	0.143	100 %
GP 1wt%	0.172	120 %
GP 2.5wt%	0.166	116 %
GP 5wt%	0.164	115 %
GP 10wt%	0.156	109 %
GP 20wt%	0.145	101 %

If we now considered the used Glycidyl-POSS as the smallest possible silica particle with surface functionalization, and further take into account, that these silica particles then take up 45 % of the incorporated G-POSS additive's weight, classically we would expect an increase in thermal conductivity as a function of the incorporated mass of the silica. This can be better understood when we apply mixing laws and calculate estimated values of the composites' thermal conductivity based on silica's thermal conductivity of 1.4 W/m·K and its density of 2.2 g/cm³ (compared to 1.2 g/cm³ of the NE). Both parameters for silica were taken from (Lide, 1994).

From Maxwell's effective medium approximation for randomly dispersed spherical particles in a matrix the effective thermal conductivity of a composite with low volume fraction of spherical particles can be deducted to (Shen et al., 2011)

$$\lambda_c = \lambda_m \frac{(2\lambda_m + \lambda_f) - 2\varphi_f(\lambda_m - \lambda_f)}{(2\lambda_m + \lambda_f) + \varphi_f(\lambda_m - \lambda_f)}. \quad (5.4)$$

with λ_c , λ_f and λ_m representing the thermal conductivities of composite, filler and matrix, and φ_f and φ_m the respective volume fractions of the composite's constituents. Following the geometric mean model, the effective thermal conductivity of a composite can be described by (Kochetov et al., 2009a)

$$\lambda_c = \lambda_f^{\varphi_f} + \lambda_m^{\varphi_m}. \quad (5.5)$$

In addition, Looyenga's formula for the dielectric permittivity which applies for spherical inclusions as well as randomly oriented ellipsoids, independent of their shape, also holds for the thermal conductivity of a composite and reads

$$\lambda_c^{1/3} = \varphi_f \lambda_f^{1/3} + \varphi_m \lambda_m^{1/3}. \quad (5.6)$$

When comparing the estimated thermal conductivities for the different composites based on the mixing laws, with the actual experimental results (see Figure 5.5) it is evident, that not the inorganic core of the Glycidyl-POSS molecule is accountable for the improvement of the thermal conductivity for low POSS loadings. Instead, we assume that the incorporation of G-POSS in the epoxy matrix has led to a re-structuration of the polymeric network, where POSS molecules serve as nodal points to form continuous pathways for phonons to move through the bulk of the composite.

It is common understanding that thermal conduction in polymeric dielectrics is based on phonons (lattice vibrations) (Cui et al., 2011; Takezawa, Akatsuka et Farren, 2003). Phonon

scattering, which can appear at either particle-particle or particle-matrix interfaces, or at the interfaces of the amorphous structure in epoxy resins itself (Takezawa, Akatsuka et Farren, 2003), lead to attenuation of the thermal conductivity within a material.

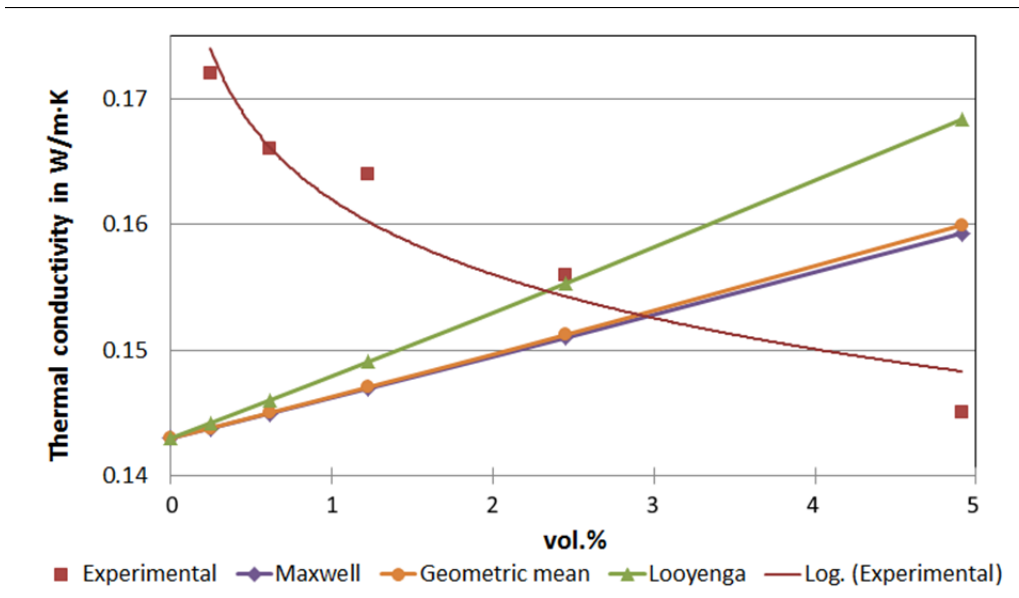


Figure 5.5 Evolution of the thermal conductivity for the POSS composites as estimated with mixing laws, compared to experimental values. While the calculations result in a continuously increasing thermal conductivity with increasing POSS content, the experimental values show a logarithmic decrease

However, it was established in (Takezawa, Akatsuka et Farren, 2003) that creating ordered structures on a nanometric level within epoxy resins, which are characterized by their amorphous structure, would cause a diminishment of phonon scattering, and hence, significantly improve the thermal conductivity of the polymer. Thus, we believe, that in the case of low G-POSS contents, and especially for the GP 1wt%, we have succeeded in re-organizing the amorphous structure of the epoxy matrix into a more organized epoxy/POSS network that enhances the phonon transport through the material and also diminishes phonon scattering. As a result, this will lead to an improved thermal conductivity for the low content POSS composites. The retrogressive trend in thermal conductivity with increasing Glycidyl-POSS contents can thus only be explained by phonon scattering that gets more pronounced, the more POSS is incorporated in the matrix. Although more pathways will be formed when

more POSS is introduced, it also increases the amount of interfaces between organic matrix and inorganic core of the POSS, where phonon scattering can occur, and hence lead to an attenuation of the thermal conductivity for higher POSS contents.

Besides that, in the case of GP 20wt% where crystalline zones have been observed (Figure 5.3), these interfaces, viz. between the bulk composite and the crystalline zones, will further lead to enhanced phonon scattering, and thus, to an ever lower thermal conductivity as compared to the other POSS composites. Coherent results were found in earlier works with a different type of POSS used (Heid, Fréchette et David, 2014c; 2015c).

5.4.6 Dielectric spectroscopy

The dielectric responses, with the real part ϵ' and the imaginary parts ϵ'' of the complex permittivity, for all test specimens obtained at different temperatures, viz. 20 °C, 60° C and 100 °C are presented in Figure 5.6. Compared with NE, both the GP 1wt% and the GP 2.5wt% composite revealed marginally lower values of ϵ' over the complete frequency range and temperatures from 20 °C to 100 °C (compare Figure 5.6a to Figure 5.6c). This phenomenon has often been observed when low contents of nanometric additives are incorporated in a polymeric matrix (Kochetov et al., 2012; Krivda et al., 2012) and results from an immobilization of the polymer chains in the vicinity of the filler. The composites with a loading of 5 wt% G-POSS and more have seen a slight increase in ϵ' , which was getting more pronounced the more POSS was incorporated (Figure 5.6a). This increase should be attributed to the inorganic silica-like core of the Glycidyl-POSS molecules, considering that silica has a higher dielectric constant than the epoxy.

Additionally, β -relaxation peaks were detected in ϵ'' for all samples in the vicinity of 100 kHz at 20 °C, as shown in Figure 5.6a'. Those β -peaks are common for amorphous polymers and appear due to secondary relaxation processes caused by movements of local groups that are attached to the main polymer chain, namely hydroxyl ether groups, in the case of the epoxy system used.

Similar to the behavior seen for ϵ' , marginally increased ϵ'' were also noted compared to NE, for all Glycidyl-POSS composites over the complete frequency range. However, it should be mentioned that the β -relaxation peaks for the POSS composites are more prominent than the one for neat epoxy. On the contrary, for nanoparticle filled epoxy composites usually no changes in the β -relaxation peak are observed (Couderc et al., 2013). The increased intensity of the β -peaks for all composites can be attributed to the additional introduced epoxy groups, forming supplementary hydroxyl ether groups during the cross-linking process. Concurrently those hydroxyl ether groups might have a higher mobility, hence leading to slightly increased dielectric losses in the frequency range of the β -relaxation peak.

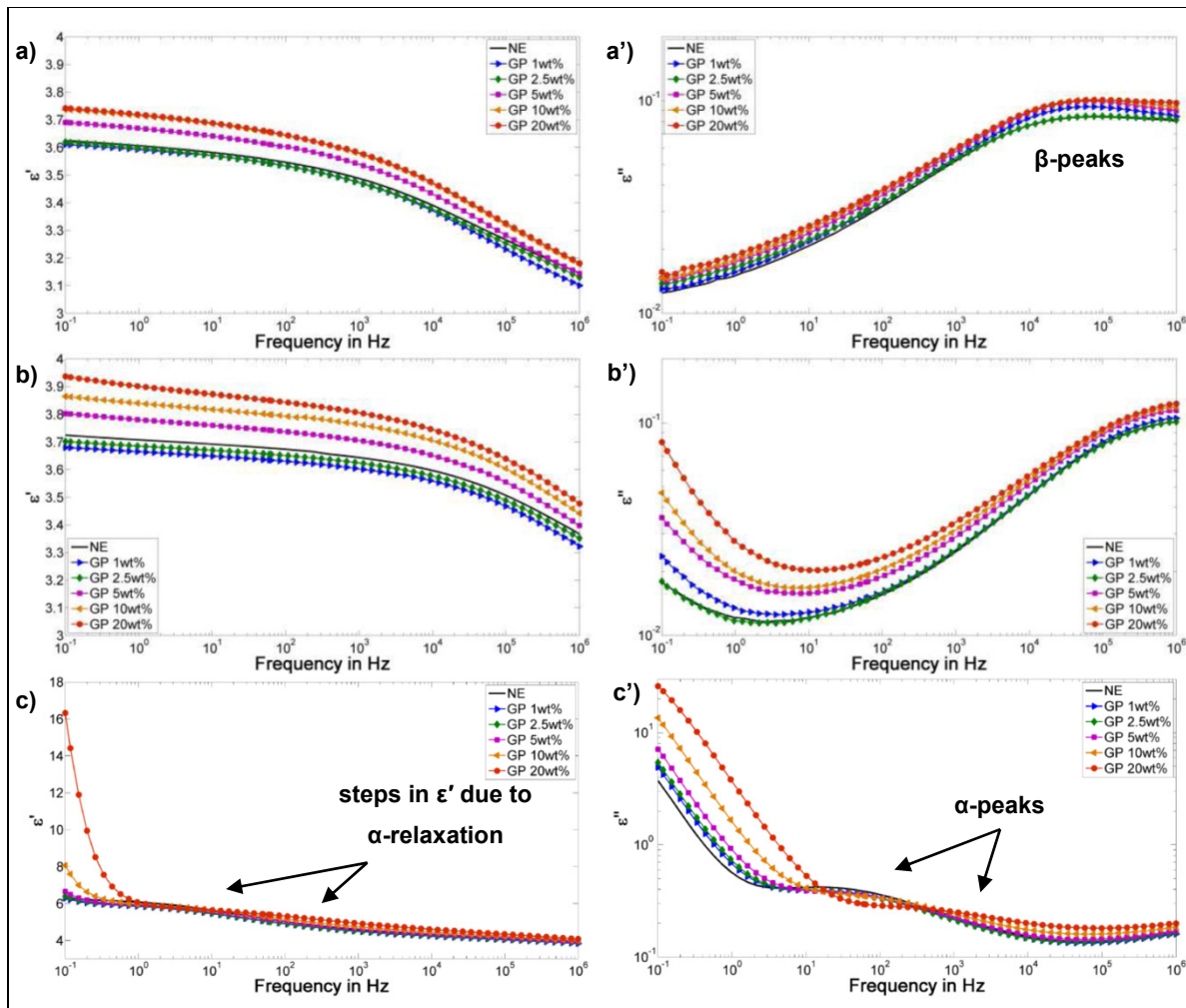


Figure 5.6 Dielectric response of NE and the POSS composites for a) 20°C, b) 60°C and c) 100°C

Most importantly, no interfacial loss peaks were found in the dielectric response of the composites, in contrast to preceding studies on different POSS additives with a lower amount of reactive epoxy groups (Heid, Fréchette et David, 2013; Heid, Fréchette et David, 2014c; 2015c), suggesting a good dispersion of the Glycidyl-POSS used in this work (Fréchette et al., 2014).

At 60 °C (see Figure 5.6b), the real part of the complex permittivity for GP 1wt% and GP 2.5wt% has seen a slight reduction compared to NE, as discussed above. For the other POSS composites though a distinct increase was found with higher POSS contents. In terms of the imaginary part of the complex permittivity (Figure 5.6b'), a more significant increase in the dielectric losses was seen for the POSS composites, which was more and more pronounced towards low frequencies and for higher POSS contents. This increase in dielectric losses supports the assumption made in paragraph 5.4.3, that POSS additives might allow localized charge movement under the influence of an electric field (Horwath et al., 2006; Nelson et Fothergill, 2004). However, GP 2.5wt% has not seen an increase in dielectric losses compared to NE, which will be analyzed more in paragraph 5.4.7.

The dielectric response at 100 °C, and thus slightly above the glass transition temperature of the specimens, is presented in Figure 5.6c and Figure 5.6c' and shows the α -relaxation peak with a loss maximum around power frequencies for NE and all the composites with exception of GP 20wt%, for which the α -peak was shifted by approximately one decade towards higher frequencies (see Figure 5.6c'). In amorphous polymers, the α -relaxation is correlated to relaxation processes of the main polymer backbone due to chain movement as a result of the glass transition phenomenon. Thus, the shift of the α -peak seen for GP 20wt% is in good correlation with its lower glass transition values reported in paragraph 5.4.2. Given that GP 20wt% has the lowest T_g , the α -relaxation process is initiated at lower temperatures, as compared to NE, and hence, the peak is shifted to slightly higher frequencies at temperatures above the T_g . In accordance with the findings for the dielectric losses, the resulting steps in ϵ' due to the α -relaxation process could be observed in the vicinity of 10 Hz

for NE and the G-POSS composites with exception of GP 20wt%, for which the α -step was also shifted by one decade to 100 Hz (Figure 5.6c).

The increasing dielectric losses at 100 °C in the low frequency domain (Figure 5.6c'), with a slope $\neq -1$ on the log-log scale, accompanied with the increasing real part of the permittivity for frequencies below 1 Hz (Figure 5.6c), translates a more complex behavior than simple DC conductivity of being responsible for the increasing dielectric losses (Iyer et al., 2011). The low frequency dispersion at 100 °C can be explained by interfacial polarization on a macroscopic level at the electrode/sample interface, the so called electrode polarization (EP) (Kremer, 2003), possibly superimposed by electronic conductivity. This is a common phenomenon for polymeric materials at elevated temperatures (Preda et al., 2013). The peak in ϵ'' due to electrode polarization was found to be more pronounced for GP 20wt% (see Figure 5.7c), which could be caused by an overlap of EP with an additional relaxation phenomenon, the so-called Maxwell-Wagner-Sillars (MWS) relaxation. MWS relaxation is caused by charge accumulation at interfaces between the polymeric matrix with inclusions (Kremer, 2003), which could be attributed to the crystalline zones that we have observed with SEM (Figure 5.3) in the case of GP 20wt%.

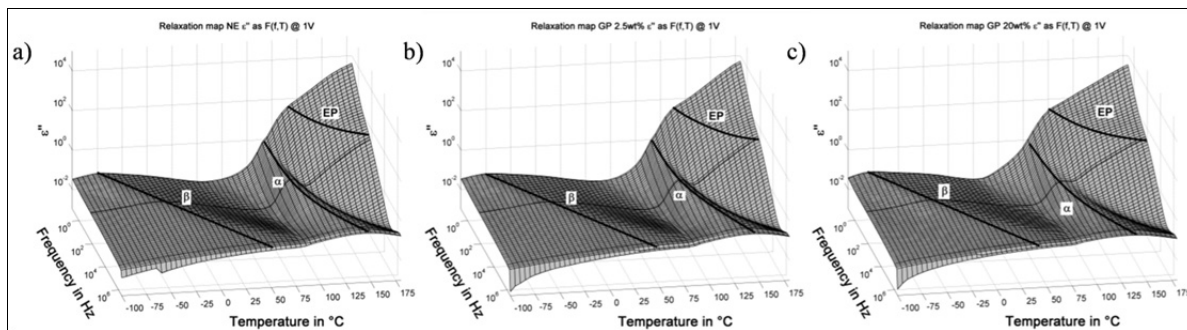


Figure 5.7 Relaxation maps of the dielectric losses as a function of applied frequency and temperature; for a) NE, b) GP 2.5wt% and c) GP 20wt%

5.4.7 Relaxation behavior

In order to further analyze the relaxation behavior of polymer composites, their dielectric responses are often fitted by an empirical equation (5.7) proposed by Havriliak and Negami

(Kremer, 2003). It is known to hold for various polymers as well as inorganic materials and it reads:

$$\varepsilon^*(\omega) = \varepsilon_\infty + \frac{\Delta\varepsilon}{(1 + (j\omega\tau_{HN})^{\alpha_{HN}})^{\beta_{HN}}} \quad (5.7)$$

The frequency-dependent complex permittivity $\varepsilon^*(\omega)$ can be approximated by (5.7), where ε_∞ is the high frequency permittivity, $\Delta\varepsilon$ the dielectric relaxation strength, ω the angular frequency ($\omega=2\pi \cdot f$), τ the relaxation time, α_{HN} and β_{HN} (with $0 < \alpha_{HN} < 1$ and $\beta_{HN} > 0$) the Havriliak-Negami parameters which designate, respectively, the symmetric and asymmetric broadening of the relaxation time distribution function. When the shape parameters (α_{HN} and β_{HN}) are equal to 1, equation (5.7) is simplified, and the relaxation law proposed by Debye (Raju, 2003) is obtained.

In our work, the relaxation behavior of all samples was therefore investigated by fitting the β -relaxation peaks of the imaginary part of the complex permittivity in order to obtain the corresponding relaxation times. After the corresponding relaxation times were obtained for the temperatures of interest, from -40 °C to $+40$ °C in the case of our test specimens, the molecular mobility of polymer chains participating in the β -relaxation process was explored, as described by the Arrhenius law:

$$\tau_\beta = \tau_{0\beta} \exp\left(\frac{E_a}{k_B T}\right) \quad (5.8)$$

According to the Arrhenius law, the relaxation time τ_β , which is inversely proportional to the molecular mobility, depends on the pre-exponential factor $\tau_{0\beta}$, the activation energy E_a of the β -relaxation process and the Boltzmann constant k_B . The global error, obtained after both the fitting of the β -relaxation and the derivation of the parameters of the Arrhenius law, was below 10 %. The obtained relaxation times are plotted in Figure 5.8 and the respective activation energies E_a , which are derived from the slope of the linear variation of the relaxation times, are listed in Table 5.6.

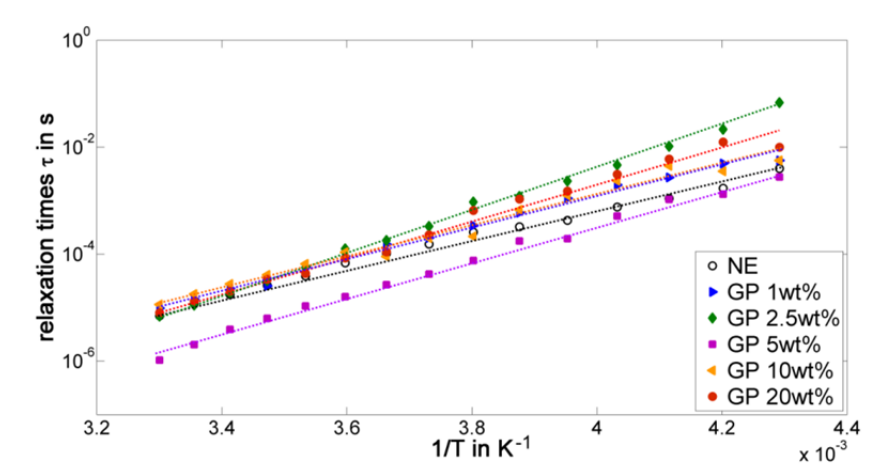


Figure 5.8 Relaxation time plots of the β -relaxation process

The resulting activation energies for the β -relaxation show that based on NE with 0.525 eV, the incorporation of Glycidyl-POSS has resulted in an increase of the activation energies for all composites, even when only marginally in the cases of GP 1wt% and GP 10wt%. The most significant increase of E_a was seen for GP 2.5wt%, which was 0.781 eV and hence about 50 % higher than for NE. Higher loadings of G-POSS have then led to decreasing activation energies of the β -relaxation process, although the GP 20wt% has seen an enhancement of E_a again.

Table 5.6 Activation energies obtained by fitting the β -relaxation process

Sample	Activation energy E_a (eV)
NE	0.525
GP 1wt%	0.593
GP 2.5wt%	0.781
GP 5wt%	0.698
GP 10wt%	0.578
GP 20wt%	0.672

The increased values of the activation energies for the POSS composites show that the molecular movements during the β -relaxation process are notably hindered. It appears that due to the good dispersion of POSS, along with the formation of covalent bonds between the filler and the epoxy, a more rigid epoxy/POSS network is obtained. Such increase in the rigidity of the molecular web is the result of incorporating the rigid silica-like cage structure of POSS into the matrix. However, if only 1 wt% of Glycidyl-POSS is added to the epoxy this effect might not be that significant, and also increasing the G-POSS content above 2.5 wt% might lead to more and more cross-linking between POSS molecules themselves, and hence to less rigidification of the polymer network.

The intriguing increase of E_a in the case of GP 20wt% appears to be attributable to the crystalline formations observed (Figure 5.3). Addition of 20 wt% Glycidyl-POSS has resulted in a semi-crystalline composite, which is quite unusual for the intrinsically amorphous epoxy resins. In the case of HDPE, which is a semi-crystalline polymer, the presence of surfaces of the crystalline zones, as well as the covalent bonds formed between amorphous and crystalline regions, have an immobilizing effect on the β -relaxation process (Suljovrujic, Micic et Milicevic, 2013), which can explain the higher activation energy found for GP 20wt% compared to GP 10wt%, where no crystalline zones were observed.

Finally, the exceptionally high value of the activation energy for GP 2.5wt% are coherent with findings of a recent study on a different type of POSS (Heid, Fr chet te et David, 2015c) and are further supported by the presented improvements in dielectric properties, viz. the BD strength and the comparably low dielectric losses, where GP 2.5wt% out-performed neat epoxy and the other composites, significantly in some cases.

5.5 Concluding remarks

Epoxy resins modified with functional Glycidyl-POSS were evaluated in terms of their potential for applications in high voltage insulation systems.

In summary, composites with low G-POSS content have excelled in high BD strengths and notably increased resistances against corona discharges, as well as enhanced thermal conductivities and low dielectric losses. The addition of 2.5 wt% of POSS in epoxy seems to be an optimal value in terms of dielectric strength and losses, also considering earlier studies on epoxy/POSS composites (Heid, Fréchet et David, 2015c). Further increase of the Glycidyl-POSS loading can then contribute towards an even higher resistance to corona discharges, whereas in terms of thermal conductivity the composites with low contents of 2.5 wt% Glycidyl-POSS and below have seen the most significant enhancements.

In conclusion, it can thus be stated that epoxy/POSS composites are indeed very promising dielectrics for a vast range of high voltage apparatus or applications, such as generator bars, spacers, bushings, cable terminations, and also for embedding materials of power electronics.

5.6 Acknowledgment

Hydro-Québec and the Natural Sciences and Engineering Research Council of Canada (NSERC) are gratefully thanked for their financial support.

CHAPTER 6

FUNCTIONAL EPOXY COMPOSITES FOR HIGH VOLTAGE INSULATION INVOLVING C-BN AND REACTIVE POSS AS COMPATIBILIZER

Thomas Heid^{1,2}, Michel Fréchet², Eric David¹

¹ Department of Mechanical Engineering, École de Technologie Supérieure,
1100 Notre-Dame West, Montreal, Quebec, (H3C 1K3) Canada

² Hydro-Québec's Research Institute,
1800 Boulevard Lionel-Boulet, Varennes, Quebec, (J3X 1S1) Canada

This article has been published in:

Journal of Materials Science

08/2015, vol. 50, issue 16, pp. 5494-5503

<http://dx.doi.org/10.1007/s10853-015-9095-9>

Abstract

Epoxy resins modified with only Polyhedral Oligomeric Silsesquioxanes (POSS) or cubic boron nitride (c-BN), as well as multiphase composites containing both, POSS and c-BN, were fabricated and investigated. Two different types of reactive liquid POSS with molecule sizes of approximately 2 nm, viz. Triglycidylisobutyl-POSS and Glycidyl-POSS were added in contents of 1 wt% to form single-phase and multiphase composites. Submicrometric c-BN, in contents of 5 wt%, was used for the respective single-phase composite as well as in the multiphase samples to create multifunctional nanostructured composites. The single-phase POSS composites have seen up to 15 % improved dielectric strengths and enhanced thermal conductivities by up to 20 %. The single-phase c-BN composite revealed the most distinct improvement in thermal conductivity of more than 25 %. SEM observations revealed a significantly improved dispersion of the c-BN particles in the presence of POSS for the multiphase composites, suggesting that POSS acts as a compatibilizer between organic epoxy matrix and inorganic filler particles.

Keywords: Compatibilizer, cubic boron nitride, dielectric spectroscopy, dielectric breakdown strength, epoxy composites, polymer nanodielectric, POSS, thermal conductivity

6.1 Introduction

Insulating systems are a crucial component of any high voltage (HV) apparatus used in power generation, energy transformation or for energy transportation. However, one of the weaknesses of the organic materials used for high voltage insulation, such as epoxy resins, is that they are subject to electrical degradation (Dissado et Fothergill, 1992). Even more, the polymer itself usually features a low thermal conductivity (Heid, Fréchet et David, 2015b; Kochetov et al., 2009b; Takezawa, Akatsuka et Farren, 2003; Tanaka et al., 2011; Tsekmes et al., 2014), which is a major limiting factor for materials that are expected to undergo high electro-thermal stresses.

For the last decade, there has been a deep interest in nano-composite research in the scientific community in numerous fields (Abenojar et al., 2012; Baker, Dutton et Kelly, 2014), and more recently also in terms of dielectric materials (Heid, Fréchet et David, 2015c; Nelson et Hu, 2005; Nelson et Fothergill, 2004; Tuncer et al., 2007a). This novel class of dielectric materials is commonly called polymer nanodielectrics. The presence of inorganic nanometric particles in the organic polymer matrix can render the resulting composites more resilient to electro-thermal stresses and improve parameters such as thermal conductivity or dielectric breakdown strength (Nelson, 2010).

Interesting filler materials, especially in the case of epoxy resins, are Polyhedral Oligomeric Silsesquioxanes (POSS). Unlike other common inorganic nanofillers, POSS is a hybrid material that features an inorganic silica-like core and organic side-groups. When these organic side-groups are of reactive nature and compatible with the epoxy system at hand, as is the case for the POSS additives further used in this study, the POSS molecules can covalently bond with the epoxy matrix. Thus, this leads to an intimate interaction between the POSS molecules (approx. 2 nm in size) and the polymer, resulting in a re-structuration of the polymer network on a nanometric scale. As a result, epoxy/POSS composites have revealed notable improvements in both, dielectric and thermal performances, as published in recent studies (Heid, Fréchet et David, 2014b; 2014c; 2015c; Huang et al., 2014).

In an effort to further enhance the thermal conductivity of polymers, Boron Nitride (BN), a highly thermally conductive ceramic, has presented itself as a promising additive (Kochetov et al., 2010; Tanaka et al., 2011; Wang et al., 2011). BN is a chemically synthesized material, which has been synthesized in different crystalline phases, of which hexagonal BN (h-BN) and cubic BN (c-BN) are commonly used. Cubic BN does not occur in nature (Klocke, 2011; Kumashiro, 2000). Recent studies have led to the conclusion that c-BN composites have seen higher improvements of thermal conductivities compared to their h-BN counterparts (Heid, Fréchet et David, 2014a; 2015b), which can be attributed to the significantly higher bulk thermal conductivity of c-BN along with its isotropic properties.

The inorganic nature of such filler particles and their tendency to agglomerate, however, can pose difficulties in terms of an intimate incorporation into an organic matrix, and for their dispersion within the polymer, when surface functionalization is not applied (Dongling et al., 2005a; Tanaka et al., 2013).

What would happen now, if the inorganic c-BN were to be incorporated in a polymeric matrix, where POSS molecules have re-organized the polymeric web due to their reactive nature, and hence, by covalent bonding with the epoxy molecules? Could the hybrid inorganic/organic POSS, incorporated in the epoxy network, affect the interaction between c-BN and the matrix?

Therefore, to answer these questions, the scope of this work was to investigate the interaction between hybrid inorganic/organic POSS and inorganic submicrometric c-BN, when both filler types are incorporated in an epoxy composite. The expected change in morphology as a result of the covalent bonding of POSS with the epoxy molecules is assumed to affect the interaction of c-BN particles with the epoxy/POSS network, possibly yielding a synergetic effect, where the hybrid POSS might act as a functionalizing agent, and hence, improve the integration of c-BN in the epoxy/POSS matrix.

6.2 Materials and sample preparation

6.2.1 Materials

DER332 epoxy resin (DOW Chemical Company) and Jeffamine D230 curing agent (Huntsman Corp.) were used as the base polymer for sample fabrication. Three distinct additives, namely a submicrometric cubic boron nitride (c-BN) with average particle sizes of 500 nm (from Diamond Innovations Inc.) and two different liquid reactive POSS types (from Hybrid Plastics Inc.), a Triglycidylisobutyl-POSS (TG-POSS) and a Glycidyl-POSS (G-POSS), were used to fabricate composites. The TG-POSS has three mono-directionally oriented epoxy groups attached to the cage-like silica core (Figure 6.1 on the left), whereas the G-POSS features 8 to 12 epoxy groups attached to the silica core (Figure 6.1 on the right).

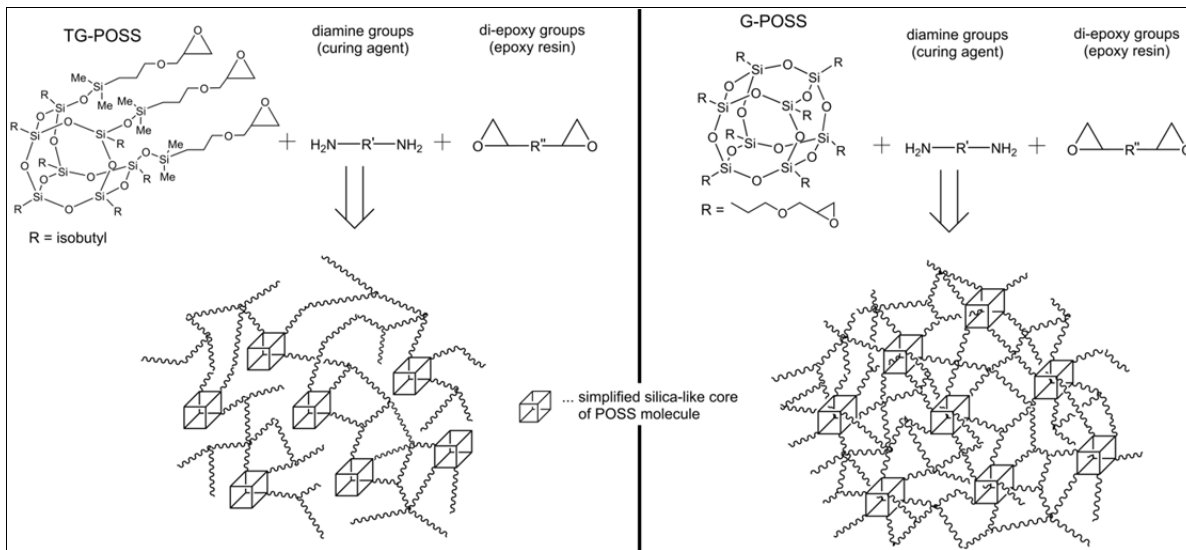


Figure 6.1 Proposed reaction of the two different POSS types with curing agent and epoxy resin, TG-POSS (left) with the three epoxy groups and the G-POSS (right) with the cage structure represented for the case of R=8 epoxy groups. The formation of covalent bonds between POSS and epoxy matrix results in nano-structured epoxy/POSS networks

Both POSS types can form covalent bonds with the epoxy system used during the curing reaction, and hence, modify the structure of the epoxy network on a nanometric level, as proposed in Figure 6.1. Due to the significantly higher amount of epoxy groups featured by

G-POSS, the incorporation of these molecules into the epoxy resin will lead to a higher cross-linking density of the resulting epoxy/POSS network compared to the case when TG-POSS is used.

The viscosity of both POSS types was comparable with that of the base epoxy, which facilitated the dispersion of POSS in the epoxy.

6.2.2 Compounding

In this study several types of composites were produced in addition to the neat epoxy (NE) reference sample: First, three composites featuring only a single additive, meaning either one of the two POSS types with a content of 1 wt%, named G-POSS and TG-POSS respectively, or containing 5 wt% of the submicrometric cubic boron nitride, named cBN, were produced. The second type of composites were multiphase composites (MP), where either type of POSS was incorporated along with 5 wt% of c-BN. Hence, one composite with 1 wt% of G-POSS plus 5 wt% c-BN (MP/G-POSS) and one composite with 1 wt% of TG-POSS plus 5 wt% c-BN (MP/TG-POSS) were obtained. A summary of the various test specimens is shown in Table 6.1, providing the sample codes to which the following work will refer, as well as the respective constituents for the single filler composites and the multiphase (MP) composites.

Table 6.1 Overview and nomenclature of prepared samples

Sample code	Sample nature	Total amount of additives
NE	Neat epoxy	N/A
G-POSS	Epoxy + G-POSS 1wt%	1 wt%
TG-POSS	Epoxy + TG-POSS 1wt%	1 wt%
cBN	Epoxy + c-BN 5wt%	5 wt%
MP/G-POSS	Epoxy + G-POSS 1wt% + c-BN 5wt%	6 wt%
MP/TG-POSS	Epoxy+ TG-POSS 1wt% + c-BN 5wt%	6 wt%

The molecules of both, TG-POSS and G-POSS, feature distinct amounts of epoxy groups surrounding the silica-like core, which will consume curing agent during the reticulation process. As a result, distinctive stoichiometric ratios of epoxy, curing agent and the respective POSS were formulated for all POSS-containing composites, in order to balance the reactive epoxy groups of resin and POSS with the amine groups of the curing agent. The stoichiometric calculations were based on the respective epoxy equivalent weights of the constituents involved.

Considering the unique nature of the different fillers, distinct fabrication procedures were established to achieve a good dispersion of the additives in the epoxy matrix. The liquid additives, TG-POSS and G-POSS, were dispersed by means of a magnetic stir on a hot plate at a temperature of 40 °C. When only POSS was incorporated in the composites, following the aforementioned step, the curing agent was added to the liquid epoxy/POSS composite and mixed as well with a magnetic stir at 40 °C. Throughout the stirring procedures, vacuum was applied directly on the mixing vessel to degas the mixture before the liquid composites were cast. The method described has shown to give homogeneous epoxy/POSS composites, for the amounts of POSS used (Heid, Fréchette et David, 2015a; 2015c).

When c-BN particles were involved, they were added either to the base epoxy, in the case of the cBN sample, or, in the cases of the two MP composites, the c-BN particles were added to the epoxy/POSS mixture, which was obtained according to the above mentioned description. Most importantly, before the curing agent was introduced, the liquid composites were sonicated, employing a high energy ultrasonic probe, to disperse the c-BN particles. After sonication, these liquid composites were thoroughly degassed, before the curing agent was added into the mixtures with a magnetic stir on a hotplate at 40 °C. Again, vacuum was applied directly on the mixing vessel during the multiple stirring procedures.

Subsequently, the liquid composites were cast in stainless steel molds and cured under vacuum at 100 °C for a period of six hours. The curing process followed a gradual cool down

to room temperature. A release agent (QZ13) applied on the molds before the composites were cast, facilitated the demolding of the fabricated sample plaques.

6.3 Experimental methods

6.3.1 Microstructure analysis

The test specimens containing submicrometric c-BN were immersed in liquid nitrogen to render them brittle and subsequently fractured in order to obtain cross-sections for observations with a Scanning Electron Microscope (SEM). The two composites containing only POSS as an additive, viz. G-POSS and TG-POSS, were mounted in epoxy and subsequently polished with abrasive materials of gradually decreasing particle sizes down to 50 nm to obtain a very smooth surface for high magnification observations with the SEM.

For all composite samples, complete cross-sections with a width of approximately 2 cm and a height of 300 μm were analyzed with an SU-70 high resolution SEM (Hitachi High Technologies America). Different magnification levels were chosen to assess the dispersion of the used filler in the epoxy matrix, depending on the respective filler sizes used for the composites. In the cases of POSS, magnifications of up to x200k were employed, considering the very small size of the POSS molecules of around 2 nm. When the submicrometric c-BN was involved in the composites, and hence, for the cBN and the two MP composites, magnifications of up to x20k were sufficient to investigate the dispersion of the c-BN particles. Prior to the SEM observations, all samples were cleaned in an ultrasonic bath to remove debris from the fracturing process. Subsequently, the specimens were sputter-coated with a 2 nm Platinum layer to avoid charging due to the electron beam during the SEM observations.

6.3.2 Dielectric spectroscopy

The dielectric response was evaluated on samples 40 mm in diameter and with an average thickness of 300 μm by the use of Broadband Dielectric Spectroscopy (BDS, Novocontrol

Technologies GmbH) at an excitation voltage of 1 V and a temperature of 20 °C, for a frequency range of 0.1 Hz to 1 MHz. The complex permittivity ε^* as given in (6.1) was obtained with the real permittivity ε' , representing the real or storage part and ε'' , the imaginary or dielectric loss part.

$$\varepsilon^*(\omega) = \varepsilon'(\omega) - i\varepsilon''(\omega) \quad (6.1)$$

6.3.3 Differential scanning calorimetry

Glass transition temperatures T_g were measured by Differential Scanning Calorimetry (DSC) with a heat flow calorimeter (Q20, TA Instruments). Each specimen was subjected to two thermal cycles with a heating rate of 10 °C/min from 20 °C to 250 °C, followed by a gradual cooling down to 20 °C also at 10 °C/min. The T_g were obtained from the second heating cycle to avoid any thermal history of the test specimens.

6.3.4 AC breakdown strength

The AC breakdown strength was retrieved based on the ASTM D149 standard. Samples were immersed in transformer oil and positioned between two ball tip electrodes with a 4 mm diameter. The short-term test was used, where a 60 Hz voltage with a ramp rate of 2 kV/s was applied between the electrodes until breakdown occurred. Twelve breakdowns were carried out for each sample type, after which the ball tip electrodes were replaced to avoid pitting. The test specimens for this experiment had a thickness of 135 μm .

6.3.5 Thermal conductivity

The thermal conductivity was obtained with a DTC-25 guarded heat flow meter (TA Instruments) in accordance with the ASTM E1530 standard. The circular samples, 50.8 mm (2 inches) in diameter and with an average thickness of 300 μm , were placed between the upper heating plate and the lower cooling plate of the instrument. Applying a pressure of 20 psi on the upper plate ensured intimate contact between the sample, the heating and the

cooling plates. The thermal conductivity values were assessed for a mean sample temperature of 25 °C. The specimens remained inside the test chamber for two hours before the thermal conductivity values were obtained, to allow a thermal stabilization of the samples.

6.4 Results and discussion

6.4.1 Microstructure analysis

The SEM micrographs revealed homogeneous bulk compositions for the G-POSS and TG-POSS samples (see Figure 6.2a and Figure 6.2b) without any particular trace of the POSS additives. Thus, both POSS additives seem to be dispersed into the polymeric matrix on a molecular level. In the case of the cBN sample (see Figure 6.2c) a rather heterogeneous bulk material was observed, with agglomerated zones packing a high density of c-BN particles, while others were lacking c-BN. In comparison to this observation, it was found that in the cases of the two multiphase composites MP/G-POSS and MP/TG-POSS (Figure 6.2d and Figure 6.2e, respectively) the incorporated c-BN particles were well dispersed throughout the bulk of the material. Thus, no clusters of c-BN particles were found for these composites.

It appears that the incorporation of the hybrid organic/inorganic POSS molecules in the organic epoxy network indeed resulted in some type of compatibilization with the inorganic c-BN. Due to the covalent bonds formed between the epoxy chains and the POSS molecules with its silica-like cores, the resulting epoxy/POSS network now features inorganic zones on a nanometric scale. This subsequently renders the per se organic epoxy into an intrinsically hybrid material with an organic backbone and inorganic silica-like regions (see Figure 6.1). Thus, it is believed that POSS acts as a compatibilizer within the polymer backbone, which enables a homogeneous dispersion of the c-BN particles in the matrix. In recent studies (Huang et al., 2012; Huang et al., 2013), POSS has been shown to perform as a functionalizing agent or compatibilizer by improving the interfacial interaction between filler particles and epoxies when the respective additives are surface treated with POSS. Consequently, homogeneous dispersions of the respective filler materials in the epoxy matrix were obtained in these studies.

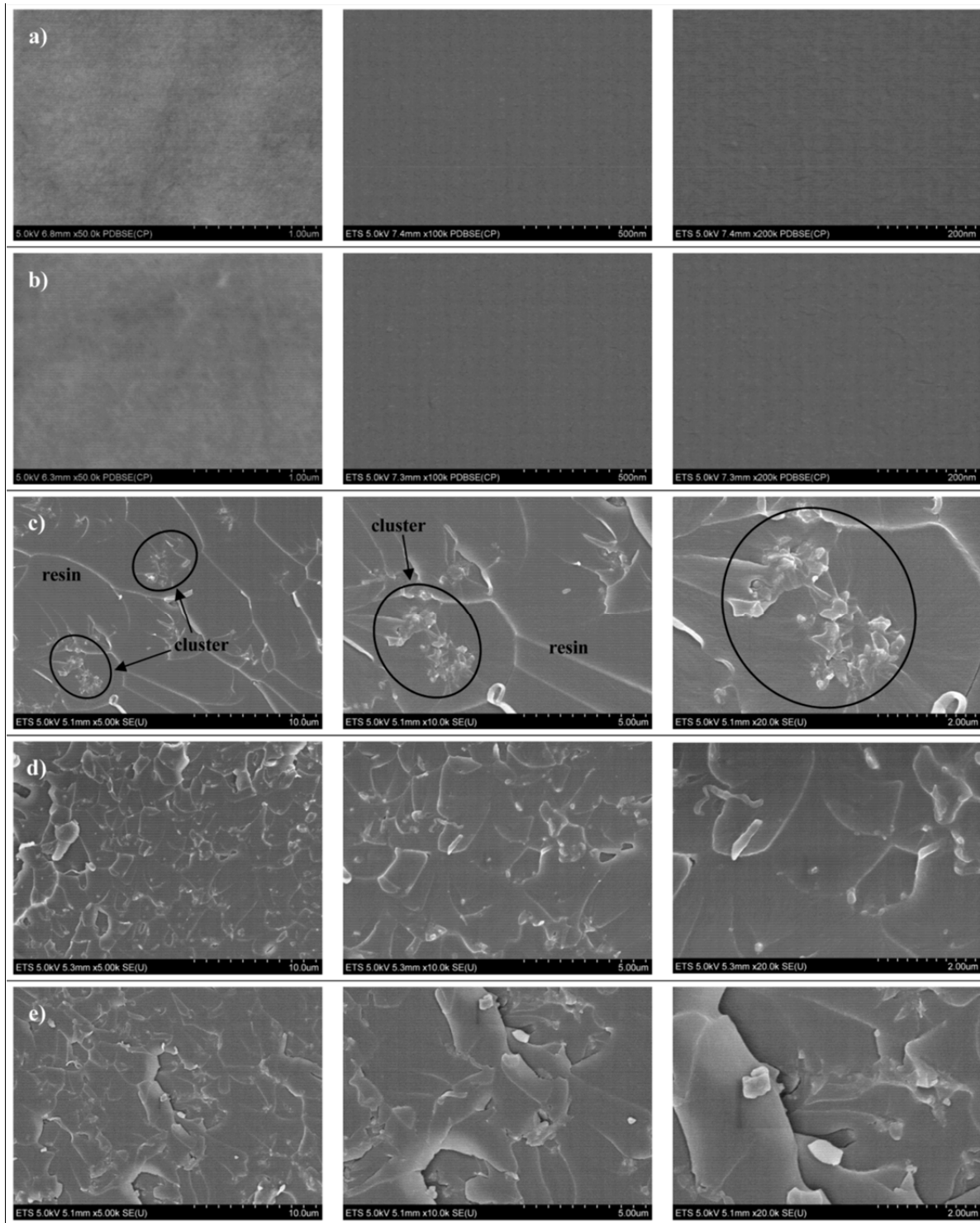


Figure 6.2 Micrographs of the composites captured at different magnifications: (a) G-POSS, (b) TG-POSS, (c) cBN, (d) MP/G-POSS and (e) MP/TG-POSS

6.4.2 Dielectric spectroscopy

The dielectric responses of the test specimens obtained show different results depending on the type of additive used, both in the real and in the imaginary parts of the complex permittivity. Compared with NE, the two single-phase POSS composites revealed slightly lower values of ϵ' , which was more evident for the G-POSS sample (see Figure 6.3a). This phenomenon has often been observed when low contents of nanometric additives are incorporated in a polymeric matrix (Kochetov et al., 2012; Krivda et al., 2012). In contrary, for the cases involving c-BN, and hence, the cBN and the two multiphase composites, ϵ' was found to be higher than what was observed for NE, especially with decreasing frequencies. Since the values of the relative permittivity for c-BN increase from high frequency $\epsilon_{\infty} = 4.5$ towards the static $\epsilon_0 = 7.1$ (Kumashiro, 2000), it appears that the submicrometric c-BN particles dictate the dielectric permittivity for the cBN and MP composites.

Additionally, β -relaxation peaks were detected in ϵ'' for all samples in the vicinity of 100 kHz, as depicted in Figure 6.3b. Those β -relaxation peaks are common for amorphous polymers and appear due to secondary relaxation processes caused by movements of local groups that are attached to the main polymer chain, namely hydroxyl ether groups, in the case of the epoxy system used. Similar to the observations made for ϵ' , increased ϵ'' were also noted compared to neat epoxy, for the composites involving c-BN, and thus, the cBN and both MP samples.

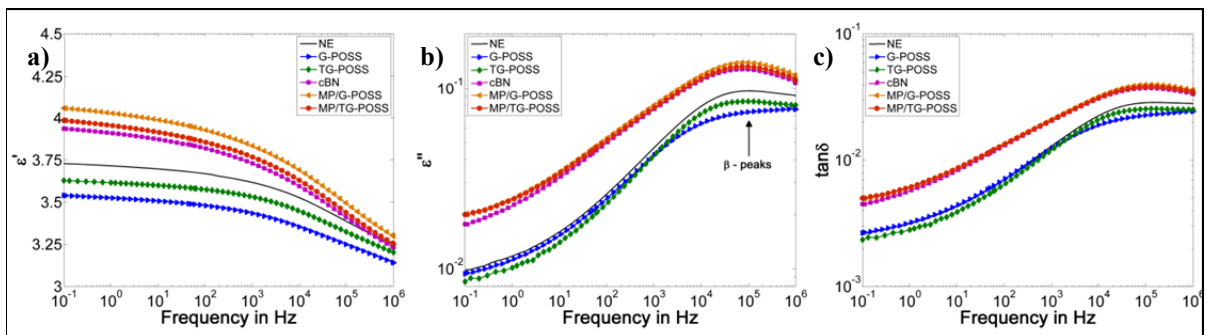


Figure 6.3 Dielectric response of test specimens at 20 °C and 1 V; (a) real part of complex permittivity, (b) imaginary part of complex permittivity and (c) the resulting loss tangent

In terms of both POSS composites though, the dielectric losses were found to be marginally lower for the frequency range from 1 kHz to 0.1 Hz, compared to the neat polymer. In the vicinity of the β -peak (around 100 kHz) however, the decrease in dielectric losses of both G-POSS and TG-POSS was more evident. It seems that the incorporation of POSS in the matrix leads to an immobilization of the side groups contributing to the β -relaxation process, as described above. The immobilization can be explained by the formation of covalent bonds between POSS and epoxy molecules due to the reactive epoxy groups of POSS, which leads to a more rigid network in the POSS composites as compared to the neat polymer. This gets even more evident, when one compares the dielectric losses of the G-POSS composite, which are lower than those of TG-POSS in the vicinity of the β -peak. Since G-POSS has 8 to 12 reactive epoxy groups that can form covalent bonds with the epoxy matrix, compared to only three epoxy groups for the TG-POSS, it is evident that the resulting epoxy/POSS network is more rigid when G-POSS is added instead of TG-POSS, and hence, the lower dielectric losses for the G-POSS composite due to the β -relaxation process.

6.4.3 Differential scanning calorimetry

The DSC experiment revealed rather close values of T_g which are summarized in Table 6.2. The glass transition phenomenon is strongly interrelated with the chain mobility of the epoxy network, which itself will be dependent on factors such as the cross-linking degree, chain

Table 6.2 Glass transition temperatures T_g of test specimens

Sample	T_g (°C)
NE	92
G-POSS	91
TG-POSS	89
cBN	93
MP/G-POSS	93
MP/TG-POSS	92

lengths, the flexibility of side-groups or chains, as well as free volume, as reported in this review (Nakka, 2010). Considering the close values of T_g for NE and all of the composites, it can be concluded that the incorporation of either filler did not contribute to any significant changes to the mobility of the molecular chains of the epoxy or epoxy/POSS network during the glass transition process.

6.4.4 AC breakdown strength

The AC breakdown (BD) data obtained were processed with the two-parameter Weibull distribution according to the IEEE 930 standard, to evaluate the AC breakdown strengths of the test specimens:

$$P(E_{BD}) = 1 - \exp \left[- \left(\frac{E_{BD}}{\alpha} \right)^\beta \right] \quad (6.2)$$

where $P(E_{BD})$ is the cumulative failure probability in %, E_{BD} is the experimental value of the dielectric breakdown strength in kV/mm, α is the scale parameter representing the breakdown strengths in kV/mm at which 62.3 % of the samples experienced electric BD, and the shape parameter β , which is an inverse measure for the scatter of the BD data, meaning the higher it is, the lower the variation of the data to the Weibull distribution. In accordance with the IEEE 930 standard, the cumulative failure probability for the experimental data of E_{BD} can be approximated by:

$$P(i, n) = \frac{i - 0.44}{n + 0.25} \quad (6.3)$$

where i denotes the result of the i^{th} rank, when all values of $E_{BD,i}$ are sorted in ascending order, and n represents the number of data points. In this work, $n=12$. The Weibull plots of the BD experiment are shown in Figure 6.4 and the respective Weibull parameters α and β are listed in Table 6.3.

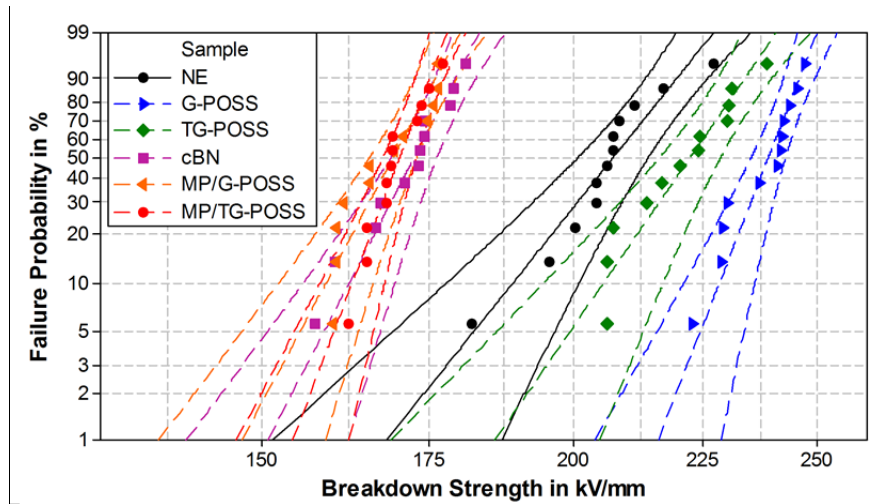


Figure 6.4 Weibull plot of the breakdown data with 95 % confidence intervals

Compared to the neat polymer NE, which had a BD strength of 211 kV/mm, both POSS composites revealed higher AC BD strengths. TG-POSS had a slightly higher BD strength of 226 kV/mm, whereas G-POSS revealed the highest BD strength, with 241 kV/mm. In terms of the cBN composite and the two multiphase (MP) composites though, significantly reduced BD strengths were recorded, compared to NE. With 174 kV/mm for the cBN composite and 172 kV/mm for both, the MP/G-POSS and MP/TG-POSS composites, it is evident that the submicrometric c-BN particles dominate the breakdown behavior of the multiphase

Table 6.3 Weibull parameters from the breakdown experiment

Sample	α (kV/mm)	β
NE	211	20.4
G-POSS	241	41.9
TG-POSS	226	23.7
cBN	174	31.5
MP/G-POSS	172	30.5
MP/TG-POSS	172	43.1

composites. The decrease in BD strength in the presence of the c-BN particles can be attributed to local electrical field enhancements in the proximity of c-BN caused by the irregular shape of the filler particles which feature pronounced edges, and also due to the mismatch of the dielectric permittivity, compared to epoxy (Heid, Fréchette et David, 2015b; Lovell, 1976; Wang et al., 2012).

It has been argued in the past, i.e. (Chen, 2012; Strachota et al., 2007), that some of the benefits of incorporation of POSS into a polymeric matrix are due to the ability of POSS to structure a polymeric network on a nanometric level, which occurs by the formation of covalent bonds between the reactive POSS types used and the epoxy, and thus leads to a more homogeneous molecular structure of the epoxy/POSS network. This fact, plus a local reinforcement of the polymer chains with inorganic silica, should give rise to the enhanced BD strengths of the POSS composites.

6.4.5 Thermal conductivity

The obtained thermal conductivities of the test specimens are summarized in Table 5.5. Our experiments showed a thermal conductivity of 0.143 W/m·K for NE, which is in accordance with previously published findings for this epoxy resin (Heid, Fréchette et David, 2014a; 2015c). Based on these values, all composite materials were found to have increased thermal conductivities. The TG-POSS composite has seen only a slightly increased thermal conductivity of 0.156 W/m·K, whereas for the G-POSS specimen, a 20 % enhancement in thermal conductivity to 0.172 W/m·K was achieved. The cBN composite, however, revealed the most important improvement in thermal conductivity, with a value of 0.180 W/m·K, representing an increase of more than 25 % compared to NE. Considering the rather similar values obtained for the multiphase composites, viz. 0.178 W/m·K for MP/G-POSS and 0.177 W/m·K for MP/TG-POSS, it is evident that no synergetic effect in terms of a further improved thermal conductivity could be attained by incorporation of both POSS and c-BN together in a multiphase composite.

Table 6.4 Evaluation of thermal conductivity measurements

Sample	Thermal conductivity (W/(m·K))	Relative values
NE	0.143	100 %
G-POSS	0.172	120 %
TG-POSS	0.156	109 %
cBN	0.180	126 %
MP/G-POSS	0.178	125 %
MP/TG-POSS	0.177	124 %

It is well established that the thermal conduction in dielectric solids is based on phonons (lattice vibrations) (Cui et al., 2011; Takezawa, Akatsuka et Farren, 2003). However, in amorphous epoxy resins the dominating process is phonon scattering, which causes a diminishment of thermal conductivity within a material. Phonon scattering can occur at matrix-filler or filler-filler interfaces, as well as at the interfaces of the amorphous structure in epoxy resins itself (Takezawa, Akatsuka et Farren, 2003).

The incorporation of low amounts of POSS in epoxy resins is believed to bring about a re-structuration of the resulting composites' molecular structure, caused by covalent bonds between epoxy and POSS. Furthermore, the reticulation between filler and matrix is considered to diminish phonon scattering in the TG-POSS and especially in the G-POSS composite, and thus leads to an enhancement of the POSS composites' thermal conductivities compared to the neat polymer.

The superior performance of the G-POSS composite in comparison with TG-POSS can accordingly be attributed to the higher degree of reactivity of G-POSS, with its 8 to 12 epoxy groups, instead of only 3 epoxy groups in the case of the TG-POSS. This allows the G-POSS to better integrate in the matrix, creating more continuous pathways for the heat conduction by inter-connecting epoxy molecules with one another. In the multiphase composites,

however, the c-BN particles with their comparatively large size of 500 nm apparently obstruct the described effect of POSS on the epoxy network. Thus, no beneficial synergetic effect of POSS and c-BN on the thermal conductivity was seen for the multiphase composites. In conclusion, the c-BN particles also dominate the heat conduction properties of both, the MP/G-POSS and MP/TG-POSS composite.

6.5 Concluding remarks

Both POSS samples, but especially the G-POSS composite, have shown notably enhanced properties in terms of BD strength and dielectric losses, as well as increased thermal conductivities compared to the neat polymer. However, in the presence of the submicrometric c-BN particles in the two multiphase composites, the re-structuration of the polymeric matrix by incorporation of POSS seems to be compromised by the comparatively large c-BN particles, with an average size of 500 nm. Thus, no additional benefit was found in terms of thermal conductivity or BD strength when both POSS and c-BN were incorporated together in a multiphase (MP) sample.

On the contrary, when comparing G-POSS with the cBN and the MP samples, besides the marginally higher thermal conductivity of cBN and both MP composites, it is evident that the G-POSS specimen features the overall best performance of a dielectric material for high voltage insulation, with lower dielectric losses, higher BD strength, as well as increased thermal conductivity, compared to the base epoxy.

It is however most intriguing that even the clearly improved dispersion of the introduced c-BN particles in the MP composites, as presented in Figure 6.2 did not contribute to any kind of enhancement in either electric or thermal performance of the respective composites. Consequently, it is believed that the choice of the sub-micrometric c-BN particles used was inadequate to benefit from the structuring abilities of POSS. Considering that the c-BN particles used were comparatively large, with an average size of 500 nm compared to approximately 2 nm for the POSS molecules, it might be of interest to conduct a similar

study involving a nanometric sized filler, with sizes closer to that of the POSS molecules used, in order to avoid the perturbation of the POSS' structuring effect, and thus, enable a synergetic effect of the two fillers.

Although no complex chemical surface treatment of the c-BN particles involved was applied in our study, yet a homogeneous dispersion of the inorganic c-BN particles was seen for the multiphase composites (see Figure 6.2d and Figure 6.2e), this effect of POSS on the compatibility between polymer and filler should be regarded as a major point of interest in nano-dielectrics or nano-composites in general. In fact, the dispersion of nanometric inorganic filler particles within polymers is still a very current problematic (Hong et Chen, 2015; Kochetov et al., 2012; Nelson, 2010; Tanaka et al., 2013).

The possibility of using POSS as a compatibilizer in industrial manufacturing processes instead of more complex chemical procedures, which might come with certain health or environmental risks, and hence, the approach of formulating epoxy composites combining reactive POSS and other additives to improve their dispersion within the epoxy matrix, could significantly contribute to the advancement of the implementation of epoxy-based nano-composites on an industrial level.

6.6 Acknowledgment

Hydro-Québec and the Natural Sciences and Engineering Research Council of Canada (NSERC) are gratefully thanked for their financial support.

CHAPTER 7

MATHEMATICAL VALIDATION AND ESTIMATION OF MATERIAL PROPERTIES

The estimation of composite materials' properties, such as the dielectric permittivity, by use of analytical or numerical methods is an interesting topic, as it enables tailoring of the engineered composite materials to meet certain specifications. Many comprehensive reviews exist on this topic (Bergman, 1978; Bánhegyi, 1986; Kremer, 2003; Raju, 2003; Shalaev, 1996; Tuncer, Serdyuk et Gubanski, 2002; Tuncer, Gubański et Nettelblad, 2001) but these approaches, also called mixing laws or rules of mixture, are usually conceived for two phase mixtures and are thus often limited to composites with micrometric filler phases, for which the influence of interphases between matrix and particles are negligible. When nanocomposites are investigated, more complex models have been proposed, e.g. (Daily et al., 2014; Preda et al., 2014; Steeman et Maurer, 1990; Todd et Shi, 2005) extending the before mentioned two phase models to three phase models, where the important impact of the interphase between a polymeric matrix and nanometric filler particles is considered.

7.1 Theoretical models for the complex permittivity of composite materials

7.1.1 Two phase models

A first approach to estimate effective medium properties, such as the dielectric permittivity of a heterogenic medium, was first proposed by Maxwell (Maxwell, 1873) based on a singular spherical inclusion with permittivity ε_2 and radius R within a medium of permittivity ε_1 (as depicted in Figure 7.1a). When an electric field E is applied, the resulting electrical potentials outside and inside of the inclusion (ϕ_1 and ϕ_2 respectively) can be obtained by solving the Laplace equations in polar coordinates:

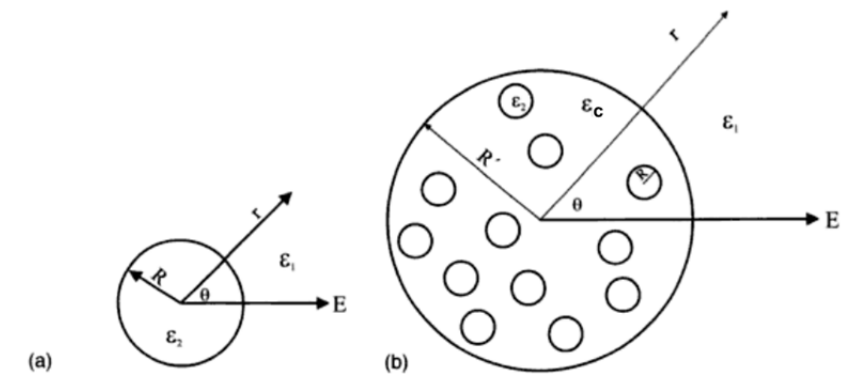


Figure 7.1 (a) Single spherical inclusion within a medium to develop Maxwell's equations for mixtures (b); the small inclusions in (b) are the same as the inclusion shown in (a)
Adapted from Kremer (2003, p. 89)

$$\nabla^2 \phi_1 = 0 \quad ; \quad \nabla^2 \phi_2 = 0. \quad (7.1)$$

Respecting the boundary condition of continuity for the electric potentials at the boundary of the inclusion, where $r = R$, one can state

$$\phi_1 = \phi_2 \quad \text{and} \quad \varepsilon_1 \frac{\partial \phi_1}{\partial r} = \varepsilon_2 \frac{\partial \phi_2}{\partial r}. \quad (7.2)$$

From (7.2) it can then further be developed that

$$\phi_1 = - \left(\frac{\varepsilon_1 - \varepsilon_2}{2\varepsilon_1 + \varepsilon_2} \frac{R^3}{r^3} + 1 \right) Er \cos \theta \quad (7.3)$$

$$\phi_2 = - \left(\frac{\varepsilon_1 - \varepsilon_2}{2\varepsilon_1 + \varepsilon_2} + 1 \right) Er \cos \theta. \quad (7.4)$$

Based on (7.3) the effective medium equations can be then derived, considering that N small inclusions with radius R are randomly dispersed in a larger sphere of radius R' (see Figure 7.1b). The potential ϕ_p outside the larger sphere can thus be expressed as (Kremer, 2003)

$$\Phi_p = - \left(\frac{\varepsilon_1 - \varepsilon_c}{2\varepsilon_1 + \varepsilon_c} \frac{R'^3}{r^3} + 1 \right) Er \cos \theta \quad (7.5)$$

where ε_c represents the effective medium permittivity of the larger sphere with the dispersed small inclusions. Similarly, the potential ϕ_p can as well be formulated as a sum of N potentials due to the small inclusions, when these don't interact with one another. It thus follows, for low concentrations of inclusions:

$$\phi_p = - \left(\frac{\varepsilon_1 - \varepsilon_2}{2\varepsilon_1 + \varepsilon_2} \frac{R^3}{r^3} N + 1 \right) Er \cos \theta . \quad (7.6)$$

The potentials of ϕ_p from equations (7.5) and (7.6) are equivalent, which then leads to the general expression of the effective medium permittivity for a composite material with spherical inclusions (Tuncer, 2013)

$$\varepsilon_c = \varepsilon_1 \frac{(2\varepsilon_1 + \varepsilon_2) - 2\varphi_f(\varepsilon_1 - \varepsilon_2)}{(2\varepsilon_1 + \varepsilon_2) + \varphi_f(\varepsilon_1 - \varepsilon_2)} \quad (7.7)$$

with the volume fraction φ_f of the small inclusions given by

$$\varphi_f = \frac{NR}{R'} . \quad (7.8)$$

The effective medium approach of Maxwell was generalized by Wagner (Wagner, 1914) to account for the complex nature of the dielectric permittivity. Sillars (Sillars, 1937) then extended the model for ellipsoidal inclusions, which applies for randomly distributed filler particles with the dielectric permittivity¹ ε_f and the volume fraction φ_f within a matrix of permittivity ε_m . The dielectric permittivity of the resulting composite ε_c is thus

¹ Note: The dielectric permittivities hereafter are of complex nature and a function of the applied angular frequency $\omega=2\pi f$

$$\varepsilon_c = \varepsilon_m \frac{[n\varepsilon_f + (1-n)\varepsilon_m] + (1-n)\varphi_f(\varepsilon_f - \varepsilon_m)}{[n\varepsilon_f + (1-n)\varepsilon_m] - n\varphi_f(\varepsilon_f - \varepsilon_m)} \quad (7.9)$$

where n presents the shape factor ($0 \leq n \leq 1$) of the filler particles in direction of the electric field lines. For the simplest case of spherical particles, where a symmetry in all three directions applies it follows that (Kremer, 2003)

$$n_x = n_y = n_z = \frac{1}{3}. \quad (7.10)$$

More values for diverse particle shapes can be found in literature, e.g. (Kremer, 2003; Torquato, 2002).

Due to the limitation of the Maxwell-Wagner-Sillars theory to low quantities of filler particles (below 20 vol.%) Bruggeman proposed a different approach using an integral technique (Bruggeman, 1935), that was later extended to estimate the complex permittivity of heterogeneous composites with ellipsoidal inclusions in a matrix material (Tuncer, Gubański et Nettelblad, 2001)

$$1 - \varphi_f = \frac{\varepsilon_f - \varepsilon_c}{\varepsilon_f - \varepsilon_m} \left(\frac{\varepsilon_m}{\varepsilon_c} \right)^n. \quad (7.11)$$

The variables and shape factor n apply in the same way as described above.

A different way to estimate the effective medium properties, based on a symmetrical integration approach, was independently developed by Looyenga (Looyenga, 1965) and Landau and Lifshitz (Landau et Lifshitz, 1960), and applies for spherical inclusions as well as randomly oriented ellipsoids, independent of their shape:

$$\varepsilon_c^{1/3} = \varphi_f \varepsilon_f^{1/3} + \varphi_m \varepsilon_m^{1/3}. \quad (7.12)$$

The general form of (7.12) is known as the Lichtenecker formula (Goncharenko, Lozovski et Venger, 2000)

$$\varepsilon_c^k = \varphi_f \varepsilon_f^k + \varphi_m \varepsilon_m^k \quad (7.13)$$

and holds for $-1 < k < 1$.

7.1.2 Three phase models

In order to account for the significant contribution of the interphase area between nanometric filler particles and the surrounding matrix, on the dielectric response of nanocomposites, three phase models have been proposed. Based on the power law equation (7.13), a three phase system can be derived to (Todd et Shi, 2005)

$$\varepsilon_c^n = \varphi_f \varepsilon_f^n + \varphi_m \varepsilon_m^n + \varphi_i \varepsilon_i^n \quad (7.14)$$

with the complex permittivity of the interphase region ε_i and its respective volume fraction φ_i and the shape factor n , as mentioned above. An interlayer model was also introduced by Steeman and Maurer (Steeman et Maurer, 1990) which, for ellipsoidal filler particles results to

$$\varepsilon_c = \frac{\varphi_f \varepsilon_f + \varphi_m \varepsilon_m S + \varphi_i \varepsilon_i R}{\varphi_f + \varphi_i R + \varphi_m S} \quad (7.15)$$

with

$$R = \frac{n\varepsilon_f + (1-n)\varepsilon_i}{\varepsilon_i} \quad (7.16)$$

$$S = \frac{[n\varepsilon_i + (1-n)\varepsilon_m][n\varepsilon_f + (1-n)\varepsilon_i] + \frac{\varphi_f}{\varphi_f + \varphi_i} n(1-n)(\varepsilon_i - \varepsilon_m)(\varepsilon_f - \varepsilon_i)}{\varepsilon_i \varepsilon_m} \quad (7.17)$$

The depolarization factor or shape factor n for different particle shapes can be found in literature, i.e. (Kremer, 2003; Torquato, 2002). For spherical particles (7.10) applies.

7.2 Theoretical models for the thermal conductivity of composite materials

Similar to the shown theoretic models to calculate dielectric permittivities, approaches for estimation of the effective thermal conductivity of composite materials can be found in literature, e.g. (Shen et al., 2011). The most basic two-phase models can be derived for layered composites, with the different layers either in parallel to the direction of the heat flow (parallel model)

$$\lambda_c = \varphi_f \lambda_f + \varphi_m \lambda_m \quad (7.18)$$

or perpendicular to the heat flow (series model)

$$\frac{1}{\lambda_c} = \frac{\varphi_f}{\lambda_f} + \frac{\varphi_m}{\lambda_m}. \quad (7.19)$$

In both cases λ_c , λ_f and λ_m represent the thermal conductivities of composite, filler and matrix, and φ_f and φ_m the respective volume fractions of the composite's constituents. Following the geometric mean model the effective thermal conductivity of a composite can be derived to (Kochetov et al., 2009a)

$$\lambda_c = \lambda_f^{\varphi_f} + \lambda_m^{\varphi_m} \quad (7.20)$$

From Maxwell's effective medium approximation for randomly dispersed spherical particles in a matrix (7.7), the effective thermal conductivity of a composite with low volume fraction of spherical particles can be deducted to (Shen et al., 2011)

$$\lambda_c = \lambda_m \frac{(2\lambda_m + \lambda_f) - 2\varphi_f(\lambda_m - \lambda_f)}{(2\lambda_m + \lambda_f) + \varphi_f(\lambda_m - \lambda_f)}. \quad (7.21)$$

Bruggeman's formula for the permittivity (7.11) also holds for the effective thermal conductivity (Shen et al., 2011)

$$1 - \varphi_f = \frac{\lambda_f - \lambda_c}{\lambda_f - \lambda_m} \left(\frac{\lambda_m}{\lambda_c} \right)^n \quad (7.22)$$

with $n=1/3$ for spherical particles. Similarly, Looyenga's formula for the dielectric permittivity (7.12), which applies for spherical inclusions as well as randomly oriented ellipsoids, independent of their shape, also holds for the thermal conductivity of a composite and reads

$$\lambda_c^{1/3} = \varphi_f \lambda_f^{1/3} + \varphi_m \lambda_m^{1/3}. \quad (7.23)$$

Most of the introduced models do, however, not consider possible interactions between a polymeric matrix and the filler particles, which is why most models are limited in their accuracy to estimate the composite materials' properties. Also phonon scattering effects are not included, which is a major drawback for these models.

In an effort to include material specific variations of the effective thermal conductivity of composites, Agari and Uno presented a semi-empiric model (Agari et Uno, 1986) that holds for many polymeric matrices and various fillers:

$$\log \lambda_c = \varphi_f C_2 \log \lambda_f + (1 - \varphi_f) \log(C_1 \lambda_m). \quad (7.24)$$

In order to include possible effects of filler particles on the polymer's morphology, such as changes in crystallinity, which could influence the matrix's thermal conductivity, the factor C_1 was introduced. The factor C_2 is related to the filler's capability to form conductive paths

with the matrix. From a more practical standpoint, C_1 is a material specific parameter, depending on the type and chemistry of the selected polymer and filler, whereas with C_2 the effects of filler shape (form factor) and even phonon scattering can be attributed for.

7.3 Comparison of theoretical models with the experimental data

7.3.1 Estimation of the thermal conductivities of h-BN composites

In Chapter 3 (Article I), it was shown that incorporating hexagonal boron nitride (h-BN) in epoxy has led to enhanced thermal conductivities of the resulting composites compared with neat epoxy. In this chapter, the applicability of mixing laws presented in paragraph 7.2 on these epoxy/h-BN composites is evaluated. Therefore, the experimental results are compared to Maxwell's formula (equation (7.21)), the Geometric mean model of the effective thermal conductivity from equation (7.20), as well as the semi-empiric formulas for the effective thermal conductivities of composites by Lichtenecker (derived from equation (7.13)) and Agari & Uno (equation (7.24)). For the thermal conductivity of h-BN, 250 W/m·K was chosen according to (Wypych, 2010). In the case of the epoxy matrix, the measured experimental value for this sample series of 0.171 W/m·K was used.

The resulting comparisons of experimental and calculated thermal conductivities for the submicrometric h-BN filler (BN205) is shown in Figure 7.2 and the comparison for the micrometric h-BN (BN600) in Figure 7.3. The used calculation parameters and the fitting parameters, in the two cases of semi-empiric formulas, are summarized in Table 7.1.

Looking at the graphs in Figure 7.2 and Figure 7.3, it is evident that both, the Maxwell and Geometric mean formulas are not fit to estimate the thermal conductivities of the h-BN composites, considering that all values calculated by Maxwell's equation are too low, whereas the values retrieved by the Geometric mean model are too high compared to the experimental data. The semi-empiric models proposed by Lichtenecker or Agari & Uno, however, are both suitable to model the thermal conductivities of the composites at hand. Due to the formula's semi-empiric nature though, they are limited to fit existing experimental

data. However, after the fitting is performed and all the parameters are determined, the obtained models can further be used to estimate thermal conductivities of composites by interpolation between the experimental data.

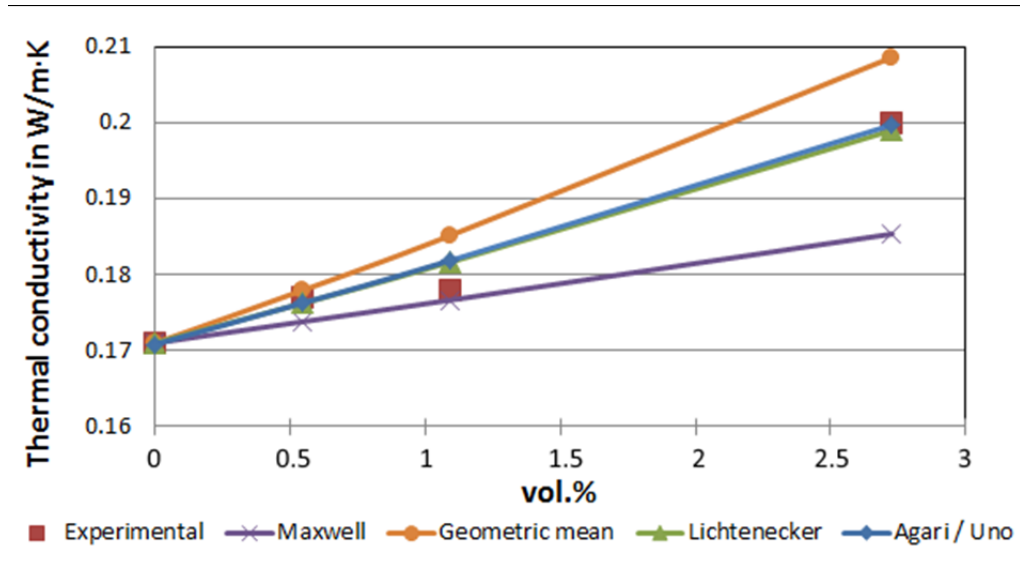


Figure 7.2 Comparison of thermal conductivities between the experimental data obtained for the submicrometric BN205 sample series and the theoretical mixing laws

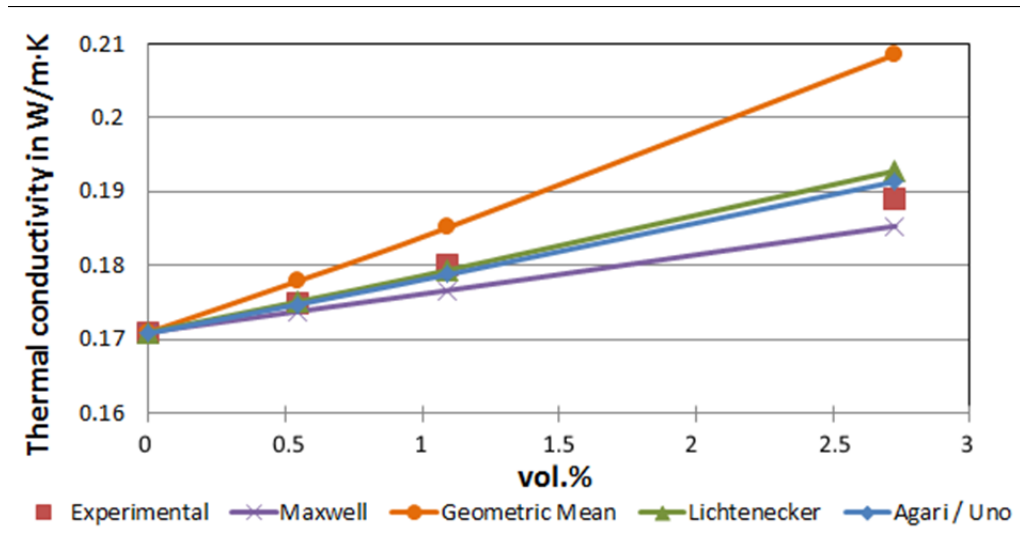


Figure 7.3 Comparison of thermal conductivities between the experimental data obtained for the micrometric BN600 sample series and the theoretical mixing laws

Table 7.1 Parameters for the comparison between the theoretical mixing laws and the experimental data for the h-BN sample series

Filler type	Density in g/cm ³		Thermal conductivity in W/(m·K)		Fitting parameters		
	epoxy	h-BN	λ_{epoxy}	$\lambda_{\text{h-BN}}$	Agari/Uno		Lichtenecker
					C ₁	C ₂	n
BN205	1.2	2.2	0.171	250	0.1	1.65	-0.08
BN600	1.2	2.2	0.171	250	0.1	1	-0.155

7.3.2 Estimation of the thermal conductivities of c-BN composites

Similar to the approach described before in paragraph 7.3.1, the experimental data of epoxy composites involving cubic boron nitride (c-BN) were compared to the same models for the thermal conductivity of composite materials, and hence, Maxwell's equation, the Geometric mean model, and Lichtenecker's as well as Agari & Uno's equations. The graph with the comparison of the experimental and calculated data is presented in Figure 7.4 and the respective parameters used for the calculations and the fitting of the two semi-empiric formulas, respectively, are listed in Table 7.2.

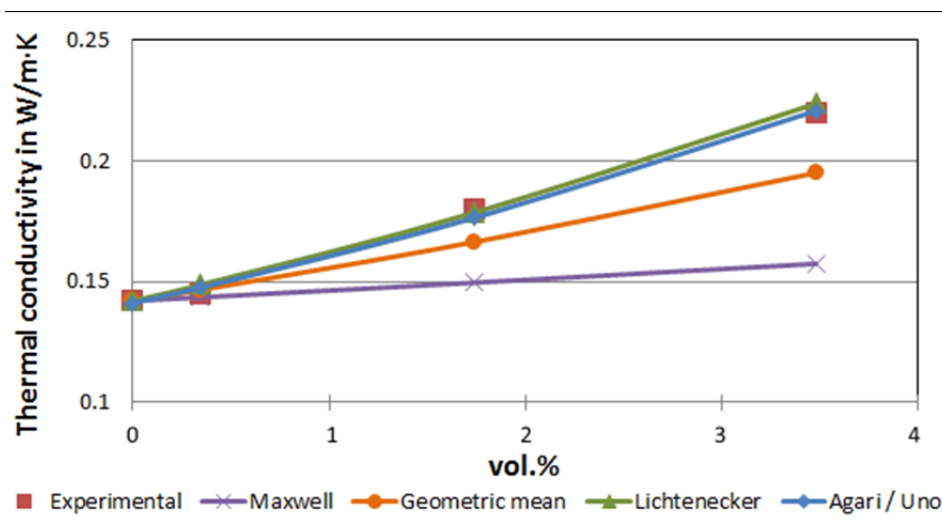


Figure 7.4 Comparison of thermal conductivities between the experimental data obtained for the submicrometric c-BN sample series and the theoretical mixing laws

Table 7.2 Parameters for the comparison between the theoretical mixing laws and the experimental data for the c-BN sample series

Filler type	Density in g/cm ³		Thermal conductivity in W/(m·K)		Fitting parameters		
	epoxy	c-BN	λ_{epoxy}	$\lambda_{\text{c-BN}}$	Agari/Uno C ₁	C ₂	Lichtenecker n
c-BN	1.2	3.45	0.142	1300	0.0775	3.5	0.078

From Figure 7.4 it is evident that both, Maxwell's equation and the Geometric mean model are not fit to estimate the thermal conductivity of the epoxy/c-BN composites. The semi-empiric formulas of Lichtenecker or Agari & Uno yet again seem applicable to model thermal conductivities of composite materials.

7.4 Conclusion on the applicability of mixing laws to estimate material properties

In this chapter, it was shown that existing models to estimate effective medium properties, such as the thermal conductivity, are not always applicable on polymer composites. A main reason in the case of the composites used in this comparison is that imperfections, which can occur due to the incorporation of micrometric and submicrometric filler particles, might significantly affect the composite's properties. Also, possible phonon scattering at the interfaces between organic matrix and inorganic filler particles can't be taken into account. Here lies the strength of semi-empiric models as the Lichtenecker or Agari & Uno's model, as they can take such effects in consideration.

In conclusion, it can be said that the semi-empiric formulas work well to model thermal conductivity of composite materials, however they are limited to fit existing experimental data. From a practical standpoint though, this could be useful to estimate thermal conductivities of composites by interpolation between existing experimental data points, or eventually also by extrapolating to slightly higher filler loadings below a possible percolation threshold of the particles used.

CHAPTER 8

3D FEM MODELING OF THE THERMAL CONDUCTIVITY OF COMPOSITE MATERIALS

As we have seen before in Chapter 7, there are certain limitations to the application of mixing laws to estimate effective medium values of composite materials such as the thermal conductivity. These limitations get even more pronounced the smaller the inclusions or filler particle are, which is the case for nanocomposites, where the volume content of the interfacial area between filler particles and matrix can significantly exceed the content of the filler particles itself, as was shown in Figure 1.1. Thus, it is crucial to implement the respective contribution of the interface on the nanocomposites' properties, like the thermal conductivity.

The following chapter presents a modeling approach for the composites' thermal conductivities by means of the finite element method (FEM) in **COMSOL Multiphysics**. Based on the experimental data of Chapter 5 and Chapter 6 (Article III and Article IV) a model for the conductive heat transfer in our functional POSS composites is proposed in several steps. Various morphological scenarios, and thus, the particle dispersion and eventual occurring interfacial effects on the thermal conductivity have been considered. This model will further allow to understand the particular results in thermal conductivity found for the POSS composites, where decreasing values in thermal conductivity were observed with increasing POSS contents, contrary to the behavior predicted by the theoretical models (Chapter 5, paragraph 5.4.5)

Accordingly, the heat transfer in single-phase epoxy composites with only cubic boron nitride (c-BN) as filler will be simulated in the first step. In the second step, the developed model will then be extended to multiphase composites containing both, POSS and c-BN. These findings will further lead to the third step, where the actual contribution of POSS to

the heat transfer in such functional POSS composites will be analyzed, subsequently leading to the proposal of a novel model explaining the conductive heat transfer in epoxy/POSS composites. In the fourth and final step, this model will then be verified by comparison with experimental data obtained in Chapter 5, for composites with varying contents of G-POSS.

8.1 Basics of heat transfer in solids

The heat flow through a solid material follows Fourier's law of heat conduction, which reads

$$q_z = -\lambda \frac{\partial T}{\partial z} \quad (8.1)$$

with the conductive heat flux per unit area q_z in z direction, the thermal conductivity λ of the material and the temperature gradient $\partial T/\partial z$ in direction of the heat flux. In case of anisotropic thermal conductivity of a composite material, λ becomes a tensor

$$\lambda = \begin{pmatrix} \lambda_{xx} & \cdots & \lambda_{xz} \\ \vdots & \ddots & \vdots \\ \lambda_{zx} & \cdots & \lambda_{zz} \end{pmatrix} \quad (8.2)$$

and the conductive heat flux then follows to

$$q_z = -\sum_i \lambda_{z,i} \cdot \frac{\partial T}{\partial z}. \quad (8.3)$$

In the steady-state case, Fourier's law can also be written in its integral form

$$\frac{\Delta Q}{\Delta t} = -\lambda \cdot A \cdot \frac{\Delta T}{\Delta z} \quad (8.4)$$

and gives the heat flow rate $\Delta Q/\Delta t$ through a material with a cross section area A in z -direction, as a function of the applied temperature difference ΔT over a distance Δz of the

material. In case of anisotropic thermal conductivities in a composite material, the effective medium thermal conductivity of a material can thus be derived by integrating the conductive heat flow over the composites' volume.

8.2 Modeling the thermal conductivity of epoxy/c-BN composites

In order to calculate the thermal conductivity of the c-BN composites in this first step, different geometries were created to match the volumetric content of cubic boron nitride in the 1 and 5 wt% composites, as can be seen in Figure 8.1. Therefore, a unit cell of 2 μm side length was established and the c-BN particles were assumed to be spherical and of average particle sizes of approx. 500 nm, as stated by the supplier. Thus, the cBN 1wt% composite could be represented by 1 sphere and the cBN 5wt% composite by 5 spheres in a unit cell, respectively. In the case of cBN 5wt%, a well dispersed system was generated (see Figure 8.1c). The case of neat epoxy (NE) (Figure 8.1a) was included mainly to verify the model and especially the resolution of the mesh used for the calculations.

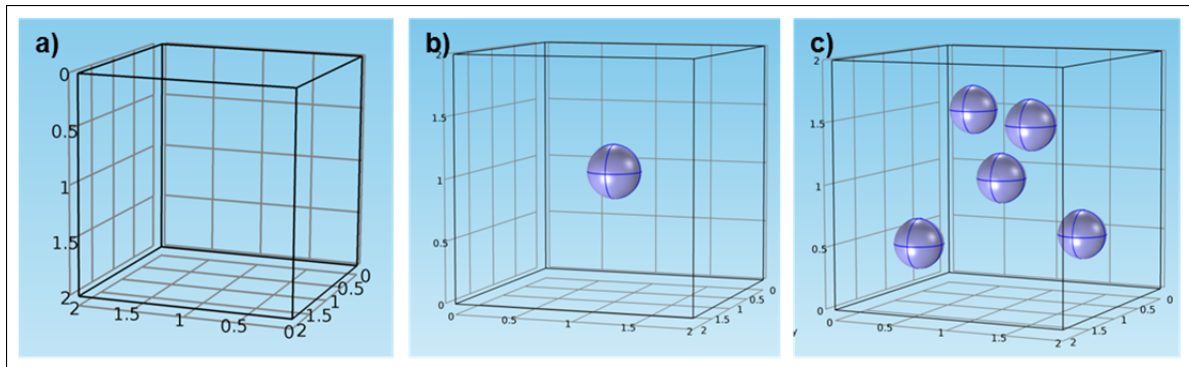


Figure 8.1 Geometries for the cases of a) neat epoxy, b) cBN 1wt% and c) cBN 5wt%

The selected boundary conditions for the simulations of the thermal conductivities of all specimens are shown in Figure 8.2. For all the simulations conducted in COMSOL, a ΔT of 34 $^{\circ}\text{C}$ between the upper and lower faces of the sample cube was applied to generate a heat flow in z-direction. The selected temperatures, 45 $^{\circ}\text{C}$ on the top and 11 $^{\circ}\text{C}$ on the bottom face, match the settings of the DTC-25 heat flow meter, with which the experimental values of thermal conductivities of the respective materials were measured.

The COMSOL simulations were further conducted for the steady-state, taking into account that during the measurements the samples were allowed to remain inside the DTC-25 heat flow meter for 2 hours to avoid transient effects on the thermal conductivity. Additionally, the remaining faces of the unit cell were defined to be thermally insulating, so that no heat flux out of the cube resulted in both, the x- and y-axis, and thus $\mathbf{q}_x = \mathbf{q}_y = \mathbf{0}$. The thermal conductivities of the materials used for the COMSOL simulations were $\lambda_{\text{epoxy}} = 0.142 \text{ W/m}\cdot\text{K}$, taken from the experimental data for our neat epoxy, and $\lambda_{\text{c-BN}} = 1300 \text{ W/m}\cdot\text{K}$, taken from (Haubner et al., 2002). Lastly, it should be mentioned that the interfacial zone around the c-BN particles was omitted for these models because it was assumed to be negligible regarding the c-BN particle sizes of approximately $0.5 \text{ }\mu\text{m}$.

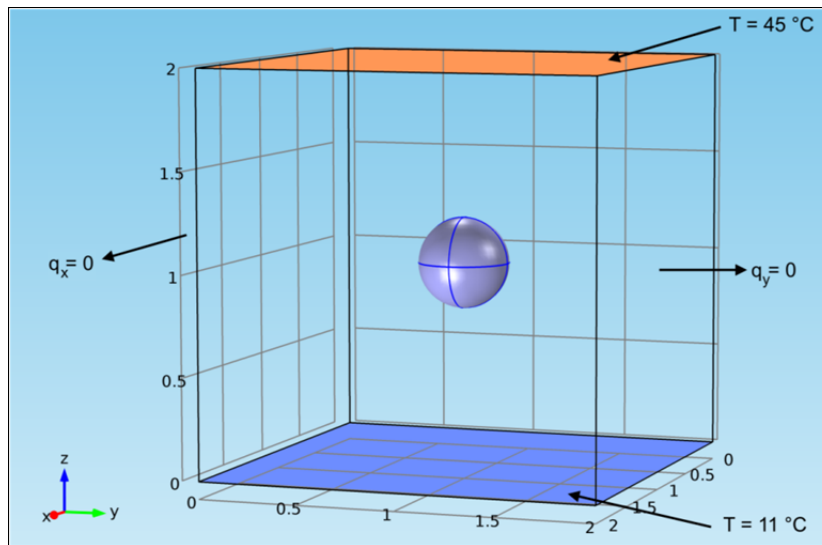


Figure 8.2 The defined boundary conditions for the models, here in case of cBN 1wt%. The temperature difference over the sample volume will cause a heat flow from top to bottom of the model. The heat flux out of the unit cell with $2 \text{ }\mu\text{m}$ side lengths was defined zero ($\mathbf{q}_x = \mathbf{q}_y = \mathbf{0}$)

The resulting values of the thermal conductivity of neat epoxy, the cBN 1wt% and the cBN 5wt% composite are listed in Table 8.1, which were obtained from the simulations based on the geometries presented in Figure 8.1. In the cases of neat epoxy and cBN 1wt%, the simulation results of the composites' thermal conductivities $\lambda_{\text{sample,sim}}$ match the experimental values found ($\lambda_{\text{sample,exp}}$).

Table 8.1 Resulting thermal conductivities obtained by COMSOL simulations (coherent results are highlighted in green, unmatched results in orange)

Sample	Thermal conductivity in W/(m·K) of composite	
	simulated $\lambda_{\text{sample,sim}}$	experimental $\lambda_{\text{sample,exp}}$
Neat epoxy	0.142	0.142
cBN 1wt%	0.147	0.147
cBN 5wt%	0.156	0.180

For the cBN 5wt% composite, however, a significantly lower value of $\lambda_{\text{cBN 5wt\%,sim}} = \mathbf{0.156}$ W/m·K was computed, compared to the measured value of $\lambda_{\text{cBN 5wt\%,exp}} = \mathbf{0.18}$ W/m·K.

Considering that the microstructure of the cBN 5wt% composite, which was presented before in Chapter 6, has revealed pronounced agglomerations of the c-BN particles (also see Figure 8.3), it is assumed that this difference in morphology between the simulated case of well dispersed c-BN and the observed agglomerated structure in the actual cBN 5wt% sample will result in the mismatch of the calculated and experimental values. Therefore, new geometries for the cBN 5wt% composite were created, taking into account the clusters with high density of c-BN particles. Hence, the influence of these agglomerations on the composites' thermal conductivity could be evaluated.

The new geometries for these simulations, based on the micrographs, are presented in Figure 8.4. In case a), the c-BN particles surrounding the center particle are positioned in a small distance to the latter. In the cases b) and c), all particles were in direct contact, forming agglomerates in shape of an “X” or an “+”, respectively, and thus, providing continuous pathways for the heat transfer over a larger distance within the composites' bulk. The results of these additional simulations are summarized in Table 8.2.

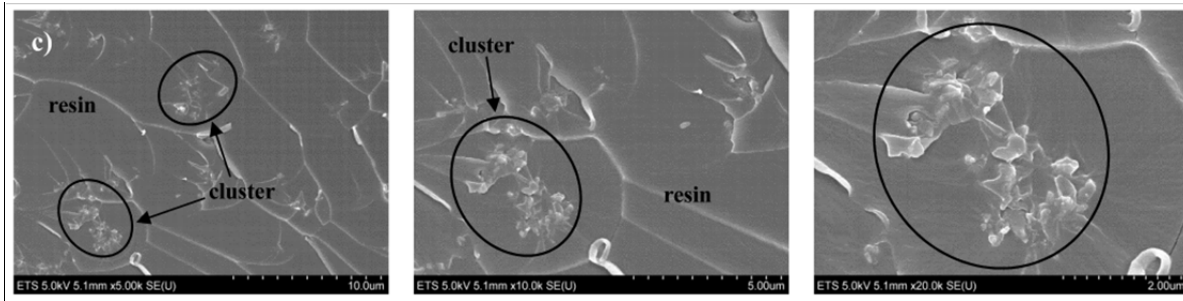


Figure 8.3 Micrograph of the cBN 5wt% sample (with increasing magnification from left to right) showing that the c-BN particles were not well dispersed in the matrix, but formed clusters with c-BN agglomerations

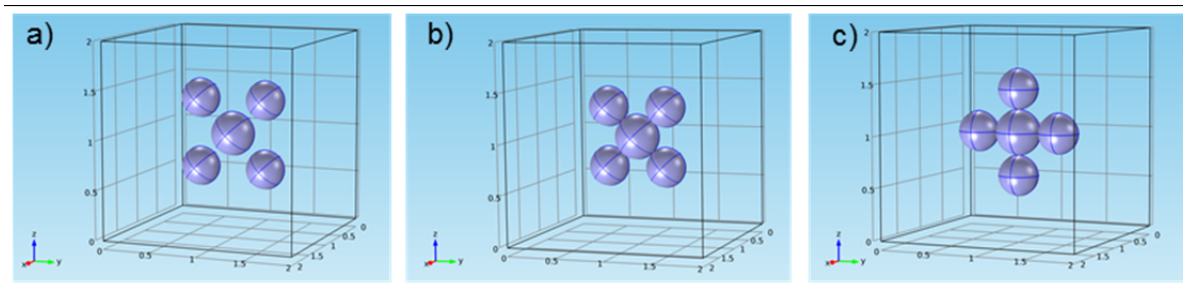


Figure 8.4 New geometries for the cBN 5wt% sample with a) small distance between the particles, b) an agglomerated “X” structure and c) an agglomerated “+” structure

Table 8.2 Comparison of simulation results with the experimental value for the thermal conductivity in the case of cBN 5wt% with clusters of c-BN particles (coherent results are highlighted in green, unmatched results in orange)

Geometry	Thermal conductivity in W/(m·K)	
	experimental $\lambda_{cBN\ 5wt\%,exp}$	simulated $\lambda_{cBN\ 5wt\%,sim}$
Case a) separated particles		0.156
Case b) clustered “X”	0.180	0.179
Case c) clustered “+”		0.183

It was found that in both cases with direct contact of the particles, cases b) and c) respectively, the calculated values of the composites’ thermal conductivities were very close compared to the experimental data. In case a), where the particles were close to each other

but still separated by a small distance, no improvement in thermal conductivity was found compared to the previously discussed case of well dispersed particles (compare with Table 8.1).

Thus, it can be concluded that the formation of continuous pathways for the heat transfer, given by agglomerated c-BN particles, was the reason for the elevated thermal conductivity measured for the cBN 5wt% sample in Chapter 6.

In contrast to dielectric properties, which usually see a worsening with agglomerated filler particles, such as the dielectric breakdown strength or the dielectric response (e.g. additional loss peaks can occur due to agglomerated particles), the observed agglomerates prove beneficial in terms of the thermal conductivity. Through the formation of continuous pathways with reduced phonon scattering and a high thermal conductivity (1300 W/m·K in case of c-BN), the heat transfer through the composite volume can be significantly boosted compared to well dispersed systems.

In order to balance the only marginally lower or higher values found in cases b) and c) with respect to the experimental value of 0.18 W/m·K, an additional geometry of 8 unit cells was created, since the clusters observed by SEM can be of random shape. This geometry contains both agglomerated scenarios in an equal amount: 4 times the case b) and 4 times the case c) (see Figure 8.5).

Based on this new geometry, a new simulation was performed and the obtained thermal conductivity for the cBN 5wt% composite was $\lambda_{\text{cBN 5wt\%,sim}} = 0.18 \text{ W/m}\cdot\text{K}$. This value exactly matched the experimental data. It thus appears that the proposed model based on random c-BN clusters is adequate to simulate the heat transfer in the c-BN composites at hand.

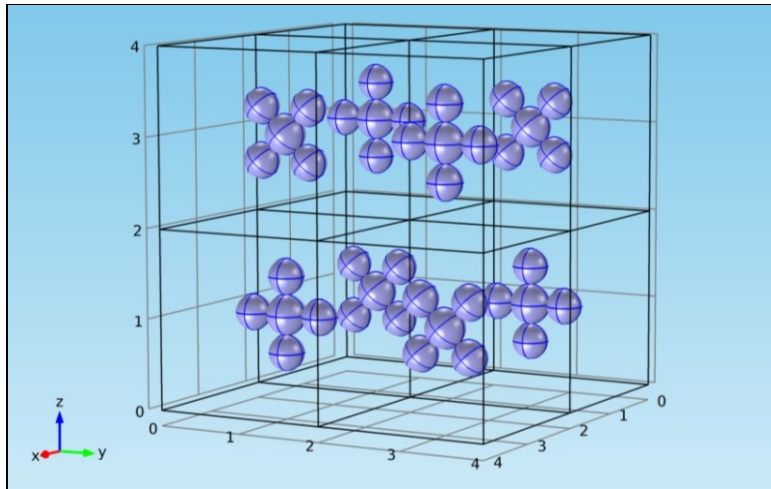


Figure 8.5 Scenario with 8 unit cells (cases b) and c) in equal numbers), representing a random structure of cBN 5wt%

8.3 Unraveling the thermal conductivity of the multiphase and functional POSS composites

In paragraph 8.2 we have established the influence of particle dispersion on the thermal conductivity and have seen that the resulting thermal conductivity was lower for well dispersed particles in epoxy compared to the case of agglomerations. However, in Chapter 6 it was reported that a significantly improved dispersion of the c-BN particles was found in the cases of the multiphase (MP) composites, and thus, when 1 wt% POSS was added to the epoxy in addition to 5 wt% of c-BN (see Figure 8.6).

Table 8.3 Overview of the sample natures and the respective measured thermal conductivities in case of cBN 5wt% and the two multiphase samples

Sample	Sample nature	Thermal conductivity in W/(m·K)
cBN 5wt%	Epoxy + 5 wt% c-BN	0.180
MP/G-POSS	Epoxy + 1 wt% G-POSS + 5 wt% c-BN	0.178
MP/TG-POSS	Epoxy + 1 wt% TG-POSS + 5 wt% c-BN	0.176

Considering though, that in the case of well dispersed c-BN particles a composite thermal conductivity of only 0.156 W/m·K was calculated before (see Table 8.1), yet in the cases of both MP samples a thermal conductivity close to the one of cBN 5wt% was noted, as summarized in Table 8.3, it is evident that the added POSS in the MP composites has to contribute to their thermal conductivity.

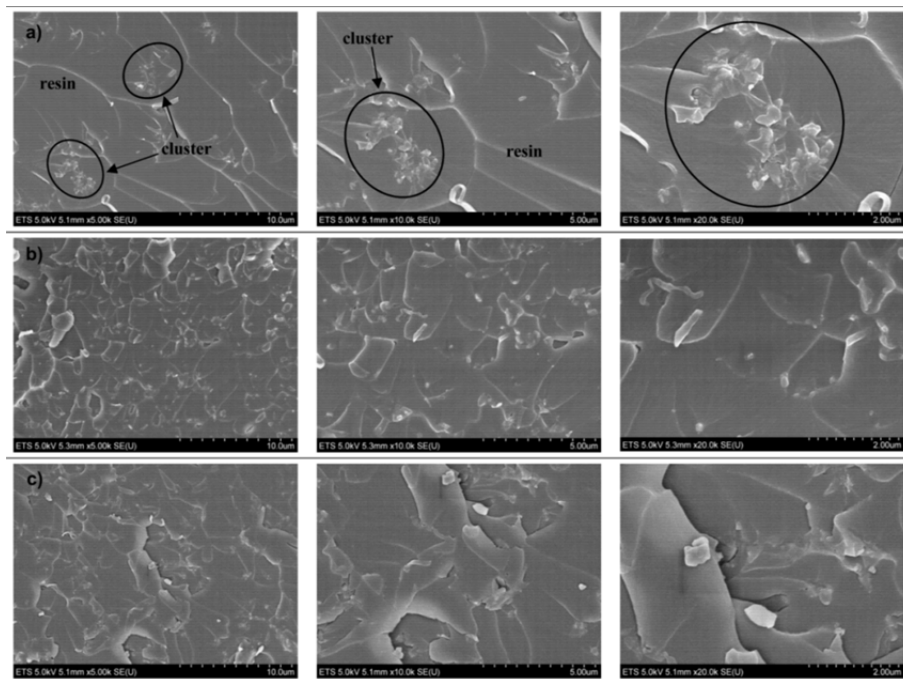


Figure 8.6 Microstructures of a) cBN 5wt%, b) MP/G-POSS and c) MP/TG-POSS. In the two MP samples a clearly improved dispersion of the c-BN particles resulted

8.4 Evaluation of POSS' contribution to the thermal conductivity in the multi-phase composites

The second step in our computational approach was to understand the contribution of POSS to the thermal conductivity in the multiphase (MP) composites. Thus, a new simulation was conducted based on the geometry of the well dispersed cBN 5wt% sample presented in Figure 8.1c. As mentioned before, the calculations conducted with this model geometry have given a bulk thermal conductivity value of only 0.156 W/m·K.

Considering that the TG-POSS and G-POSS (in the used contents of 1 wt%) have been successfully dispersed on a molecular level (as shown in Chapters 4 and 5), it was assumed that POSS is intimately incorporated in the epoxy. Thus, epoxy plus POSS form the actual matrix in case of the MP composites, where the c-BN particles will then be introduced.

Based on this assumption, a series of simulations were conducted, where the thermal conductivity of the matrix for the well dispersed cBN 5wt% model was varied, having the thermal conductivity measured for neat epoxy (0.142 W/m·K) as the lower limit and the thermal conductivity of the 1 wt% G-POSS composite (0.172 W/m·K) as the upper limit. The results of these simulations, based on the geometry shown in Figure 8.1c and the varying thermal conductivity of the matrix from 0.142 to 0.172 W/m·K, are summarized in Table 8.4.

It was found that in case of MP/TG-POSS, the thermal conductivity of the matrix would need to be $\lambda_{\text{matrix}} = 0.164 \text{ W/m}\cdot\text{K}$, and $\lambda_{\text{matrix}} = 0.166 \text{ W/m}\cdot\text{K}$ in case of MP/G-POSS, in order to achieve the $\lambda_{\text{MP composites}}$ of 0.176 and 0.178 W/m·K, respectively. These enhanced values in thermal conductivity of the respective epoxy/POSS matrices, compared to neat epoxy with $\lambda_{\text{epoxy}} = 0.142 \text{ W/m}\cdot\text{K}$, must thus be attributable to the addition of POSS in the epoxy.

Now that we have established in which extend POSS will have to contribute to the thermal conductivity in the multiphase composites, additional simulations were conducted in the next modelization step, in order to further understand the mechanisms of how the incorporation of POSS in epoxy can contribute to the heat transfer in the respective composites. In the following simulation steps only the case of G-POSS will be investigated.

8.4.1 Simulations based on the assumption that POSS is represented only by its silica core

When we consider that G-POSS is a hybrid inorganic/organic material with common molecular sizes of 2-5 nm, consisting of a silica-like core that has organic epoxy groups attached, which are compatible with the epoxy system used in our studies, it seems

appropriate for our simulations to implement POSS as a very small silica particle which is surrounded by functional groups.

Table 8.4 Simulation results of bulk thermal conductivity for the MP composite (right column) as a function of a variation in the matrix' thermal conductivity (left column). The values for λ_{matrix} which will lead to the measured values of $\lambda_{\text{MP composite}}$ are highlighted in green

Variation of thermal conductivity of the matrix in W/(m·K) λ_{matrix} with 1 wt% POSS	Simulation results of thermal conductivity for the MP composite in W/(m·K) $\lambda_{\text{MP composite}}$
0.142	0.154
0.144	0.156
0.146	0.158
0.148	0.160
0.150	0.162
0.152	0.164
0.154	0.166
0.156	0.168
0.158	0.170
0.160	0.172
0.162	0.174
0.164	0.176 ⁽²⁾
0.166	0.178 ⁽³⁾
0.168	0.180
0.170	0.182
0.172	0.185

² This value corresponds to the experimental value found for the MP/TG-POSS composite

³ This value corresponds to the experimental value found for the MP/G-POSS composite

Taking into account the molecular weight of G-POSS with 1338 g/mol, the silica content in G-POSS can be established to be approximately 45 wt%. Based on these assumptions, a new model was established with well dispersed silica particles representing 1 wt% of G-POSS and accordingly 0.45 wt% of silica (see Figure 8.7). The unit cell in this case had side lengths of 25 nm and the 1 wt% of G-POSS was embodied by 9 silica particles with a chosen radius of 1 nm. As stated before, for the GP 1wt% composite a thermal conductivity of $\lambda_{\text{GP1wt\%}} = 0.172 \text{ W/m}\cdot\text{K}$ was found experimentally in Chapter 6. The computed results, based on the geometry of 9 dispersed silica spheres with a radius of 1 nm, as well as the simulation parameters used for this case are listed in Table 8.5.

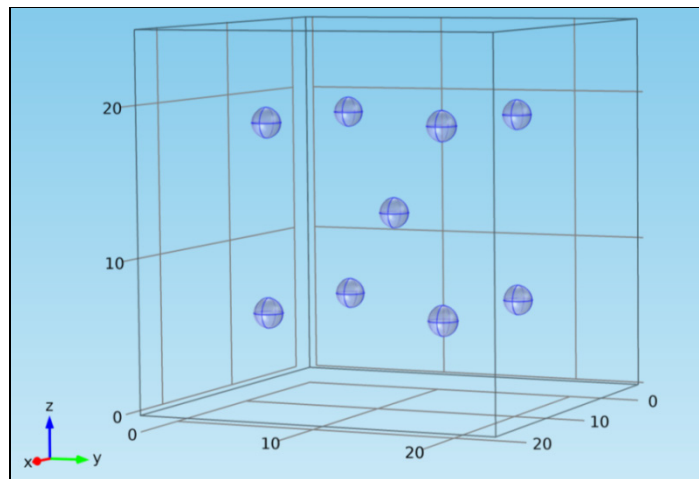


Figure 8.7 The geometry for the calculation of the thermal conductivity of GP 1wt%, with G-POSS represented by 9 well dispersed silica spheres

Table 8.5 Simulation parameters and resulting thermal conductivities for the GP 1wt% composite, where POSS was embodied by 9 silica spheres (unmatched results highlighted in orange)

Composite	Thermal conductivity in W/(m·K)			
	of constituents		of composite	
	λ_{epoxy}	λ_{silica}	simulated $\lambda_{\text{GP1wt\%,sim}}$	experimental $\lambda_{\text{GP1wt\%,exp}}$
GP 1wt%	0.142	1.38	0.143	0.172

From these simulations it was found that simple incorporation of 0.45 wt% of silica particles with the selected size does not contribute to a significant enhancement of the thermal conductivity – with $\lambda_{\text{GP1wt\%,sim}} = 0.143 \text{ W/m}\cdot\text{K}$ being close to $\lambda_{\text{epoxy}} = 0.142 \text{ W/m}\cdot\text{K}$.

Therefore, it can be concluded that the reactive nature of G-POSS, with the epoxy groups surrounding the silica core, must have an impact on the morphology of the epoxy/POSS network, in a way that enhances phonon transport through the bulk composite, and thus increases the thermal conductivity of the POSS composites.

8.4.2 Proposal of the Interfacial Restructuration Model (IFRM) for conductive heat transfer in functional POSS composites

Since the simple presence of silica, representing the POSS, in the host polymer does not explain the 20 % increase in thermal conductivity for the GP 1wt% composite, it appears that the incorporation of the reactive POSS in the epoxy matrix leads to a nanostructured epoxy/POSS network, as it was proposed in Figure 6.1 in Chapter 6. This restructuring of the polymeric matrix will then provide continuous pathways for the phonon transport through the bulk composite by inter-connecting epoxy chains with POSS molecules (see Figure 8.8).

The radius of influence on the restructuring of the epoxy/POSS network surrounding the silica core of POSS, and thus the *interfacial restructuring zone (IFRZ)* might change as a function of POSS content in the composite, considering the retrogressive trend found for the thermal conductivities of the POSS composites with increasing POSS content; which is in contradiction to the existing mixings laws, as it was shown in Figure 5.5 in Chapter 5.

Furthermore, in the presence of an additional type of filler in the same composite, these additional particles might interact with the IFRZ of POSS, and hence alter its radius of influence. This could further lead to the slight difference in thermal conductivity of the modified matrix (epoxy + 1 wt% of G-POSS), seen in the simulation of the multiphase composite, with $\lambda_{\text{matruix}} = 0.166 \text{ W/m}\cdot\text{K}$ instead of $0.172 \text{ W/m}\cdot\text{K}$ experimentally found for the GP 1wt% composite (Table 8.4).

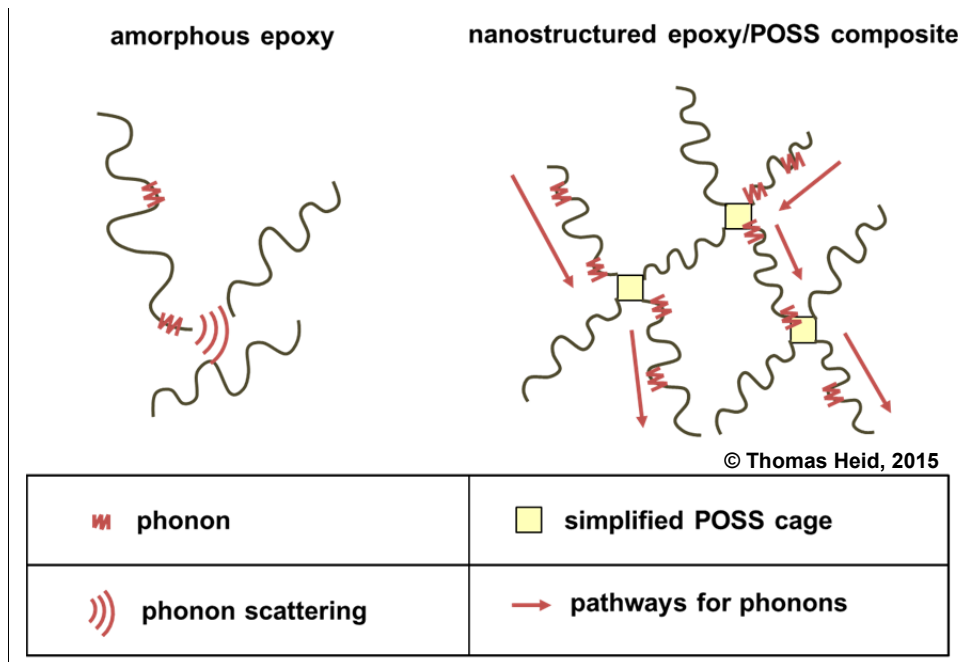


Figure 8.8 Schematic to explain the enhanced phonon transport in POSS composites compared to neat epoxy, caused by an interfacial restructuring of the polymeric network due to covalent bonding between epoxy and POSS

In order to evaluate the interaction of the POSS molecules with each other, and also the interaction between POSS and the c-BN particles (in the case of our multiphase composites), and thus, their respective effects in terms of the IFRZ of POSS, additional simulations were performed, which represent the third step in our simulation-based analysis of the conductive heat transfer in composites containing POSS.

8.4.3 Evaluation of the interfacial restructuring zone (IFRZ) of POSS by means of 3D FEM simulations

In this paragraph, to further understand the IFRZ of G-POSS when incorporated in epoxy, new FEM simulations of the heat transfer through the GP 1wt% composite will be conducted. Therefore, the IFRZ around the silica particles will be realized in COMSOL by concentric spherical regions surrounding the silica core, based on the geometry established for GP 1wt% in Figure 8.7.

In order to find the impact of the IFRZ on the thermal conductivity of the bulk composite, the IFRZ was implemented with 2 variable parameters:

- the size (radius) of the IFRZ was varied from 0.75-5 nm, measured from the silica particle surface;
- the thermal conductivity of the IFRZ was varied from 0.1-1.4 W/m·K.

These limits were chosen as follows: The minimum radius of 0.75 nm for the IFRZ was selected by taking into account the chemical structure of G-POSS, and more specifically the epoxy side groups with their bond lengths and angles, based on which these side groups can span over a distance of approximately 0.75 nm, when reticulating with epoxy molecules. The maximum radius of 5 nm for the IFRZ was based on a geometric cause, because it represents the particular case when an overlap between neighboring IFRZs occurs, which results in the IFRZs spanning over the complete unit cell of the COMSOL model, as you can see in Figure 8.9c. The selection of the thermal conductivities attributed to the IFRZs was based on the assumption that the restructuration of the polymeric web can't lead to a higher thermal conductivity than for silica itself, which is 1.38 W/m·K according to (Lide, 1994), but should just slightly enhance the phonon transport in the IFRZ-affected regions of the composite.

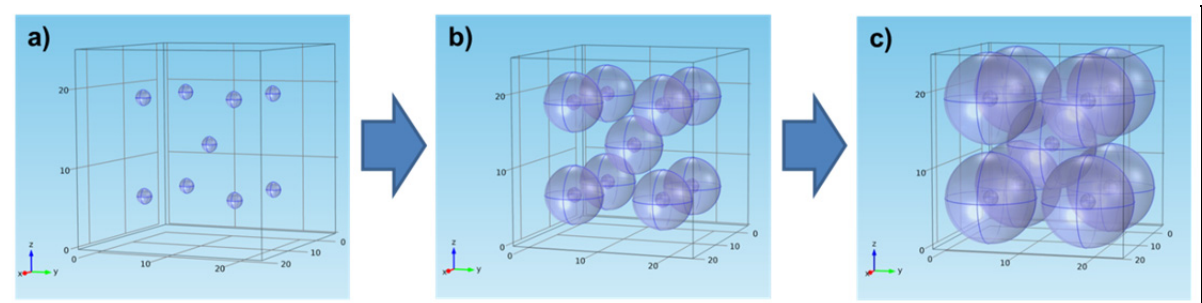


Figure 8.9 Different geometries used for the simulations of the impact of the IFRZ on the thermal conductivity of GP 1wt%, showing the varying size of the IFRZ for a) no IFRZ at all (0 nm), b) with a 3 nm and c) with a 5 nm IFRZ

In Figure 8.9, the change in morphology of the GP 1wt% is shown, as the *interfacial restructuration zone* is expanded up to 5 nm, as it is the case in Figure 8.9c, in which the

center IFRZ will then slightly overlap with the 8 surrounding IFRZs. This represents the case when these IFRZs span over the complete composite, and thus create continuous pathways for the phonon conduction throughout the bulk composite, which is the aforementioned reason for the upper limit of 5 nm for the IFRZ radius.

The simulation results of the bulk thermal conductivity calculated for the different morphologies of GP 1wt%, as a function of IFRZ radius and its thermal conductivity are presented in Figure 8.10. By analysing the presented curves, it can be seen that, in the cases of small IFRZs, for 2 nm in radius and below, the experimental value of 0.172 W/m·K for the bulk thermal conductivity cannot be achieved. Thus, the IFRZ in the GP 1wt% must have a size larger than 2 nm in radius.

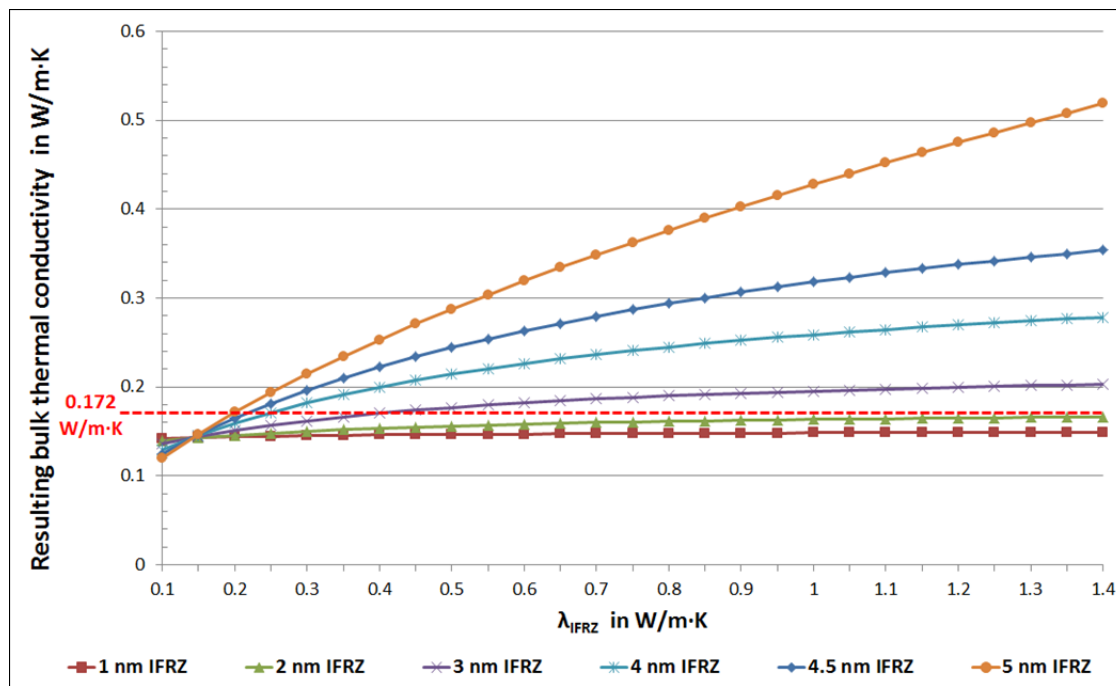


Figure 8.10 Computed bulk thermal conductivity of the GP 1wt% composite as a function of radius and thermal conductivity of the IFRZs. The dashed red line shows the experimental value of the GP 1wt% composite, which is the desired bulk thermal conductivity for our model cases

Also, considering that the IFRZ is defined by its organic nature and only causes a restructuring of the epoxy chains in its vicinity, therefore the effective thermal conductivity

of the IFRZs might be close to the actual thermal conductivity found for the neat epoxy, yet slightly higher as a result of the restructuration of the matrix in vicinity of the POSS core.

In Table 8.6, multiple possible combinations of the thermal conductivity λ_{IFRZ} of the interfacial restructuration zone and its radius are presented. They yield close values of the computed bulk thermal conductivity compared to the 0.172 W/m·K measured for the GP 1wt% composite. All the values were obtained by COMSOL simulations by varying the two parameters λ_{IFRZ} and the IFRZ's radius. The values listed in Table 8.6 represent the cases for which the curves of varying λ_{IFRZ} and IFRZ radius in Figure 8.10 intersect with the dotted red line, which denotes the required bulk thermal conductivity of 0.172 W/m·K for the GP 1wt% composite.

Table 8.6 The calculated bulk thermal conductivities of GP 1wt% in W/(m·K) as a function of the interfacial restructuration zone's λ_{IFRZ} and its radius around the silica core. Possible combinations of λ_{IFRZ} and its radius giving the same bulk thermal conductivity as measured for GP 1wt% are highlighted in green

λ_{IFRZ} in W/(m·K)	Calculated bulk thermal conductivity of GP 1wt% in W/(m·K) as a function of λ_{IFRZ} and its radius around the silica core				
	3 nm radius	3.5 nm radius	4 nm radius	4.5 nm radius	5 nm radius
0.2	0.151	0.155	0.159	0.165	0.172
0.25	0.157	0.163	0.171	0.181	0.194
0.3	0.162	0.171	0.182	0.196	0.215
0.35	0.167	0.177	0.191	0.210	0.235
0.4	0.170	0.183	0.200	0.222	0.253
0.45	0.174	0.188	0.207	0.234	0.271

Starting from the largest IFRZ-radius of 5 nm, where a λ_{IFRZ} of 0.2 W/m·K would result in the searched bulk thermal conductivity of GP 1wt% (0.172 W/m·K), we observe that with decreasing IFRZ-radii, slightly increasing values of λ_{IFRZ} are required (see Table 8.6), in order to achieve the necessary bulk thermal conductivity of 0.172 W/m·K.

In order to further evaluate which of the above-listed combinations of IFRZ-radius and its thermal conductivity (from Table 8.6) is the most plausible, another set of simulations were added, to unravel the heat transfer phenomenon in G-POSS composites. Therefore, additional geometries for G-POSS composites with higher contents of POSS were created and their resulting thermal conductivities were calculated and compared to their respective experimental results, which were presented in Chapter 5, Table 5.5.

8.4.4 Validation of the proposed model of the interfacial restructuring zones

In this fourth and final part of our simulation-based analysis, the cases of GP 2.5wt%, GP 5wt%, GP 10wt% and GP 20wt% were implemented in COMSOL in the same way GP 1wt% was treated. Thus, in all the cases of different POSS contents, the IFRZs around the silica core have been varied in size and thermal conductivity, to find the suitable combinations of these two parameters, to match the computed results of the composites' bulk thermal conductivity with the experimental values obtained for the respective POSS composites. The final combinations of the IFRZs' thermal conductivity and its respective sizes, found for the simulations of the different POSS composites, are listed in Table 8.7.

Table 8.7 Final results of the COMSOL simulations on the bulk thermal conductivity of the G-POSS composites showing matching parameter combinations for the IFRZs

Composite	Suitable combinations of IFRZ parameters		Thermal conductivity in $W/(m \cdot K)$	
	λ_{IFRZ}	radius of IFRZ	simulated $\lambda_{composite,sim}$	experimental $\lambda_{composite,exp}$
GP 1wt%	0.2 $W/m \cdot K$	5 nm	0.172	0.172
GP 2.5wt%	0.2 $W/m \cdot K$	3 nm	0.166	0.166
GP 5wt%	0.2 $W/m \cdot K$	2 nm	0.164	0.164
GP 10wt%	0.2 $W/m \cdot K$	0.75 nm	0.159	0.156
GP 20wt%	0.1 $W/m \cdot K$	0.75 nm	0.146	0.145

The respective geometries for the POSS composites with the final sizes of the IFRZs, which lead to matching computed values with the experimentally found thermal conductivities, are shown in Figure 8.11.

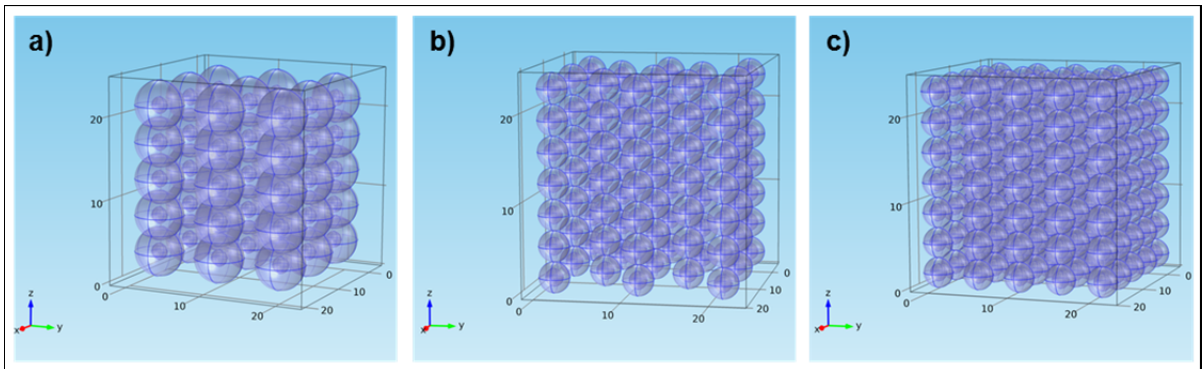


Figure 8.11 The final geometries for the cases of a) GP 5wt%, b) GP 10wt% and c) GP 20wt% with the IFRZ sizes that gave the matching results for the calculations compared with the experimental data

It was found that for G-POSS contents up to 10 wt% the choice of a constant λ_{IFRZ} with a value of 0.2 W/m·K and a varying size of the IFRZs, i.e. decreasing with increasing POSS content, resulted in matching results of the computed bulk thermal conductivities of the G-POSS composites with the experimental data. These findings show, according to the assumption made in paragraph 8.4.2, that with increasing POSS addition the IFRZ radius will be affected, becoming smaller and smaller with increasing POSS content in the composite.

However, in case of the GP 20wt% a distinct change from this pattern was seen. In this specific case, the resulting thermal conductivity just by implementing the 20 wt% of G-POSS embodied by its equivalent amount of silica particles, which is 9 wt% of silica, would result in a bulk thermal conductivity of 0.16 W/m·K for the respective GP 20wt% composite. This is an unrealistic value, given that it would be significantly higher as the experimental value of 0.145 W/m·K found for this composite.

Considering this, the low experimental value of 0.145 W/m·K for GP 20wt% can thus only be attributed to pronounced phonon scattering occurring at such high POSS contents at the interfaces between the organic matrix and the inorganic silica core and even more, at the interfaces between the bulk composite and the crystalline structures observed by SEM (see Chapter 5).

In the COMSOL simulations, therefore, a lower value for λ_{IFRZ} of only **0.1 W/m·K** was needed to match the computed value of the bulk thermal conductivity with the measured value in the case of the GP 20wt% composite. This value of $\lambda_{\text{IFRZ}} = 0.1 \text{ W/m}\cdot\text{K}$ is lower than the thermal conductivity measured for neat epoxy ($\lambda_{\text{epoxy}} = 0.142 \text{ W/m}\cdot\text{K}$).

8.5 Concluding remarks on the interfacial restructuring zones in functional POSS composites

The simulations have confirmed that the restructuring of the matrix, in vicinity of the incorporated POSS molecules, leads to a slightly enhanced phonon transport around the POSS core, i.e. in the proposed interfacial restructuring zone (IFRZ). Thus, higher bulk thermal conductivities of the POSS composites result.

The IFRZ was shown to have a thermal conductivity $\lambda_{\text{IFRZ}} = \mathbf{0.2 \text{ W/m}\cdot\text{K}}$, and even more, it was revealed that the reach of this interfacial restructuring zone will vary based on the content of POSS additive in the epoxy matrix. More specifically, the IFRZ radius will decrease with increasing POSS content.

Additionally, the performed simulations have led to the conclusion that 1 wt% of G-POSS in the MP composite needs to result in a thermal conductivity of approximately 0.166 W/m·K of the epoxy/POSS matrix, in order to achieve a bulk thermal conductivity of 0.178 W/m·K when both, 1 wt% of G-POSS and 5 wt% of c-BN are incorporated in the MP/G-POSS multiphase sample. Based on the results found by the COMSOL simulations, suggesting a constant value of the IFRZs' thermal conductivity of $\lambda_{\text{IFRZ}} = \mathbf{0.2 \text{ W/m}\cdot\text{K}}$ for G-POSS contents $\leq 10 \text{ wt}\%$, a suitable scenario for the IFRZ's thermal conductivity and radius can

hence be derived for the case of the MP/G-POSS composite. Here, a λ_{IFRZ} of also **0.2 W/m·K** and an IFRZ radius of approximately 4.5 nm would lead to a value of 0.165 W/m·K in thermal conductivity (see Table 8.8) for the epoxy/POSS matrix. This value is very close to the necessary 0.166 W/m·K required for the matrix of epoxy + POSS, so that the calculations conducted on the multiphase samples with varying thermal conductivities for the matrix are matched (as presented in Table 8.4).

It thus appears that, besides POSS itself, the presence of other filler particles can as well influence the range of the interfacial restructuration zones (IFRZ) due to the POSS addition in epoxy.

Table 8.8 Final results of the COMSOL simulations presenting the matching combinations of IFRZ parameters to achieve a $\lambda_{\text{matrix}} = \mathbf{0.166 \text{ W/m}\cdot\text{K}}$ by incorporation of 1 wt% G-POSS in the multiphase composite

Composite	Suitable combinations of IFRZ parameters		Thermal conductivity in W/(m·K) simulated
	λ_{IFRZ}	radius of IFRZ	$\lambda_{\text{MP/G-POSS,sim}}$
Matrix of epoxy + 1 wt% G-POSS	0.2 W/m·K	4.5 nm	0.165

In conclusion, it can thus be stated that the proposed *Interfacial Restructuration Model* or *IFRM* was appropriate to clarify the heat transfer phenomenon for the functional POSS composites at hand and proves to be adequate to explain the specific influence of reactive POSS on the conductive heat transfer in epoxy/POSS composites, unlike other theoretical models such as the mixing laws.

CONCLUSION

In this chapter a comprehensive synthesis of this work is provided. Due to the manuscript-based nature of this thesis, the main conclusions will be presented in accordance with the published articles in the respective chapters.

The aim of this PhD thesis was to design and analyze innovative nanostructured multiphase epoxy composites, which would take advantage of the specific features of both POSS and BN as filler materials, and thus exhibiting improvements such as reduced degradation due to electrical discharges and enhanced thermal conductivities.

In Chapter 1, a review of the materials used in this research project was presented along with an introduction to dielectrics and nanodielectrics. Chapter 2 offers a synthesis of the physical properties of polymer dielectrics. In Chapters 3 to 6, the thermal and dielectric properties of different epoxy based composites were presented and debated.

In Chapter 3, epoxy composites with low contents, i.e. up to 5 wt% of submicrometric and micrometric hexagonal boron nitride particles were analyzed. It was found that:

- The AC breakdown strength of h-BN composites was found to be diminished with increasing content of h-BN particles, although the deterioration of the breakdown strength for submicrometric BN205 composites was found to be less distinct compared to their micrometric BN counterparts, because micrometric particles are more likely to introduce defects in the epoxy matrix during the fabrication process;
- The resistance to erosion due to electrical discharge has been remarkably increased by up to 50 % less eroded volume for the h-BN composites. Composites with only 1 wt% h-BN content were found to have the best erosion resistance due to less introduced defects in the epoxy matrix with less filler particles. The micrometric BN600 composites performed better than the submicrometric BN205 ones, which was attributed to the larger specific surface area of BN600, offering better protection against the electrical discharges;

- The thermal conductivity of composites with less than 5 wt% h-BN did not show any significant increase. The submicrometric BN205 5wt% composite revealed a noteworthy increase of 17 % in thermal conductivity compared to neat epoxy, the micrometric BN600 5wt% composite, however, an increase of 11 %. The superior performance of the submicrometric h-BN composite over the micrometric one could be attributed to the larger volume fraction in the composites for submicrometric h-BN particles, as well as augmented phonon scattering at particle-matrix interfaces for the micrometric BN particles due to their larger specific surface area;
- In summary, it was shown in this first study that incorporation of very low weight fractions of h-BN particles in an epoxy resin could result in noticeable improvements of dielectric and thermal performance of the resulting composites. Although the composites with a loading of 5 wt% h-BN revealed a deterioration in AC breakdown strength, it should be mentioned that the respective breakdown strengths found (more than 130 kV/mm) are still significantly higher than common electric stresses in high voltage insulation systems (e.g. 2 to 3 kV/mm in stator bars for rotating machines). Therefore the improvements in erosion resistance and thermal conductivity should be granted a higher emphasis.

In Chapter 4, the dielectric and thermal properties of novel epoxy/POSS composites, were investigated along with POSS' effect on the nanostructuration of epoxy composites. By incorporation of Triglycidylisobutyl-POSS, which has three reactive epoxy groups that can form covalent bonds with the epoxy system used, we have shown that:

- The addition of low amounts of Triglycidylisobutyl-POSS (≤ 5 wt%) lead to improved dielectric breakdown strengths by more than 10 % in case of the 2.5 wt% POSS composite;
- The corona resistance of the fabricated Triglycidylisobutyl-POSS composites has seen notable improvements, especially in the cases when 1 and 2.5 wt% of Triglycidylisobutyl-POSS were incorporated in the epoxy resin, which resulted in approximately 60 % less eroded sample volume due to corona discharges;

- The thermal conductivities of the resulting nanostructured epoxy/POSS composites have seen an enhancement compared with the neat polymer. The composites with 1 and 2.5 wt% revealed 10 % higher thermal conductivities, whereas with increasing Triglycidylisobutyl-POSS contents lower values were found;
- In terms of the complex permittivity distinct interfacial loss peaks were seen for the POSS composites with 5 and 10 wt% of Triglycidylisobutyl-POSS. Such interfacial loss peaks occur due to local conduction phenomena caused by agglomerations of the filler, and hence, the POSS additive. Accordingly, for these two cases such agglomerated structures were found by SEM analysis;
- In summary, it was shown that the formation of covalent bonds between POSS and the epoxy matrix significantly improves the filler/matrix interaction, leading to intimate *interfaces* instead of undefined *interphases*, and hence, contributes to the distinct improvements in dielectric and thermal performances reported for the Triglycidylisobutyl-POSS composites. This was further supported by the superior performances of the lower content composites ePOSS 1wt% and ePOSS 2.5wt%, where no agglomerations were found, and hence, where the dispersion of POSS in the epoxy can be considered to be at a molecular level.

In Chapter 5, epoxy resins modified with functional Glycidyl-POSS were evaluated in terms of their potential for applications in high voltage insulation systems. This particular kind of POSS has a higher number of reactive epoxy groups than the Triglycidylisobutyl-POSS used in Chapter 4 (8-12 epoxy groups vs. 3 epoxy groups, respectively). Thus, it was expected to better integrate in the epoxy matrix by covalent bonding, and hence, lead to more pronounced enhancement of the dielectric and thermal properties of Glycidyl-POSS composites. In this chapter, we have shown that:

- The addition of Glycidyl-POSS has led to more distinctly improved dielectric breakdown strengths of all Glycidyl-POSS composites compared to the neat polymer. In case of the 2.5 wt% POSS composite by more than 17 %;
- The corona resistance of the produced Glycidyl-POSS composites has seen notable improvements, which was getting more pronounced with higher Glycidyl-POSS contents.

By incorporation of 1 wt% Glycidyl-POSS the corona resistance could be doubled, whereas by incorporation of 20 wt% Glycidyl-POSS the corona resistance can be enhanced by more than seven times;

- The thermal conductivities of the resulting nanostructured Glycidyl-POSS composites have seen an enhancement compared with the neat epoxy. The composite with 1 wt% Glycidyl-POSS revealed a by 20 % higher thermal conductivity. Similar to what was reported in Chapter 4, with increasing Glycidyl-POSS contents lower values followed;
- The Glycidyl-POSS used could be dispersed at a molecular level in the epoxy matrix at much higher loadings as the Triglycidylisobutyl-POSS used in the former study (Chapter 4). This could be concluded from the complex permittivity found for the Glycidyl-POSS composites, where no distinct interfacial loss peaks were observed. High resolution SEM and TEM analysis have confirmed the molecular dispersion for the Glycidyl-POSS composites;
- Crystalline zones were found for the 20 wt% Glycidyl-POSS composite, which are untypical for amorphous epoxies. These crystalline zones therefore must occur due to the Glycidyl-POSS added in such a high concentration, leading to the formation of such ordered, crystalline structures;
- In summary, it was shown that composites with low G-POSS content have excelled in high BD strengths and notably increased resistances against corona discharges, as well as enhanced thermal conductivities and low dielectric losses. The addition of 2.5 wt% of POSS in epoxy seems to be an optimal value in terms of dielectric strength and losses. Further increase of the Glycidyl-POSS loading can then contribute towards an even higher resistance to corona discharges, whereas in terms of thermal conductivity the composites with low contents of 2.5 wt% Glycidyl-POSS and below have seen the most significant enhancements.

In Chapter 6, we have investigated the interaction between the hybrid inorganic/organic POSS and inorganic cubic boron nitride (c-BN), when both filler types were incorporated in an epoxy composite. Both types of POSS, and hence, the Glycidyl-POSS and the Triglycidylisobutyl-POSS were used to produce such multiphase samples. The obtained

multiphase samples were compared in terms of their dielectric and thermal properties with the respective single-phase composites, where only POSS or c-BN was incorporated in epoxy. In this work we have found that:

- Although no complex chemical surface treatment of the c-BN particles involved was applied in our study, yet a homogeneous dispersion of the inorganic c-BN particles was seen for the multiphase composites. This effect of POSS, which was shown to act as a dispersant of the inorganic c-BN filler should be regarded as a major point of interest in nano-dielectrics or nano-composites in general, as the dispersion of nanometric inorganic filler particles within polymers is still a very current problematic. And thus, the approach of formulating epoxy composites combining reactive POSS and other filler particles to improve their dispersion within the epoxy matrix, could significantly contribute to the advancement of the implementation of epoxy-based nano-composites on an industrial level;
- In the presence of the submicrometric c-BN particles in the multiphase composites, the re-structuration of the polymeric matrix by incorporation of POSS was assumed to be hindered by the comparatively large c-BN particles, with an average size of 500 nm. Thus, no additional benefit was seen in terms of thermal conductivity or breakdown strengths when both POSS and c-BN were incorporated together in a multiphase sample;
- In summary, by comparing the G-POSS with the c-BN and the multiphase samples, besides the marginally higher thermal conductivity of the 5 wt% c-BN and both multiphase composites, it is evident that the G-POSS specimens feature the overall best performance of a dielectric material for high voltage insulation, with lower dielectric losses, higher BD strength, as well as increased thermal conductivity, compared to the base epoxy.

The 7th Chapter of this work consists of a comprehensive review of theoretical models, which are commonly used to estimate the dielectric permittivity or the thermal conductivity of polymer composites. A comparison between calculated values based on such theoretical models, also called mixing laws, with experimentally obtained results of the thermal conductivity of our fabricated h-BN and c-BN composites was conducted. It was shown that

the classical models based on the effective mean field approach could not be applied to estimate the thermal conductivities of the BN composites, as those models cannot account for effects such as phonon scattering. However, some semi-empirical models, the ones of Lichtenecker and Agari & Uno to be more precise, were shown to give coherent values of the effective medium thermal conductivity.

In order to further comprehend the complex behavior of our single and multiphase composites, an approach to model the thermal conductivities of these composites was presented in Chapter 8. Therefore, 3D FEM simulations of the conductive heat transfer in selected epoxy composites were conducted in COMSOL Multiphysics, to further analyze the heat transport phenomenon found for the POSS composites, where increasing POSS contents have led to a diminishment of the measured thermal conductivities of the respective composites. This trend is in contradiction with all existing mixing laws. These simulation-based analyses finally led to the proposal of a novel model, which can explain the heat transport phenomenon in the presented POSS composites. In this chapter it was shown that:

- The formation of continuous pathways for the heat transfer, given by agglomerated c-BN particles, was the result for the elevated thermal conductivity measured for the cBN 5wt% sample, which was approximately by 15 % higher in case of agglomerated c-BN structures compared to well dispersed c-BN particles in the same content;
- Considering the well dispersed c-BN particles in the multiphase composites though, which should lead to a lower composite's thermal conductivity, according to the findings by COMSOL simulations, it was proven that the incorporation of POSS in the multiphase samples has contributed to the heat conduction mechanism in these multiphase composites. Thus, the nanostructuring ability of POSS should not be considered as completely hindered, but slightly restricted when POSS is incorporated with other fillers in a multiphase composite;
- The silica-like core of POSS alone does not contribute to the enhanced thermal conductivity of the POSS composites, which was confirmed by COMSOL simulations. Thus, the restructuring of the epoxy matrix, which occurs due to the incorporation of reactive POSS additives, must lead to a locally enhanced phonon transport in the vicinity

of the POSS core. These **interfacial restructuration zones (IFRZ)** were found to have a slightly higher thermal conductivity (approximately 0.2 W/m·K) compared to the base epoxy used (0.142 W/m·K). Additionally, the size of the IFRZ around the POSS core will depend on the amount of POSS content. It was proven to decrease with increasing POSS content and also when other filler particles, e.g. c-BN, were incorporated in the same composite;

- Based on these findings it was concluded that the reactive nature of POSS, with the epoxy groups surrounding the silica core, must have an impact on the morphology of the epoxy/POSS network, in a way that enhances phonon transport through the bulk composite. This conclusion finally led to the proposal of the **Interfacial Restructuration Model (IFRM)**, to explain the particular results of thermal conductivities in the presented POSS composites.

Based on the presented results it can thus be stated that the developed nanostructured POSS composites have shown the potential to significantly improve the dielectric and thermal performances of epoxy based insulation materials. Due to the reactivity of POSS and its epoxy-like viscosity, it can be implemented into various production and processing methods, such as casting (e.g. bushings, spacers and cable terminations) and even in Vacuum-Pressure-Impregnation (VPI) or Resin-Rich (RR) processes for rotating machine insulation. Additionally, POSS offers the possibility to tailor the properties of the epoxy composite according to its specification, such as improved thermal conductivity and enhanced erosion resistance with low POSS contents for applications in i.e. rotating machines, or very high POSS contents for substantially improved resistance to erosion due to electrical discharges, which could be interesting for applications such as spacers for gas insulated switchgear (GIS) or gas insulated lines (GIL).

RECOMMENDATIONS

In order to further investigate the influence of POSS on the dispersion of inorganic filler particles in epoxy composites, it would be of interest to conduct additional studies involving nanometric filler, especially considering that the c-BN particles used in Chapter 6 were comparatively large, with an average size of 500 nm compared to approximately 2 nm for the POSS molecules. The use of nanometric sized filler, with sizes closer to that of the POSS molecules, might then allow to fully benefit from a synergetic effect of the two fillers. This could be embodied by a combination of high dielectric strength and further enhanced thermal conductivity for instance.

Even a slightly increased electrical conductivity, by one or two orders of magnitude compared to the neat epoxy, yet still maintaining a high dielectric strength could be achieved with the selection of an appropriate combination of POSS with electrically conductive filler. Tailoring the electrical conductivity of an epoxy composite at such a level could help prevent charge trapping in the resulting composites, which would make them interesting for application in HVDC insulation systems, where space charge accumulation can cause inhomogeneous electric field stresses of the insulators, which subsequently can cause premature breakdown of the insulator or surface flashovers.

Additionally, conducting space charge measurements on the POSS composites themselves could be of interest, to investigate if the nanostructuring of the epoxy/POSS network has resulted in more homogeneous bulk composites, and thus, in reduced charge trapping sites.

APPENDIX I

PERSONAL PUBLICATION LIST

JOURNAL PUBLICATIONS

- **T. Heid**, M. Fréchet and E. David: *Enhanced Electrical and Thermal Performances of Nanostructured Epoxy/POSS Composites*. IEEE Transactions on Dielectrics and Electrical Insulation, submitted 07/2015;
- **T. Heid**, M. Fréchet and E. David: *Functional epoxy composites for high voltage insulation involving c-BN and reactive POSS as compatibilizer*. Journal of Materials Science, vol. 50(16), 08/2015;
- **T. Heid**, M. Fréchet, and E. David: *Nanostructured Epoxy/POSS composites: Enhanced Materials for High Voltage Insulation Application*. IEEE Transactions on Dielectrics and Electrical Insulation, vol. 22(3), 06/2015;
- **T. Heid**, M. Fréchet, and E. David: *Epoxy/BN Micro- and Meso-composites: Dielectric and Thermal Properties of Enhanced Materials for High Voltage Insulation Systems*. IEEE Transactions on Dielectrics and Electrical Insulation, vol. 22(2), 04/2015;
- M. Toselli, D. Fabiani, P. Mancinelli, M. Fréchet, **T. Heid**, E. David, A. Sacconi: *In situ thermal reduction of graphene oxide forming epoxy nanocomposites and their dielectric properties*. Polymer Composites 02/2014;
- T. Berg, J. Fabian, **T. Heid**, T. Judendorfer, M. Lerchbacher, J. Podesser: *Ausgewählte technologische Entwicklungen in der Hochspannungstechnik*. e & i Elektrotechnik und Informationstechnik 06/2012.

CONFERENCE PROCEEDINGS

- **T. Heid**, M. Fréchet, and E. David: *Dielectric and Thermal Properties of Nanostructured Epoxy Composites Involving Reactive POSS and c-BN*. IEEE Electrical Insulation Conference (EIC), 2015;

- **T. Heid**, M. Fréchet, and E. David: *Dielectric and Thermal Properties of Submicrometric Epoxy/c-BN Composites*. IEEE Conference on Electrical Insulation and Dielectric Phenomena (CEIDP), 2014;
- **T. Heid**, M. Fréchet, and E. David: *Nanostructured Epoxy/POSS composites: High Performance Dielectrics with Improved Breakdown Strength and Corona Resistance*. IEEE Conference on Electrical Insulation and Dielectric Phenomena (CEIDP), 2014;
- M.F. Fréchet, I. Preda, H. Alamdari, P. Lewin, A. Holt, **T. Heid**: *Exploratory dielectric study involving ultra-low content of Si-C-Al in epoxy*. IEEE Conference on Electrical Insulation and Dielectric Phenomena (CEIDP) 2014;
- **T. Heid**, M. Fréchet, and E. David: *Nanostructured Epoxy/POSS composites: High Performance Dielectrics with Improved Corona Resistance and Thermal Conductivity*. IEEE Electrical Insulation Conference (EIC), 2014;
- H. Couderc, M. F. Fréchet, **T. Heid**, and E. David: *Evaluation of a new technique for preparation of HDPE / silica nanocomposites*. IEEE Electrical Insulation Conference (EIC), 2014;
- **T. Heid**, M. Fréchet, E. David: *Dielectric properties of epoxy/POSS composites*. IEEE Conference on Electrical Insulation and Dielectric Phenomena (CEIDP), 2013;
- **T.F. Heid**, N. Freebody, M.F. Fréchet, H. Couderc, C. Vanga, E. David, A.S. Vaughan: *Dielectric properties of epoxy/BN micro- and meso-composites: Dielectric response at low and high electrical field strengths*. IEEE Electrical Insulation Conference (EIC), 2013;
- **T. Heid**, S. Savoie, C. Vanga, M. Fréchet, E. David, N. Freebody, A. Vaughan: *Surface resistance of epoxy/BN micro- and Meso-composites exposed to electrical discharges*. IEEE International Conference on Solid Dielectrics (ICSD), 2013;
- I. Preda, J. Castellon, S. Agnel, P. Notingher, M. Fréchet, **T. Heid**, H. Couderc, N. Freebody, A.S. Vaughan: *Conduction currents and time to frequency domain transformation for epoxy resin nanocomposites*. IEEE International Conference on Solid Dielectrics (ICSD), 2013;

- M.F. Fréchet, M. Guo, **T. Heid**, E. David, S. Savoie, S. Sutton, S.J. Han: *Dielectric response of polyethylene modified with nanosilica*. IEEE Electrical Insulation Conference (EIC), 2013;
- P. Mancinelli, D. Fabiani, A. Saccani, M. Toselli, **T. Heid**, M. Fréchet, S. Savoie, E. David: *Preparation and dielectric behavior of epoxy resin containing graphene oxide*. IEEE International Conference on Solid Dielectrics (ICSD), 2013;
- C. Vanga-Bouanga, **T.F. Heid**, E. David, M.F. Fréchet, S. Savoie: *Tailoring of the electrical properties of silicon carbide for field grading application*. IEEE Electrical Insulation Conference (EIC), 2013;
- P. Mancinelli, **T. F. Heid**, D. Fabiani, A. Saccani, M. Toselli, M. F Fréchet, S. Savoie, E. David: *Electrical conductivity of graphene-based epoxy nanodielectrics*. IEEE Conference on Electrical Insulation and Dielectric Phenomena (CEIDP), 2013;
- P. Mancinelli, **T. F Heid**, D. Fabiani, A. Saccani, M. Toselli, M. F Fréchet, S. Savoie, E. David: *Thermal in situ reduction of graphene oxide in epoxy-based nanodielectrics: Influence on dielectric properties*. IEEE Conference on Electrical Insulation and Dielectric Phenomena (CEIDP), 2013.

LIST OF BIBLIOGRAPHICAL REFERENCES

- Abenojar, J., M. A. Martínez, M. Pantoja, F. Velasco et J. C. Del Real. 2012. « Epoxy Composite Reinforced with Nano and Micro SiC Particles: Curing Kinetics and Mechanical Properties ». *Journal of Adhesion*, vol. 31, n° 2, p. 418-434.
- Agari, Y., et T. Uno. 1986. « Estimation on thermal conductivities of filled polymers ». *Journal of Applied Polymer Science*, vol. 32, n° 7, p. 5705-5712.
- Andritsch, T., R. Kochetov, Y. T. Gebrekiros, P. H. F. Morshuis et J. J. Smit. 2010. « Short term DC breakdown strength in epoxy based BN nano- and microcomposites ». In *IEEE International Conference on Solid Dielectrics (ICSD)*.
- Andritsch, T., R. Kochetov, P. H. F. Morshuis et J. J. Smit. 2011. « Proposal of the polymer chain alignment model ». In *Electrical Insulation and Dielectric Phenomena (CEIDP), 2011 Annual Report Conference on.* (16-19 Oct. 2011), p. 624-627.
- Andritsch, T.M. 2010. « Epoxy Based Nanodielectrics for High Voltage DC Applications: Synthesis, Dielectric Properties and Space Charge Dynamics ». Dissertation. Delft University of Technology.
- Arora, Ravindra, et Wolfgang Mosch. 2011. « Electric Fields, their Control and Estimation ». In *High Voltage and Electrical Insulation Engineering*. p. 11-68. John Wiley & Sons, Inc. < <http://dx.doi.org/10.1002/9780470947906.ch2> >.
- Baker, Alan, Stuart Dutton et Donald Kelly. 2014. *Composite Materials for Aircraft Structures (2nd Edition)*. American Institute of Aeronautics and Astronautics.
- Bergman, David J. 1978. « The dielectric constant of a composite materialA problem in classical physics ». *Physics Reports Physics Reports*, vol. 43, n° 9, p. 377-407.
- Blythe, A. R., et D. Bloor. 2005. *Electrical properties of polymers*. Cambridge; New York: Cambridge University Press.
- Bocek, J., L. Matejka, V. Mentlik, P. Trnka et M. Slouf. 2011. « Electrical and thermomechanical properties of epoxy-POSS nanocomposites ». *European Polymer Journal*, vol. 47, n° 5, p. 861-872.
- Brockschmidt, M., F. Pohlmann, S. Kempen et P. Groppel. 2011. « Testing of nano-insulation materials: Some ideas, some experiences ». In *IEEE Electrical Insulation Conference (EIC)*.

- Bruggeman, D. A. G. 1935. « Berechnung verschiedener physikalischer Konstanten von heterogenen Substanzen. I. Dielektrizitätskonstanten und Leitfähigkeiten der Mischkörper aus isotropen Substanzen ». *Annalen der Physik*, vol. 416, n° 7, p. 636-664.
- Bánhegyi, G. 1986. « Comparison of electrical mixture rules for composites ». *Colloid and Polymer Science*, vol. 264, n° 12, p. 1030-1050.
- Calventus, Y., S. Montserrat et J. M. Hutchinson. 2001. « Enthalpy relaxation of non-stoichiometric epoxy-amine resins ». *Polymer*, vol. 42, n° 16, p. 7081-7093.
- Chen, George, Junwei Zhao, Shengtao Li et Lisheng Zhong. 2012. « Origin of thickness dependent dc electrical breakdown in dielectrics ». *Applied Physics Letters*, vol. 100, n° 22, p. 222904.
- Chen, Jiangfeng. 2012. « Nanostructuring of epoxy networks by using polyhedral oligomeric silsesquioxanes POSS and its copolymers ». Lyon, Institut national des sciences appliquées.
- Chisholm, Nathaniel, Hassan Mahfuz, Vijaya K. Rangari, Adnan Ashfaq et Shaik Jeelani. 2005. « Fabrication and mechanical characterization of carbon/SiC epoxy nanocomposites ». *Composite Structures*, vol. 67, n° 1, p. 115-124.
- Couderc, H., M. Frechette, E. David et S. Savoie. 2013. « Study of dielectric relaxation of epoxy composites containing micro and nano particles ». *IEEE Transactions on Dielectrics and Electrical Insulation*, vol. 20, n° 2, p. 592-600.
- Cui, Wei, Feipeng Du, Jinchao Zhao, Wei Zhang, Yingkui Yang, Xiaolin Xie et Yiu-Wing Mai. 2011. « Improving thermal conductivity while retaining high electrical resistivity of epoxy composites by incorporating silica-coated multi-walled carbon nanotubes ». *Carbon*, vol. 49, n° 2, p. 495-500.
- Daily, C. S., W. Sun, M. R. Kessler, X. Tan et N. Bowler. 2014. « Modeling the interphase of a polymer-based nanodielectric ». *Dielectrics and Electrical Insulation, IEEE Transactions on*, vol. 21, n° 2, p. 488-496.
- Dakin, T. W. 2006. « Conduction and Polarization Mechanisms and Trends in Dielectrics ».
- David, E., et M. Fréchet. 2013. « Polymer nanocomposites-major conclusions and achievements reached so far ». *Electrical Insulation Magazine, IEEE*, vol. 29, n° 6, p. 29-36.
- Dissado, L. A., et J. C. Fothergill. 1992. *Electrical degradation and breakdown in polymers*. London: P. Peregrinus.

- Dongling, Ma, A. Hugener Treese, W. Siegel Richard, Christerson Anna, Mårtensson Eva, Öneby Carina et S. Schadler Linda. 2005a. « Influence of nanoparticle surface modification on the electrical behaviour of polyethylene nanocomposites ». *Nanotechnology*, vol. 16, n° 6, p. 724-731.
- Dongling, Ma, A. Hugener Treese, W. Siegel Richard, Christerson Anna, Mårtensson Eva, Öneby Carina et S. Schadler Linda. 2005b. « Influence of nanoparticle surface modification on the electrical behaviour of polyethylene nanocomposites ». *Nanotechnology*, vol. 16, n° 6, p. 724.
- Fabiani, D., G. C. Montanari, A. Krivda, L. E. Schmidt et R. Hollertz. 2010. « Epoxy based materials containing micro and nano sized fillers for improved electrical characteristics ». In *IEEE International Conference on Solid Dielectrics (ICSD)*. p. 1-4.
- Friedrich, K., J. Ulanski, G. Boiteux et G. Seytre. 2001. « Time-of-flight ion mobility measurements in epoxy-amine systems during curing ». *Dielectrics and Electrical Insulation, IEEE Transactions on*, vol. 8, n° 3, p. 572-576.
- Fréchette, M. F. 2009. « Innovation in dielectric materials: from macro to nanoscales ». In *IEEE Electrical Insulation Conference (EIC)*. (May 31 2009-June 3 2009), p. 514-523.
- Fréchette, M. F., S. Savoie, M. Reading, A. S. Vaughan, H. Couderc, J. Castellon et L. Banet. 2012. « Surface resistance of epoxy-based composites to electrical discharge ». In *Electrical Insulation (ISEI), Conference Record of the 2012 IEEE International Symposium on*. (10-13 June 2012), p. 632-636.
- Fréchette, M. F., M. Trudeau, H. D. Alamdari et S. Boily. 2001. « Introductory remarks on nanoDielectrics ». In *2001 Annual Report Conference on Electrical Insulation and Dielectric Phenomena, October 14, 2001 - October 17, 2001*. (Kitchener, ON, Canada), p. 92-99. Coll. « Conference on Electrical Insulation and Dielectric Phenomena (CEIDP), Annual Report »: Institute of Electrical and Electronics Engineers Inc. < <http://dx.doi.org/10.1109/CEIDP.2001.963496> >.
- Fréchette, M., I. Preda, J. Castellon, A. Krivda, R. Veillette, M. Trudeau et E. David. 2014. « Polymer composites with a large nanofiller content: a case study involving epoxy ». *IEEE Transactions on Dielectrics and Electrical Insulation*, vol. 21, n° 2, p. 434-443.
- Goncharenko, A. V., V. Z. Lozovski et E. F. Venger. 2000. « Lichtenecker's equation: applicability and limitations ». *Optics Communications*, vol. 174, n° 1-4, p. 19-32.
- Haubner, R., M. Wilhelm, R. Weissenbacher et B. Lux. 2002. « Boron Nitrides — Properties, Synthesis and Applications ». In *High Performance Non-Oxide Ceramics II*, sous la

dir. de Jansen, Martin. Vol. 102, p. 1-45. Coll. « Structure & Bonding »: Springer Berlin / Heidelberg. < http://dx.doi.org/10.1007/3-540-45623-6_1 >.

- Heid, T. F., N. Freebody, M. F. Fréchet, H. Couderc, C. Vanga, E. David et A. S. Vaughan. 2013a. « Dielectric properties of epoxy/BN micro- and meso-composites: Dielectric response at low and high electrical field strengths ». In *IEEE Electrical Insulation Conference (EIC)*.
- Heid, T. F., M. Fréchet et E. David. 2013. « Dielectric Properties of Epoxy/POSS composites ». In *IEEE Conference on Electrical Insulation and Dielectric Phenomena (CEIDP)*. p. 751 - 755.
- Heid, T., M. Fréchet et E. David. 2014a. « Dielectric and thermal properties of submicrometric epoxy/c-BN composites ». In *IEEE Conference on Electrical Insulation and Dielectric Phenomena (CEIDP)*. (19-22 Oct. 2014), p. 719-722.
- Heid, T., M.F. Fréchet et E. David. 2014b. « Nanostructured Epoxy/POSS composites: High Performance Dielectrics with Improved Breakdown Strength and Corona Resistance ». In *IEEE Conference on Electrical Insulation and Dielectric Phenomena (CEIDP)*. p. 659-662.
- Heid, T., M.F. Fréchet et E. David. 2014c. « Nanostructured Epoxy/POSS composites: High Performance Dielectrics with Improved Corona Resistance and Thermal Conductivity ». In *IEEE Electrical Insulation Conference (EIC)*. p. 316-319.
- Heid, T., M. Fréchet et E. David. 2015a. « Dielectric and Thermal Properties of Nanostructured Epoxy Composites Involving Reactive POSS and c-BN ». In *IEEE Electrical Insulation Conference (EIC 2015)*. (Seattle).
- Heid, T., M. Fréchet et E. David. 2015b. « Epoxy/BN Micro- and Submicro-Composites: Dielectric and Thermal Properties of Enhanced Materials for High Voltage Insulation Systems ». *IEEE Transactions on Dielectrics and Electrical Insulation*, vol. 22, n° 2, p. 1176-1185.
- Heid, T., M. Fréchet et E. David. 2015c. « Nanostructured Epoxy/POSS composites: Enhanced Materials for High Voltage Insulation Applications ». *IEEE Transactions on Dielectrics and Electrical Insulation*, vol. Vol. 22, n° 3, p. 1594-1604.
- Heid, T., S. Savoie, C. Vanga, M. Fréchet, E. David, N. Freebody et A. Vaughan. 2013b. « Surface resistance of epoxy/BN micro- and Meso-composites exposed to electrical discharges ». In *IEEE International Conference on Solid Dielectrics (ICSD)*. (June 30 2013-July 4 2013), p. 872-875.
- Hong, R. Y., et Q. Chen. 2015. « Dispersion of Inorganic Nanoparticles in Polymer Matrices: Challenges and Solutions ». In *Organic-Inorganic Hybrid Nanomaterials*, sous la dir.

- de Kalia, Susheel, et Yuvaraj Haldorai. Vol. 267, p. 1-38. Coll. « Advances in Polymer Science »: Springer International Publishing.
< http://dx.doi.org/10.1007/12_2014_286 >.
- Horwath, J., D. Schweickart, G. Garcia, D. Klosterman et M. Galaska. 2005. « Improved performance of polyhedral oligomeric silsesquioxane epoxies ». In *Electrical Insulation and Dielectric Phenomena, 2005. CEIDP '05. 2005 Annual Report Conference on.* (16-19 Oct. 2005), p. 155-157.
- Horwath, John C., Daniel L. Schweickart, Guido Garcia, Donald Klosterman, Mary Galaska, Amanda Schrand et Lawrence C. Walko. 2006. « Improved electrical properties of epoxy resin with nanometer-sized inorganic fillers ». In *IEEE International Power Modulator Conference (IPMC)*. p. 189-191.
< <http://dx.doi.org/10.1109/MODSYM.2006.365213> >.
- Huang, X., Y. Li, F. Liu, P. Jiang, T. Iizuka, K. Tatsumi et T. Tanaka. 2014. « Electrical properties of epoxy/POSS composites with homogeneous nanostructure ». *Dielectrics and Electrical Insulation, IEEE Transactions on*, vol. 21, n° 4, p. 1516-1528.
- Huang, Xingyi, Tomonori Iizuka, Pingkai Jiang, Yoshimichi Ohki et Toshikatsu Tanaka. 2012. « Role of Interface on the Thermal Conductivity of Highly Filled Dielectric Epoxy/AlN Composites ». *The Journal of Physical Chemistry C*, vol. 116, n° 25, p. 13629-13639.
- Huang, Xingyi, Chunyi Zhi, Pingkai Jiang, Dmitri Golberg, Yoshio Bando et Toshikatsu Tanaka. 2013. « Polyhedral Oligosilsesquioxane-Modified Boron Nitride Nanotube Based Epoxy Nanocomposites: An Ideal Dielectric Material with High Thermal Conductivity ». *Advanced Functional Materials*, vol. 23, n° 14, p. 1824-1831.
- Ishai P.B, Levy E., Feldman Y., Talary M. S. et Caduff A. 2013. « Electrode polarization in dielectric measurements: A review ». *Meas. Sci. Technol. Measurement Science and Technology*, vol. 24, n° 10.
- Iyer, G., R. S. Gorur et A. Krivda. 2012. « Corona resistance of epoxy nanocomposites: experimental results and modeling ». *IEEE Transactions on Dielectrics and Electrical Insulation*, vol. 19, n° 1, p. 118-125.
- Iyer, G., R. S. Gorur et A. Krivda. 2014. « Understanding electrical discharge endurance of epoxy micro- and nano-composites through thermal analysis ». *IEEE Transactions on Dielectrics and Electrical Insulation*, vol. 21, n° 1, p. 225-229.
- Iyer, G., R. S. Gorur, R. Richert, A. Krivda et L. E. Schmidt. 2011. « Dielectric properties of epoxy based nanocomposites for high voltage insulation ». *IEEE Transactions on Dielectrics and Electrical Insulation*, vol. 18, n° 3, p. 659-666.

- Jonscher, A. K. 1983. *Dielectric relaxation in solids*. London: Chelsea Dielectrics Press.
- Jonscher, A. K. 1996. *Universal relaxation law : a sequel to Dielectric relaxation in solids*. London: Chelsea Dielectrics Press.
- Katayama, J., Y. Ohki, N. Fuse, M. Kozako et T. Tanaka. 2013. « Effects of nanofiller materials on the dielectric properties of epoxy nanocomposites ». *Dielectrics and Electrical Insulation, IEEE Transactions on*, vol. 20, n° 1, p. 157-165.
- Klocke, Fritz. 2011. *Manufacturing Processes I Cutting*. Berlin, Heidelberg: Springer-Verlag Berlin Heidelberg.
- Kochetov, R., T. Andritsch, U. Lafont, P. H. F. Morshuis, S. J. Picken et J. J. Smit. 2009a. « Thermal behaviour of epoxy resin filled with high thermal conductivity nanopowders ». In *IEEE Electrical Insulation Conference (EIC)*. p. 524-528.
- Kochetov, R., T. Andritsch, U. Lafont, P. H. F. Morshuis et J. J. Smit. 2009b. « Thermal conductivity of nano-filled epoxy systems ». In *IEEE Conference on Electrical Insulation and Dielectric Phenomena (CEIDP)*.
- Kochetov, R., T. Andritsch, P. H. F. Morshuis et J. J. Smit. 2010. « Effect of filler size on complex permittivity and thermal conductivity of epoxy-based composites filled with BN particles ». In *IEEE Conference on Electrical Insulation and Dielectric Phenomena (CEIDP)*.
- Kochetov, R., T. Andritsch, P. H. F. Morshuis et J. J. Smit. 2012. « Anomalous behaviour of the dielectric spectroscopy response of nanocomposites ». *IEEE Transactions on Dielectrics and Electrical Insulation*, vol. 19, n° 1, p. 107-117.
- Kozako, M., S. Kuge, T. Imai, T. Ozaki, T. Shimizu et T. Tanaka. 2005. « Surface erosion due to partial discharges on several kinds of epoxy nanocomposites ». In *IEEE Conference on Electrical Insulation and Dielectric Phenomena (CEIDP)*. p. 162-165.
- Kremer, F. Schönhals A. 2003. *Broadband dielectric spectroscopy*. Berlin; New York: Springer.
- Krivda, A., T. Tanaka, M. Fréchette, J. Castellon, D. Fabiani, G. C. Montanari, R. Gorur, P. Morshuis, S. Gubanski, J. Kindersberger, A. Vaughan, S. Pelissou, Y. Tanaka, L. E. Schmidt, G. Iyer, T. Andritsch, J. Seiler et M. Anglhuber. 2012. « Characterization of epoxy microcomposite and nanocomposite materials for power engineering applications ». *IEEE Electrical Insulation Magazine*, vol. 28, n° 2, p. 38-51.
- Kumashiro, Yukinobu. 2000. *Electric refractory materials*. New York: Marcel Dekker.

- Kuo, Shiao-Wei, et Feng-Chih Chang. 2011. « POSS related polymer nanocomposites ». *Progress in Polymer Science (Oxford)*, vol. 36, n° 12, p. 1649-1696.
- Küchler, Andreas. 2009. *Hochspannungstechnik Grundlagen - Technologie - Anwendungen*. Dordrecht; New York: Springer.
- Landau, L. D., et E. M. Lifshitz. 1960. *Electrodynamics of continuous media vol. 8*. Pergamon Press.
- Laskowski, J., et J. A. Kitchener. 1969. « The hydrophilic-hydrophobic transition on silica ». *Journal of Colloid and Interface Science*, vol. 29, n° 4, p. 670-679.
- Lee, J. Y., Y. W. Song, S. W. Kim et H. K. Lee. 2003. « Dielectric and molecular dynamic studies of sub- T_g by thermally stimulated current (TSC) analysis for liquid crystalline epoxy thermosets ». *Materials Chemistry and Physics*, vol. 77, n° 2, p. 455-460.
- Lewis, T. J. 2004. « Interfaces are the dominant feature of dielectrics at the nanometric level ». *Dielectrics and Electrical Insulation, IEEE Transactions on*, vol. 11, n° 5, p. 739-753.
- Lewis, T. J. 2005. « Interfaces: nanometric dielectrics ». *Journal of Physics D: Applied Physics*, vol. 38, n° 2, p. 202.
- Li, Zhe, K. Okamoto, Y. Ohki et T. Tanaka. 2009. « Role of nano-filler on partial discharge resistance and dielectric breakdown strength of micro- Al_2O_3 / epoxy composites ». In *Properties and Applications of Dielectric Materials, 2009. ICPADM 2009. IEEE 9th International Conference on the*. (19-23 July 2009), p. 753-756.
- Li, Zhe, K. Okamoto, Y. Ohki et T. Tanaka. 2011. « The role of nano and micro particles on partial discharge and breakdown strength in epoxy composites ». *IEEE Transactions on Dielectrics and Electrical Insulation*, vol. 18, n° 3, p. 675-681.
- Lide, David R. 1994. *CRC Handbook of chemistry and physics: a ready-reference book of chemical and physical data*. Boca Raton, FL: CRC Press.
- Looyenga, H. 1965. « Dielectric constants of heterogeneous mixtures ». *Physica*, vol. 31, n° 3, p. 401-406.
- Lovell, R. 1976. « The Effect of Specimen Size on the Electric Breakdown of Unfilled and Filled Epoxy Polymers ». *Electrical Insulation, IEEE Transactions on*, vol. EI-11, n° 4, p. 110-114.
- Maxwell, James Clerk. 1873. *A treatise on electricity and magnetism*. Oxford: Clarendon Press.

- Mazzanti, G., G C Montanari et A Motori. 1994. « An insight into thermal life testing and characterization of EPR-insulated cables ». *Journal of Physics D: Applied Physics*, vol. 27, n° 12, p. 2601.
- Nakka, John Suman. 2010. « Tailoring of epoxy material properties ». Delft, Delft University of Technology.
- Nelson, J. K., et Y. Hu. 2005. « Nanocomposite dielectrics—properties and implications ». *Journal of Physics D: Applied Physics*, vol. 38, n° 2, p. 213.
- Nelson, J. K., et John C Fothergill. 2004. « Internal charge behaviour of nanocomposites ». *Nanotechnology*, vol. 15, n° 5, p. 586.
- Nelson, J.K. 2010. *Dielectric Polymer Nanocomposites*. Springer Science+Business Media.
- Nguyen, V. T., A. S. Vaughan, P. L. Lewin et A. Krivda. 2015. « The effect of resin stoichiometry and nanoparticle addition on epoxy/silica nanodielectrics ». *IEEE Transactions on Dielectrics and Electrical Insulation*, vol. 22, n° 2, p. 895-905.
- Nguyen, V., A. S. Vaughan, P. L. Lewin et A. Krivda. 2011. « Stoichiometry and effects of nano-sized and micro-sized fillers on an epoxy based system ». In *IEEE Conference on Electrical Insulation and Dielectric Phenomena (CEIDP)*.
< <http://dx.doi.org/10.1109/CEIDP.2011.6232656> >.
- Osswald, Tim A., et Georg Menges. 2012. *Material Science of Polymers for Engineers (3rd Edition)*. Hanser Publishers.
- Pakdel, Amir, Chunyi Zhi, Yoshio Bando et Dmitri Golberg. 2012. « Low-dimensional boron nitride nanomaterials ». *Materials Today*, vol. 15, n° 6, p. 256-265.
- Park, Won Ho, et Jong Keun Lee. 1998. « Study on isothermal cure behavior of an epoxy-rich/anhydride system by differential scanning calorimetry ». *Journal of Applied Polymer Science*, vol. 67, n° 6, p. 1101-1108.
- Preda, I., J. Castellon, S. Agnel, H. Couderc, M. Fréchet, F. Gao, R. Nigmatullin, S. Thompson et A. F. Vaessen. 2013. « Dielectric response of various partially cured epoxy nanocomposites ». *IEEE Transactions on Dielectrics and Electrical Insulation*, vol. 20, n° 2, p. 580-591.
- Preda, I., J. Castellon, M. Fréchet et S. Agnel. 2014. « Modelling the dielectric permittivity of nanocomposites - the overlap model ». In *Electrical Insulating Materials (ISEIM), Proceedings of 2014 International Symposium on*. (1-5 June 2014), p. 17-21.

- Preetha, P., et M. J. Thomas. 2011. « AC breakdown characteristics of epoxy nanocomposites ». *IEEE Transactions on Dielectrics and Electrical Insulation*, vol. 18, n° 5, p. 1526-1534.
- Raetzke, Stephanie, et Josef Kindersberger. 2006. « The effect of interphase structures in nanodielectrics ». *IEEJ Transactions on Fundamentals and Materials*, vol. 126, n° 11, p. 1044-1049.
- Raju, G.G. 2003. *Dielectrics in Electric Fields*. New York, USA: Marcel Dekker.
- Reading, M., A. S. Vaughan et P. L. Lewin. 2011. « An investigation into improving the breakdown strength and thermal conduction of an epoxy system using boron nitride ». In *IEEE Conference on Electrical Insulation and Dielectric Phenomena (CEIDP)*. (16-19 Oct. 2011), p. 636-639.
- Reading, Martin, Zhiqiang Xu, Alun Vaughan et Paul Lewin. 2011a. « The effect of sample thickness on the relative breakdown strength of epoxy systems ». In *Dielectrics 2011*.
- Reading, Martin, Zhiqiang Xu, Alun Vaughan et Paul Lewin. 2011b. « The importance and methods of dispersing fillers into epoxy resin ». In *Dielectrics 2011*.
- Roy, M., J. K. Nelson, R. K. MacCrone, L. S. Schadler, C. W. Reed et R. Keefe. 2005. « Polymer nanocomposite dielectrics-the role of the interface ». *Dielectrics and Electrical Insulation, IEEE Transactions on*, vol. 12, n° 4, p. 629-643.
- Shalaev, Vladimir M. 1996. « Electromagnetic properties of small-particle composites ». *Physics Reports*, vol. 272, n° 2-3, p. 61-137.
- Shen, Ming-xia, Yin-xin Cui, Jing He et Yao-ming Zhang. 2011. « Thermal conductivity model of filled polymer composites ». *International Journal of Minerals, Metallurgy, and Materials*, vol. 18, n° 5, p. 623-631.
- Sillars, R. W. 1937. « The properties of a dielectric containing semiconducting particles of various shapes ». *Electrical Engineers, Journal of the Institution of*, vol. 80, n° 484, p. 378-394.
- Steeman, P. A. M., et F. H. J. Maurer. 1990. « An interlayer model for the complex dielectric constant of composites ». *Colloid and Polymer Science*, vol. 268, n° 4, p. 315-325.
- Strachota, Adam, Paul Whelan, Jiří Kříž, Jiří Brus, Martina Urbanová, Miroslav Šlouf et Libor Matějka. 2007. « Formation of nanostructured epoxy networks containing polyhedral oligomeric silsesquioxane (POSS) blocks ». *Polymer*, vol. 48, n° 11, p. 3041-3058.

- Suljovrujic, E., M. Micic et D. Milicevic. 2013. « Structural changes and dielectric relaxation behavior of uniaxially oriented high density polyethylene ». *J. Eng. Fibers Fabr. Journal of Engineered Fibers and Fabrics*, vol. 8, n° 3, p. 131-143.
- Takala, M., M. Karttunen, J. Pelto, P. Salovaara, T. Munter, M. Honkanen, T. Auletta et K. Kannus. 2008. « Thermal, mechanical and dielectric properties of nanostructured epoxy-polyhedral oligomeric silsesquioxane composites ». *IEEE Transactions on Dielectrics and Electrical Insulation*, vol. 15, n° 5, p. 1224-1235.
- Takezawa, Y., M. Akatsuka et C. Farren. 2003. « High thermal conductive epoxy resins with controlled high order structure ». In *Proceedings of the 7th International Conference on Properties and Applications of Dielectric Materials*. Vol. 3, p. 1146-1149.
- Tanaka, T., T. Iizuka, Y. Ohki, X. Huang et P. Jiang. 2013. « Dielectric properties and thermal conductivity of epoxy/AlN composites with several kinds of filler-matrix interfaces ». In *IEEE International Conference on Solid Dielectrics (ICSD)*. (June 30 2013-July 4 2013), p. 377-380.
- Tanaka, T., et T. Imai. 2013. « Advances in nanodielectric materials over the past 50 years ». *Electrical Insulation Magazine, IEEE*, vol. 29, n° 1, p. 10-23.
- Tanaka, T., M. Kozako, N. Fuse et Y. Ohki. 2005. « Proposal of a multi-core model for polymer nanocomposite dielectrics ». *Dielectrics and Electrical Insulation, IEEE Transactions on*, vol. 12, n° 4, p. 669-681.
- Tanaka, T., Y. Matsuo et K. Uchida. 2008. « Partial Discharge Endurance of Epoxy / SiC Nanocomposite ». In *IEEE Conference on Electrical Insulation and Dielectric Phenomena (CEIDP)*. (26-29 Oct. 2008), p. 13-16.
- Tanaka, T., Z. Wang, T. Iizuka, M. Kozako et Y. Ohki. 2011. « High thermal conductivity epoxy/BN composites with sufficient dielectric breakdown strength ». In *Power and Energy Systems (ICPS), 2011 International Conference on*. (22-24 Dec. 2011), p. 1-4.
- Tian, F., et Y. Ohki. 2014. « Charge transport and electrode polarization in epoxy resin at high temperatures ». *Journal of physics. D, applied physics.*, vol. 47, n° 4, p. 045311.
- Todd, Michael G., et F. G. Shi. 2005. « Complex permittivity of composite systems: a comprehensive interphase approach ». *Dielectrics and Electrical Insulation, IEEE Transactions on*, vol. 12, n° 3, p. 601-611.
- Torquato, S. 2002. *Random heterogeneous materials : microstructure and macroscopic properties*. New York: Springer.

- Tsekmes, I. A., R. Kochetov, P. H. F. Morshuis et J. J. Smit. 2014. « Modeling the thermal conductivity of polymeric composites based on experimental observations ». *IEEE Transactions on Dielectrics and Electrical Insulation*, vol. 21, n° 2, p. 412-423.
- Tuncer, E. 2013. « Dielectric mixtures-importance and theoretical approaches ». *Electrical Insulation Magazine, IEEE*, vol. 29, n° 6, p. 49-58.
- Tuncer, E., C. Cantoni, Karren L. More, D. R. James, G. Polizos, I. Sauers et A. R. Ellis. 2010. « Breakdown properties of epoxy nanodielectric ». In *IEEE Conference on Electrical Insulation and Dielectric Phenomena (CEIDP)*. (17-20 Oct. 2010), p. 1-4.
- Tuncer, E., Y. V. Serdyuk et S. M. Gubanski. 2002. « Dielectric mixtures: electrical properties and modeling ». *Dielectrics and Electrical Insulation, IEEE Transactions on*, vol. 9, n° 5, p. 809-828.
- Tuncer, Enis, Stanisław M. Gubański et B. Nettelblad. 2001. « Dielectric relaxation in dielectric mixtures: Application of the finite element method and its comparison with dielectric mixture formulas ». *Journal of Applied Physics*, vol. 89, n° 12, p. 8092-8100.
- Tuncer, Enis, Isidor Sauers, D. Randy James, Alvin R. Ellis, M. Parans Paranthaman, Tolga Aytuğ, Srivatsan Sathyamurthy, Karren L More, Jing Li et Amit Goyal. 2007a. « Electrical properties of epoxy resin based nano-composites ». *Nanotechnology*, vol. 18, n° 2, p. 025703.
- Tuncer, Enis, Isidor Sauers, D. Randy James, Alvin R. Ellis, M. Parans Paranthaman, Amit Goyal et Karren L. More. 2007b. « Enhancement of dielectric strength in nanocomposites ». *Nanotechnology*, vol. 18, n° 32, p. 325704.
- Ulański, J., K. Friedrich, G. Boiteux et G. Seytre. 1997. « Evolution of ion mobility in cured epoxy-amine system as determined by time-of-flight method ». *Journal of Applied Polymer Science*, vol. 65, n° 6, p. 1143-1150.
- Vahid, Mirjalili, Yourdkhani Mostafa et Hubert Pascal. 2012. « Dispersion stability in carbon nanotube modified polymers and its effect on the fracture toughness ». *Nanotechnology*, vol. 23, n° 31.
- Virtanen, S., T. M. Krentz, J. K. Nelson, L. S. Schadler, M. Bell, B. Benicewicz, H. Hillborg et Zhao Su. 2014. « Dielectric breakdown strength of epoxy bimodal-polymer-brush-grafted core functionalized silica nanocomposites ». *IEEE Transactions on Dielectrics and Electrical Insulation*, vol. 21, n° 2, p. 563-570.
- Wagner, KarlWilly. 1914. « Erklärung der dielektrischen Nachwirkungsvorgänge auf Grund Maxwellscher Vorstellungen ». *Archiv für Elektrotechnik*, vol. 2, n° 9, p. 371-387.

- Wang, Qi, Zhe Li, Jiandong Wu et Yi Yin. 2012. « The thermal conductivity and electrical strength of epoxy resin with different filler content of micro and nano alumina ». In *Condition Monitoring and Diagnosis (CMD), 2012 International Conference on*. (23-27 Sept. 2012), p. 1110-1113.
- Wang, Z., T. Iizuka, M. Kozako, Y. Ohki et T. Tanaka. 2011. « Development of epoxy/BN composites with high thermal conductivity and sufficient dielectric breakdown strength part I - sample preparations and thermal conductivity ». *IEEE Transactions on Dielectrics and Electrical Insulation*, vol. 18, n° 6, p. 1963-1972.
- Wen, Dongsheng, et Yulong Ding. 2004. « Effective Thermal Conductivity of Aqueous Suspensions of Carbon Nanotubes (Carbon Nanotube Nanofluids) ». *Journal of Thermophysics and Heat Transfer*, vol. 18, n° 4, p. 481-485.
- Wypych, George. 2010. *Handbook of Fillers (3rd Edition)*. ChemTec Publishing.
- Yang, Li, Miao Yin, Xiuyun Li et Hanbing Ma. 2012. « Thermal and dielectric properties of inorganic-organic nanocomposites involving epoxy resin and polyhedral oligomeric silsesquioxanes ». In *3rd International Conference on Manufacturing Science and Engineering, ICMSE 2012, March 27, 2012 - March 29, 2012*. (Xiamen, China) Vol. 476-478, p. 665-669. Coll. « Advanced Materials Research »: Trans Tech Publications. < <http://dx.doi.org/10.4028/www.scientific.net/AMR.476-478.665> >.
- Zengbin, Wang, T. Iizuka, M. Kozako, Y. Ohki et T. Tanaka. 2011a. « Development of epoxy/BN composites with high thermal conductivity and sufficient dielectric breakdown strength part II - breakdown strength ». *Dielectrics and Electrical Insulation, IEEE Transactions on*, vol. 18, n° 6, p. 1973-1983.
- Zengbin, Wang, T. Iizuka, M. Kozako, Y. Ohki et T. Tanaka. 2011b. « Development of epoxy/BN composites with high thermal conductivity and sufficient dielectric breakdown strength part I - sample preparations and thermal conductivity ». *Dielectrics and Electrical Insulation, IEEE Transactions on*, vol. 18, n° 6, p. 1963-1972.
- Zou, Chen, J. C. Fothergill et S. W. Rowe. 2008. « The effect of water absorption on the dielectric properties of epoxy nanocomposites ». *IEEE Transactions on Dielectrics and Electrical Insulation*, vol. 15, n° 1, p. 106-117.